



12-1999

An investigation into the web defect known as 'shot' in the melt-blowing process used to create non-woven fabrics

William Todd Taylor

Follow this and additional works at: https://trace.tennessee.edu/utk_gradthes

Recommended Citation

Taylor, William Todd, "An investigation into the web defect known as 'shot' in the melt-blowing process used to create non-woven fabrics. " Master's Thesis, University of Tennessee, 1999.
https://trace.tennessee.edu/utk_gradthes/10035

This Thesis is brought to you for free and open access by the Graduate School at TRACE: Tennessee Research and Creative Exchange. It has been accepted for inclusion in Masters Theses by an authorized administrator of TRACE: Tennessee Research and Creative Exchange. For more information, please contact trace@utk.edu.

To the Graduate Council:

I am submitting herewith a thesis written by William Todd Taylor entitled "An investigation into the web defect known as 'shot' in the melt-blowing process used to create non-woven fabrics." I have examined the final electronic copy of this thesis for form and content and recommend that it be accepted in partial fulfillment of the requirements for the degree of Master of Science, with a major in Mechanical Engineering.

Mancil W. Milligan, Major Professor

We have read this thesis and recommend its acceptance:

R. Arimilli, M. Parang

Accepted for the Council:

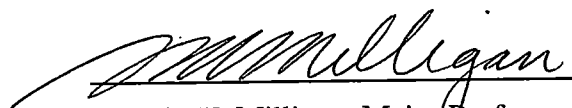
Carolyn R. Hodges

Vice Provost and Dean of the Graduate School

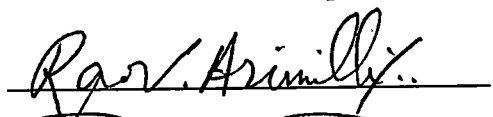
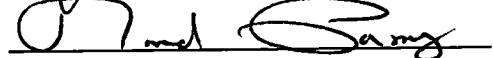
(Original signatures are on file with official student records.)

To the Graduate Council:

I am submitting a thesis written by William Todd Taylor entitled "An Investigation into the Web Defect known as 'Shot' in the Melt-Blowing Process used to Create Non-Woven Fabrics." I have examined the final copy of this thesis for form and content and recommend that it be accepted in partial fulfillment of the requirements for the degree of Master of Science, with a major in Mechanical Engineering.


Mancil W. Milligan, Major Professor

We have read this thesis
And recommend its acceptance:

Accepted for the Council:



Associate Vice Chancellor and
Dean of the Graduate School

AN INVESTIGATION INTO THE WEB DEFECT KNOWN AS
"SHOT" IN THE MELT-BLOWING PROCESS USED TO CREATE
NON-WOVEN FABRICS

A Thesis

Presented for the

Master of Science

Degree

The University of Tennessee, Knoxville

William Todd Taylor

December 1999

Dedication

This thesis is dedicated to
my lovely wife, Rachele
Thank you for all your help and kindness!

also

to the members of my family who have
crossed over the river during my time here
at the University of Tennessee

Mrs. Lucille Morris Taylor
(1904 – 1997)

Mr. Samuel Morris Taylor
(1927 – 1999)

Mr. Donald Boland Aycock
(1931 – 1997)

Acknowledgments

I would like to thank my major professor, Dr. Mancil Milligan, for his support and guidance during this research and preparation of this thesis. I would also like to thank Dr. R. Arimilli and Dr. M. Parang for their comments and assistance during their review of this thesis.

I am very grateful to the Exxon Chemical Company for their financial support during my graduate program and to Dr. Milligan for selecting me to receive this support.

I would like to offer a special thanks to Mr. Brian Herndon for his countless hours of assistance in data analysis and I wish him all the best during his own graduate work at Penn State University. I also offer a special thanks to Mr. Imad Qashou for his help during the ladder stages of this research. His knowledge of polymers was greatly appreciated.

Finally, I would like to thank my parents, John William Taylor and Jamie Aycock Taylor, for their continuous support and encouragement during my graduate career.

Abstract

An extensive experimental investigation was undertaken to study the influence of processing parameters, die configurations and resin type on the production of shot in the melt-blowing process. The addition of nucleating agents to a base resin and the effect these agents have on shot production was also investigated. The processing variables that were investigated included: die air pressure (related to air jet velocity), processing temperature (air and polymer temperature) and polymer mass throughput. The die configuration was varied between a single hole die and a thirty hole die for both conventional and metallocene resins. Data was collected in order to establish the individual effect of varying a single processing parameter on the production of shot. This data was then used to create an empirical model to predict the amount of shot produced using a single hole die.

The thirty hole per inch die produced more shot than the single hole die with all other processing conditions being equal. The metallocene resins also produced more shot than the conventional resins with all other processing conditions being equal. Die air pressure had a strong effect on the shot production; an increase in die air pressure produced more shot in the web sample. Processing temperature produces a similar trend; an increase in process temperature produced more shot in the web sample. Polymer throughput was different in that an increase in polymer throughput might either increase or decrease the amount of shot in the web sample.

A couple of empirical models were created using the experimental data collected during this research. These models utilized a dimensionless form of the processing parameters or more traditional fluid mechanics dimensionless variables to predict the amount of shot that would be present in the web sample. The processing parameter model and the traditional variable model both captured the shot production trends of the melt blowing process.

Nucleating agents were added to a base resin to increase the base resin's crystallization kinetics in an attempt to reduce shot production. The shot production and the average fiber diameter of the nucleated resins were the same as that of the base resin. Laboratory tests indicated that these additives do provide the accelerated crystallization kinetics in a quiescent environment even though the influence of these additives was not realized in the highly turbulent air jet of the melt-blowing process.

Table of Contents

CHAPTER		PAGE
I.	Introduction	1
	Background	1
	Objective	4
II.	Literature Review	6
III.	Experimental Apparatus and Procedures	9
	Single Hole and Multiple Hole Meltblowing Facility	9
	Polymer Extrusion System	11
	Die Test Section	14
	Air Supply System	17
	Melt Blown Web Collection System	19
	Experimental Procedures	22
	Melt Blown Web Creation	22
	Analysis of Web Samples	24
	Average Fiber Diameter Determination	24
	Number of Shot per Area Determination	32
	Effect of Processing Parameters on WebPro Shot Detection	39
IV.	Investigation into Shot Production of Six Different Resins	44

V.	Experimental Investigation into Process Parameters	59
	Die Air Pressure	62
	Process Temperature (Air and Polymer Temperature) ...	74
	Polymer Throughput	79
	Summary and Conclusions of Observation from Data Collection and Analysis	88
	Previous Investigator's Fiber Diameter Empirical Model	89
	Relationship Between Average Fiber Diameter and Shot Production	94
VI.	Single Hole Shot Production Model	105
	Method for Developing the Empirical Model	106
	Single Variable Empirical Model	121
	Multiple Variable Empirical Model	123
	Shot Production Model Based on Fundamental Fluid Mechanics Dimensionless Variables	149
VII.	Investigation into the use of Nucleating Agents to Reduce Shot Production	156
VIII.	Conclusions and Recommendations	171
	Experimental Investigation Process Summary	171
	Experimental Investigation Summary	171
	Six resin study	171
	Experimental investigation into process Parameters	172

Comparison between experimental average fiber Diameter ratio and Spencer's empirical average fiber diameter ratio	173
Single hole shot production model	173
Investigation into the use of Nucleating Agents to Reduce Shot Production	174
Recommendations	174
List of References	175
Appendices	178
Appendix I (Derivation of Air Jet Exit Area Expression) ...	179
Appendix II (Derivation of Air Flow Rate Expression)	183
Appendix III (Derivation of Air Jet Exit Velocity Exp.)	186
Vita	191

List of Figures

FIGURE		PAGE
1.1	SEM image of melt-blown web with shot	5
1.2	SEM image of melt-blown web without shot	5
3.1	Schematic of the melt blowing facility at the University of Tennessee	10
3.2	Cross-sectional view of the single screw extruder and the die test section	12
3.3	Detailed view of a typical extruder	13
3.3	Polymer extrusion system used for this investigation	13
3.5	Cross-sectional view of the test section	15
3.6	Die test section with side removed (with and without face plates)	16
3.7	Test section nosepieces (single hole and 30 hole)	18
3.8	Schematic of supply air entering test section	20
3.9	Actual view of supply air entering test section	20
3.10	Collection process for the web samples and definition of DCD	21
3.11	Views of variable speed collector	23
3.12	Potentiometer setting vs. collector RPM	25
3.13	Data collection sheet	26
3.14	Methodology used to determine the average fiber diameter for previous and current investigation	27
3.15	Drawing of view through the microscope during diameter analysis	29

3.16	Average fiber diameter vs. process conditions for two Measurement methods (optical microscope and SEM) ...	31
3.17	Average fiber diameter vs. process conditions for two Measurement methods (optical microscope and WebPro)	33
3.18	Schematic of WebPro system	35
3.19	Actual view of WebPro shot analysis system	36
3.20	View of web samples' orientation during WebPro analysis	36
3.21	WebPro image before scanning process	38
3.22	WebPro image after the scanning process	38
3.23	WebPro shot analysis output – shot diameter Distribution	40
3.24	WebPro shot analysis output – shot orientation distribution	41
3.23	WebPro shot analysis output – shot aspect ratio distribution	42
4.1	Number of shot per in ² for various resins (0.8 grams/min./hole, single hole die)	46
4.2	Average fiber diameter for various resins (0.8 grams/min./hole, single hole die)	48
4.3	Number of shot per in ² for various resins (1.3 grams/min./hole, single hole die)	49
4.4	Number of shot per in ² for various resins (0.8 grams/min./hole, 30 hole die)	51
4.5	Average fiber diameter for various resins (0.8 grams/min./hole, 30 hole die)	52
4.6	Number of shot per in ² vs. process condition (0.8 grams/min./hole, 30 hole die, comparison between ZN1 and M4)	53

4.7	Number of shot per in ² vs. process condition (M2 resin, 0.8 grams/min./hole, comparison between single and 30 hole dies)	54
4.8	Number of shot per in ² vs. process condition (M3 resin, 0.8 grams/min./hole, comparison between single and 30 hole dies)	55
4.9	Number of shot per in ² vs. process condition (ZN1 resin, 0.8 grams/min./hole, comparison between single and 30 hole dies)	56
4.10	Number of shot per in ² vs. process condition (ZN2 resin, 0.8 grams/min./hole, comparison between single and 30 hole dies)	57
4.11	Number of shot per in ² vs. process condition (ZN3 resin, 0.8 grams/min./hole, comparison between single and 30 hole dies)	58
5.1	Test matrix of the processing conditions at which the web samples were collected	61
5.2	Relationship between air jet exit velocity and die air pressure	63
5.3	Relationship between shot area percentage and number of shot per in ²	64
5.4	Number of shot per in ² vs. die air pressure (M2 resin, 0.4 grams/min./hole)	66
5.5	Number of shot per in ² vs. air velocity (M2 resin, 0.4 grams/min./hole)	67
5.6	Average fiber diameter vs. die air pressure (M2 resin, 0.4 grams/min./hole)	68
5.7	Number of shot per in ² vs. die air pressure (M2 resin, 0.8 grams/min./hole)	69
5.8	Average fiber diameter vs. die air pressure (M2 resin, 0.8 grams/min./hole)	71

5.9	Number of shot per in ² vs. die air pressure (M2 resin, 1.3 grams/min./hole)	72
5.10	Average fiber diameter vs. die air pressure (M2 resin, 1.3 grams/min./hole)	73
5.11	Number of shot per in ² vs. process temperature (M2 resin, 0.4 grams/min./hole)	75
5.12	Average fiber diameter vs. process temperature (M2 resin, 0.4 grams/min./hole)	76
5.13	Number of shot per in ² vs. process temperature (M2 resin, 0.8 grams/min./hole)	77
5.14	Average fiber diameter vs. process temperature (M2 resin, 0.8 grams/min./hole)	78
5.15	Number of shot per in ² vs. process temperature (M2 resin, 1.3 grams/min./hole)	80
5.16	Average fiber diameter vs. process temperature (M2 resin, 1.3 grams/min./hole)	81
5.17	Number of shot per in ² vs. polymer throughput (M2 resin, Die Air Pressure = 10 psig)	82
5.18	Number of shot per in ² vs. polymer throughput (M2 resin, Die Air Pressure = 8 psig)	84
5.19	Number of shot per in ² vs. polymer throughput (M2 resin, Die Air Pressure = 5 psig)	85
5.20	Number of shot per in ² vs. polymer throughput (M2 resin, Die Air Pressure = 3 psig)	86
5.21	Number of shot per in ² vs. polymer throughput (M2 resin, single hole die)	87
5.22	Modified average fiber diameter ratio vs. momentum flux ratio (Ψ), (comparison between actual data and empirical relationship without polymer MFR variable)	92

5.23	Experimental average fiber diameter ratio vs. empirical fiber diameter ratio , (comparison between actual data and empirical relationship without polymer MFR variable)	93
5.24	Modified average fiber diameter ratio vs. momentum flux ratio (Ψ), (comparison between actual data and empirical relationship with polymer MFR variable)	95
5.25	Experimental average fiber diameter ratio vs. empirical fiber diameter ratio , (comparison between actual data and empirical relationship without polymer MFR variable)	96
5.26	Single hole melt blowing line filament flight dynamics	98
5.27	Number of shot per in ² vs. average fiber diameter (M2 resin, single hole die)	99
5.28	Number of shot per in ² vs. web fiber diameter coefficient of variation (M2 resin, single hole die)	100
5.29	Number of shot per in ² vs. web fiber diameter coefficient of variation (M2 resin, 0.4 grams/min.)	102
5.30	Number of shot per in ² vs. web fiber diameter coefficient of variation (M2 resin, 0.8 grams/min.)	103
5.31	Number of shot per in ² vs. web fiber diameter coefficient of variation (M2 resin, 1.3 grams/min.)	104
6.1	Number of shot per area ratio vs. die air pressure ratio (M2 resin, 0.4 grams/min./hole)	108
6.2	Number of shot per area ratio vs. die air pressure ratio (M2 resin, 0.8 grams/min./hole)	109
6.3	Number of shot per area ratio vs. die air pressure ratio (M2 resin, 1.3 grams/min./hole)	110
6.4	Number of shot per area ratio vs. process temperature ratio (M2 resin, 0.4 grams/min./hole)	111

6.5	Number of shot per area ratio vs. process temperature ratio (M2 resin, 0.8 grams/min./hole)	112
6.6	Number of shot per area ratio vs. process temperature ratio (M2 resin, 1.3 grams/min./hole)	113
6.7	Number of shot per area ratio vs. polymer throughput ratio (M2 resin, Die Air Pressure = 10 psig)	114
6.8	Number of shot per area ratio vs. polymer throughput ratio (M2 resin, Die Air Pressure = 8 psig)	115
6.9	Number of shot per area ratio vs. polymer throughput ratio (M2 resin, Die Air Pressure = 5 psig)	116
6.10	Number of shot per area ratio vs. polymer throughput ratio (M2 resin, Die Air Pressure = 3 psig)	117
6.11	Non-linear regression model input window	119
6.12	Non-linear model constant initial guess window	119
6.13	SPSS non-linear regression output	120
6.14	Experimental number of shot per area ratio vs. empirical number of shot per area ratio	125
6.15	Modified number of shot per area ratio vs. polymer throughput ratio for $P_d = 10$ psig	127
6.16	Modified number of shot per area ratio vs. polymer throughput ratio for $P_d = 8$ psig	128
6.17	Modified number of shot per area ratio vs. polymer throughput ratio for $P_d = 5$ psig	129
6.18	Modified number of shot per area ratio vs. polymer throughput ratio for $P_d = 3$ psig	130
6.19	Empirical number of shot per area ratio vs. experimental number of shot per area ratio	132
6.20	Figure 6.19's inverse slope value vs. polymer throughput ratio	133

6.21	Corrected empirical number of shot per area ratio vs. experimental number of shot per area ratio	135
6.22	Number of shot per area ratio vs. die air pressure ratio (both experimental and empirical values plotted, 0.4 grams/min.)	136
6.23	Number of shot per area ratio vs. die air pressure ratio (both experimental and empirical values plotted, 0.8 grams/min.)	137
6.24	Number of shot per area ratio vs. die air pressure ratio (both experimental and empirical values plotted, 1.3 grams/min.)	138
6.25	Number of shot per area ratio vs. process temperature ratio (both experimental and empirical values plotted, 0.4 grams/min.)	139
6.26	Number of shot per area ratio vs. process temperature ratio (both experimental and empirical values plotted, 0.8 grams/min.)	140
6.27	Number of shot per area ratio vs. process temperature ratio (both experimental and empirical values plotted, 1.3 grams/min.)	141
6.28	Number of shot per area ratio vs. polymer throughput ratio (both experimental and empirical values plotted, Die Air Pressure = 10 psig)	142
6.29	Number of shot per area ratio vs. polymer throughput ratio (both experimental and empirical values plotted, Die Air Pressure = 8 psig)	143
6.30	Number of shot per area ratio vs. polymer throughput ratio (both experimental and empirical values plotted, Die Air Pressure = 5 psig)	144
6.31	Number of shot per area ratio vs. polymer throughput ratio (both experimental and empirical values plotted, Die Air Pressure = 3 psig)	145
6.32	Comparison between empirical model and experimental data (all M2 resin, single hole die data)	147

6.33	Comparison between empirical model and experimental data for a modified data set, (M2 resin, single hole die data, higher process Temperatures only)	148
6.34	Elongational viscosity of 700 MFR polypropylene vs. polymer temperature	151
6.35	Empirical shot cover percentage vs. experimental shot cover percentage, (single empirical relationship)	153
6.36	Empirical shot cover percentage vs. experimental shot cover percentage, (multiple empirical relationships)	155
7.1	Number of shot per in ² vs. process conditions (two NA-1 resins, 30 hole die, 0.8 grams/min./hole)	159
7.2	Average fiber diameter vs. process conditions (two NA-1 resins, 30 hole die, 0.8 grams/min./hole)	160
7.3	Number of shot per in ² vs. process conditions (four NA-1 resins, 30 hole die, 0.8 grams/min./hole)	161
7.4	Average fiber diameter vs. process conditions (four NA-1 resins, 30 hole die, 0.8 grams/min./hole)	163
7.5	Number of shot per in ² vs. process conditions (two NA-2 resins, 30 hole die, 0.8 grams/min./hole)	164
7.6	Average fiber diameter vs. process conditions (two NA-2 resins, 30 hole die, 0.8 grams/min./hole)	165
7.7	Crystallization half-time vs. crystallization temperature (for all NA-1 resins, NA-2 resins and M2 base resin)	166
AI.1	Exploded view of the die tip and face plates	181

List of Symbols and Abbreviations

ASME	American Society of American Engineers
A_{exit}	air jet exit area
DCD	Die to Collector Distance
d_g	die gap
d_s	die setback
h	air jet exit height
h_m	orifice pressure drop in inches of water
m_o	air mass flow rate at the orifice
m_{ts}	air mass flow rate at the test section
MFR	melt flow rate
P_{ts}	static pressure of air at the test section exit
P_{tso}	stagnation pressure of air at the test section exit
P_{die}	die air pressure or die stagnation pressure
P_{∞}	atmospheric pressure
R	specific gas constant
RPM	revolutions per minute
SCFM	standard cubic feet per minute
SEM	scanning electron microscope
TANDEC	Textiles and Nonwovens Development Center
T_{ts}	static temperature of air at the exit of test section
T_{tso}	stagnation temperature of air at the exit of the test section

T_a	temperature of air measured with thermocouples
T_p	polymer temperature
T_{pipe}	temperature of the air at the measuring orifice
V_e	air jet exit velocity
w	air exit width

Greek Symbols

α	included angle of the die
β	polymer throughput ratio
Γ	air to polymer mass flux ratio
γ	specific heat ratio
δ	fiber diameter ratio
η	number of shot per area ratio
μ	polymer elongational viscosity
ρ_{air}	density of air
Θ	process temperature ratio
θ	air jet exit angle
Φ	die air pressure ratio
Ψ	air to polymer momentum flux ratio

Chapter I

Introduction

Background

In order to understand the effect of process conditions on the production of non-woven fabrics in the melt-blowing process, one must first understand the nature of both non-woven fabrics and the melt-blowing process. Fortunately, a non-woven fabric is exactly what it sounds like. These fabrics are materials that are not constructed using the traditional “mechanical” weaving methods that the vast majority of people are familiar with in one form or another. The term “non-woven fabric” is defined by the American Standard for Testing Materials (ASTM) [1] as:

A structure produced by bonding or the interlocking of fibers, or both, accomplished by mechanical, chemical, thermal, or solvent means and the combination thereof. The term does not include paper or fabrics that are woven, knitted, tufted, or those made by wool or other felting processes.

With this definition of a non-woven fabric, one might be surprised how often he or she comes in contact or uses these materials. Some examples of everyday uses for non-woven materials are as follows: tea bags, large envelopes, car covers, face masks, disposable clothing, filter media and floppy disks liners.

Since the above uses of non-woven are not extremely plentiful one might wonder why this area warrants academic study. The simple answer to this question is growing markets. The non-woven market is not static; it is growing considerably. In 1990, the world production of non-woven fabric was twelve billion square yards and

in 1994 the world production had increased to thirty-eight billion square yards [2]. In financial terms, it has been estimated that the total United States dollar value of non-woven materials and products that presently utilize non-woven materials was about \$31 billion in 1994 [2]. This industry as a whole is expanding at an average rate of 5% per year in the United States and greater elsewhere [2].

There are many competing technologies in the production of non-woven fabric. All non-woven production technologies are classified into three categories [3]: dry laid, wet laid and polymer-laid. The melt-blowing process is a method of producing a non-woven fabric or "web" in the polymer-laid category and is defined in this manner [4]:

Melt-blowing is a process in which a fiber forming polymer is melted and extruded through a die containing a number of small orifices (from one to the limit of die construction). Convergent streams of hot air are used to attenuate the extruded polymer streams to form extremely fine diameter fibers. The attenuated fibers are eventually carried by the high velocity heated air onto a collector screen and thus form a fine fibered self-bonded non-woven melt blown web.

One of the most significant factors in the increased use of non-woven fabric is that the fabrics themselves are made directly from raw materials and therefore do not require as many steps to reach final phase as that of conventional textiles. The melt-blowing process adheres to the minimization of processing steps to create a melt-blown fabric or web in its final form. A few example of melt-blown products in today's industry are oil spill containment devices, wipes, surgical gowns and face

masks, clothing insulation, filter media and feminine hygiene products [5].

Another advantage of the melt-blowing system for producing non-woven fabrics is that this system is capable of producing extremely fine fibers. The production of very fine fibers enables the creation of webs with very high surface area to mass ratios and therefore this process is very effective at producing high efficiency filtration media. Nearly all non-wovens can be tailored to the filtration industry and this is evident in the growing market share of non-wovens in that industry. The latest available data indicates that the filtration industry is the number one user for durable non-wovens, with annual sales in excess of one billion square yards. The melt-blown portion of the non-woven filtration business is approximately 18% with annual sales of \$230 million in 1994 [2].

The growth of the melt-blown industry is inherently linked to understanding of the process itself. The original purpose of the process was to create ultra fine fibers for filtration purposes. A great deal of energy has been exercised in understanding the parameters of the process that produce these small fibers. However, during these studies a processing defect, later labeled as "shot", was discovered. This defect or shot occurs when an amount of the polymer is not attenuated to its design fiber stage and eventually appears as a "globule" of polymer in the final non-woven fabric. As previously stated, the melt blown process allows for the creation of filtration fabrics with very high surface area to mass ratios. The production of shot is detrimental to this ratio and reduces the fabric's filtration efficiency. The presence of shot also adversely affects the general appearance and

feel of the final non-woven fabric. Therefore most studies of the melt-blown process investigate the process conditions or resin characteristics that optimize the fiber diameter for specific applications and to minimize the production of shot. For clarification purposes, Figure 1.1 and Figure 1.2 are scanning electron microscope (SEM) images of melt blown webs with and without shot.

Objective

The objectives of this research effort are best summarized as follows:

- To investigate the differences in shot production for six different resins provided by the Exxon Chemical Company. These resins were comprised of different catalyst types and resin melt flow rates.
- To determine the effects of polymer throughput, polymer and air temperature and air velocity on average fiber diameter and shot content of the final web.
- To develop an empirical model for the shot production in terms process parameters and also in terms of classical fluid mechanics dimensionless variables.
- Investigate the use of additives in the polymers themselves to aid in the reduction of shot. Determine the effect (if any) these additives might have on the average fiber diameter.

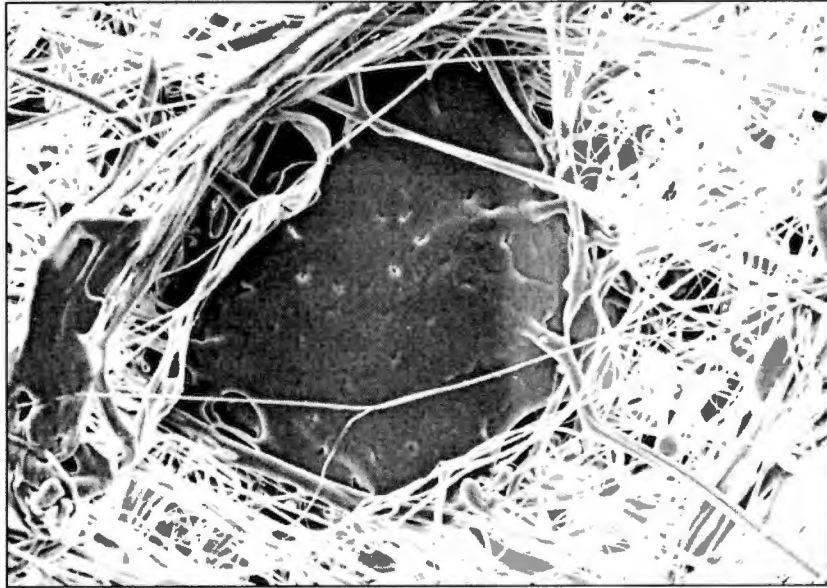


Figure 1.1: SEM image of melt-blown web with shot

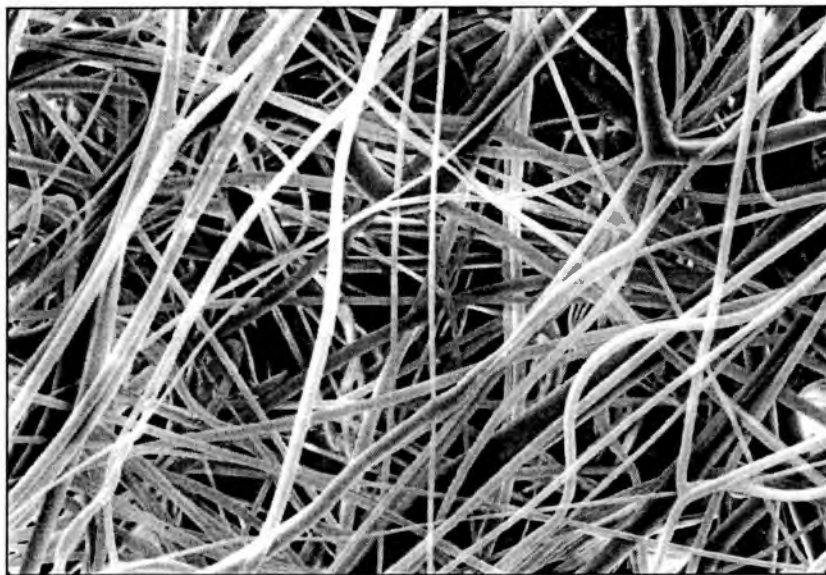


Figure 1.2: SEM image of melt-blown web without shot

Chapter II

Literature Review

As stated in the introduction, a great deal of study has occurred concerning the effects of processing parameters on the melt blowing process. Most studies have been concerned with the fiber diameter for the purpose of making smaller fibers. Wentz [6] was an early pioneer in the production of fibers less than one micron. Wentz's work was performed in the 1950's for the Naval Research Laboratory with the purpose of creating micron-sized fibers for filtration applications. The methods used by Wentz in the 1950's were the foundation for the melt-blowing system currently licensed to the Exxon Chemical Corporation. Even though Wentz was primarily concerned with the production of small fibers for filtration purposes, he noticed that filter efficiencies dropped due to the presence of particles in the web he later referred to as "shot". Wentz described shot as a globule of solid material larger than diameters of the surrounding fibers. He also stated that these globules were most likely produced when the molten polymer filament was fractured and the end at the fracture would form a globule of polymer since it could no longer be attenuated. This first study by Wentz introduced shot production at the beginning of the melt-blowing process development.

Other investigators have noticed and documented this shot phenomenon as well. Buntin and Lohkamp [7] stated that the converging high-speed air streams caused the molten polymer streams to be severed or broken continuously into small

lengths. The broken ends would snap back on its own stream and create a polymer globule or shot. Shambaugh [8] continued work with Buntin and Lohkamp's snap back theory in order to determine the processing range in which shot was not produced. Shambaugh concluded that the melt blowing process was comprised of three distinct regions and he performed a dimensional analysis in order to determine the dominant variables for each region. He labeled these regions as I, II and III. Region I is the low gas (air) velocity region and is similar to melt spinning in that the melt fibers are continuous. He also stated that fibers in this region are typically greater than 10 μm . Region II was described as the "unstable region" and is entered into when the gas velocity is increased. In this region the polymer streams break in shorter length filaments and create shot. Shambaugh states that these shot are usually greater than 0.3 mm in diameter and induce an undesirable coarseness into the final product. Region II also has fiber diameters in the range of 0.5 μm to 10 μm . Shambaugh's last region, Region III, is entered when the gas velocity is raised even further than that of Region II. The shot is still present in this region, but the shot has been attenuated to diameters of less than 0.3 mm. Fiber diameters in this region are from 10 μm down to 0.1 μm .

In 1991, Milligan and Haynes [10] performed melt-blowing studies using stop motion photography and a single hole die to demonstrate that the fibers that were produced in the melt blown webs were actually continuous filaments. This was an important departure from the broken fiber "snap-back" theory of shot creation since

there must be another mechanism for shot production if the fibers did not break very often.

In 1993, Utsman [11] examined the effects of polymer temperature and air velocity on shot production and average fiber diameter. He concluded that average fiber diameters decrease as polymer temperature increases and air velocity increases. Utsman also found that shot intensity decreased as polymer temperature decreased and as air velocity increased. Shot intensity is a parameter Utsman created in order to account for various basis weight samples. He defined shot intensity as the number of shot per area divided by the mass of the sample. Utsman used stop motion photography to examine the plane motion of multi-hole and single-hole die extruded fibers in flight. This stop motion photographic study verified the preliminary work done by Milligan and Haynes [10] that the primary mechanism for shot production was not the snap back phenomenon previously believed, but a collision of molten polymer streams during their attenuation and crystallization time.

Milligan and Bogard [12] created a broad model for the formation of shot in the melt-blowing process. This model was entirely based on the polymer filament collision theory of shot production. This model was primarily concerned with the changes in the heat transfer rates for a fused filament pair as opposed to that of a single filament.

Chapter III

Experimental Apparatus and Procedures

This chapter describes the experimental apparatus used to produce the melt-blown fabrics and the procedures used to analyze these fabrics. The discussion in this chapter is divided into three sections. The first section is a description of the melt-blown facility equipment used to produce the melt-blown fabrics. The second section describes the methods used to collect the melt-blown fabrics. The last section provides a description of the methods used to analyze the experimental data and the processes used to determine average fiber diameter and shot quantity from the collected fabrics. This research effort is part of a continuing investigation supported by the Exxon Chemical Corporation at the University of Tennessee and therefore the Exxon Chemical Corporation provides all resins used throughout this project. The resins used throughout this investigation are polypropylene resins.

Single Hole and Multiple Hole Meltblowing Facility

The meltblowing facility used through out this study is located in room M1 on the mezzanine floor of Dougherty Engineering Building at the University of Tennessee, Knoxville. As stated by Spencer[13] and Utsman [11], the meltblowing facility is composed of four main components. These four components consist of the polymer extrusion system, die test section, air delivery system and the melt-blown fabric collection system. A schematic showing the arrangements of these components is provided in Figure 3.1 [11].

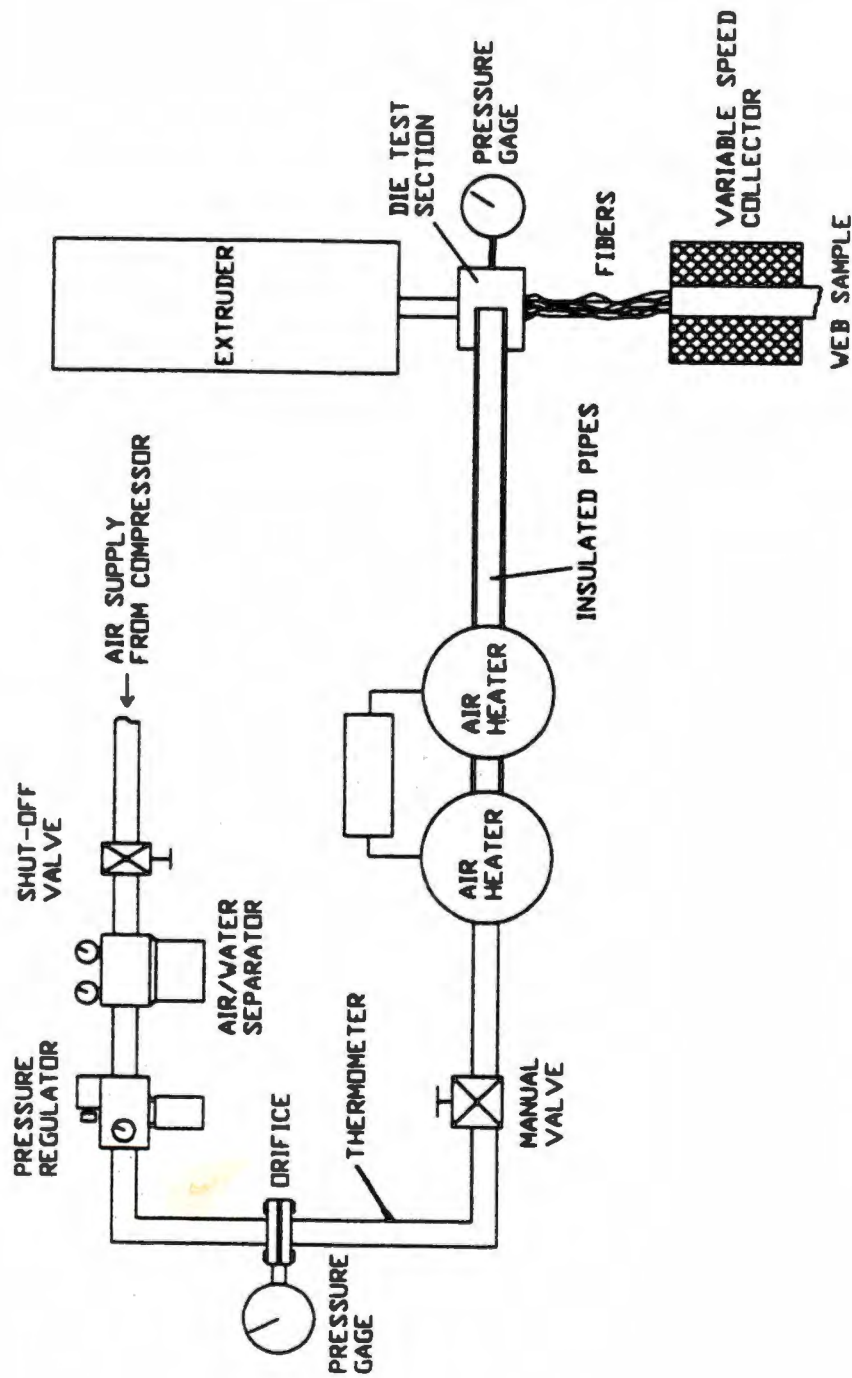


Figure 3.1: Schematic of the melt blowing facility at the University of Tennessee

Source: Utzman, F.M., An Experimental Investigation on the Production of Microfibers and the Web Defect Known as Shot for the Melt Blowing Process, Thesis, University of Tennessee, Knoxville, 1995.

Polymer Extrusion System

The function of the polymer extrusion system is to supply the die test section with a constant flow of molten polymer. The polymer extrusion system used throughout this investigation is a Killion single screw extruder (series KLB, Model 075-125) capable of delivering molten polymer at flow rates from 0.2 to 48.0 grams/minute to the die test section. The extruder screw is powered by a variable speed three horsepower motor, which drives the screw via a worm and gear 90° coupling. Raw polymer is fed into the extrusion system through the hopper and the melting of the polymer is accomplished through five independently controlled zones (or stages) using band heaters fixed to the exterior of the extruder barrel assembly. These band heaters are controlled with Eurotherm temperature controllers. This extrusion system is shown schematically in Figure 3.2 [11] and a more detailed drawing of a typical extruder is shown in Figure 3.3 [14].

The flow rate of the polymer is varied by increasing or decreasing the motor/screw RPM. A digital RPM meter indicates the speed of the screw and a pressure transducer is used to monitor the pressure of the molten polymer. The molten polymer pressure is a very important indicator in order to maintain constant polymer throughput for a given resin and polymer temperature. This pressure transducer is a Dynisco PT422A with a least count of 1 psig. The molten polymer pressure is measured between zones four and five as shown in Figure 3.2 [11]. The actual polymer extrusion system used throughout this investigation is shown in Figure 3.4.

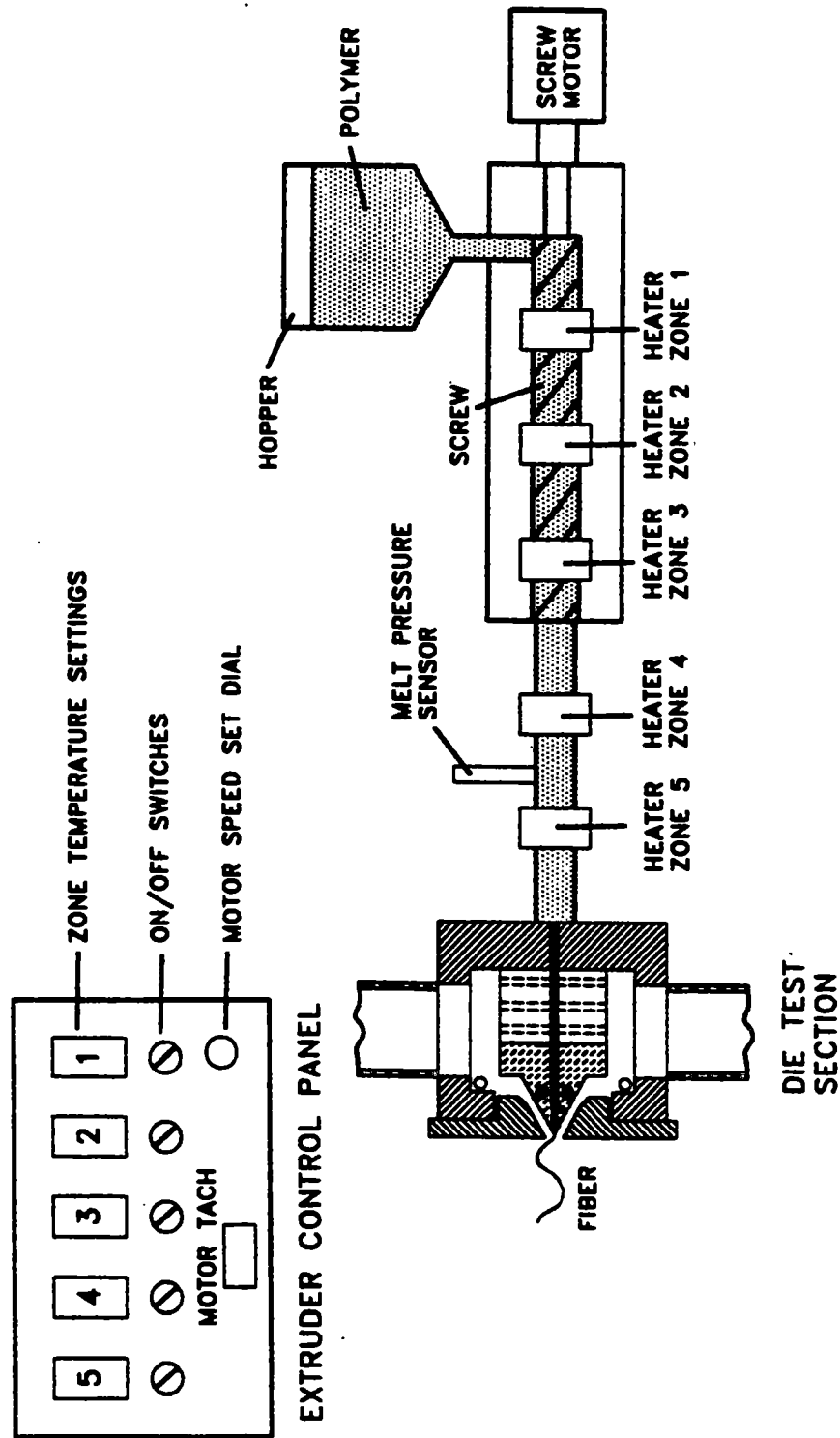


Figure 3.2: Cross-sectional view of the single screw extruder and the die test section

Source: Utsman, F.M., An Experimental Investigation on the Production of Microfibers and the Web Defect Known as Shot for the Melt Blowing Process, Thesis, University of Tennessee, Knoxville, 1995.

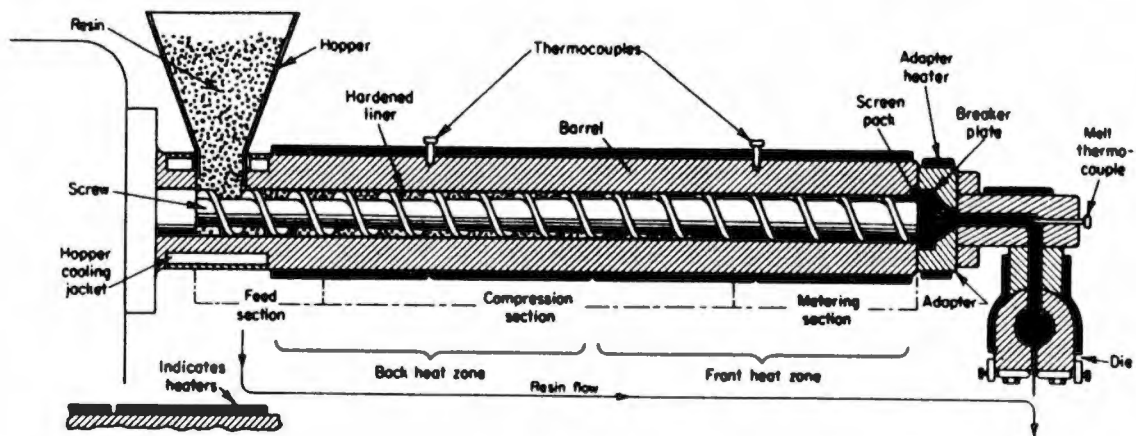


Figure 3.3: Detailed view of a typical extruder

Source: Rodriguez, Ferdinand, Principles of Polymer Systems, fourth edition, Taylor and Francis, New York, 1996.

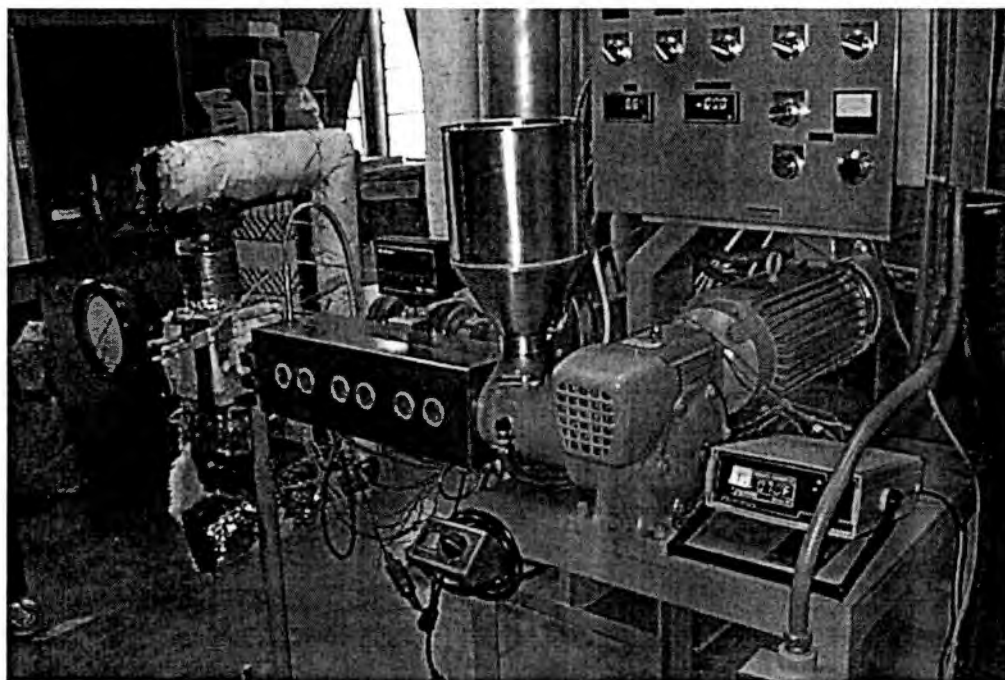
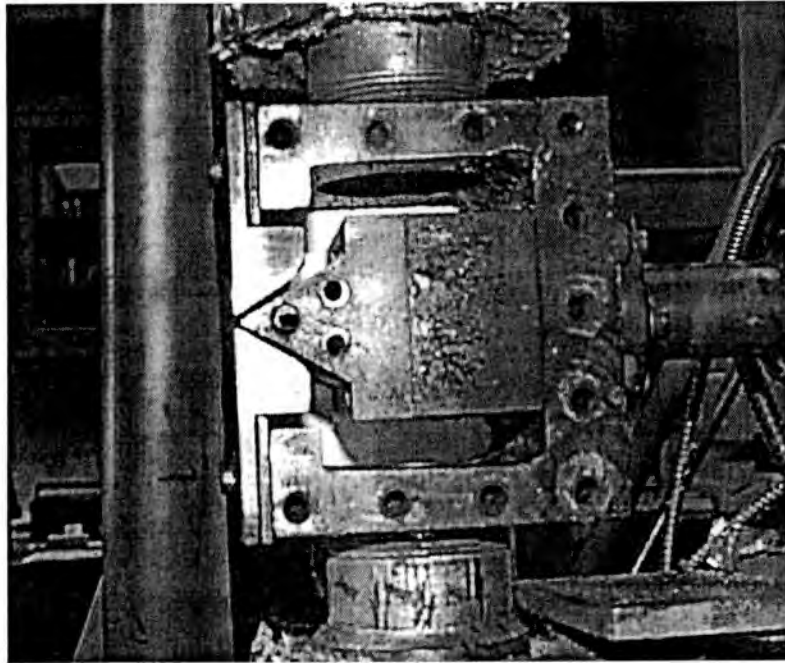


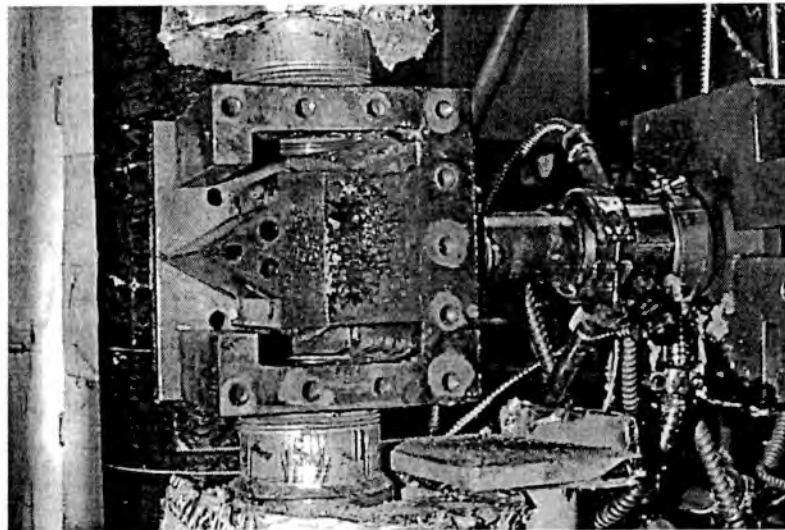
Figure 3.4: Polymer extrusion system used for this investigation

Die Test Section

Once the molten polymer exits the extrusion system it enters the die test section. The die test section is composed of an adapter flange, nosepiece, adjustable upper and lower faceplates, spacer block and housing. Figure 3.5 [13] shows a cross-sectional schematic of the test section. Figure 3.6 shows actual photographs of the test section with the side of the test section removed. Once the molten polymer exits the extruder it enters the die test section through the adapter flange. The adapter flange has a coarse screen to catch any large particles before they enter the smaller passages of the test section. The molten polymer passes through the spacer block before entering the nosepiece. This spacer block is essentially an adapter between the back wall of the housing and the nosepiece. There is a fine screen between the spacer block and the nosepiece to prevent any non-molten polymer particles from clogging the very small orifices at the nosepiece discharge. The spacer block has holes drilled through it connecting the upper and lower air chambers. These holes allow the upper and lower air chambers' air pressure to equalize and create one stagnation chamber. The temperature and pressure of the heated air in this stagnation chamber were measured using a Type K thermocouple and a pressure gage. The nosepiece contains two 280 watt cartridge heaters to aid in maintaining the desired polymer temperature at the nosepiece exit and another Type K thermocouple to measure the exit polymer temperature. The molten polymer exits the die test section through the nosepiece orifice. This investigation utilized two different nosepieces: one nosepiece had a single $356 \mu\text{m}$ (1.4×10^{-2} [in]) diameter orifice and the other had thirty orifices of the



face plates installed



face plates removed

Figure 3.6: Die test section with side removed

same size equally spaced in a one-inch length. The two nosepieces were identical in every other aspect and are shown in Figure 3.7 for clarity. The molten polymer is forced through the nosepiece's orifice by the upstream polymer pressure, but the molten polymer is carried away from the orifice exit by the drag force of the two converging heated air streams. The converging air streams are created by the passage between the nosepiece and the adjustable face plates. These face plates can be moved either vertically or horizontally to create the required test configuration. The placement of these face plates influence the exit area through which the air from the stagnation chamber flows. A complete derivation of the exit area as a function of face plate location was derived by Spencer [13] and is provided in Appendix I.

Air Supply System

The air for the converging air streams used in the die test section is provided by the air supply system. This system is portrayed schematically in Figure 3.1. The airflow into the system is supplied by one of two compressors. The first of these compressors is located in the penthouse of Dougherty Engineering Building and the second is located in the Dabney/Buehler mechanical room across the street from Dougherty Engineering Building. The main portion of the airflow is provided by the Dougherty Engineering Building penthouse compressor and it can supply 250 SCFM at 110 psig. The compressed air enters the lab in a 2-inch inside diameter (I.D.) steel pipe. As shown in Figure 3.1, the air passes through a shut off valve, an air/water separator and a pressure regulator before passing through the air flow measuring orifice. The pressure regulator reduces the air pressure from about 110 psig to

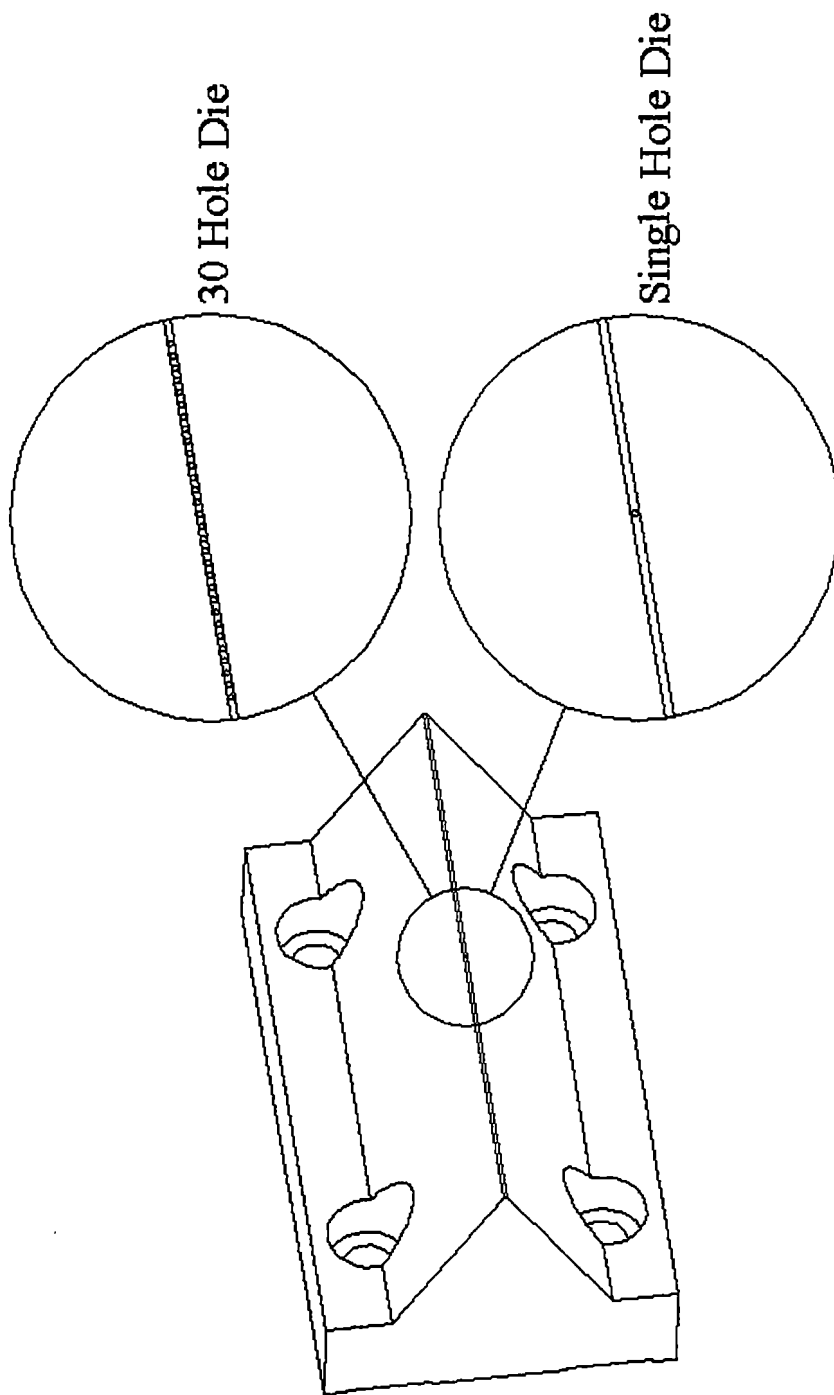


Figure 3.7: Test section nosepieces

50 psig. The pressure drop across the measuring orifice (h_m) is measured with one of two pressure gages. The first pressure gage is calibrated in inches of water and is scaled for pressures between zero and twenty-five inches of water. If higher airflows are required, a second pressure gage is calibrated in feet of water and the air system will not provide pressures that will exceed the range of this pressure gage. The purpose of the measuring orifice is to determine the mass flow rate of air entering the die test section. The measuring orifice is constructed and installed per the ASME Flow Measurement Code [15]. Once the air passes through the orifice the air temperature in the pipe (T_{pipe}) is measured with a mercury thermometer, and the airflow is regulated with a manual throttling valve. The air then enters two Accutherm electric resistance heaters that are arranged in series and controlled by measuring the air temperature out of the heaters with a thermocouple and varying the heater setting on the heater control panel until the test air temperature (T_{iso}) is obtained. The heated air then exits the heaters through an insulated 2 inch I.D. steel pipe until the pipe splits into two 2 inch I.D. insulated steel pipes that serve the top and bottom of the die test section. This setup is shown schematically in Figure 3.8 and in actual form in Figure 3.9.

Melt-Blown Web Collection System

The attenuated fibers are collected using a variable speed cylindrical collector. This collector has an 18.5 inch diameter drum covered with a fine metal mesh screen. The placement of this collection system in relation to the die test section is shown in Figure 3.10 [11]. A $\frac{1}{4}$ horsepower motor with a variable speed drive control rotates

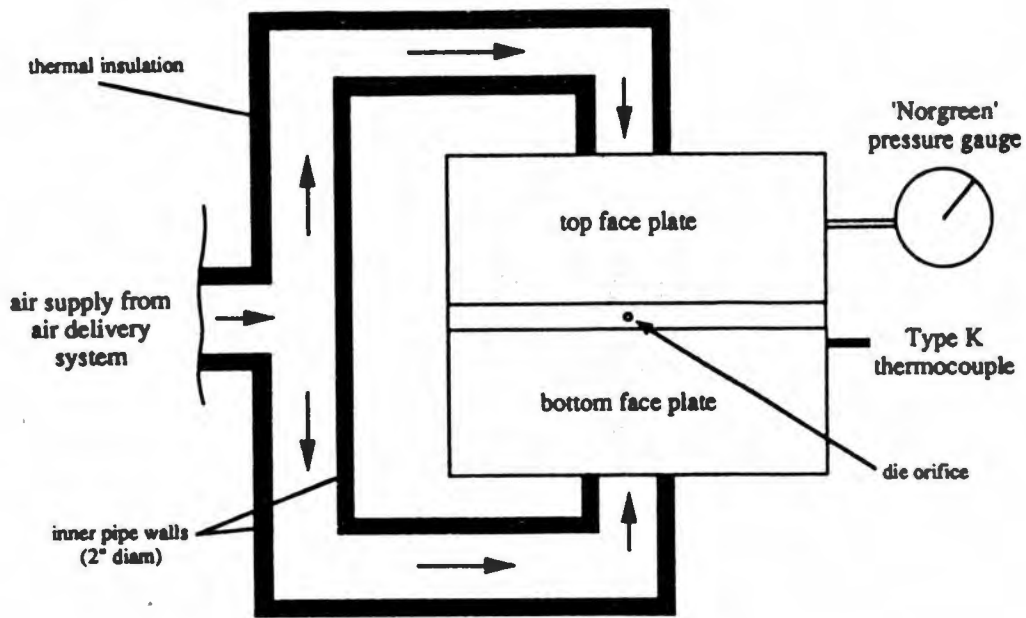


Figure 3.8: Schematic of supply air entering test section

Source: Spencer, E.G., An Experimental Investigation of Processing Parameters for the Production of Micro Fibers Using the Melt Blowing Process, Thesis, University of Tennessee, Knoxville, 1994.

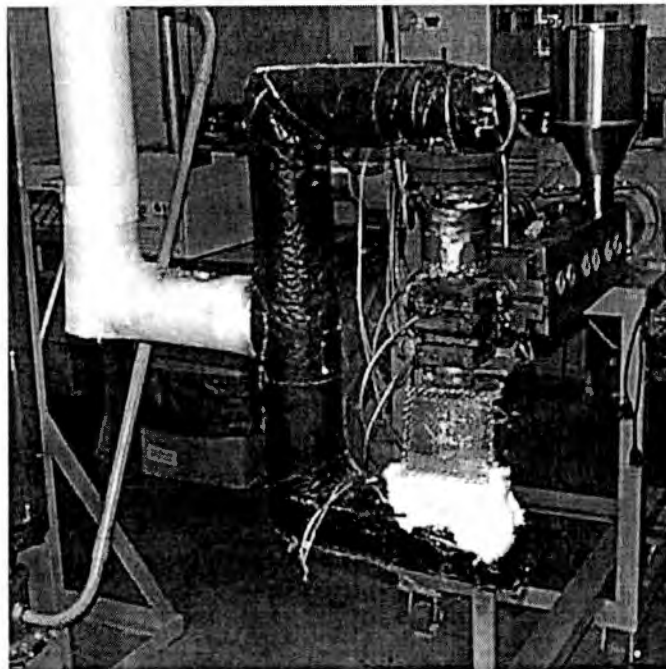


Figure 3.9: Actual view of supply air entering test section

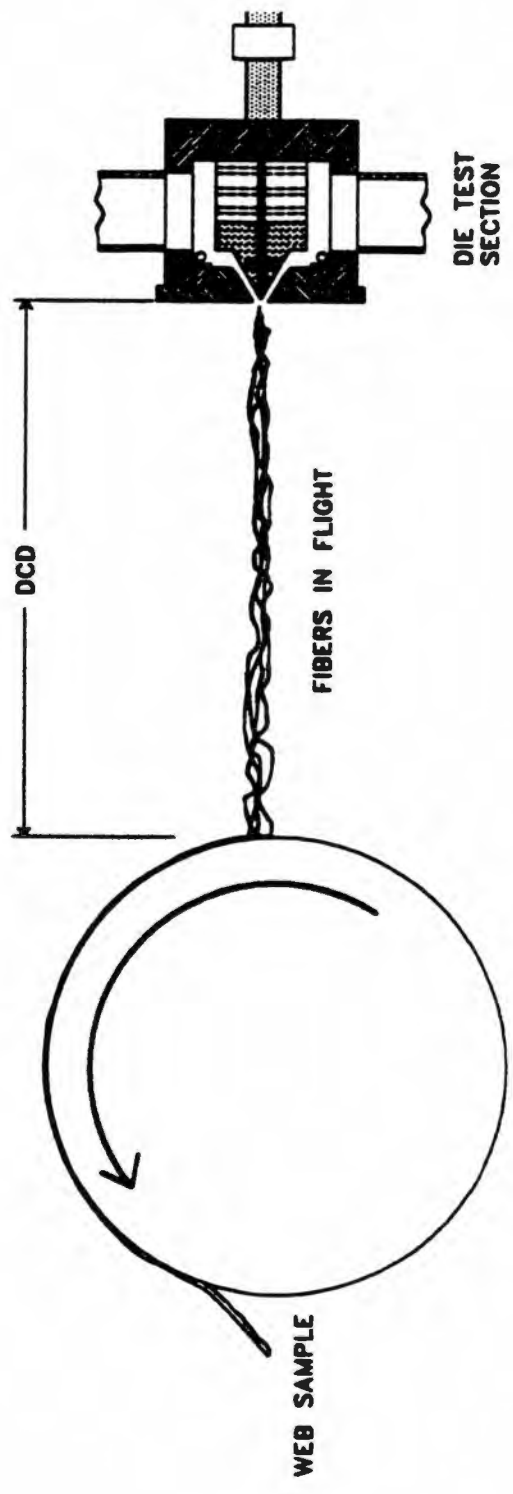


Figure 3.10: Collection process for the web samples and definition of DCD

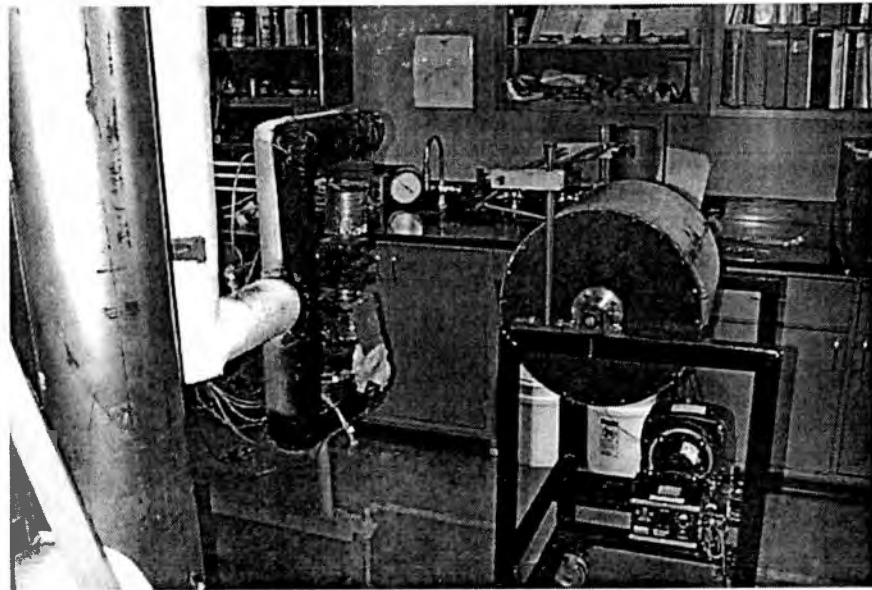
Source: Utsman, F.M., An Experimental Investigation on the Production of Microfibers and the Web Defect Known as Shot for the Melt Blowing Process, Thesis, University of Tennessee, Knoxville, 1995.

the drum. Photographs of the actual collection system are shown in Figure 3.11.

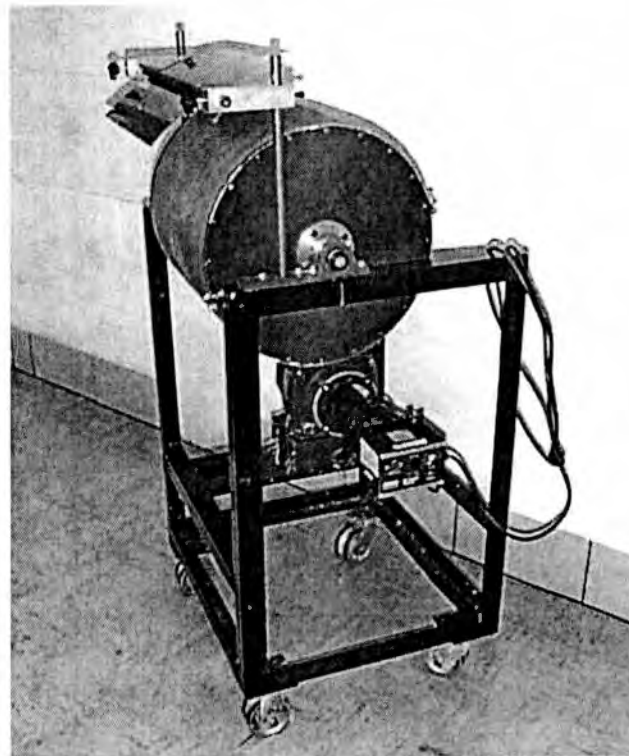
Experimental Procedures

Melt-Blown Web Creation

In order to create a melt blown web sample, the first operation that must be performed is the determination of the process conditions and the resin. This involves choosing the following: resin/polymer itself, polymer throughput, polymer temperature, test section die geometry, air temperature, air flow rate/die pressure, die to collector distance (DCD) and basis weight of melt blown web. Once the desired experimental parameters are determined the actual production of the web samples can proceed. First, a steady state operating condition must be obtained. This was done by opening the shut off valve and opening the manual valve until the pressure gage read two inches of water. The cooling water for the extruder and the digital balance were turned on. The air heaters and five zone heaters along the extruder were set to the specified process temperatures. Once the five zone heaters had reached the temperature set point, the cartridge heater was activated to heat the die tip. When the cartridge heater had reached its desired set point, the extruder motor is engaged. The screw motor speed is varied to provide the desired polymer throughput. This throughput is verified by collecting a sample of the web over a specific time and measuring its mass using the digital balance. With the throughput set and melt pressure noted, the air velocity is increased by increasing the die pressure to its specified value and the air heater set point is increased or decreased in order to obtain



Collection system shown in web sample collection location
with respect to test section



Close up view of collectorFigure

3.11: Views of variable speed collector

the proper air temperature at the specified die air pressure. The basis weight of the web is controlled by the collector drum RPM. The RPM of the collector drum was controlled by the ten turn potentiometer which varied the $\frac{1}{4}$ horsepower electric motor RPM. Figure 3.12 is a calibration curve for the drum RPM as a function of potentiometer setting. Figure 3.13 is a data collection sheet. This sheet was used to record all the settings previously mentioned and is used as a permanent record. The temperature and pressure for the air and the die test section geometry allow one to calculate the air velocity and air momentum exiting the test section. The methodology used to calculate the air velocity value is shown in Appendix III.

Analysis of Web Samples

Average Fiber Diameter Determination

Once the melt-blown samples were collected, the average fiber diameter and shot production per area were determined. The average fiber diameter was determined using one of three methods. These methods consist of the microscope, SEM and WebPro analysis method. The microscope method is performed with an optical microscope with a scaled eyepiece and a total magnification of 400. Previous experimenters [11,13,16,17] have all determined the average diameter of the web sample by cutting a one-inch square sample, Figure 3.14, and placing the sample under the microscope. Three locations in the sample were then selected and the diameters of at least eleven individual fibers were measured using the scaled eyepiece for a total of at least thirty-three fibers. The sizes of these thirty-three fibers, based on

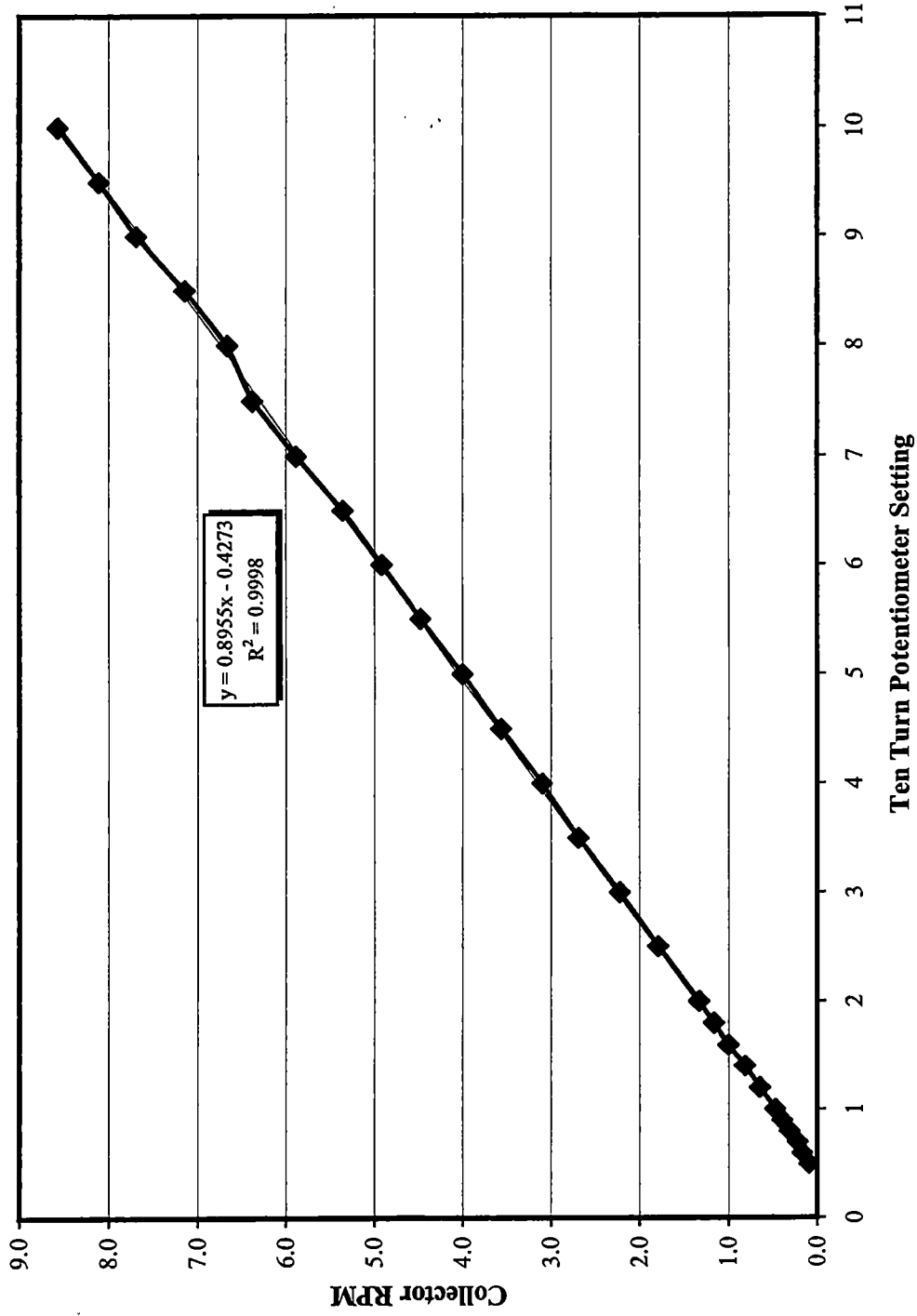
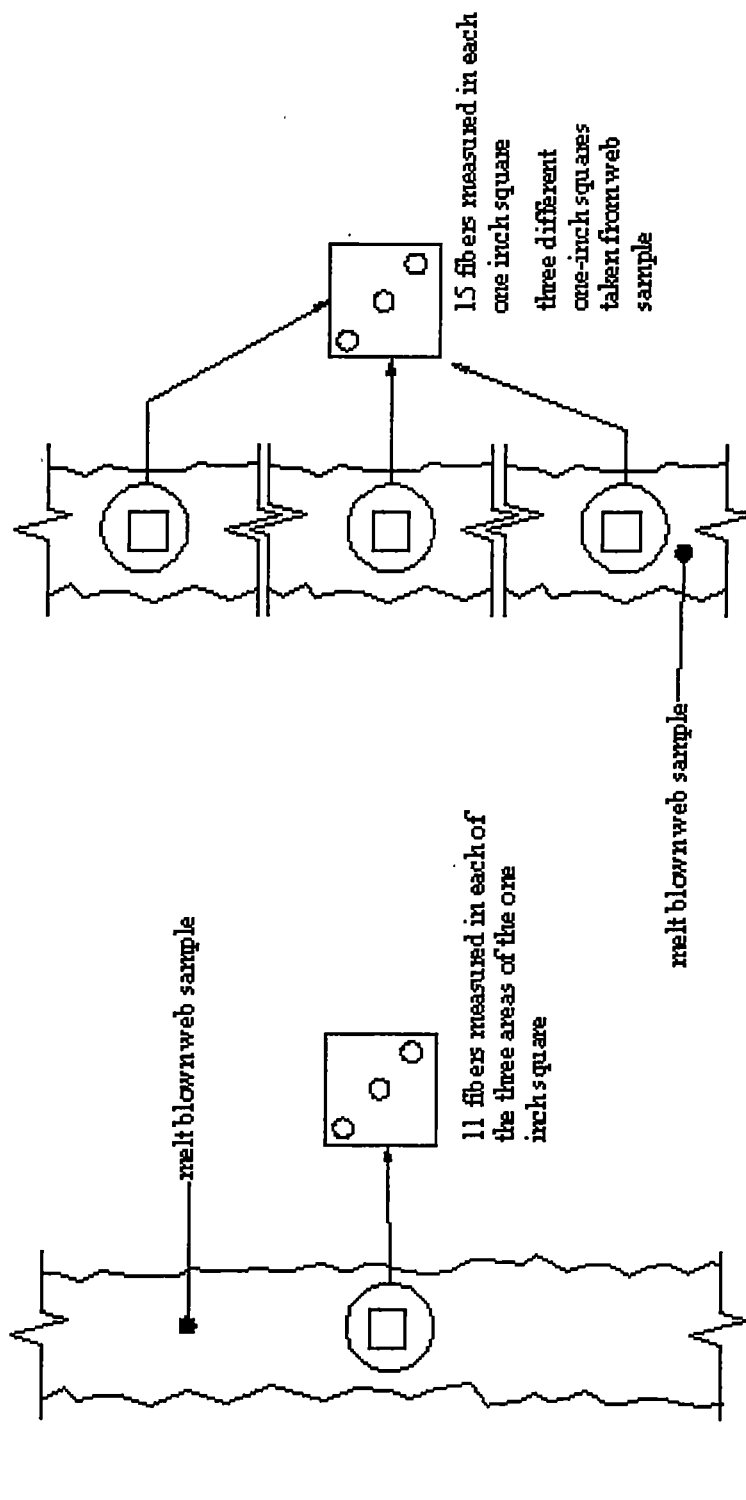


Figure 3.12: Potentiometer setting vs. collector RPM



Previous Research
Diameter Analysis

Current Research
Diameter Analysis

Figure 3.14: Methodology used to determine the average fiber diameter for previous and current investigation

the divisions of the scaled eyepiece, were entered into a BASIC program and using the known magnification of the microscope, the average fiber diameter, standard deviation, coefficient of variation, fiber dispersity and diameter histogram were determined. The methodology used to determine the average fiber diameter for this investigation was similar to that of previous experimenters [11,13,16]. The only variation was that this research did not remove just one square inch sample from the melt-blown sample for all diameter measurements. In this study, three one-inch square samples, Figure 3.14, were removed from three locations in the web sample and fifteen diameter measurements were taken from each of the three samples using the same scaled eyepiece, for a total of forty-five diameter measurements. The purpose of the change was to take diameter measurements from different locations in the web sample itself not just three locations in same one-inch square sample. The only other deviation from the methods used previously was the use of a spreadsheet to calculate the parameters previously calculated by the BASIC program. The use of an optical microscope for diameter measurements is very susceptible to human influences. In order to reduce this influence, the same person performed all optical microscope diameter measurements used throughout this research. The researcher used the microscope eyepiece to select the fibers that would be measured. Once a location in the web sample was selected for diameter measurements, the microscope was focused into the web sample and any fiber that could be brought into focus and crossed the scale in the eyepiece was measured. Figure 3.15 attempts to illustrate this process. In this figure the three white lines are fibers and the scale is shown in the center of the microscope view. In this figure the two smaller diameter fibers actually

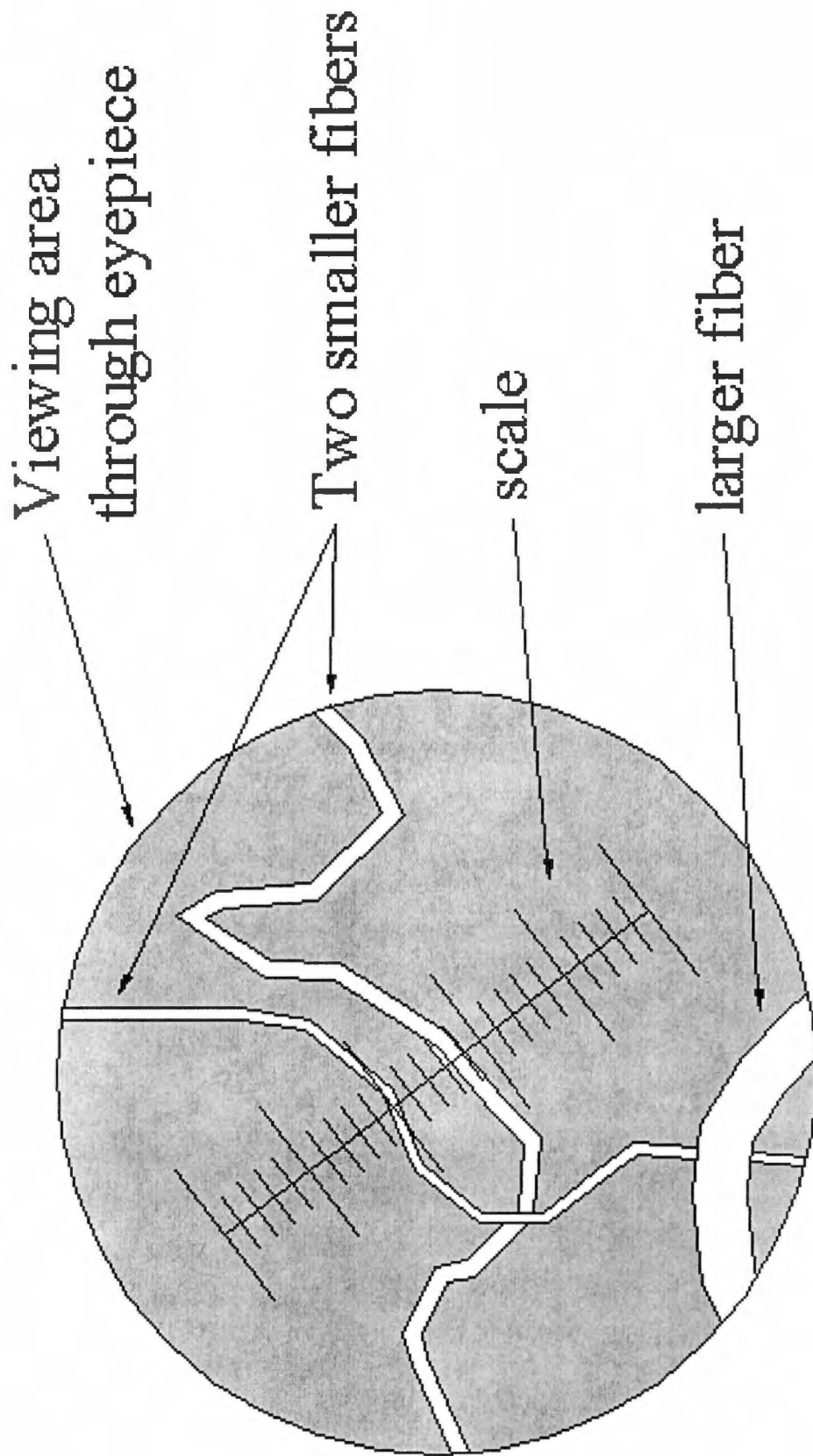


Figure 3.15: Drawing of view through the microscope during diameter analysis

cross the scale where the larger fiber in the lower left does not. Therefore the two smaller fibers are measured and the larger, more easily measured, fiber is not. This process helps reduce any human influences as long as the microscope table is not moved and the fiber selections are consistently made from the top of the web sample down once the diameter process has begun at a particular location.

Another popular method for the determination of average fiber diameter is use of a scanning electron microscope (SEM). This method allows the researcher to make the SEM image and measure the diameters of the fibers from the image. The SEM image allows the web sample's depth to be captured on one image and recorded on a 4 inch by 5 inch photograph. This photograph is then scanned using a flatbed scanner and a personal computer. The scanned image is then imported into an imaging program, and the diameters of any selected fiber are recorded by knowing the magnification of the SEM image. The researcher can measure the diameter of as many fibers as he or she wishes. Usually, a line is drawn across the image and any fiber crossing the line is measured. Again, this is done to remove any human influence in the choices of which fibers to measure. The SEM diameter trends agree with the optical microscope tests performed by this research group and are compared in Figure 3.16 for the same web sample. One example of a SEM photograph of a collection of fibers in a given web is shown in Figure 1.2.

The last method used to determine fiber diameters was the use of the WebPro image analysis program. This web analysis program was used to determine shot and

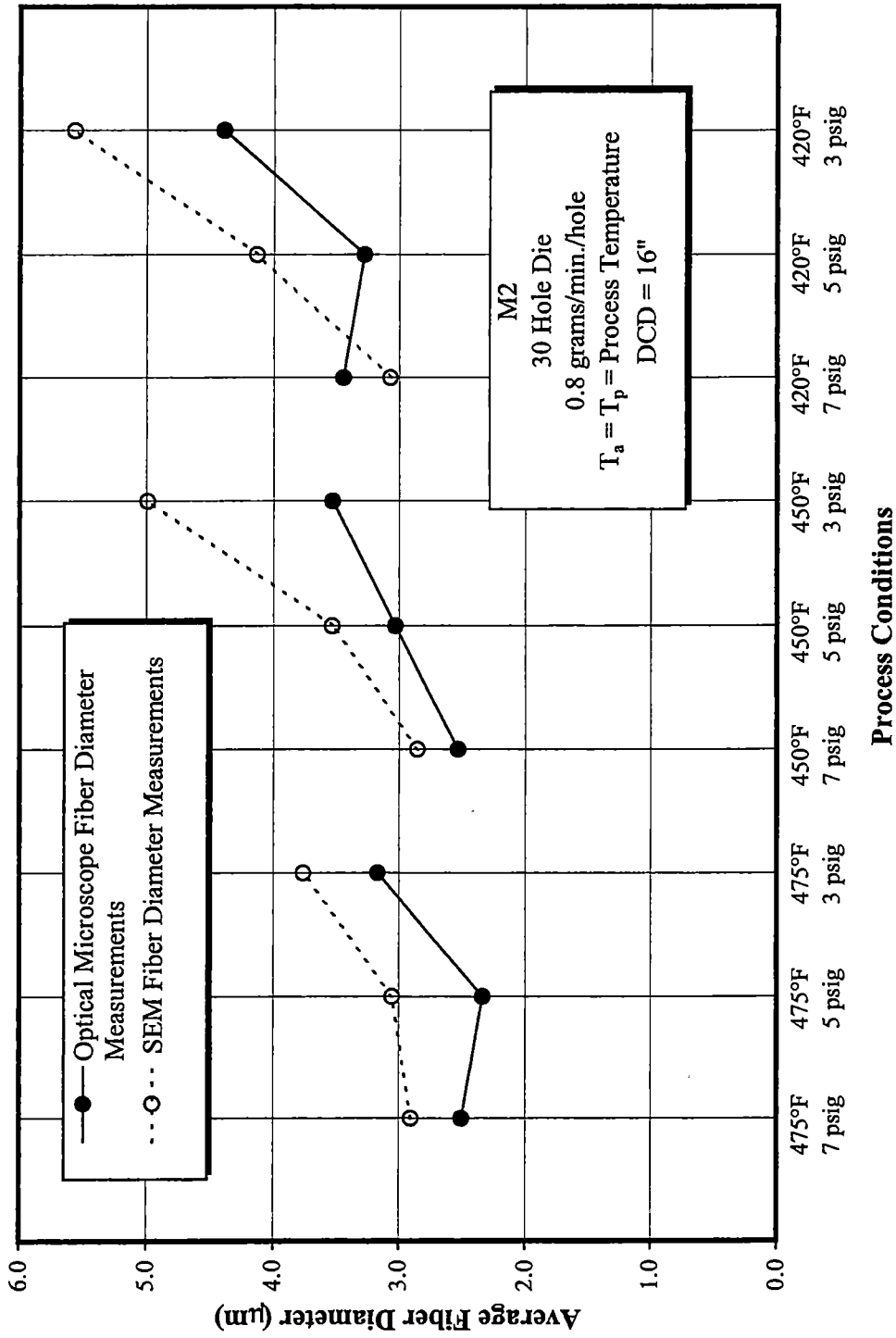


Figure 3.16: Average fiber diameter vs. process conditions for two measurement methods

will be discussed in the next section. However, this program can also perform fiber diameter analysis and was used for a small number of measurements. The Textile Science Department performed the analysis and therefore no first hand knowledge of this analysis is available. The WebPro diameter trends did agree with optical microscope tests performed by this research group and this comparison is shown in Figure 3.17.

Number of Shot per Area Determination

Since shot has already been defined as a globule of polymer that has a diameter much greater than that of the average diameter of the surrounding fibers, it is important to determine a method to count shot properly. Previous experimenters [11,17] used a shot rating and/or shot intensity system. The shot rating system is a system developed by TANDEC to evaluate the shot quantity in a web sample by assigning each sample a rating from one to five. These numbers correspond to a baseline group of webs that have previously been assigned one of these values. The sample to be rated must have the same basis weight as that of the baseline group. The sample to be rated is then placed on a light table where the shot particles become much more visible. This is due to the fact that the light passes through the shot easily, but light can not easily pass through the fiber. With this knowledge, the shot particles appear as bright spots in a diffuse background due to the surrounding fibers. This method has been used in the past but it is limited by the basis weight aspect of the rating system and the fact that a true quantitative shot value is not produced. For this reason, Utsman [11] developed the shot intensity method. This method involves

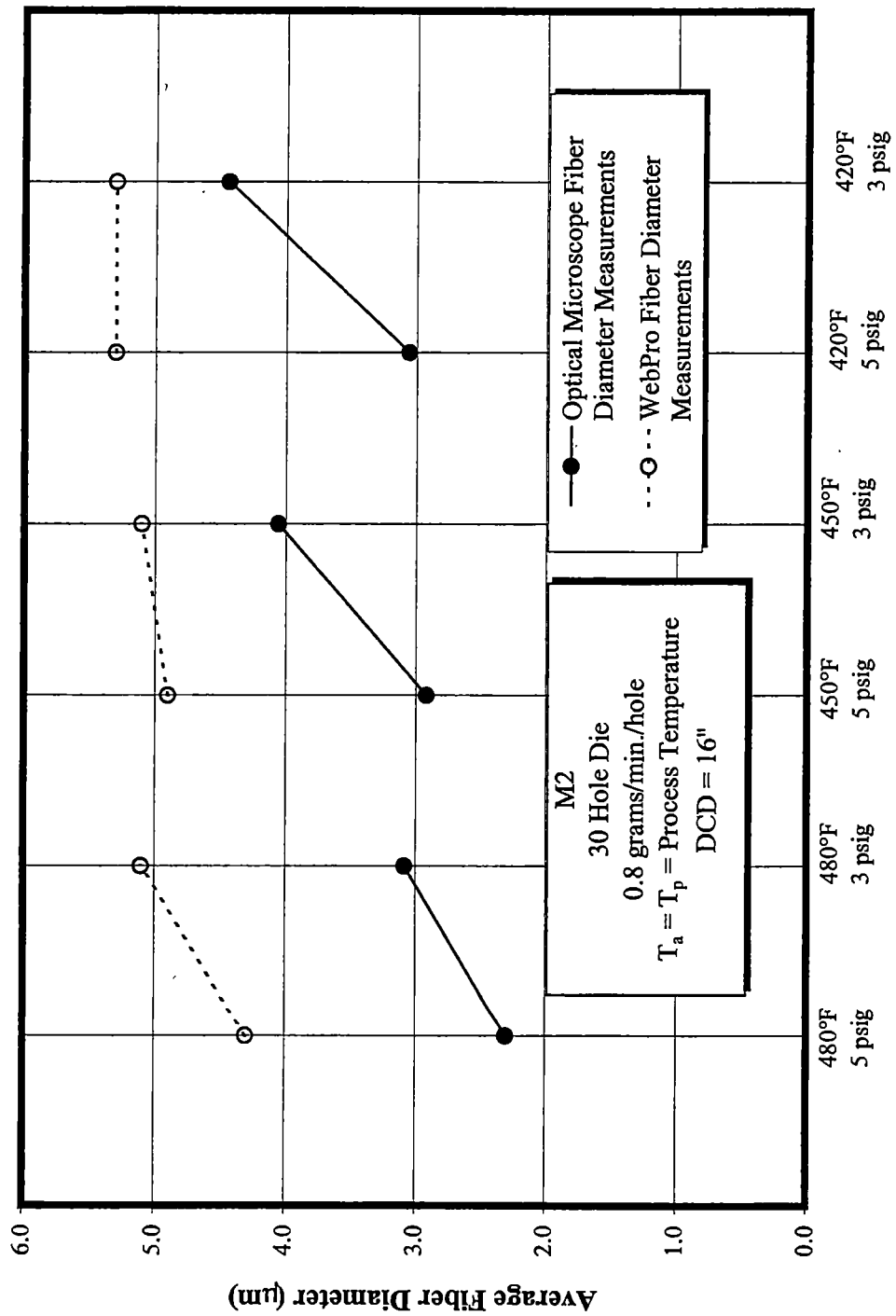


Figure 3.17: Average fiber diameter vs. process condition for two measurement methods

counting the number of shot greater than $100\mu\text{m}$ (3.94×10^{-3} [in]) in a one-inch square sample and dividing that value by the mass of the sample. The number of shot is counted using an optical microscope. Shot is detected in the same manner as the shot rating method and a scaled eyepiece is used to determine the size of the detected shot. This method is quantitative in that an actual number is produced as an output but it is extremely tedious and time consuming.

The shot determination method chosen for this research effort is the computer operated WebPro method. The Webpro shot determination method is similar to the two previous methods in that it also uses the contrast in light level between the fibrous web area and the shot itself. A complete description of the Webpro system is provided in a paper by Breese and Yan [18] but a brief description is included here for convenience. A schematic of the WebPro system is shown in Figure 3.18 [18]. This system includes a diffuse light source, a motorized table with x-y motion capability, a video camera, and a computer to capture the video images and run the WebPro software program. Figure 3.19 is a photograph of the WebPro system used in this research. The web sample is placed between two pieces of glass in order to flatten the sample. The sample's orientation between the glass plates is determined by the size of the motorized table. The orientation of the samples used throughout this research is shown in Figure 3.20. Control of the WebPro shot detection analysis is maintained through operator controlled parameters. These parameters are comprised of light source intensity as detected by the video camera, light contrast level, and threshold value or detection sensitivity. The program assigns a light level

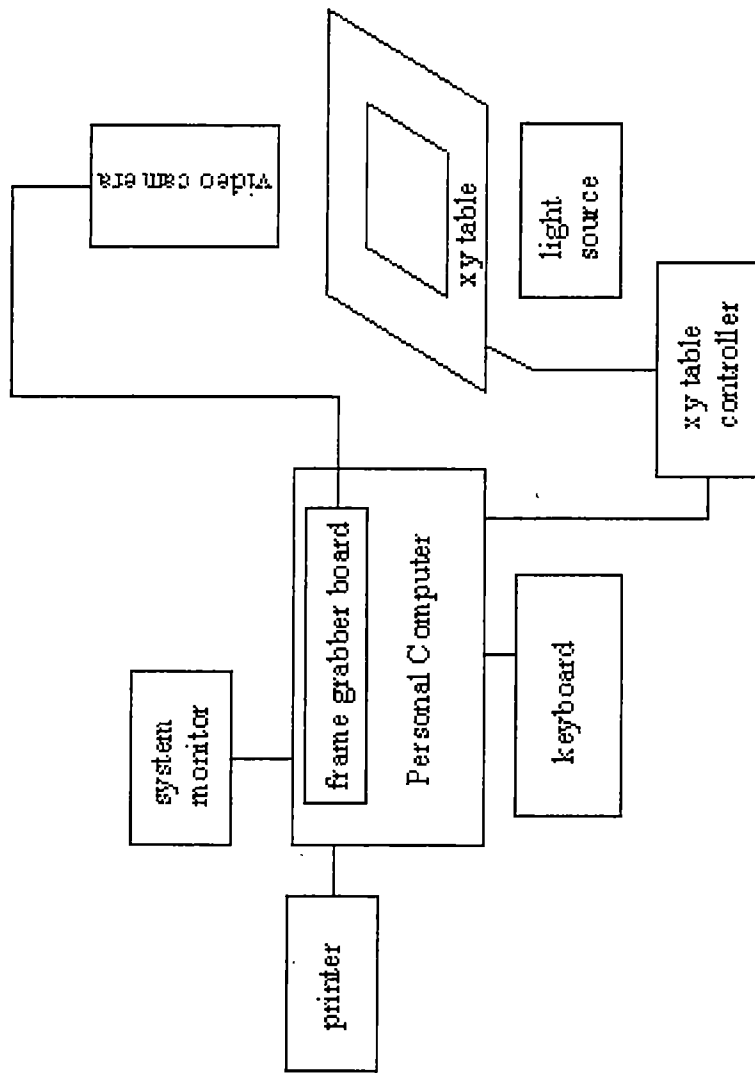


Figure 3.18: Schematic of WebPro system

Source: Yan, Z. and Bresse, R.R., "Characterizing Nonwoven-web Structure by Using Image-analysis Techniques Part V: Analysis of Shot in Meltblown Webs", The Journal of Textile Institute, Volume 89, 1998, p. 328.

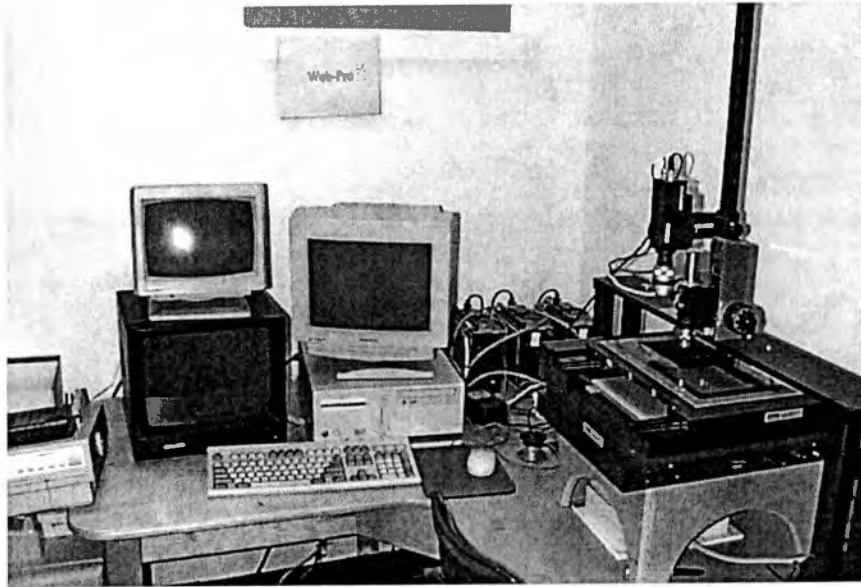


Figure 3.19: Actual view of WebPro shot analysis system

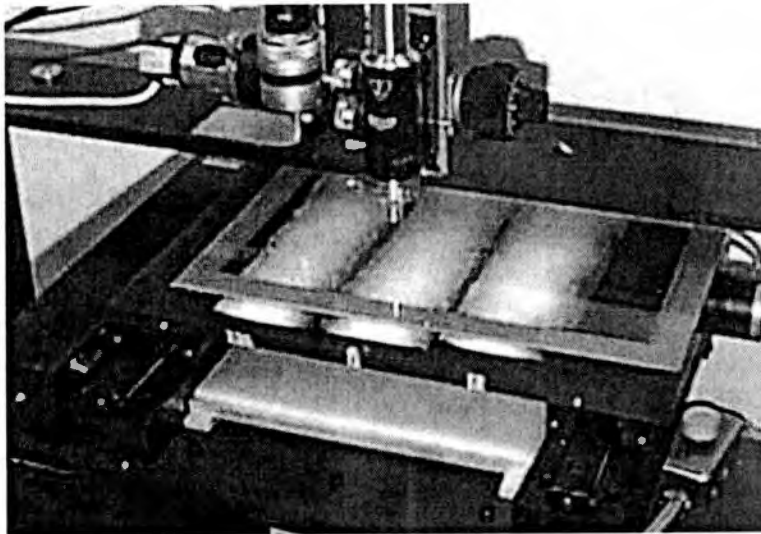


Figure 3.20: View of web samples' orientation during WebPro analysis

to each pixel the video camera views. The program then scans the pixel light levels and when it discovers a bright pixel next to a darker pixel, it marks the pixel boundary. Once the computer completes its scan it has marked a boundary between the dark and light pixels. An example image of the process is provided in Figures 3.21 and 3.22.

The WebPro system is advantageous in that it is automated and more than one square inch of the web sample is examined for shot. The amount of web area that can be scanned by WebPro's video camera is determined by the size of the motorized table and the physical characteristics of the web sample itself. The physical characteristic of the web that is most important is web uniformity. The edges of a web sample are "ragged" or non-uniform and therefore the web area inside the samples edges is scanned by WebPro. The samples created on the melt blowing line in Dougherty Engineering building are approximately three inches in width. Once the ragged edges are ignored, there is approximately a $\frac{3}{4}$ inch to one inch strip down the center of the produced sample. The WebPro setup used for this research allowed for the analysis of thirty-three web samples that were 0.63 in. by 0.47 in. (1.6 cm by 1.2 cm). This sampling amount is almost ten times the area of the optical shot intensity method, and therefore is more representative of the shot in the entire sample. WebPro returns the following values from its analysis: number of shot [Shot (N)], shot per cm² [N/cm²], mean shot size [Mean], maximum shot size [Max], minimum shot

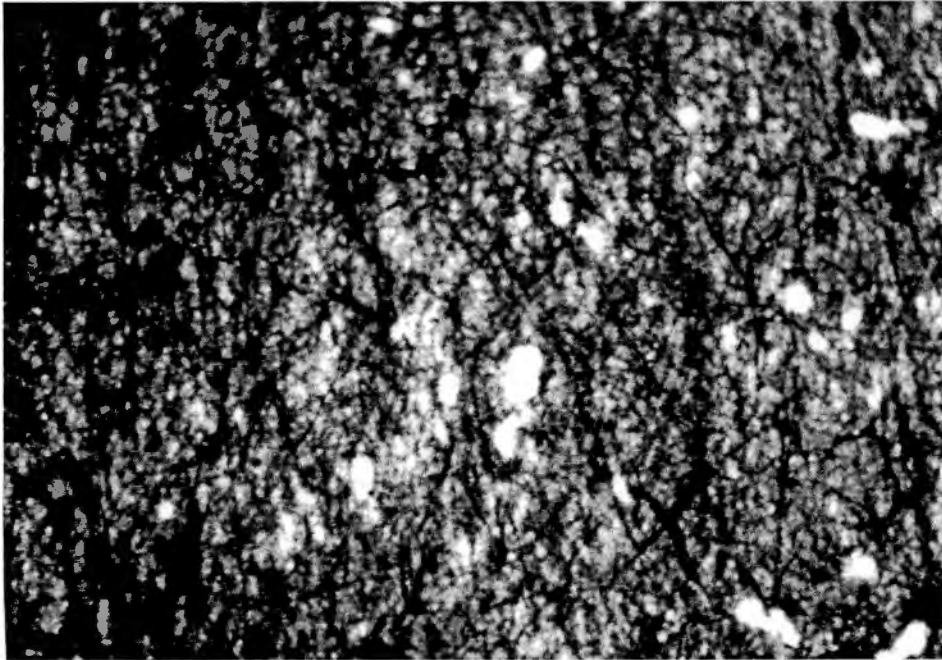


Figure 3.21: WebPro image before scanning process (bright spots are shot)

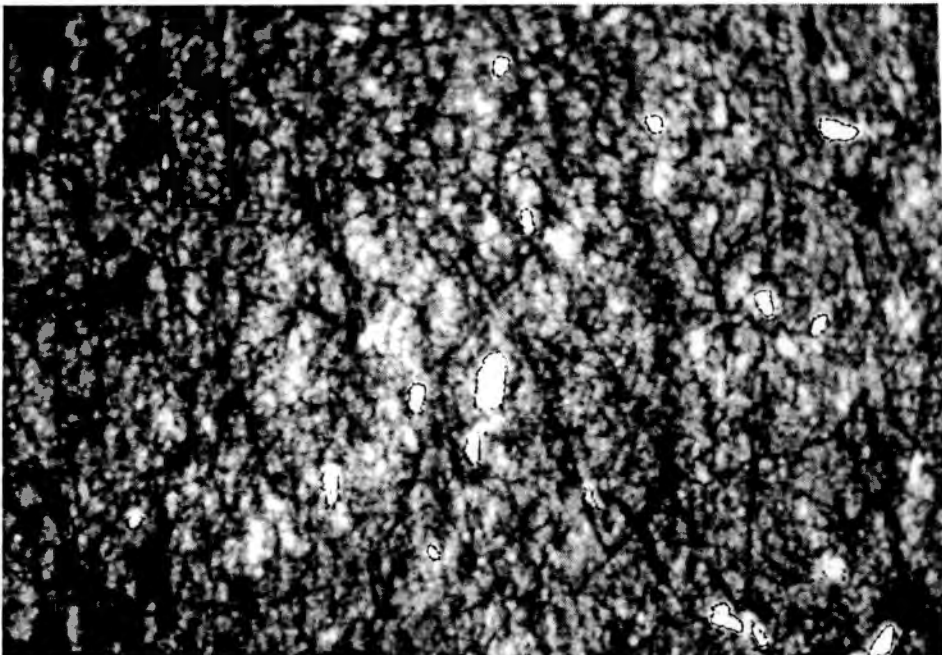
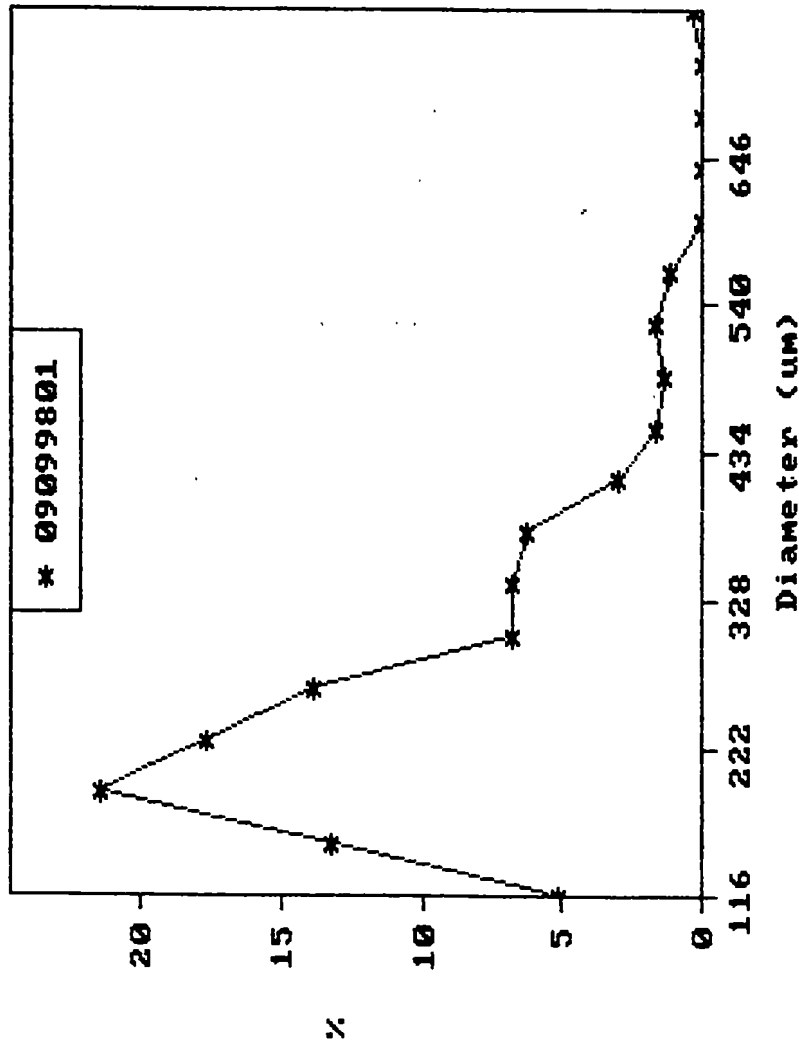


Figure 3.22: WebPro image after scanning process (notice line around bright spots)

size [Min] and % shot cover area [Cover (%)] of the measured sample. The program also produces a graph displaying the shot size distribution in the analyzed sample. Figures 3.23 through 3.25 are examples of a typical WebPro analysis output. Figure 3.23 provides the shot diameter distribution in the web sample. This figure also provides important statistical data for the detected shot. The most useful information provided in this figure is the shot per cm^2 and the shot cover percentage. Even though Figure 3.23 contains most of the information that was utilized in this research, WebPro also provides information about the shot orientation distribution and the shot aspect ratio distribution in the web samples. This information is shown in Figures 3.24 and 3.25.

Effect of Processing Parameters on WebPro Shot Detection

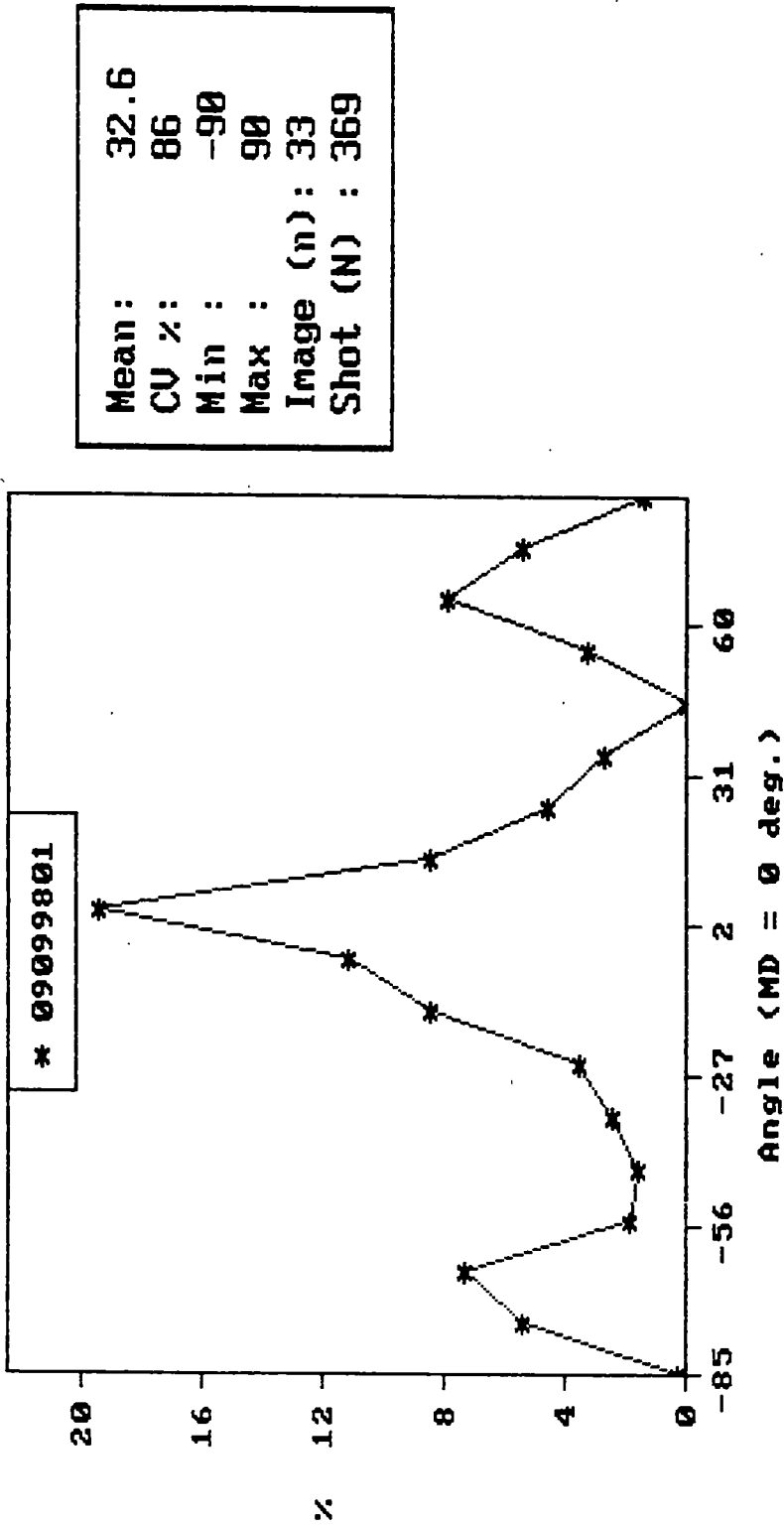
During the shot data reduction process, a few WebPro anomalies were encountered. The most important of these anomalies is the effect of process temperature and die air pressure on the effectiveness of the WebPro shot detection process. As previously shown by other experimenters [13,16], and reiterated in the following chapters, the average fiber diameter decreases inversely with process temperature and die air pressure. With the production of small fibers comes a finer, denser web sample. This type of web is more optically opaque and a shot particle will transmit light more easily than the average web and thus a distinct bright spot in the web is produced. As the process temperature and die air pressure is decreased the web fibers are larger and the light transmittance of the web sample is drastically increased. The light transmittance of the larger fiber web samples is due to the larger



Mean:	254
CV %:	39.4
Min :	97.7
Max :	770.5
Image (n):	33
Shot (N) :	369
N / cm ² :	5.8
Cover (%) :	0.4

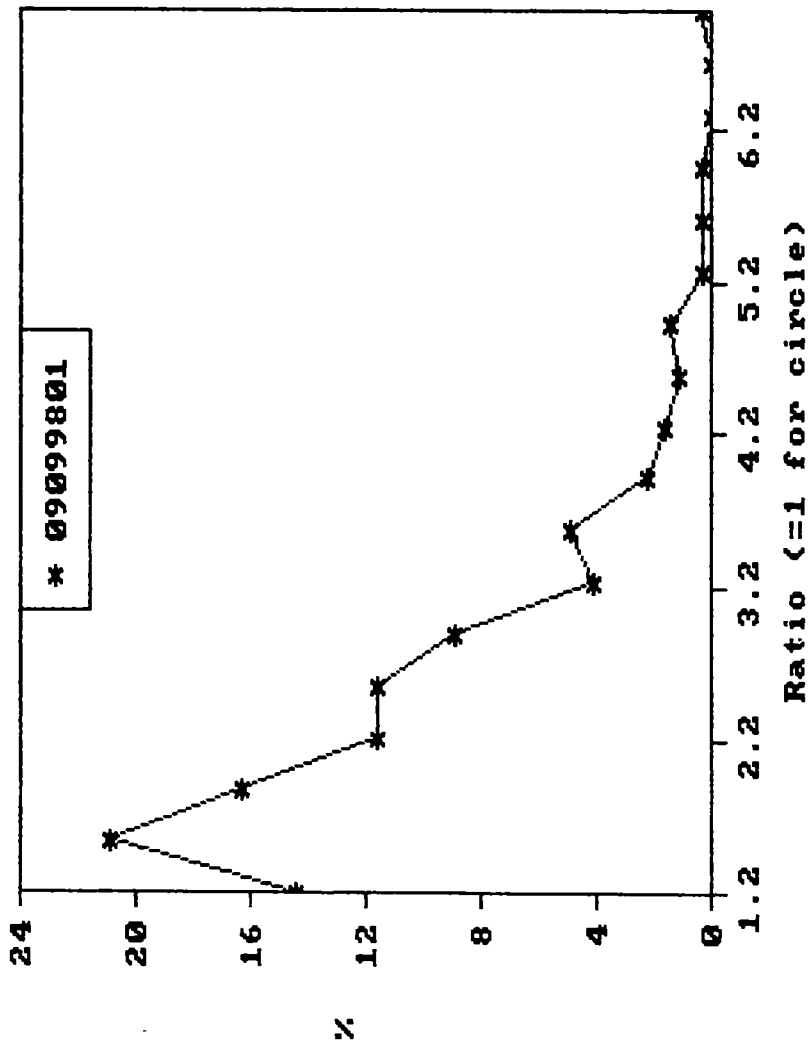
Shot diameter distribution.

Figure 3.23: WebPro shot analysis output – shot diameter distribution



Shot orientation distribution.

Figure 3.24: WebPro shot analysis output – shot orientation distribution



Mean:	2.23
CV %:	42.19
Min :	1.01
Max :	7.12
Image (n):	33
Shot (N) :	369

Shot aspect ratio distribution.

Figure 3.25: WebPro shot analysis output – shot aspect ratio distribution

open spaces between fibers and WebPro evaluates this light transmittance as shot particles. Therefore at the lower process temperatures and die air pressures the web sample is visually inspected and if no shot is seen the sample is graded as having zero shot. If numerous shot particles are viewed during this inspection then the sample is carefully analyzed using WebPro. With this type of web the shot threshold value in WebPro must be increased to a value where this light transmittance is not detected as shot. Even with this increased shot threshold value, any light transmittance that is still detected as shot and is not shot can be manually removed from the shot output file. This process allows the experimenter to exercise more control over the WebPro analysis in order to obtain shot data at the lower process conditions.

Chapter IV

Investigation into the Shot Production of Six Different Resins

Six Resins were provided by the Exxon Chemical Company for this research that varied in resin catalyst type and resin melt flow rate (MFR). In the past the polypropylene resins provided for melt blowing applications were primarily Ziegler-Natta (ZN) or conventional resins. These resins are the standard resins for most melt blowing applications. Over the past few years a new group of resins have been developed that use a different catalyst in the resin polymerization than that of the ZN resins. These new resins, with a different catalyst, are referred to as metallocene resins. These metallocene resins were developed in an attempt to "engineer" resins with narrow molecular weight distributions. It was believed that a resin with a narrower molecular weight distribution would create more uniform web samples when used in the melt blowing process. It was also believed that these narrower molecular weight distribution resins would be less likely to produce shot when melt blown. The melt flow rate of a resin is indicative of a resin's ability to flow in molten form. The MFR of the resin is similar to the reciprocal of the viscosity of a fluid. The higher the MFR number of the resin the less viscous a resin is at a particular polymer temperature. The following list indicates the type and MFR of the resins investigated.

Resin Designation	Resin Type	Resin MFR
M1	Metallocene	695
M2	Metallocene	795
M3	Metallocene	760
ZN1	Zigler-Natta	1990
ZN2	Zigler-Natta	1260
ZN3	Zigler-Natta	1020

These six resins were melt blown at the same process conditions in order to understand the effect the resin itself has on the production of shot. These resins were all processed with a single hole die with a throughput of 0.8 grams/minute. The original object of this study was to melt blow different resins at the same process conditions and video tape the filaments in flight in order to determine if different resins had different filament flight characteristics. The flight characteristics at individual process conditions could then be compared to the level of shot production at these same conditions in order to better understand the connection between filament flight dynamics and shot production, if any connection exists.

This limited filament flight dynamics study did not provide any insight into shot production for the 0.8 grams/minute throughput, single hole die situation. It is hoped that future video investigations will provide more significant results. Since the shot data had already been collected, the number of shot per square inch was plotted as a function of resin type in order to determine best and worst resins for shot production. Figure 4.1 indicates that the metallocene resins are the most shot producing resins. Again, the metallocene resins were developed to have a narrower molecular weight distribution and it was believed this would lead to more uniform

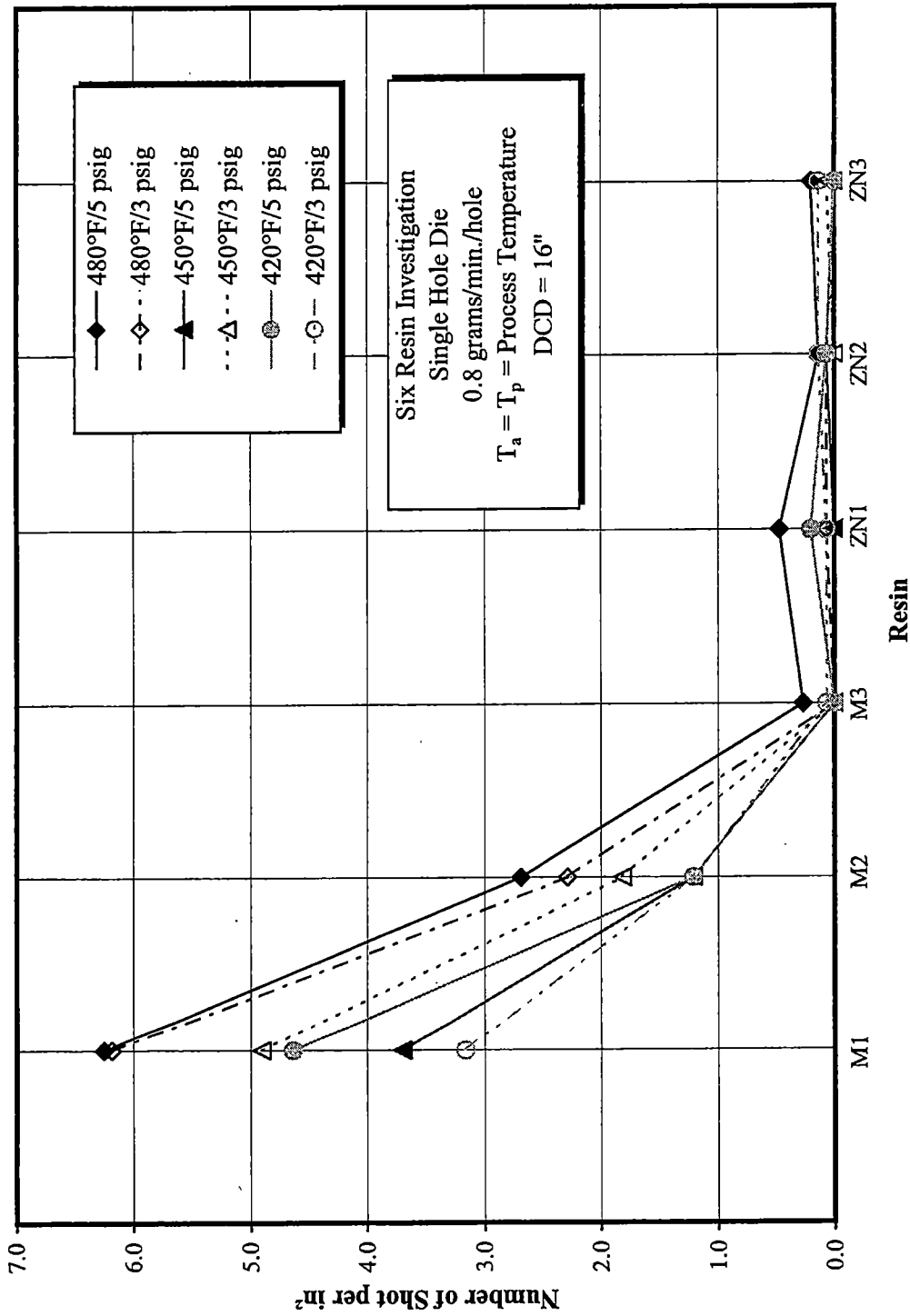


Figure 4.1: Number of shot per in² for various resins

melt blown webs with less shot. Figure 4.1 indicates that this is not the case. A similar plot for average fiber diameter is presented in Figure 4.2. This figure indicates, for the most part, the higher the MFR the lower the average fiber diameter. The only noticeable exception to this statement is the ZN3 resin, which has the third highest MFR but produced the largest fibers.

The next investigation performed with these resins involved the same single hole die test with an 1.3 grams/minute polymer throughput. Four of the six resins were processed in this higher polymer throughput investigation. The four resins are M1, M2, M3 and ZN1. These four resins were processed at the same conditions as the previous 0.8 grams/minute tests. The processing of these four resins at 1.3 grams/minute was video taped with similar results to that of the previous tests. The shot production data for this higher throughput is presented in Figure 4.3 in the same manner as that of Figure 4.1. This figure also indicates that the metallocene resins produce more shot than the single conventional resin (ZN1) tested. Average fiber diameter measurements were not performed for these 1.3 grams/minute polymer throughput web samples.

The last investigation performed with these resins involved processing six resins using a thirty hole die and 0.8 grams/minute/hole. Five out of six of the resins used in this test were the same as those used in the first test. The only difference in resins was the substitution of M4 for that of M1 due to a lack of the M1 resin. This M4 resin is a metallocene resin that has a MFR approximately equal to that of ZN1.

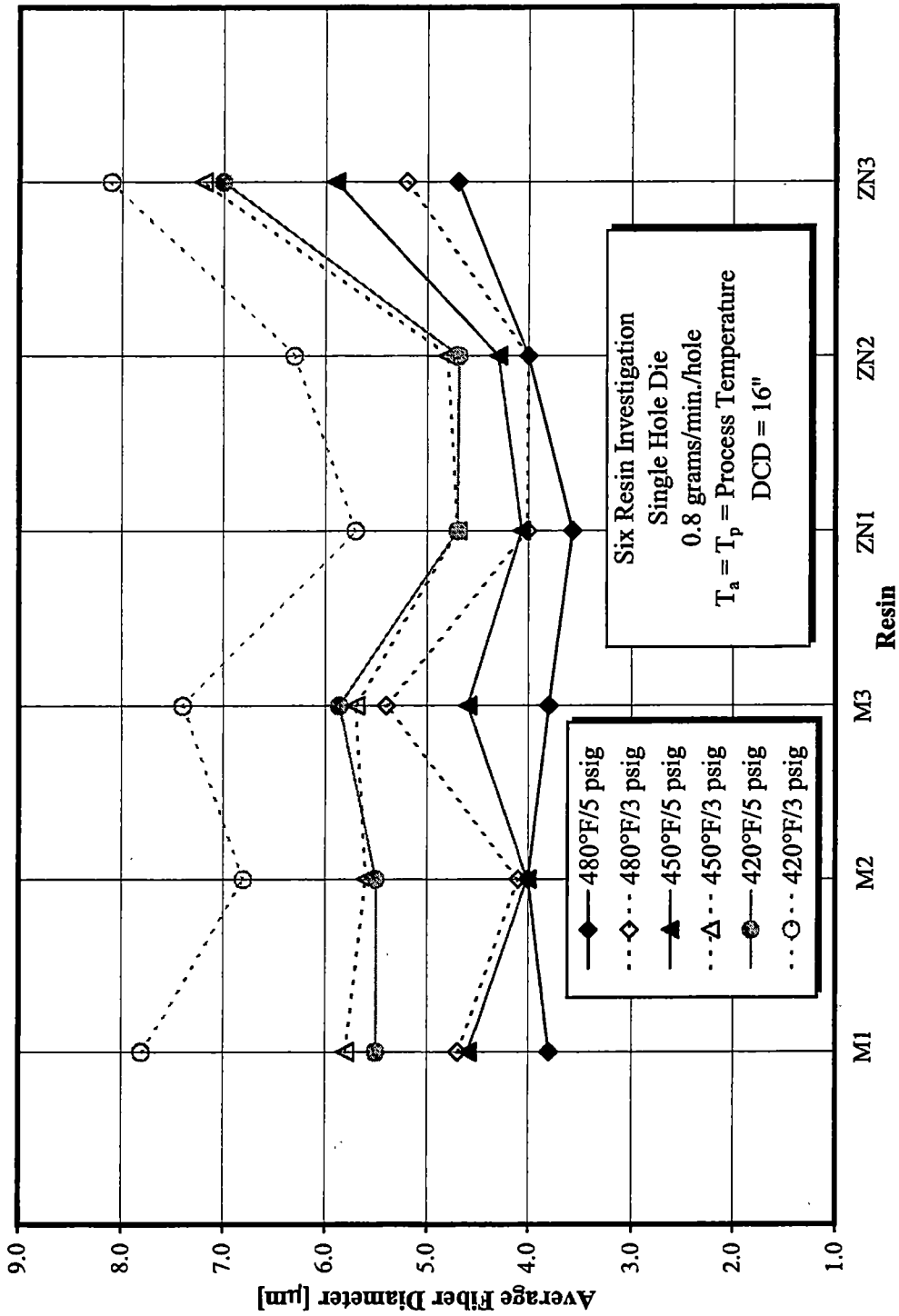


Figure 4.2: Average fiber diameter for various resins

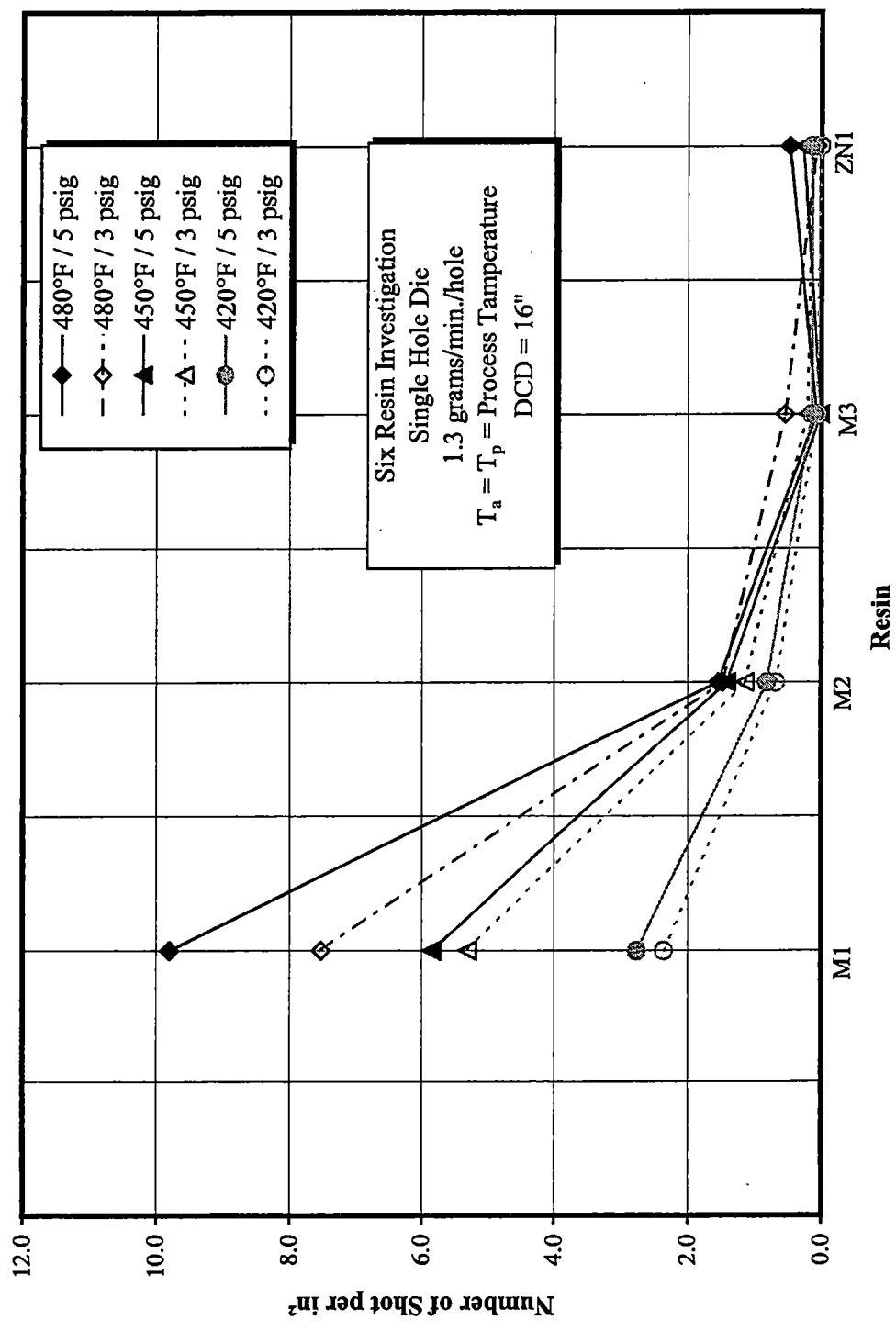


Figure 4.3: Number of shot per in² for various resins

The shot production for the thirty hole die web samples is shown in Figure 4.4. The high MFR M4 resin that replaced the M1 resin has the highest shot per square inch value for all the 5 [psig] die air pressures. Again, the metallocene resins have higher shot production values than that of the conventional ZN resins. Figure 4.5 provides the fiber diameter results for the resins produced using a thirty hole die. In comparing the two types of resins used in the single hole study, the MFR for the conventional resins is higher than that of the metallocene resins. This was the reason for the introduction of the M4 resin in the multihole study. Figure 4.6 more clearly compares the shot per square inch of resins ZN1 and M4. M4's shot production is consistently greater than the shot production of ZN1. Again, the only difference between these two resins is the resin type since the MFR difference has been removed. Therefore, it can be stated that the metallocene resins produce more shot at each of the processing conditions used in this study.

Other observations that can be made with this experimental data is that melt blown webs produced with thirty hole die have more shot than that of the single hole die. This is demonstrated in Figures 4.7 through 4.11 for each resin tested using both die configurations. Figures 4.7 through 4.11 do not include die comparisons for M1 and M4 since these resins were not processed with both dies.

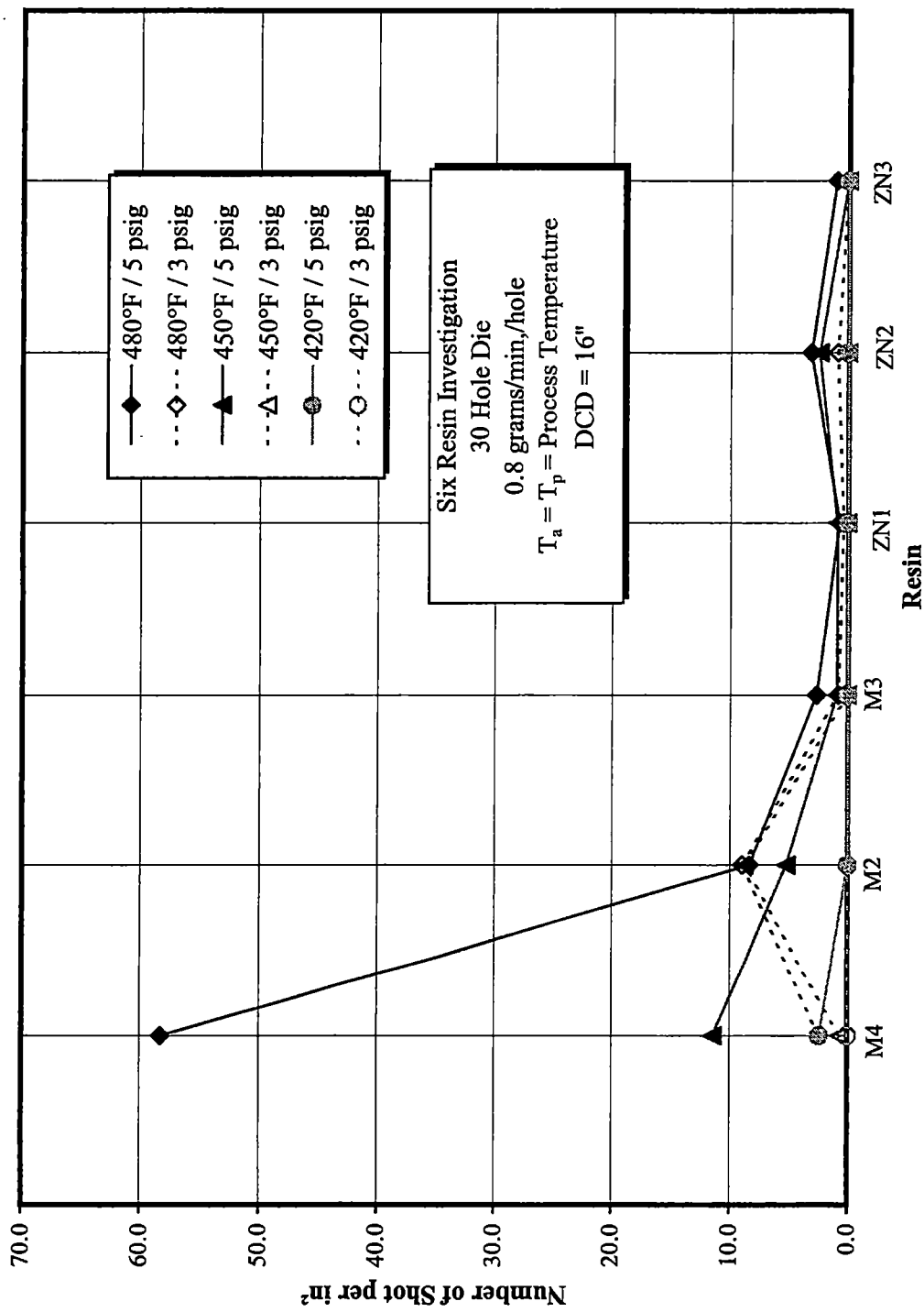


Figure 4.4: Number of shot per in² for various resins

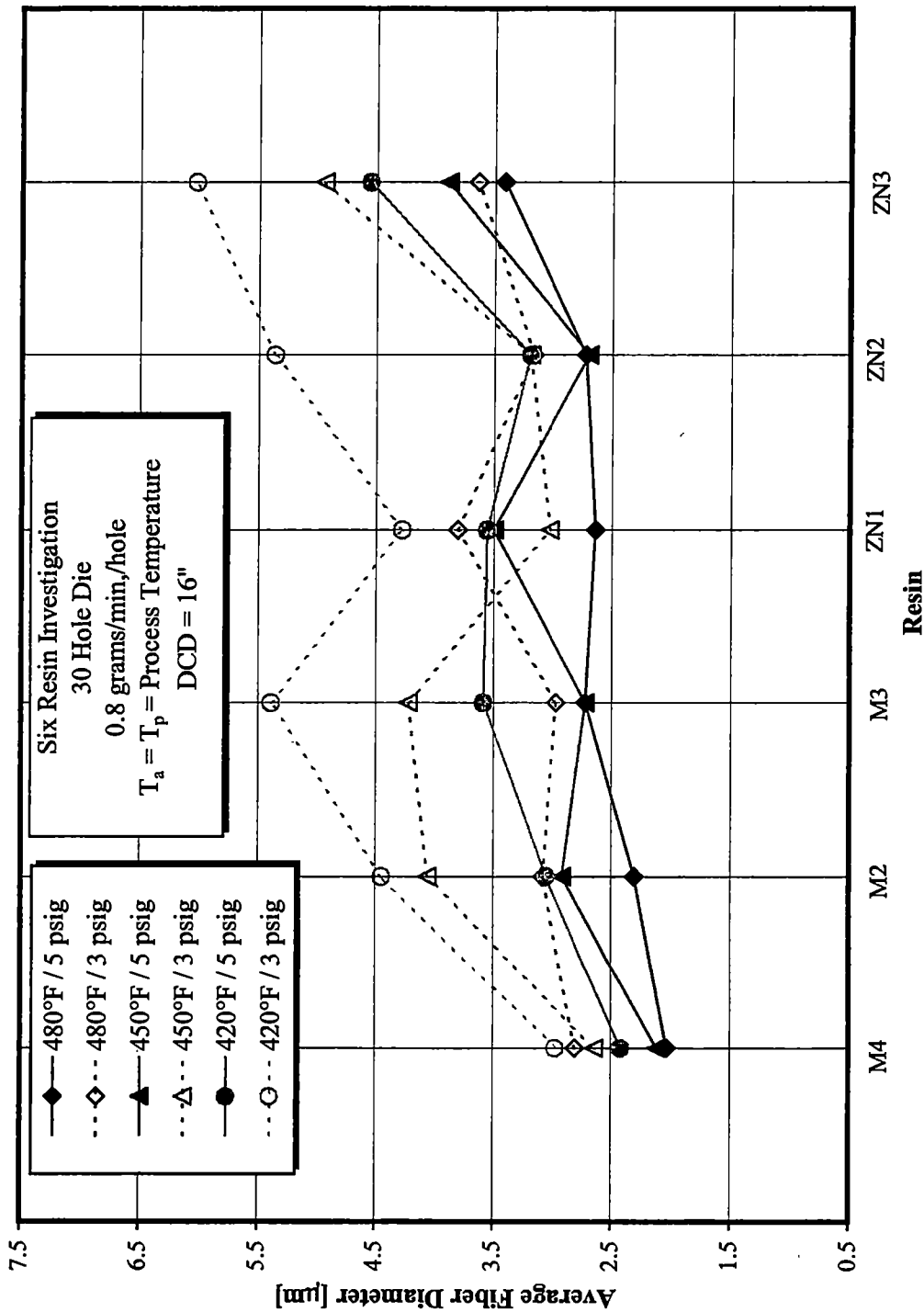


Figure 4.5: Average fiber diameter for various resins

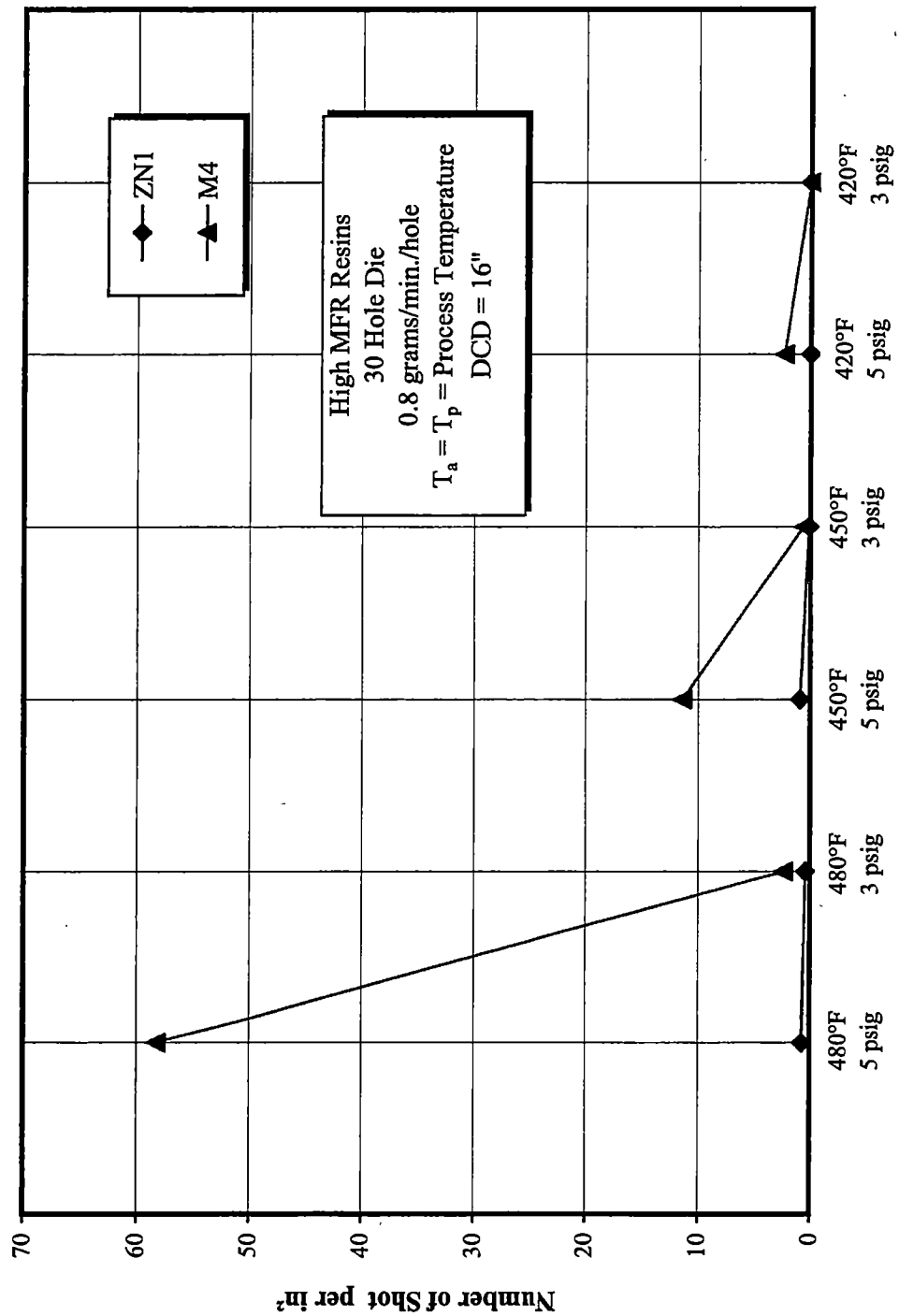


Figure 4.6: Number of shot per in² vs. process condition

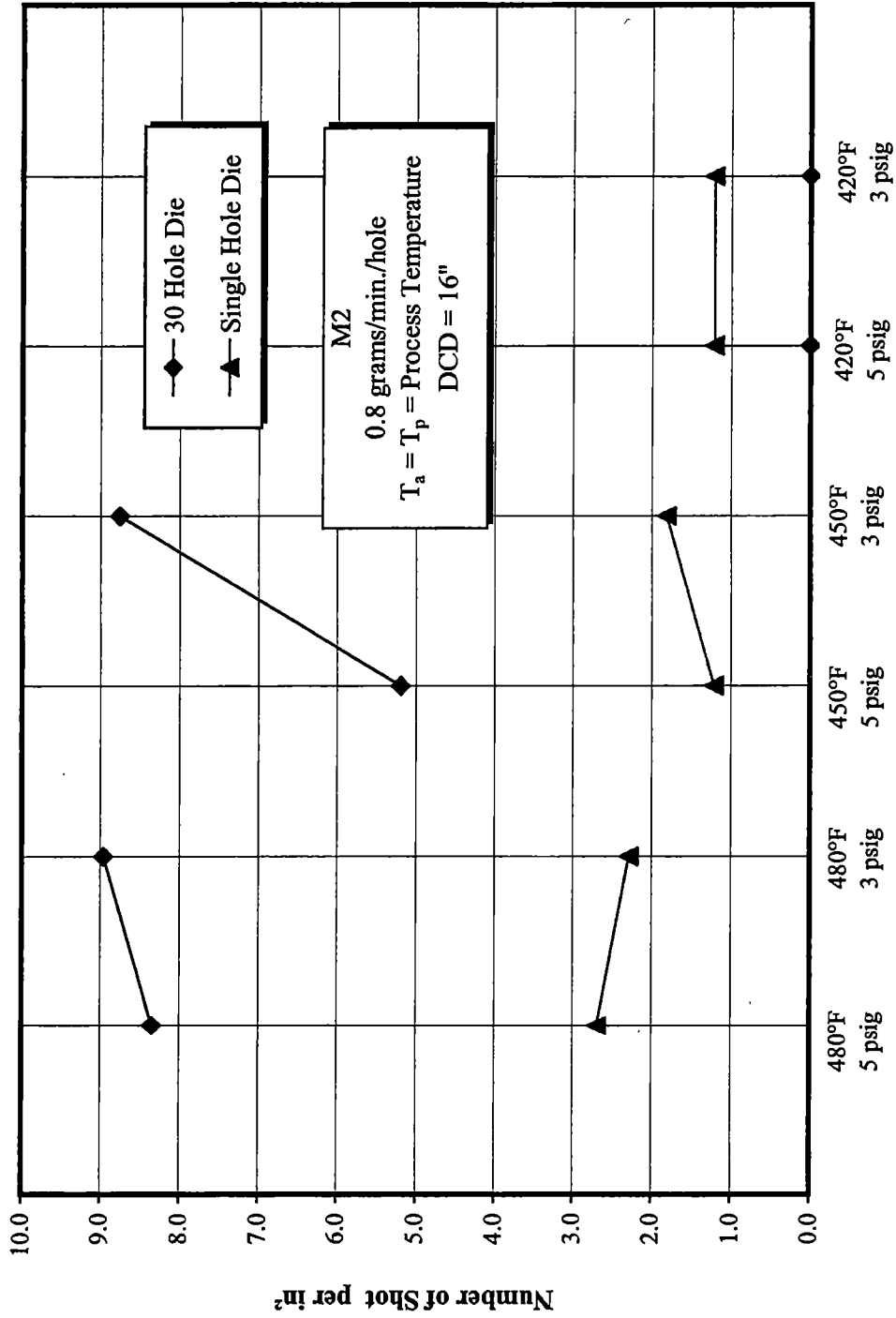


Figure 4.7: Number of shot per in² vs. process conditions

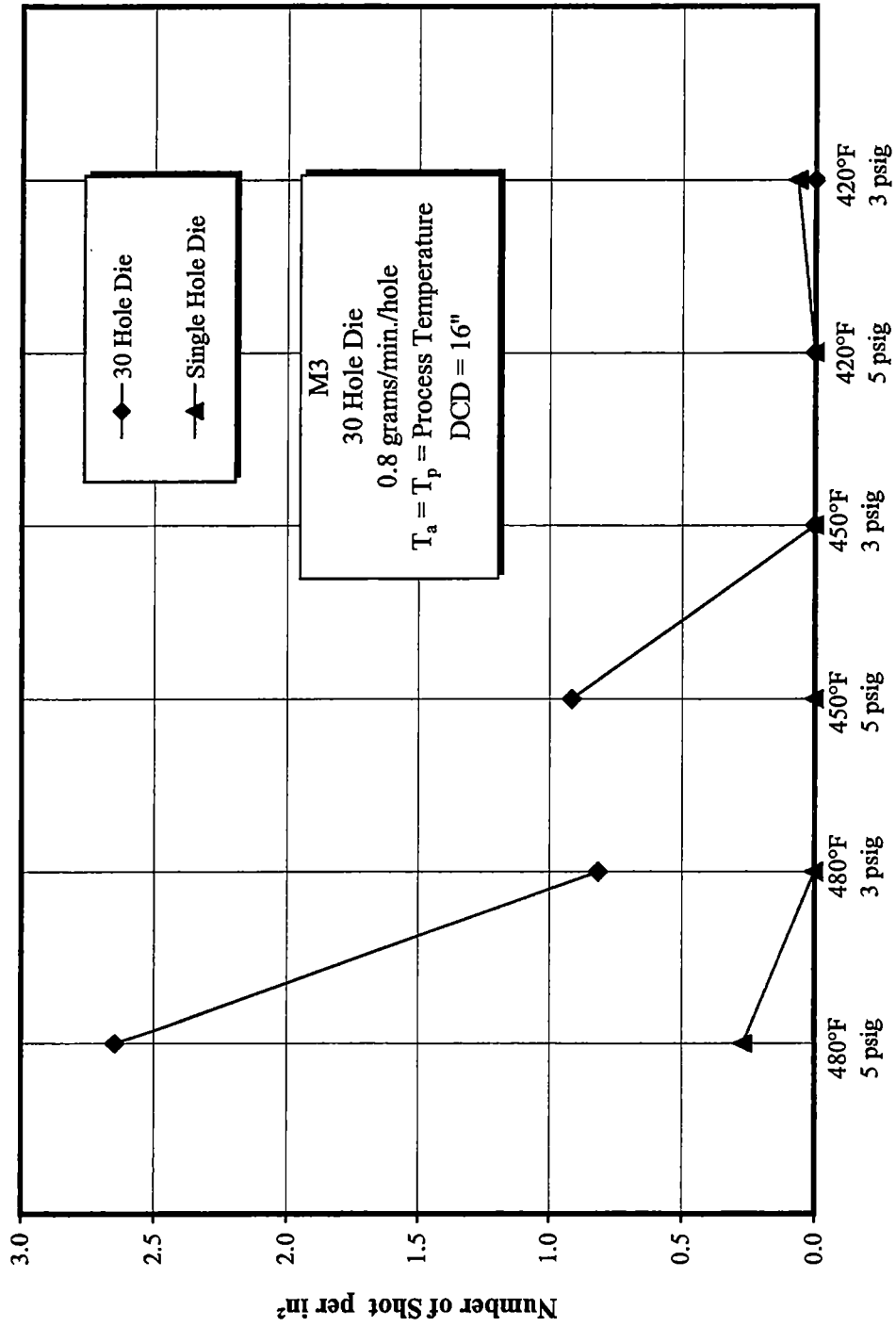


Figure 4.8: Number of shot per in² vs. process condition

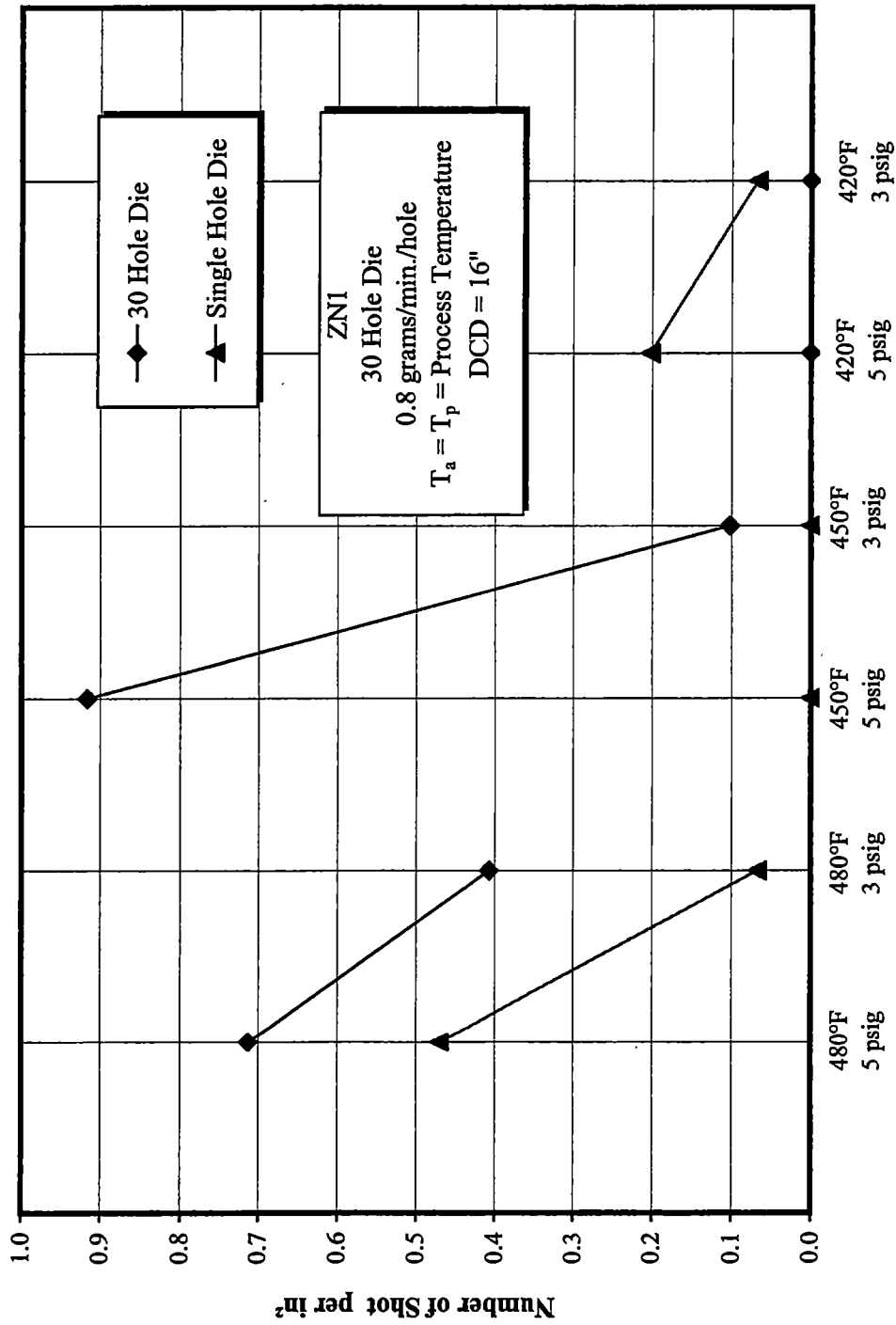


Figure 4.9: Number of shot per in² vs. process condition

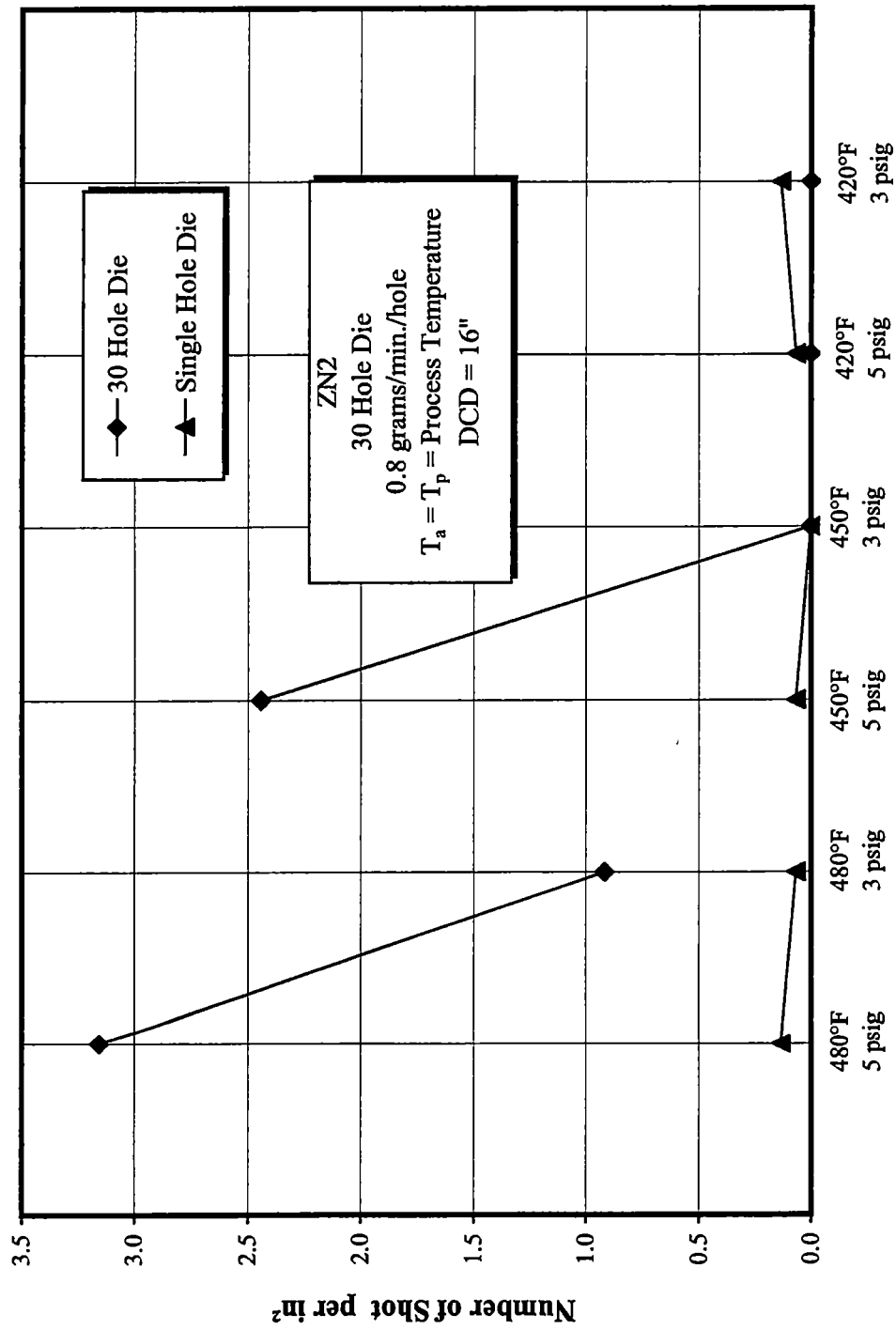


Figure 4.10: Number of shot per in² vs. process condition

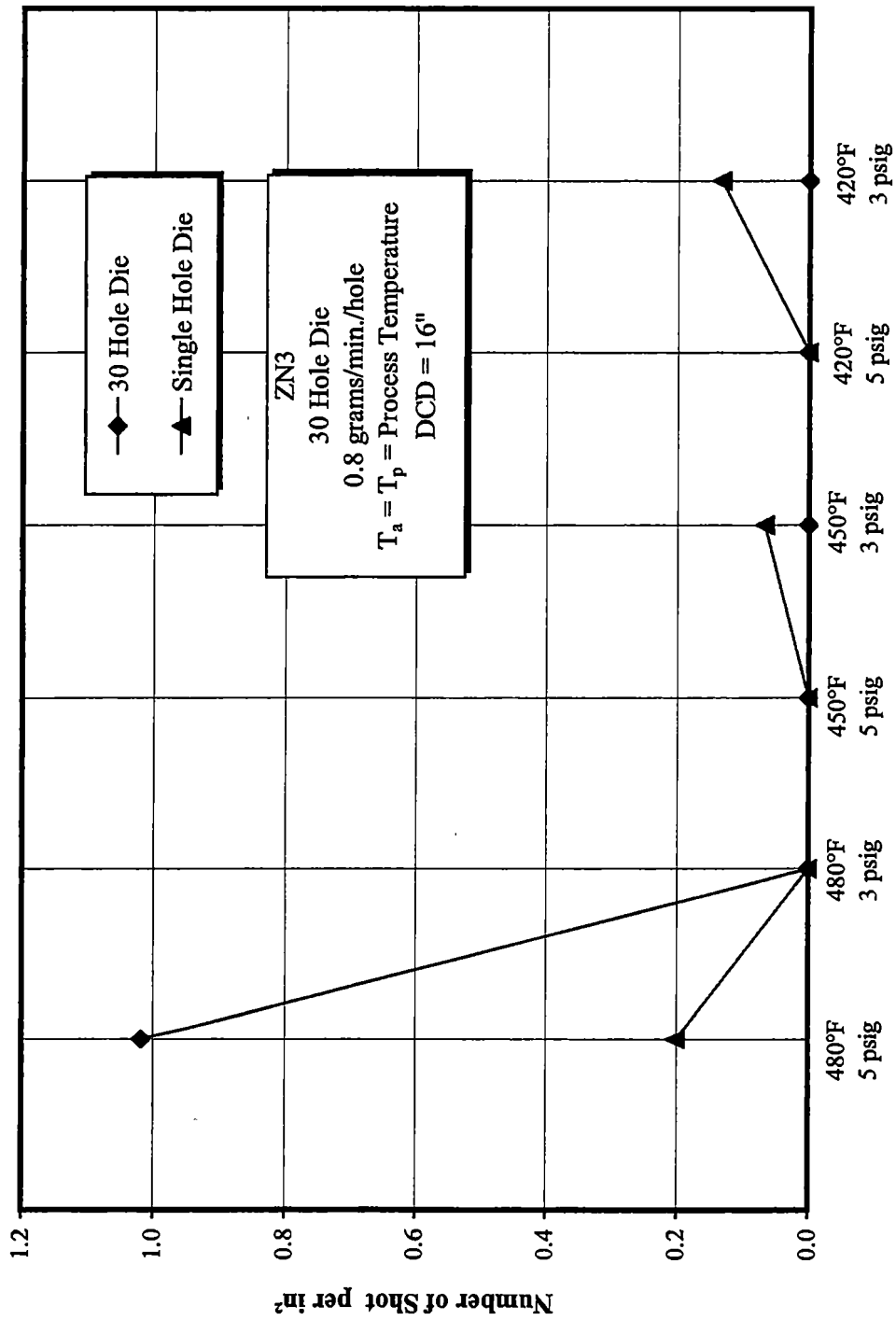


Figure 4.1.1: Number of shot per in² vs. process condition

Chapter V

Experimental Investigation into Process Parameters

As stated in the objectives in Chapter I, one goal of this effort was to determine an empirical model for the formation of shot in a melt-blowing process utilizing a single hole die. The construction of an empirical model will be attempted using shot data collected at many process conditions. The most important factor in the determination of an empirical model is good, reliable data. There has been much data generated in this area at the University of Tennessee [11,13,16]. The data reduction, fiber diameter and shot evaluations have been performed by various methods and by numerous experimenters. With this in mind, it was determined that new samples would be created and all possible care would be used to ensure that the desired data reduction and web generation techniques would be maintained throughout the investigation. Once the samples were collected, the data reduction for average fiber diameter and shot production would be performed by one individual for each and therefore obtain the most consistent set of data possible for the empirical evaluation. It is important to note that the average fiber diameter measurements were performed for two reasons since the fiber diameter measurements were not required for the empirical shot model. The first of these reasons is that it is important not to lose sight of the importance of fiber diameter in this search to decrease the shot production. A second reason is that there has been a great deal of study into fiber diameters and one will be able to test previous theories and monitor one's work in order to ensure that his or her webs are similar to those created in previous

experiments. All fiber diameter measurements were performed using the optical microscope method. The process condition ranges were selected to demonstrate the actual processing conditions, which might be utilized in an actual melt-blowing production facility. The processing parameter ranges were selected in consultation with Dr. Mancil Milligan. The polymer temperature (T_p) and air temperature (T_a) were selected to be equal since not all production facilities have the capability to vary these two temperatures independently. The test section air pressure was selected to remain between 10 psig and 3 psig. The polymer throughput to be used would be 0.4, 0.8 or 1.3 grams per minute. The processing matrix is shown in Figure 5.1. The remaining parameters would be held constant and are as follows: die setback (ds) and die gap (dg) both equal to 0.079 inches (2 mm), die to collector distance (DCD) equal to 16 inches, 60° included angle die nose piece. The web basis weight would be held constant at approximately 4.6 oz/yd² by controlling the collector drum RPM. This basis weight was selected for its optical density for WebPro use. The only remaining parameter to be discussed is the polymer itself. The polymer chosen for this study was the M2 resin discussed in the previous chapter. This resin was selected for two reasons. First, the University of Tennessee lab has a great deal of this polymer in reserve and second, this particular resin is a metallocene resin which tends to produce more shot than the conventional resins as shown in the previous chapter. This type of an investigation would allow for this M2 resin to be thoroughly investigated in the hope of gaining some insight into Chapter IV's metallocene results.

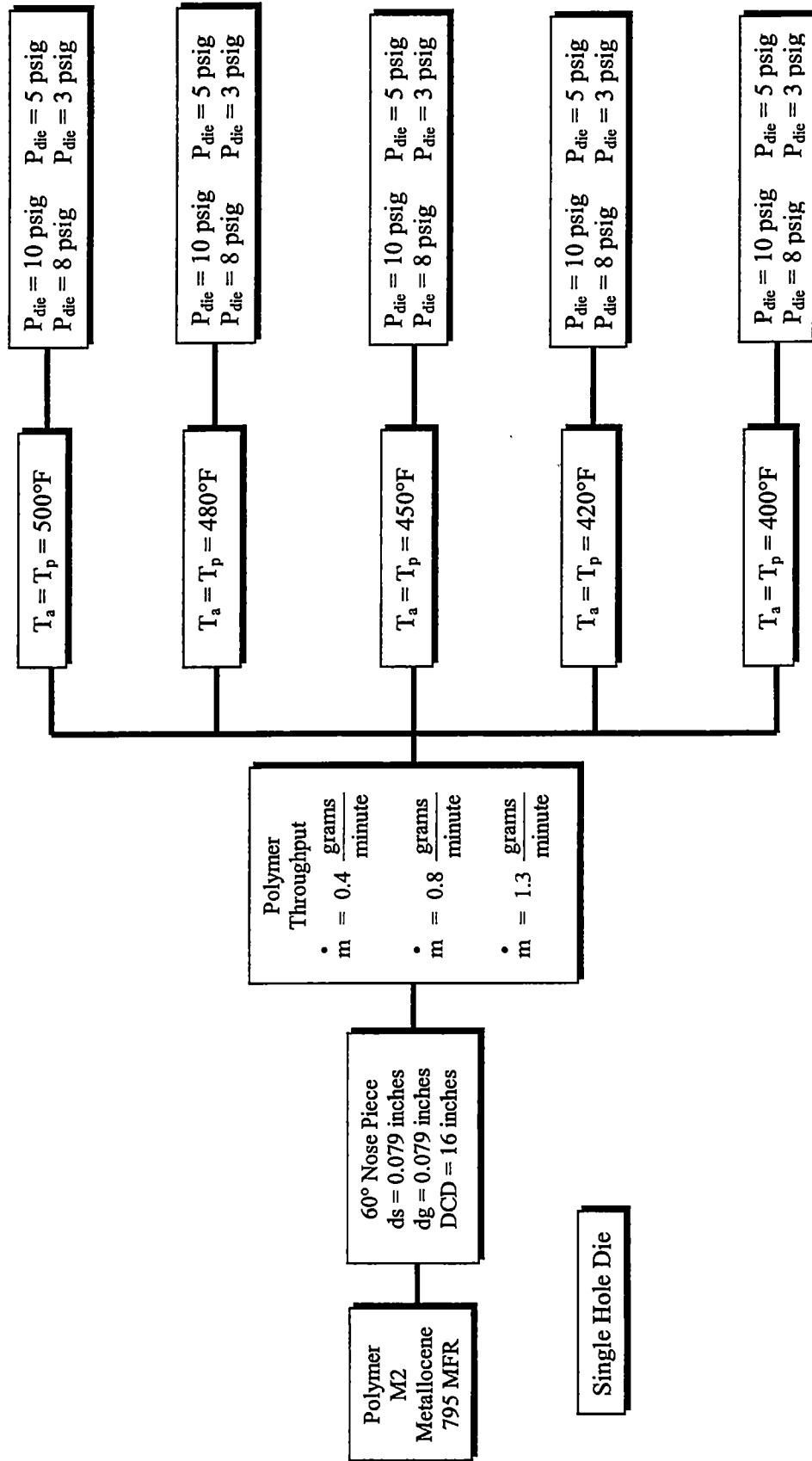


Figure 5.1 : Test matrix of the processing conditions at which the web samples were collected

Die Air Pressure

Previous researchers [11,13,16] have pointed out the importance air exit velocity plays in the production of small fibers in the melt-blowing process. If it is presumed that shot is formed from the “snapping back” model, the “filament interaction “ model, or any combination thereof then air jet velocity should play an important role in shot production as well. Even though the aerodynamics forces created by the velocity of the air jet is what breaks the fibers or causes them to collide in mid flight, the parameter used in this study is die air pressure or more correctly: die stagnation air pressure. This is appropriate since die air pressure is the dominant parameter in determining the air velocity from a fixed geometry jet with a constant air temperature. The effect of die air pressure on air velocity is clearly shown in Figure 5.2. The method used to calculate the air velocity from the known processing conditions is shown in detail in Appendix III. Another area of concern in representing the results is the shot counting output. As shown in the WebPro output in Figure 3.21, the WebPro program returns two quantitative answers in this area. The first of these is the number of shot per area (N/cm^2) and the second is the shot area percentage (cover (%)). Each of these results is used in the following presentations and discussion. Figure 5.3 shows that shot cover area is directly related to the number of shot per area (either in^2 or cm^2) for these data. Therefore, as with die air pressure and air velocity, either method of representing the data is acceptable. This investigation will primarily use number of shot per area to present the experimental results.

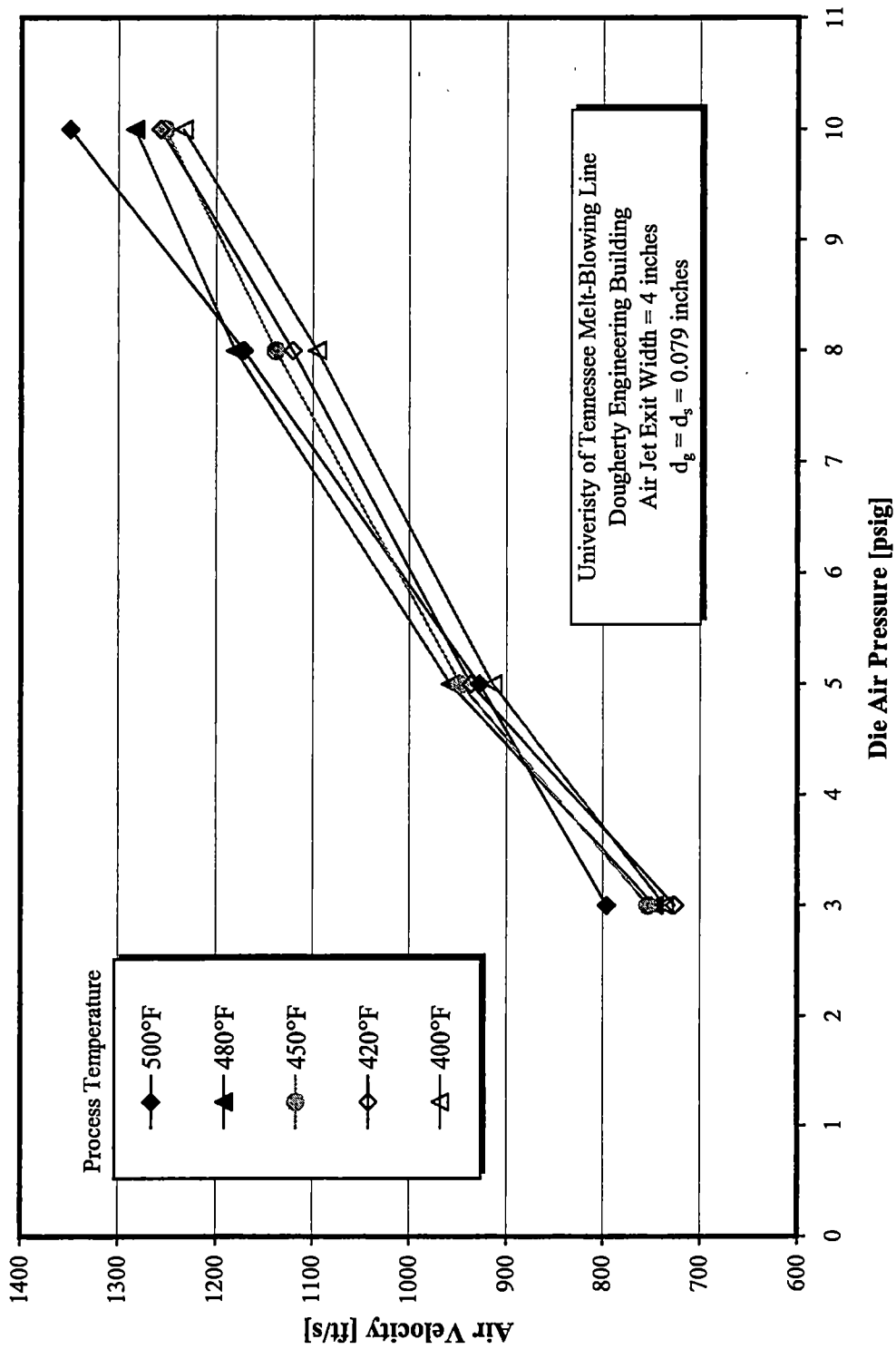


Figure 5.2: Relationship between air jet exit velocity and die air pressure

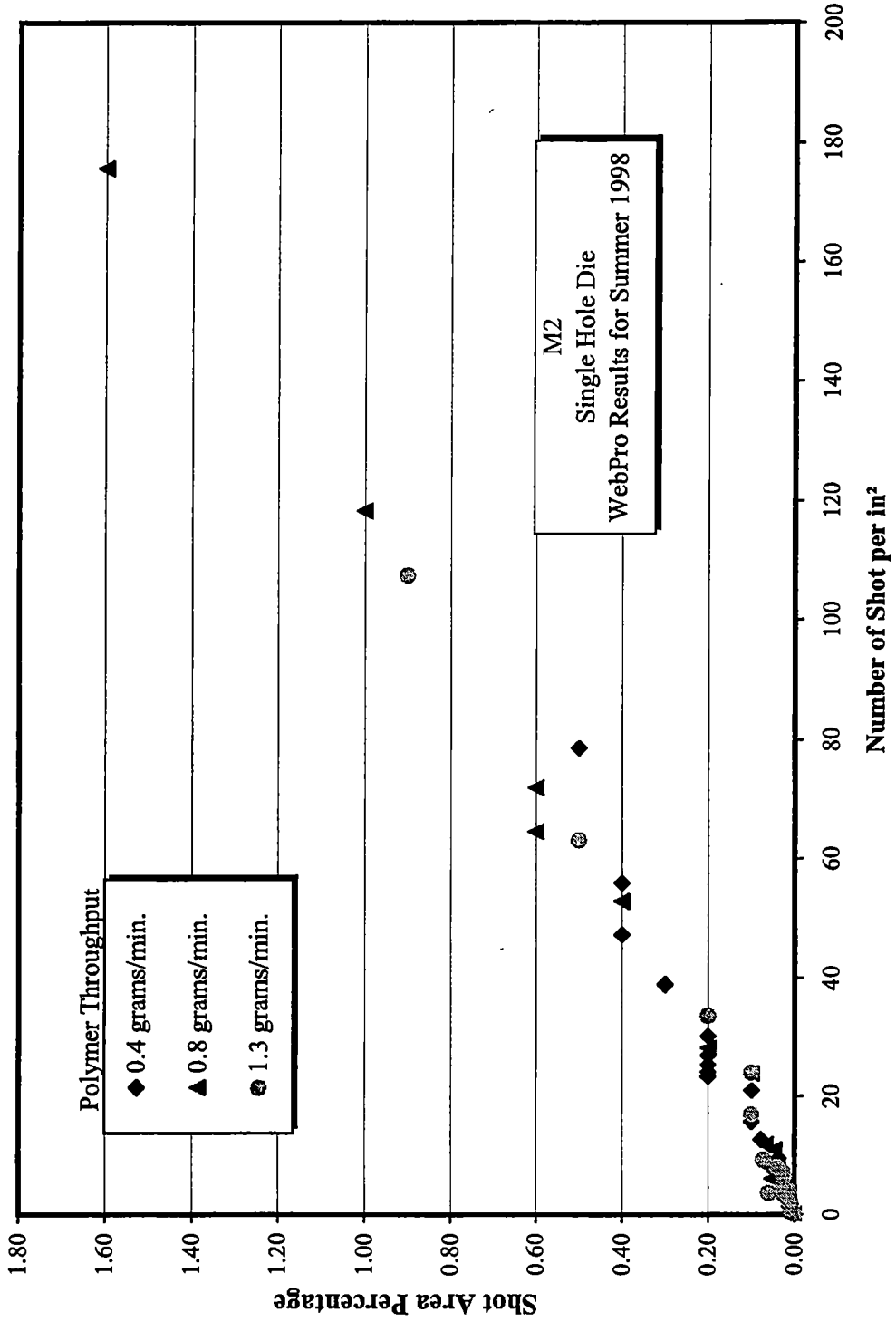


Figure 5.3: Relationship between shot area percentage and number of shot per in²

The test matrix indicates that tests were performed by setting the polymer throughput and then performing the temperature and die air pressure variations before altering the polymer throughput again. Figure 5.4 shows how shot production is influenced by die air pressure for constant process temperatures with a polymer throughput of 0.4 grams per minute. This figure shows that the number of shot per square inch increases in a near linear fashion as die pressure increases. Previous statements indicated that plotting the results in terms of die air pressure as opposed to air velocity was acceptable since the die air pressure is the dominant parameter in the air velocity. Figure 5.5 is the same as Figure 5.4 except that Figure 5.5 is plotted with the air velocity as the dependent variable. The only difference between Figure 5.4 and Figure 5.5 is the shifted location of the data points along the x-axis. Even though these points are shifted, the curves are the same relative to each other. Figure 5.6 shows how average fiber diameter changes as die pressure is increased for constant process temperatures for the same polymer throughput as Figure 5.4. Overall, the average diameters tend to decrease as the die air pressure is increased. Previous research has shown [11,13,16] this trend, but for these data no conclusion can be drawn because the uncertainty in the diameter measurement, $\pm 1.25 \mu\text{m}$, is between 65 and 35 percent of the experimental diameter values. This negligible change in fiber diameter is probably due to the low polymer throughput. The polymer throughput is already low enough to produce small fibers such that the die air pressure does not play a large role. Meaning that it is difficult for the air stream to attenuate a fiber that is already very small. Figure 5.7 is the same as Figure 5.4 except that the polymer throughput in Figure 5.7 is 0.8 grams/minute. This figure is

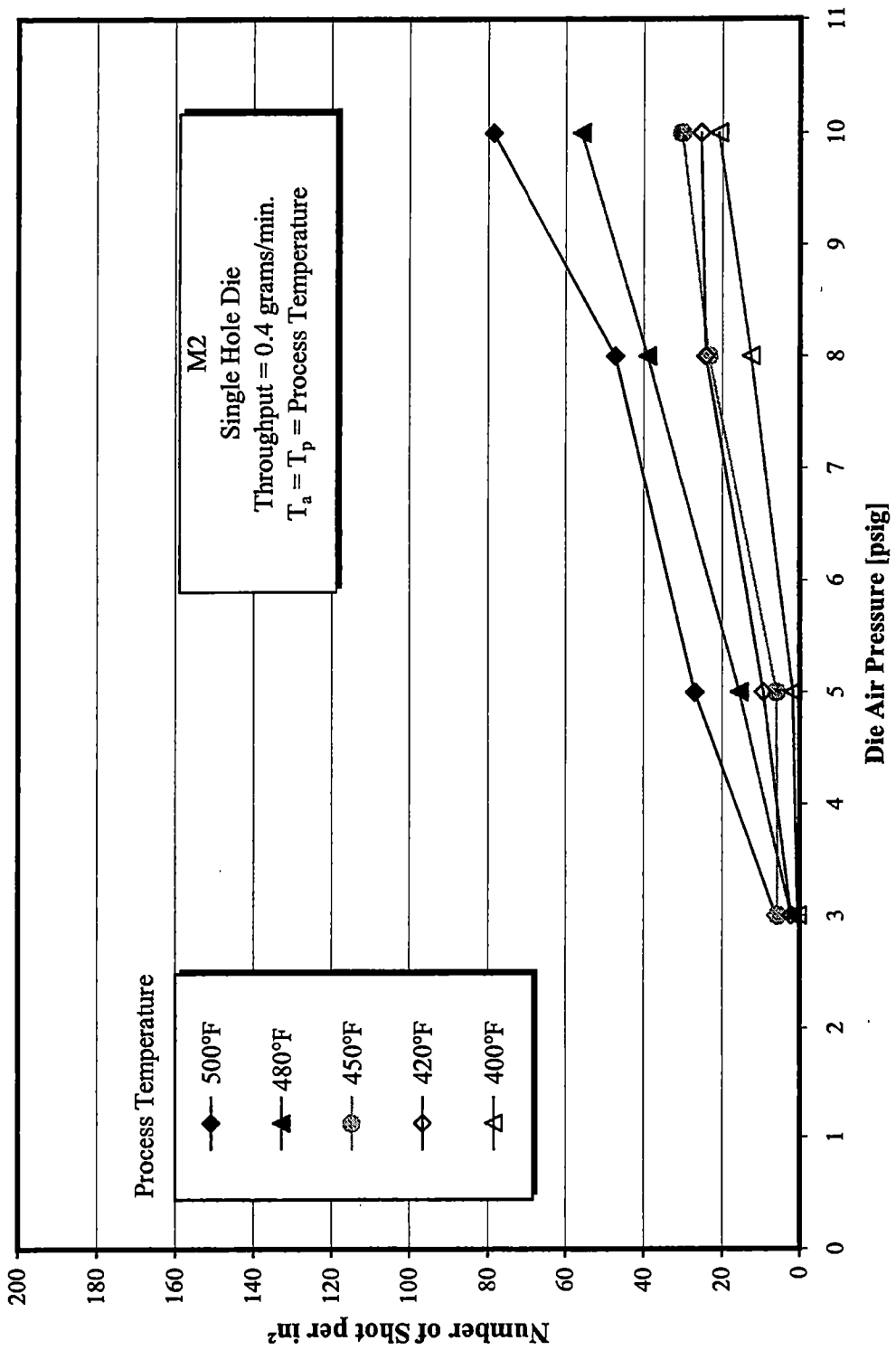


Figure 5.4: Number of shot per in² vs. die air pressure

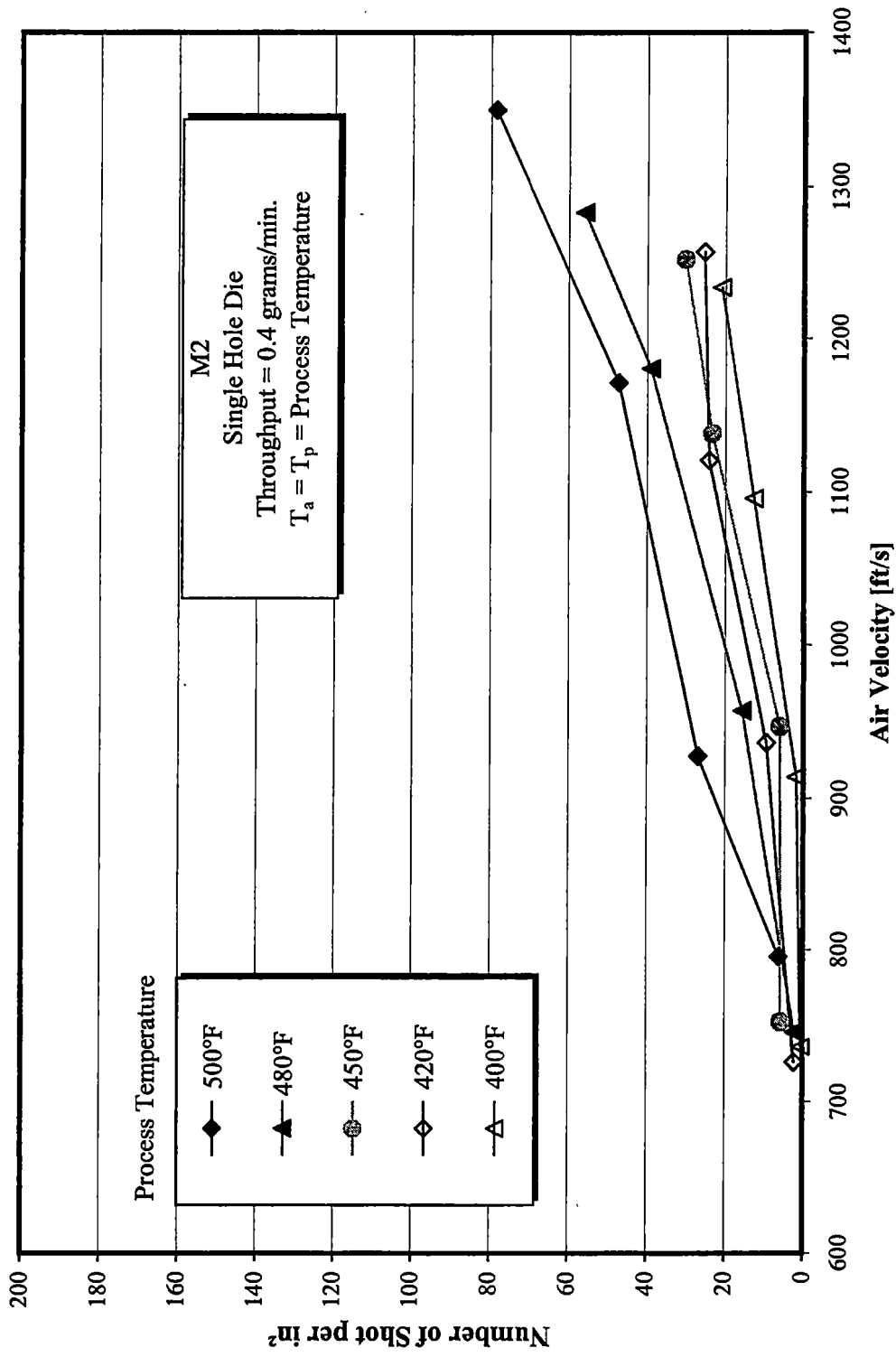


Figure 5.5: Number of shot per in² vs. air velocity

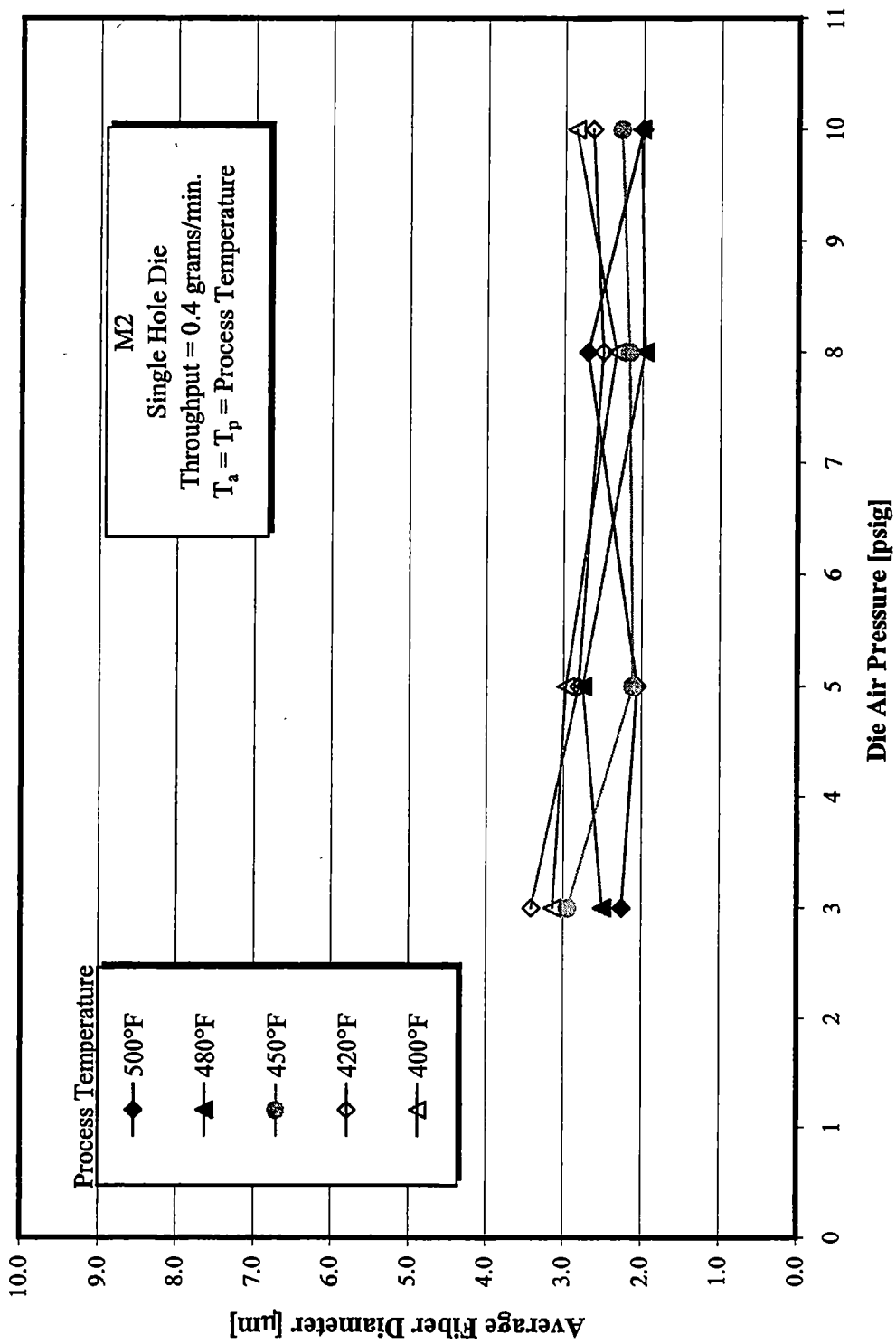


Figure 5.6: Average fiber diameter vs. die air pressure

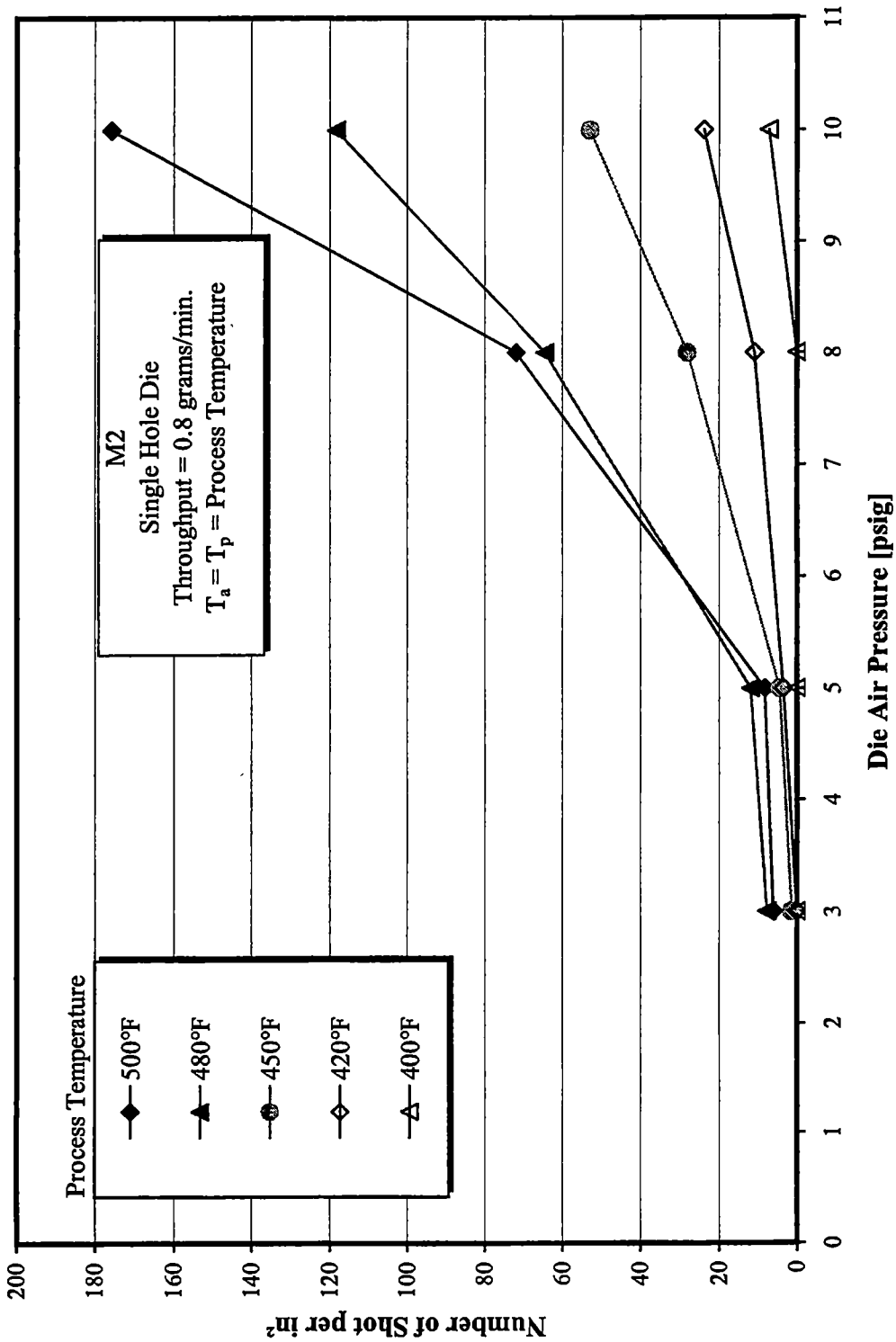


Figure 5.7: Number of shot per in² vs. die air pressure

similar to Figure 5.4 in that the shot production increases with increasing die air pressures. The change in shot production as die air pressure increases is definitely nonlinear in form. Figure 5.7 would seem to indicate that the curves are power functions with the power exponents increasing as temperature increases. Figure 5.8 shows how the average fiber diameter changes with increasing die air pressure with the 0.8 grams per minute polymer throughput. This figure is very different from its 0.4 gram per minute counterpart. Figure 5.8 demonstrates a clear decrease in average fiber diameter for all but the highest process temperatures. The two higher temperature diameter variations are less than the experimental uncertainty, but the other temperatures indicate the diameter reductions even with the uncertainty taken into account. Figures 5.9 and 5.10 represent the influence of die air pressure on shot production and average fiber diameter for the 1.3 gram per minute polymer throughput case. Figure 5.9 shows an increase in shot production as die air pressure is increased. These curves again appeared to be similar to a power function with the power exponent increasing as process temperatures increase. The values of the shot production for the 1.3 grams per minute case did not increase above that of the 0.8 gram per minute case. This was surprising since one would expect the shot production to increase from the 0.8 grams per minute case to the 1.3 grams per minute case as it did from the 0.4 grams per minute case to the 0.8 grams per minute case. Figure 5.10 shows the same decrease in average fiber diameter as die air pressure is increased. The reduction in diameter in Figure 5.10 is more dramatic than either Figure 5.6 or Figure 5.8. It seems apparent that the influence of die air pressure on the average fiber diameter increases as the polymer throughput increases. This

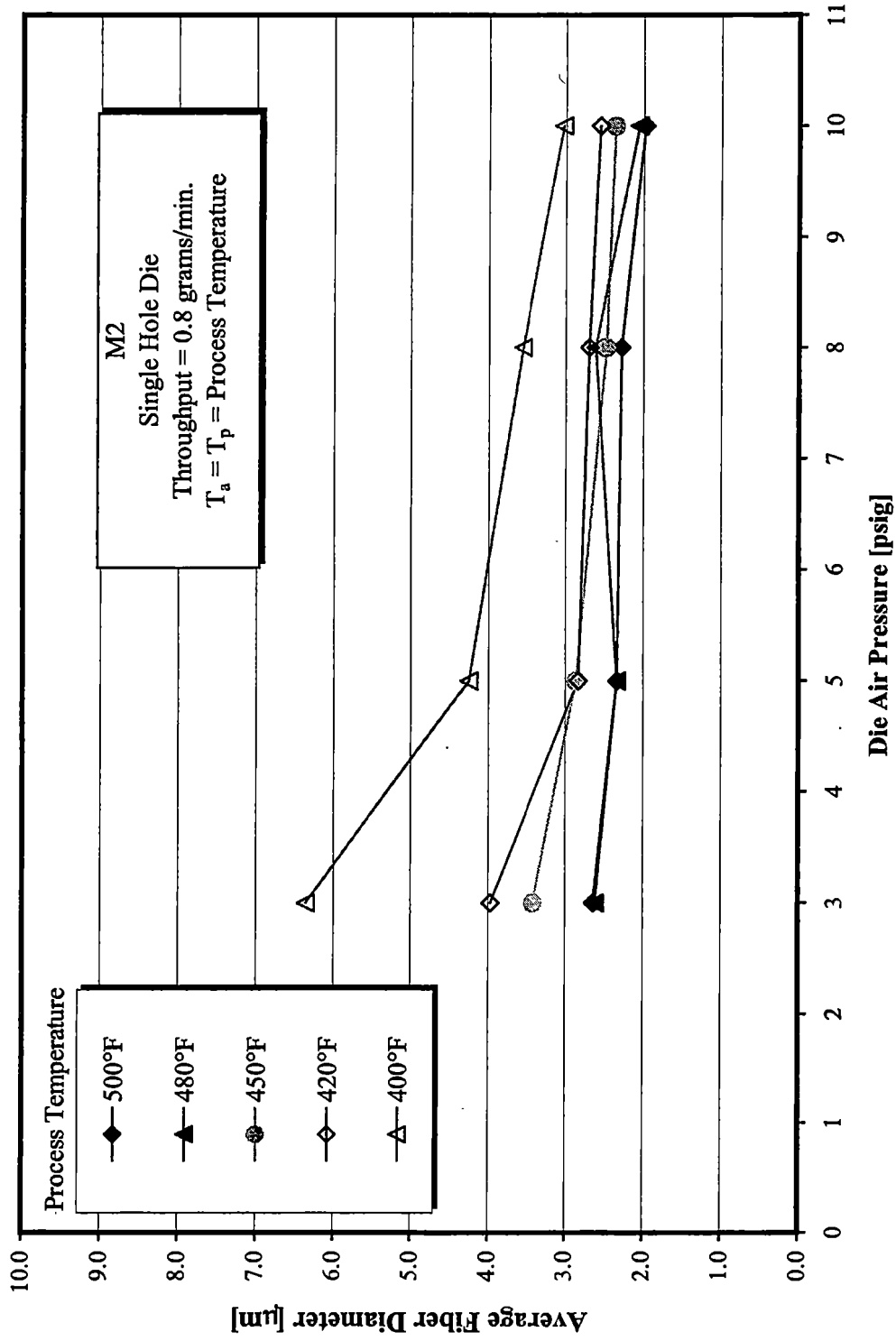


Figure 5.8: Average fiber diameter vs. die air pressure

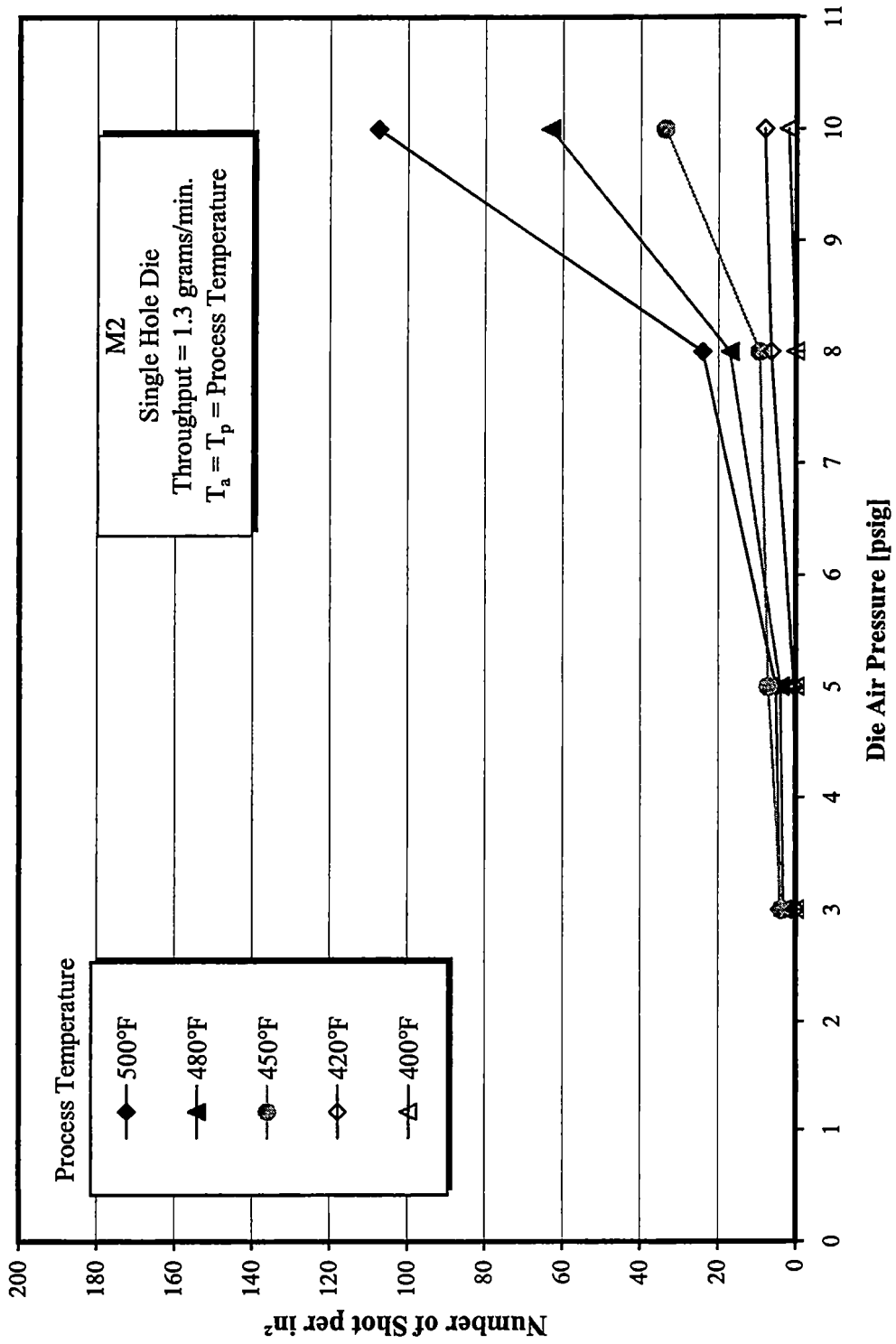


Figure 5.9: Number of shot per in² vs. die air pressure

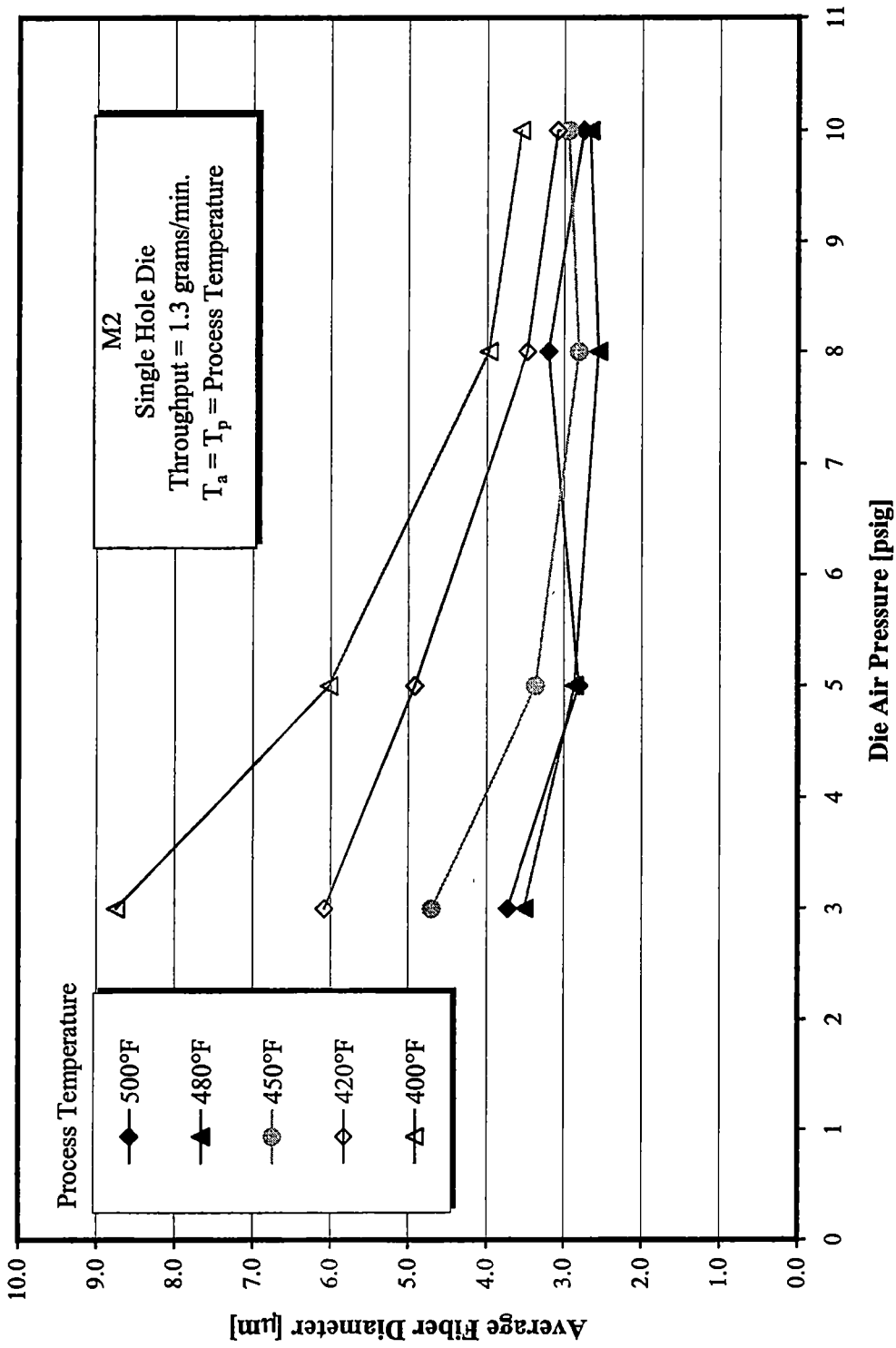


Figure 5.10: Average fiber diameter vs. die air pressure

observation is in agreement with the empirical relationships put forth by Haynes [16] and Spencer [13].

Process Temperature (Air Temperature and Polymer Temperature)

Even though the influence of process temperature on shot production and fiber diameter was shown in the previous figures, this section is presented for further visualization of the process temperature influence. Figures 5.11 and 5.12 represent the shot production and average fiber diameter versus process temperature for the 0.4 grams per minute polymer throughput case. Figure 5.11 shows that shot production increases as process temperature increases. Figure 5.12 indicates little about the influence of process temperature on average fiber diameter. This was expected since Figure 5.6 demonstrated the same negligible changes in fiber diameter for die air pressure variations at this low polymer throughput. Again, the small changes in fiber diameter are overwhelmed by the uncertainty in the fiber diameter measurements. Figures 5.13 and 5.14 represent the shot production and average fiber diameter versus process temperature for the 0.8 grams per minute polymer throughput case. Figure 5.13 shows the influence of process temperature on shot production. Here the first two curves (10 psig and 8 psig) are very distinct but the later two (5 psig and 3 psig) seem to merge into a single curve. Figure 5.14 indicates the effect of process temperature on the average fiber diameter. This figure shows that the average fiber diameter decreases as the process temperature increases. The effect of process temperature is more dominant for the lower die air pressure regions. Again, the reduction in fiber diameter for the high die air pressure cases are within the

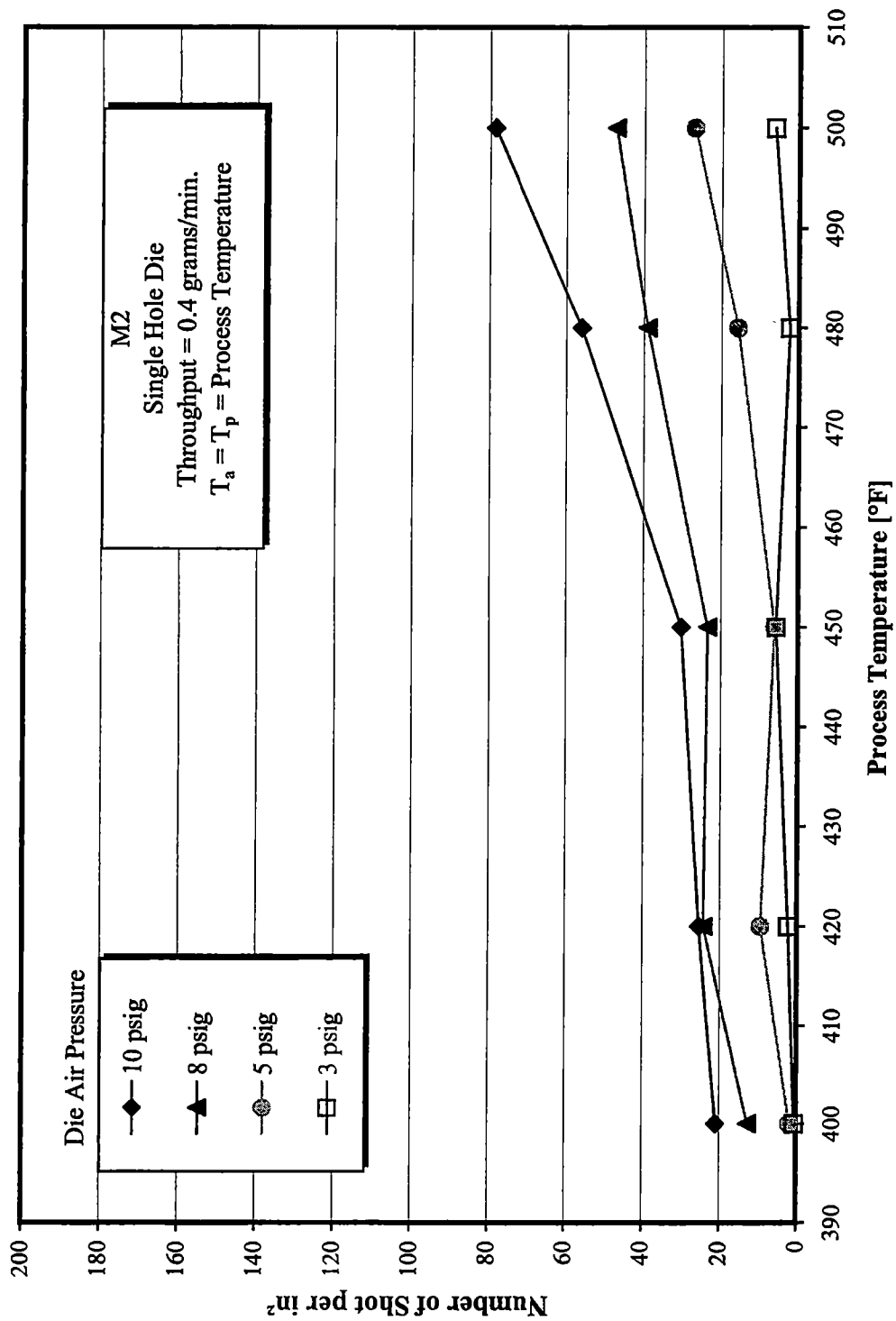


Figure 5.11: Number of shot per in² vs. process temperature

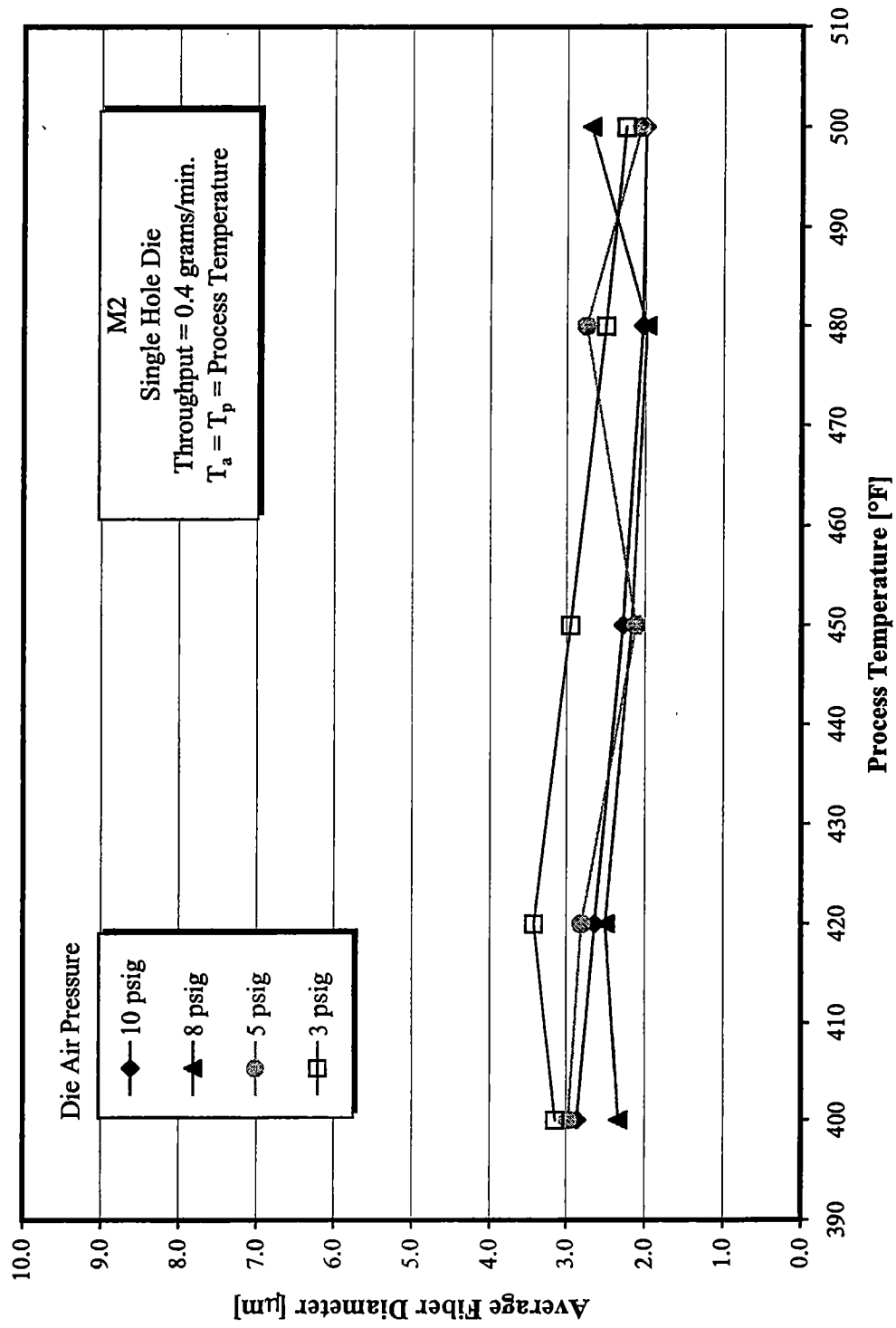


Figure 5.12: Average fiber diameter vs. process temperature

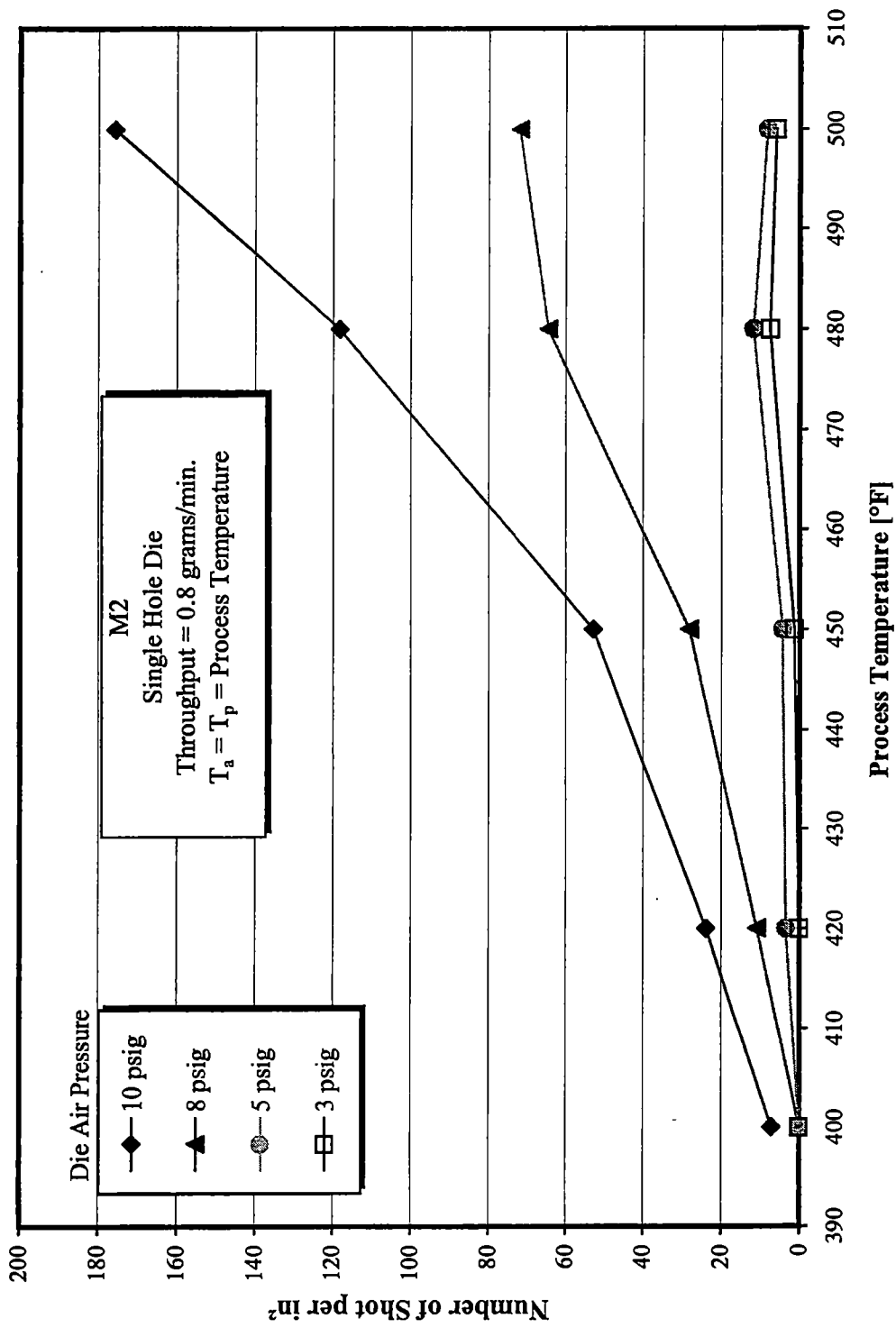


Figure 5.13: Number of shot per in² vs. process temperature

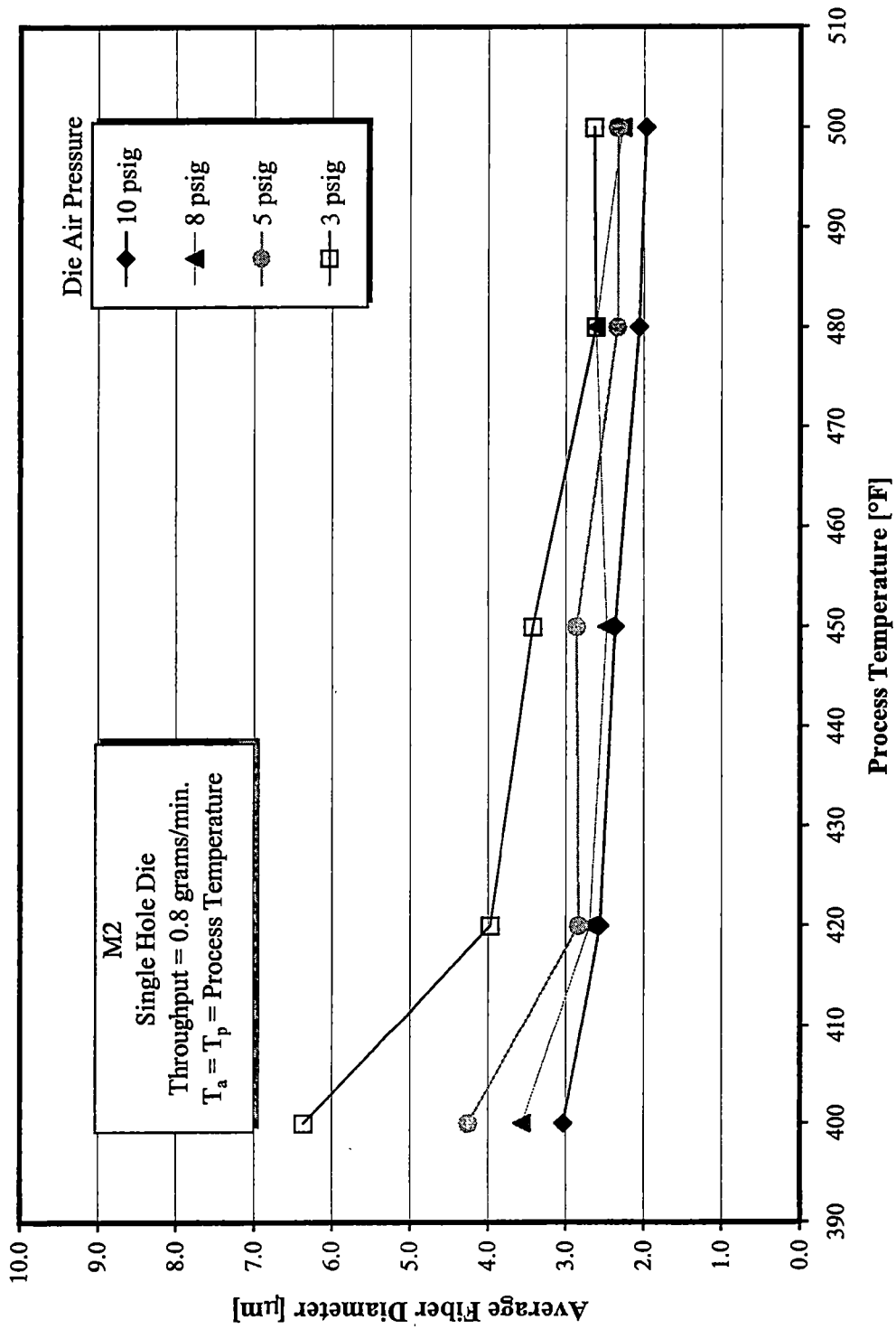


Figure 5.14: Average fiber diameter vs. process temperature

measurement uncertainty of the fiber diameter. Figure 5.15 and 5.16 represent the shot production per area and average fiber diameter versus process temperature for a polymer throughput of 1.3 grams per minute. The shot production trends in Figure 5.15 are almost identical to that of its 0.8 grams per minute counterpart shown in Figure 5.13. Figure 5.15 shows that shot production increases as process temperature increases and that the higher die air pressure curves are distinct while the lower die air pressure curves seem to merge into a single curve. Figure 5.16 demonstrates that the average fiber diameter decreases as process temperature increases. The same observations concerning the measurement uncertainty of the diameter in Figure 5.14 are applicable in Figure 5.16 also.

Polymer Throughput

Since the polymer throughput was a variable, the influence of polymer throughput can be determined for situations where the process temperature and die air pressure are held constant. This section presents the results from the polymer throughput study in four figures. Each of the following graphs represents the influence of polymer throughput on shot production for a constant die air pressure. Figure 5.17 is a graph of shot production versus polymer throughput for a die air pressure of 10 psig. The individual curves represent constant process temperatures. This figure demonstrates a phenomenon that was present in the previous graphs but not entirely obvious. The phenomenon is the observation that the shot production actually increases between throughput values of 0.4 to 0.8 but decreases between values of 0.8 to 1.3. This is demonstrated for the majority of process temperatures in

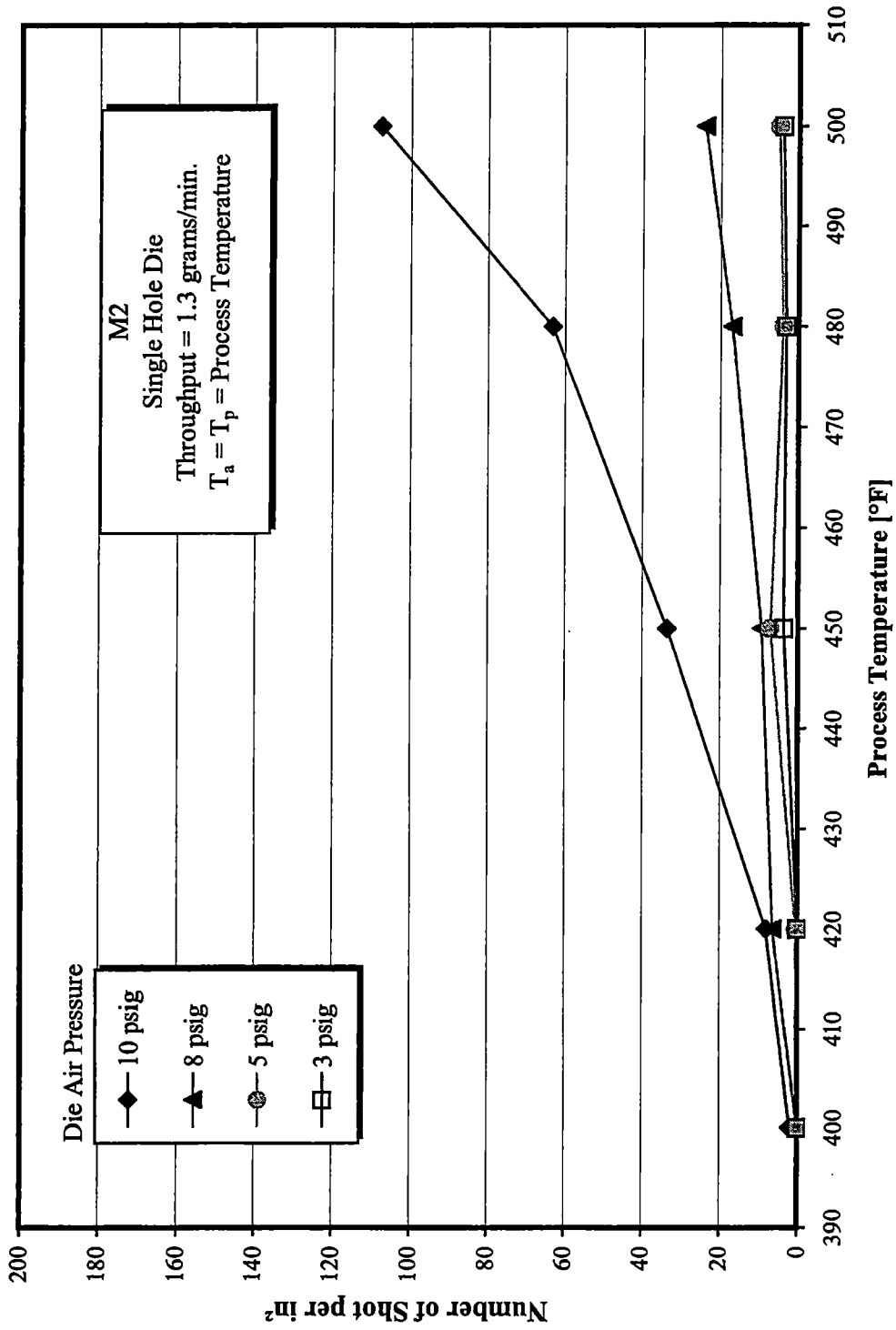


Figure 5.15: Number of shot per in² vs. process temperature

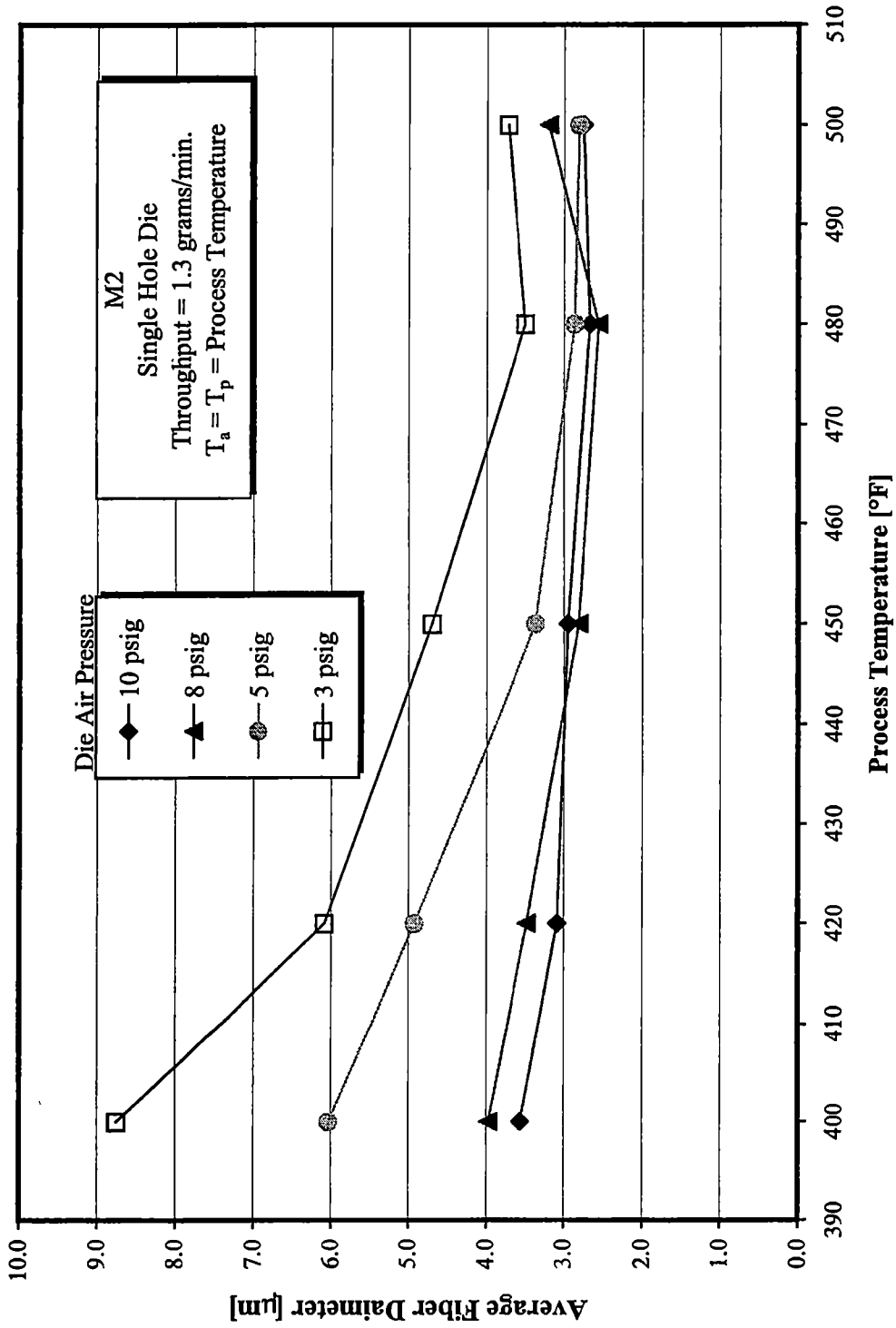


Figure 5.16: Average fiber diameter vs. process temperature

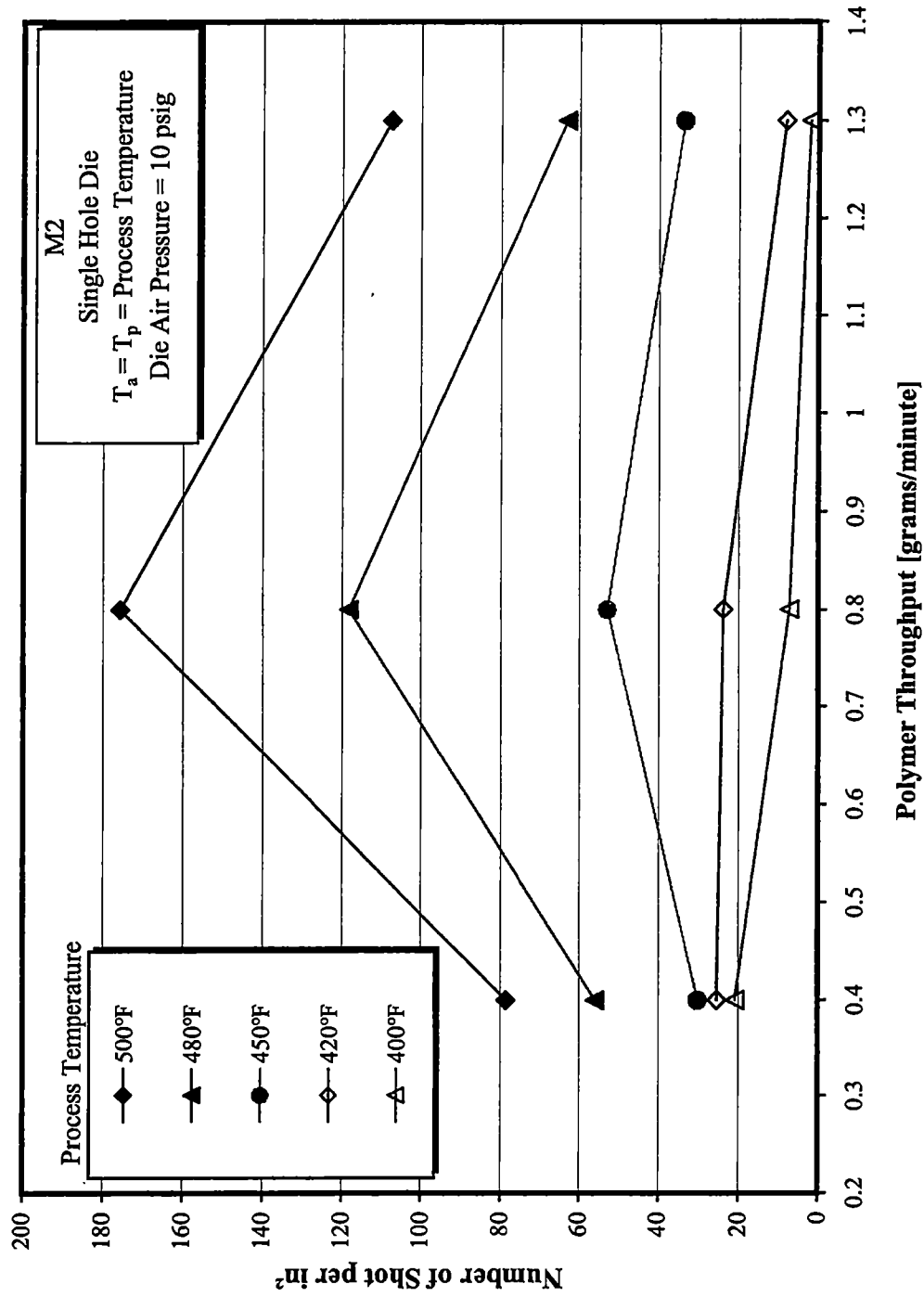


Figure 5.17: Number of shot per in² vs. polymer throughput

Figure 5.17 and is opposite to what one might expect. Figure 5.18 is the same as Figure 5.17 except that Figure 5.18 is for a die air pressure of 8 psig. Again the same observation that dominated Figure 5.17 is present in this figure for the majority of process temperatures. Figures 5.19 and 5.20 are the shot production versus polymer throughput graphs for die air pressure of 5 psig and 3 psig respectively. Figure 5.19 does not possess the same increase and decrease in shot production from 0.4 to 1.3 grams per minute as previous figures. The shot does however tend to decrease as the throughput is increased in the majority of these process temperature curves. Figure 5.20 does not indicate any strong influence of polymer throughput in the production of shot for a die air pressure of 3 psig. Even though Figure 5.20 does not indicate the shot reduction between 0.8 and 1.3 grams per minute, other experimental data at the same processing condition have indicated that this phenomena is present at this die pressure.

The inverse relationship between shot production and polymer throughput for the 0.8 to 1.3 polymer throughput range has proven to be very interesting. At first, this phenomena was treated as a mistake in data analysis until the web samples were reanalyzed on WebPro and produced the same results. In a further check of this situation, previous single hole die experiments were analyzed in which the same resin (M2) was extruded at some of the same conditions as the data represented in this section. The shot production results of these experiments are shown in Figure 5.21. This data was only collected at 5 and 3 psig die air pressure for various process temperatures and polymer throughputs. The biggest difference between this section's

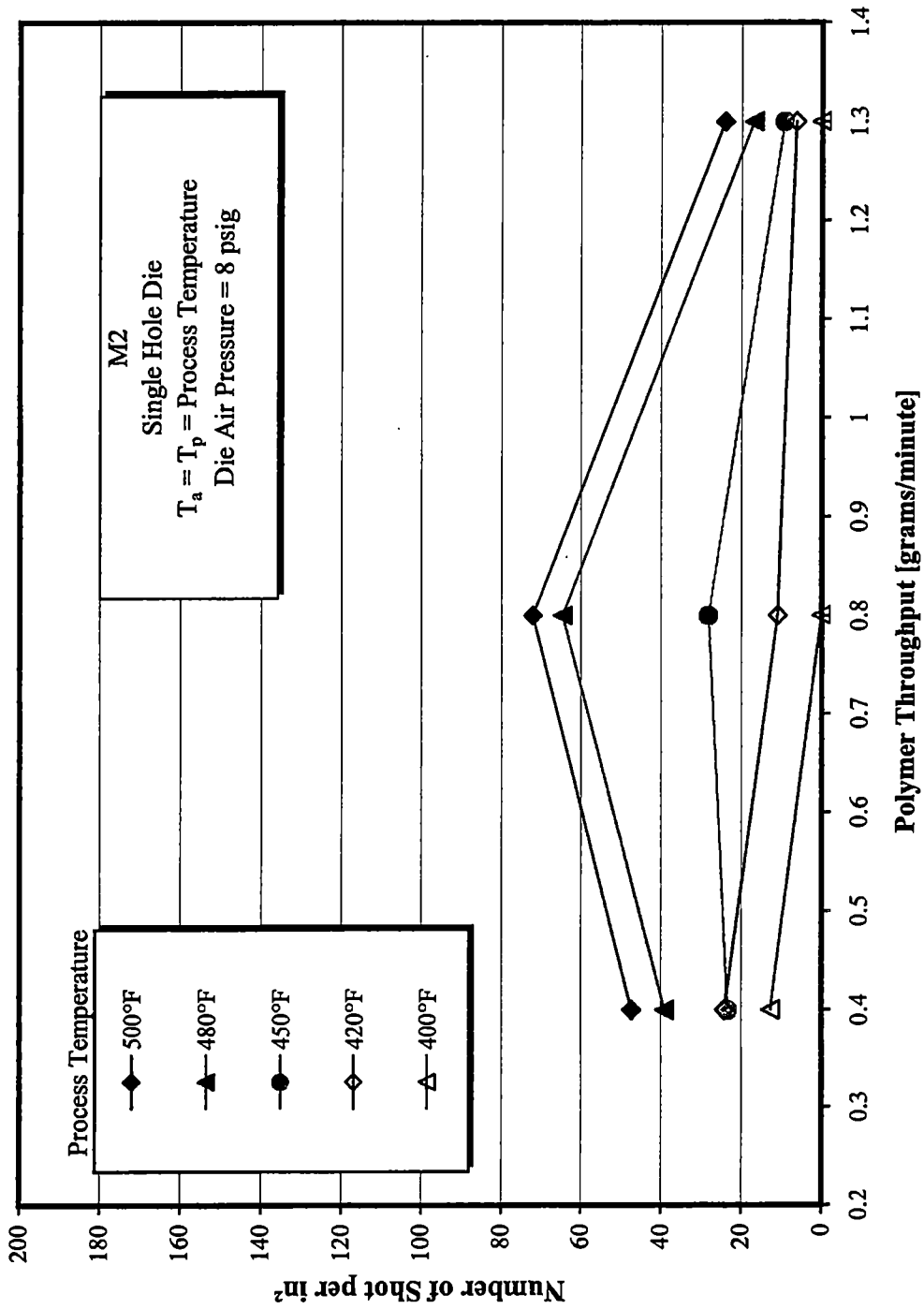


Figure 5.18: Number of shot per in² vs. polymer throughput

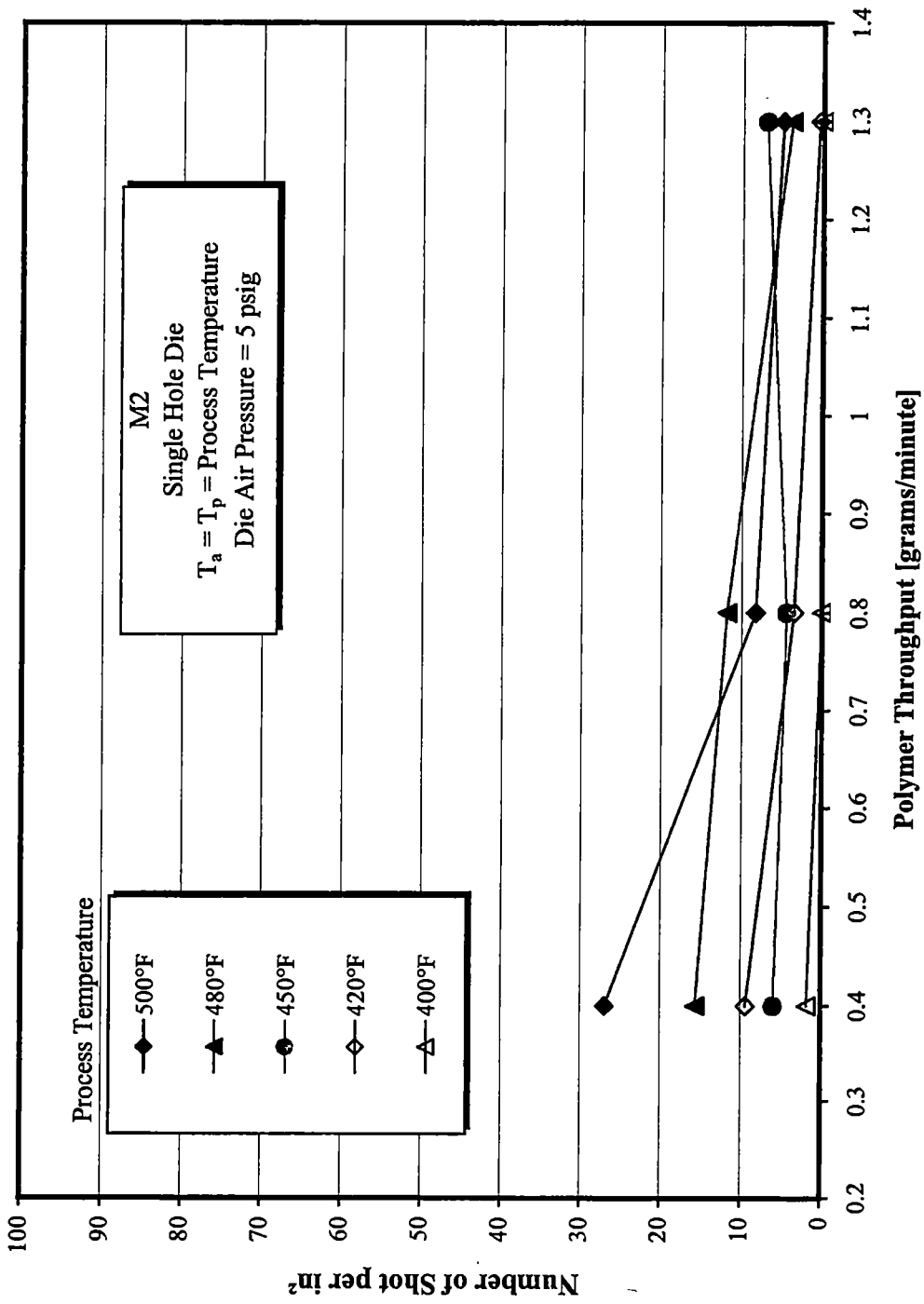


Figure 5.19: Number of shot per in² vs. polymer throughput

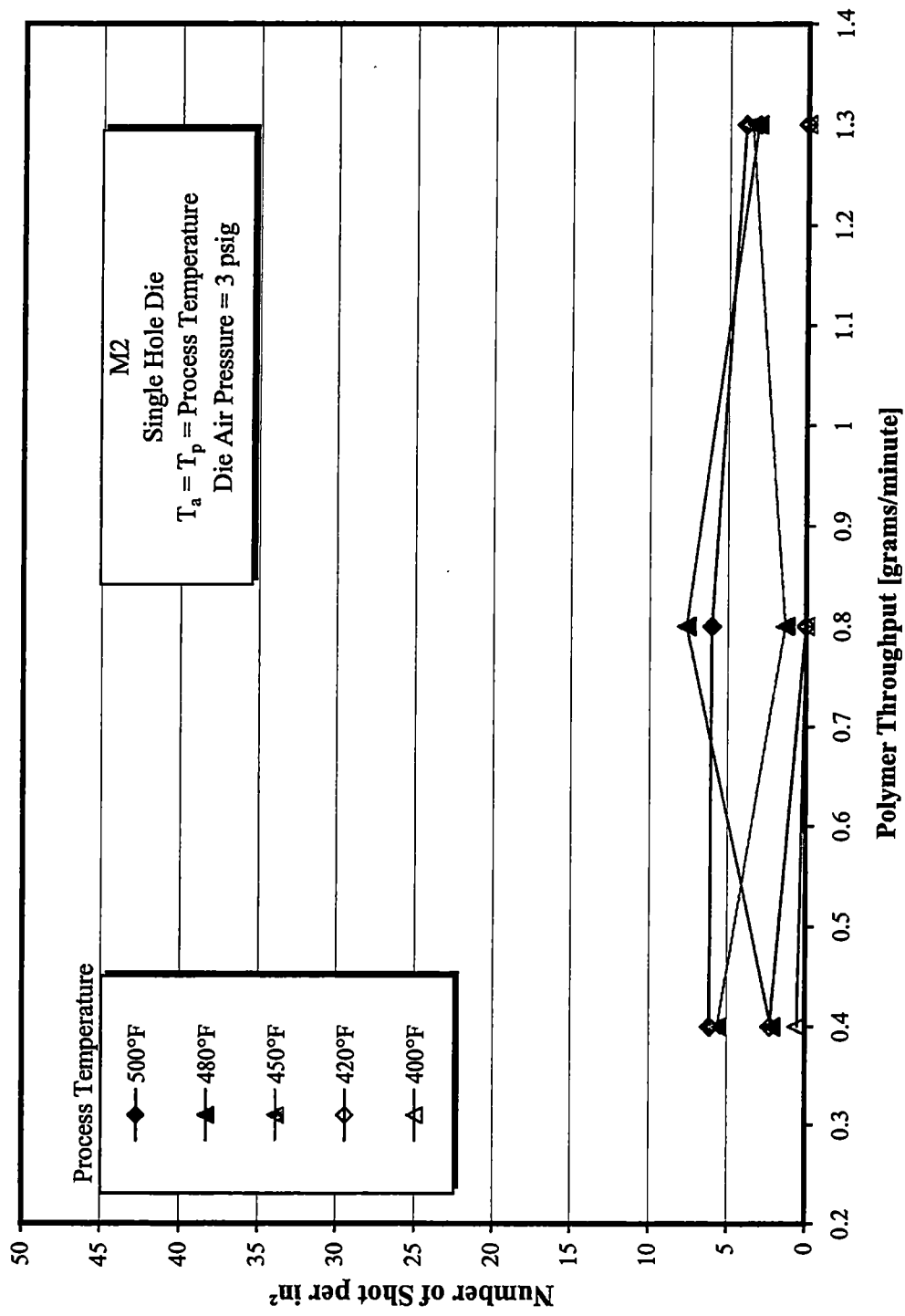


Figure 5.20: Number of shot per in² vs. polymer throughput

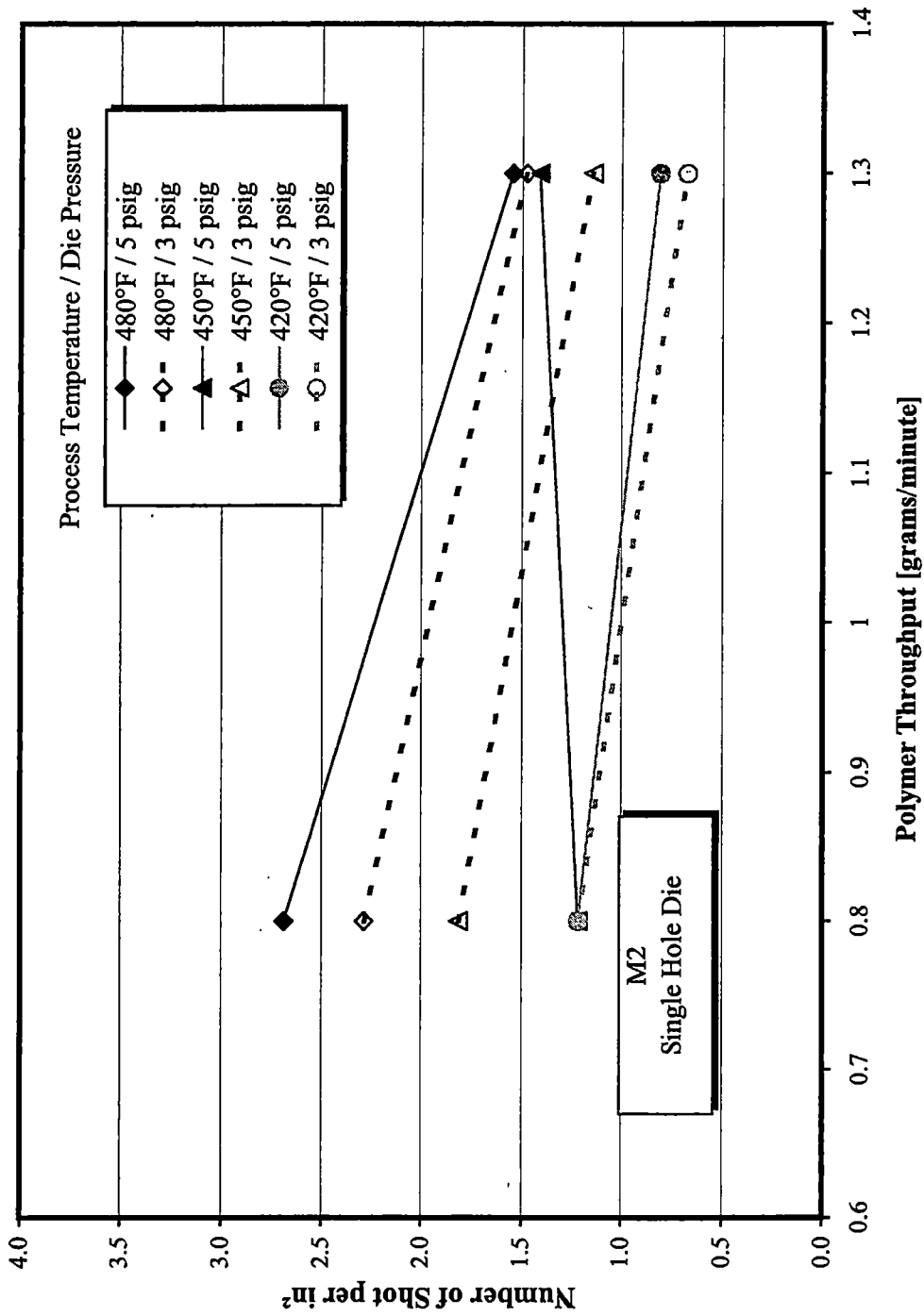


Figure 5.21: Number of shot per in² vs. polymer throughput

data and Figure 5.21 data was that another University of Tennessee research group performed the WebPro shot analysis. This experimental data was collected jointly with the other research group in February and April of 1998 during a melt blowing study in which the molten resin stream exiting the die face was video taped with a high speed camera. The actual video taping was performed by the other research group at the university in an attempt to recognize any molten polymer stream flight characteristics as mentioned in the previous chapter.

Summary and Conclusions of Observations from Data Collection and Analysis

In looking at the previous figures, one can make the following summary statements:

- Average fiber diameter decreases with increasing die air pressure (air velocity) for a constant process temperature and polymer throughput.
- Average fiber diameter decreases with increasing process temperature for a constant die air pressure and polymer throughput.
- Shot production increases with increasing die air pressure (air velocity) for a constant process temperature and polymer throughput.
- Shot production increases with increasing process temperature for a constant die air pressure and polymer throughput.
- Shot production both increases and decreases with increasing polymer throughput for a constant process temperature and die air pressure and depends on the magnitude of the polymer throughput and air velocity.
- Average fiber diameter generally increases with increasing polymer throughput for a constant process temperature and die air pressure.

Most of the previous statements are in agreement with the results from previous investigations [11, 13, 16]. Only Utsman [11] performed experiments that investigated shot production. Utsman's work reported that shot production decreased as air velocity (die air pressure) increased. The only major difference between Utsman's work and this effort was Utsman's use of a thirty hole die, resin type and data reduction methods. The shot production dependence on process temperature is in agreement with Utsman's work.

Previous Investigator's Fiber Diameter Empirical Model

As previously stated, there has been a great deal of study into the average fiber diameter of melt blown webs. Two previous investigators [13, 16] used a statistical analysis program to determine an empirical relationship for a dimensionless fiber diameter given the process parameters in non-dimensionalized form. The following two empirical relationships are available from Spencer's [13] research.

$$\delta_{32} = 0.004 + 5.8 \Psi^{-0.81} \Theta^{-6.46} \beta^{-0.85} \Phi^{-0.44} \xi^{-1.05} \Pi^{0.66} \quad 5.1$$

$$\delta_{33} = 0.002 + 3.5 \Psi^{-0.72} \Theta^{-6.26} \beta^{-0.73} \Phi^{-0.38} \xi^{-1.07} \Pi^{0.58} \Omega^{-0.44} \quad 5.2$$

The non-dimensionalized parameters used in Equations 5.1 and 5.2 are defined in Table 5.1 [13]. These parameters are almost identical to the parameters used in this investigation in the following chapter. Equation 5.1 was determined statistically using data collected while processing a 650 MFR conventional resin. Equation 5.2 was determined when the statistical sample was expanded to include other resins with different MFRs. These equations are both constructed around the momentum flux

Table 5.1: List of Spencer's dimensionless variables

Variable	Expression	Reference Value
β - Polymer Throughput Ratio	$\frac{\dot{m}_p}{(\dot{m}_p)_{ref}}$	0.8 $\left[\frac{\text{grams}}{\text{minute}} \right]$
Ψ - air polymer momentum ratio	$\frac{\dot{m}_a V_{air}/A_e}{\dot{m}_p V_p/A_{die}}$	Not Applicable
δ - average fiber diameter ratio	$\frac{d}{d_{die}}$	Not Applicable
Φ - Air Jet Exit Height Ratio	$\frac{h}{(h)_{ref}}$	0.079 [in]
Θ - Polymer Temperature Ratio (Rankine)	$\frac{T_p}{(T_p)_{ref}}$	960 [°R]
ξ - Air Temperature Ratio (Rankine)	$\frac{T_a}{(T_a)_{ref}}$	835 [°R]
Π - Air Jet Injection Angle Ratio	$\frac{\theta}{(\theta)_{ref}}$	45°
Ω - Polymer MFR Ratio	$\frac{MFR}{(MFR)_{ref}}$	650 [MFR]

ratio parameter (Ψ). This was a deviation of Spencer's work from that of Hayne's work. Haynes performed a similar investigation with the exception that Hayne's empirical models were constructed around the mass flux ratio parameter (Γ). Since Spencer's investigation expanded on that of Haynes it was decided to use Spencer's empirical relationships for this comparison. The resin used throughout this investigation was a 795 MFR metallocene (M2) resin. Therefore it would be interesting to investigate how closely Equation 5.1 and 5.2 predict the average fiber diameter of the experimental data. Spencer compared Equations 5.1 and 5.2 to experimental data by creating modified average fiber diameter relationships from these equations. These modified average fiber diameter equations are shown below and allow for the comparisons to be made in terms of the air-polymer momentum flux ratio (Ψ).

$$\Delta_{32} = \frac{\delta_{32} - 0.004}{5.8 \Theta^{-6.46} \beta^{-0.85} \Phi^{-0.44} \xi^{-1.047} \Pi^{0.66}} \quad 5.3$$

$$\Delta_{33} = \frac{\delta_{33} - 0.002}{3.5 \Theta^{-6.26} \beta^{-0.73} \Phi^{-0.38} \xi^{-1.07} \Pi^{0.58} \Omega^{-0.44}} \quad 5.4$$

Figure 5.22 is a plot of modified average fiber diameter (Δ_{32}) versus momentum flux ratio (Ψ) for both the experimental data generated in this study and the Equation 5.3 prediction. This plot demonstrates that Equation 5.1 is a good model for determining the average fiber diameter. A better test of Equation 5.1 is a plot of the predicted average fiber diameter ratio versus the experimental average fiber diameter ratio. This plot is shown in Figure 5.23 and demonstrates that Equation 5.1 is a good

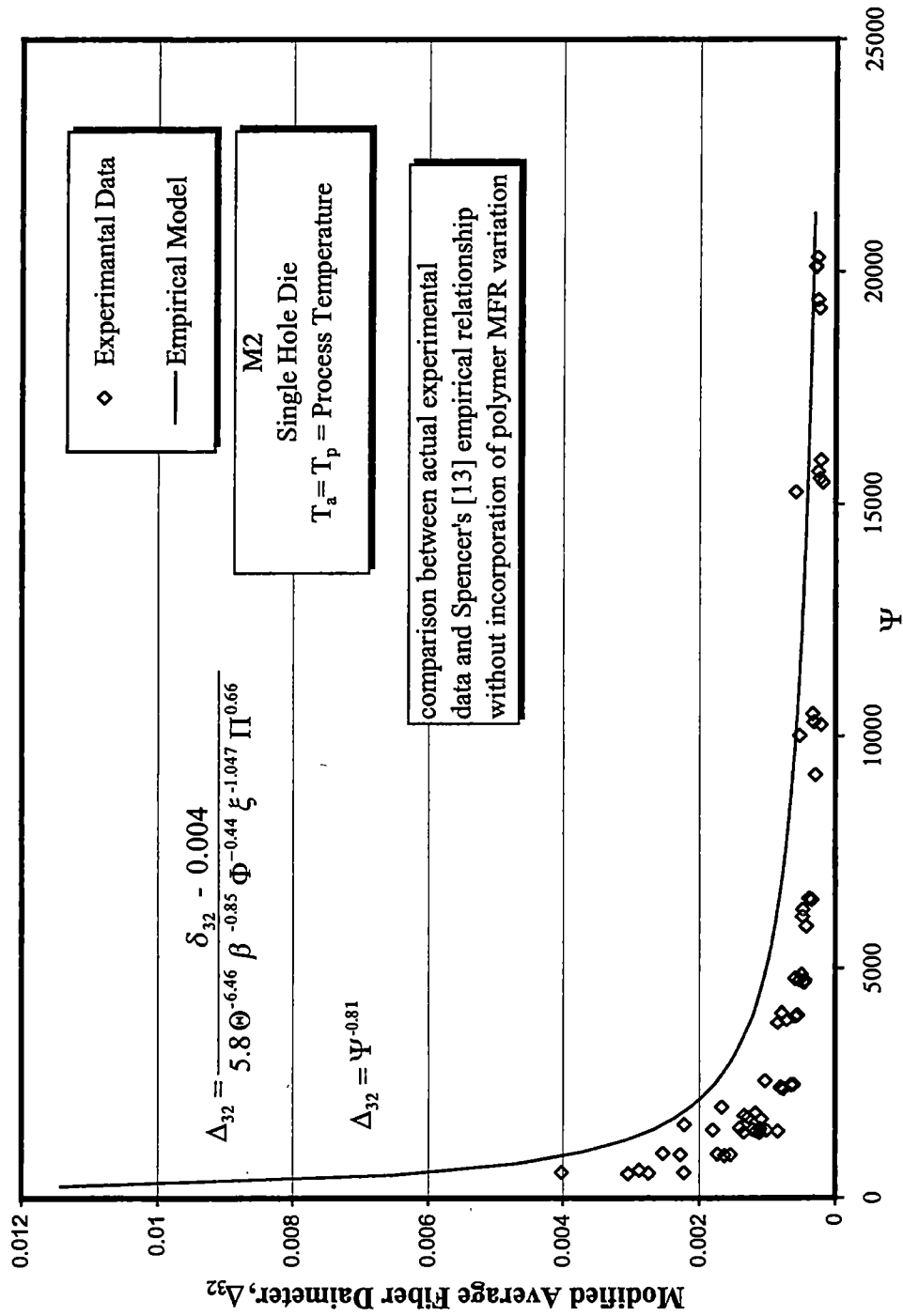


Figure 5.22: Modified average fiber diameter ratio vs. momentum flux ratio (Ψ)

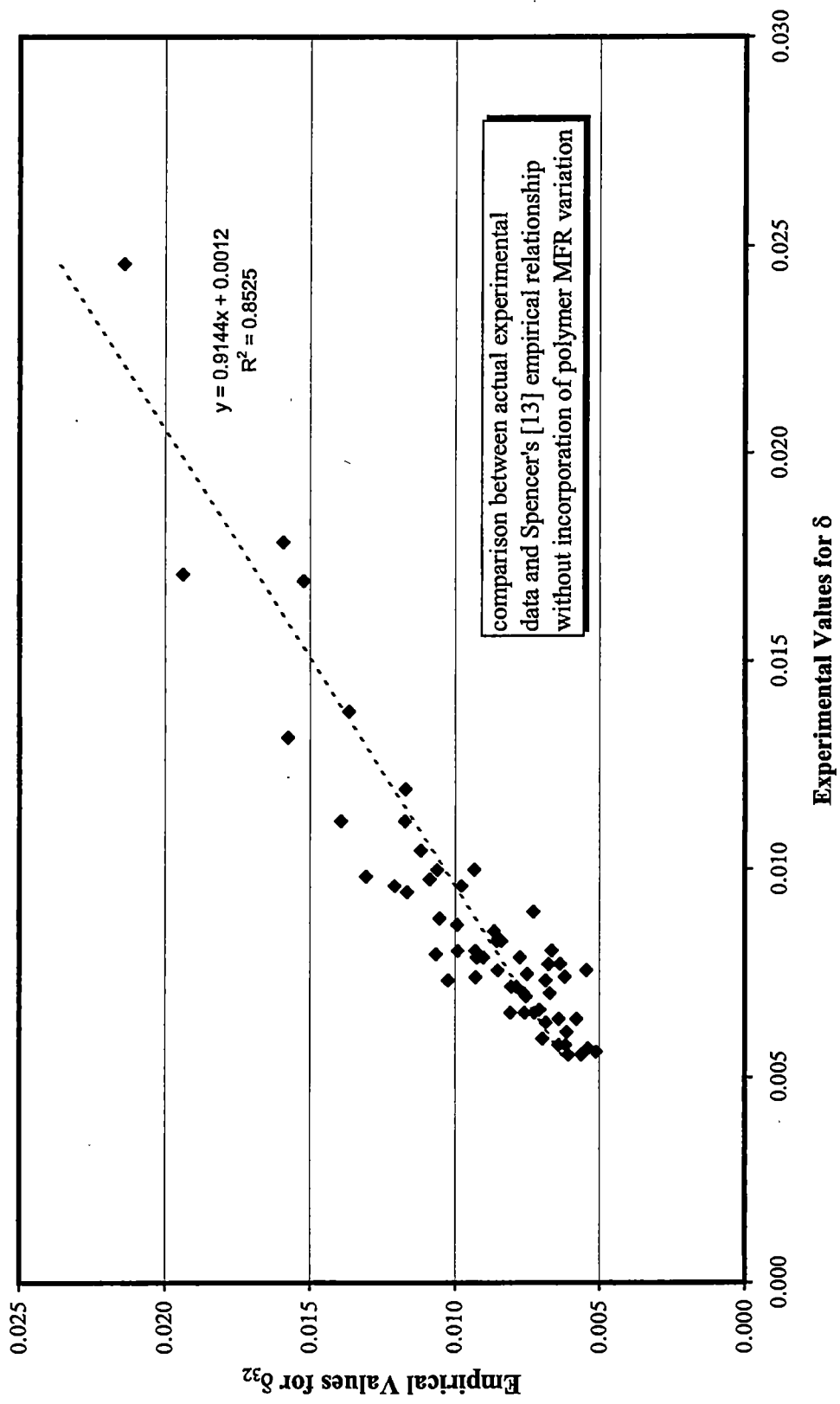


Figure 5.23: Experimental average fiber diameter ratio vs. empirical fiber diameter ratio

predictor for the average fiber diameter. Figure 5.24 is similar to Figure 5.22 except that Figure 5.24 utilizes Equation 5.4 as the empirical relationship. The addition of the polymer MFR parameter in Equation 5.2 does not appear to model the average fiber diameter ratio any better than the relationship without the polymer MFR parameter. Figure 5.25 is a plot of predicted average fiber diameter versus experimental average fiber diameter. This figure is almost identical to Figure 5.24 and the slope and R^2 terms are practically the same. With this in mind the result of this comparison is that Equations 5.1 and 5.2 are good predictors of the average fiber diameter given the processing parameters. These equations are good considering these equations were created using data from lower MFR resin and resin MFR is a major component in web average fiber diameter.

Relationship Between Average Fiber Diameter and Shot Production

The previous figures have indicated that the average fiber diameter decreases with an increase in die air pressure for a given process temperature. These same figures also indicate that an increase in die air pressure will also cause an increase in shot production for a given process temperature. This decrease in average fiber diameter as die air pressure increases is due to the increased form drag on the filament due to an increase in fiber flapping in the attenuation air stream. This flapping or oscillatory filament motion induces variable aerodynamic forces and would seem to create fibers of varying diameters. As previously stated, recent work has indicated that the production of shot is due in part to filament collisions that create more massive polymer globules which are incapable of solidifying during the

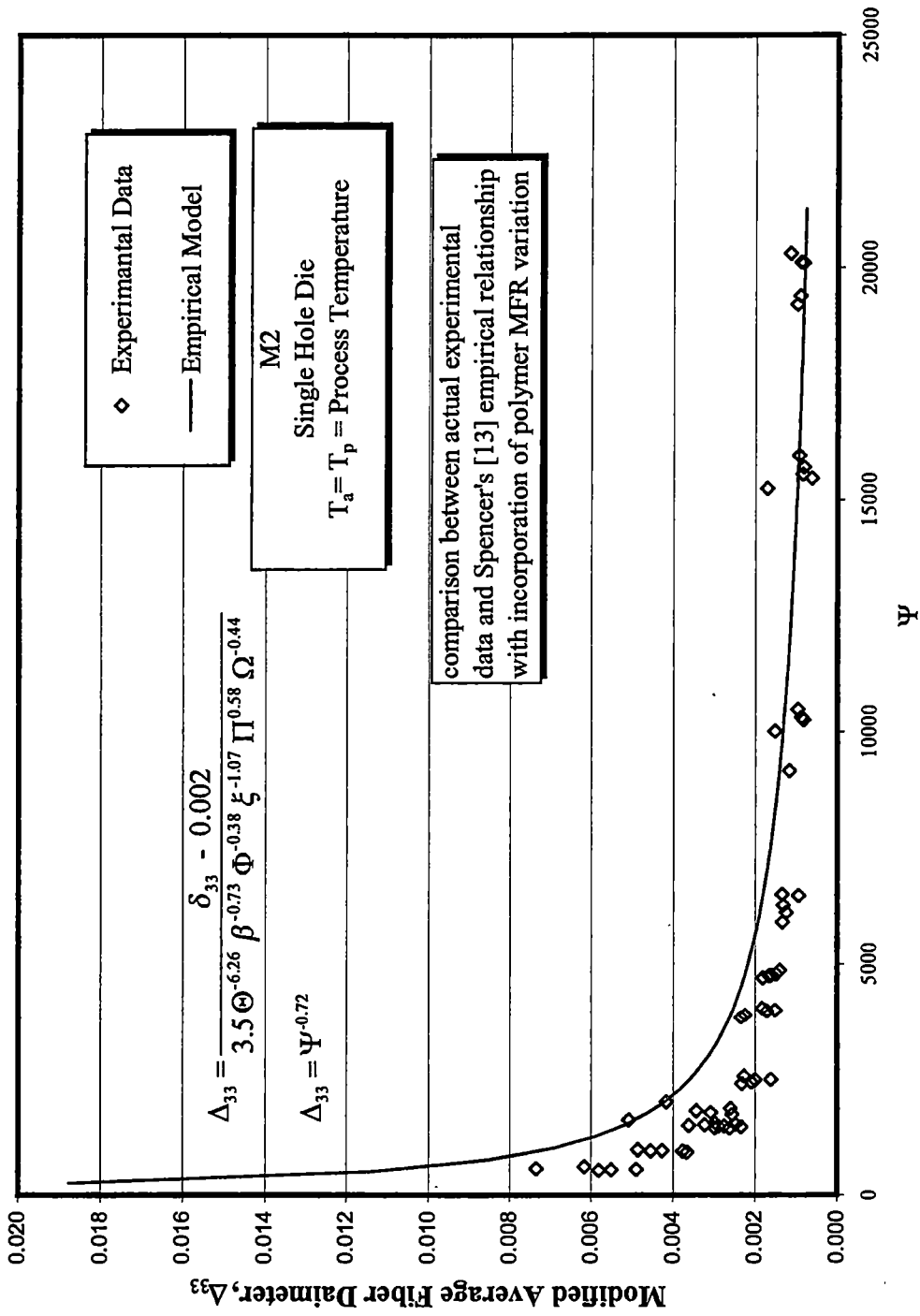


Figure 5.24: Modified average fiber diameter ratio vs. momentum flux ratio (Ψ)

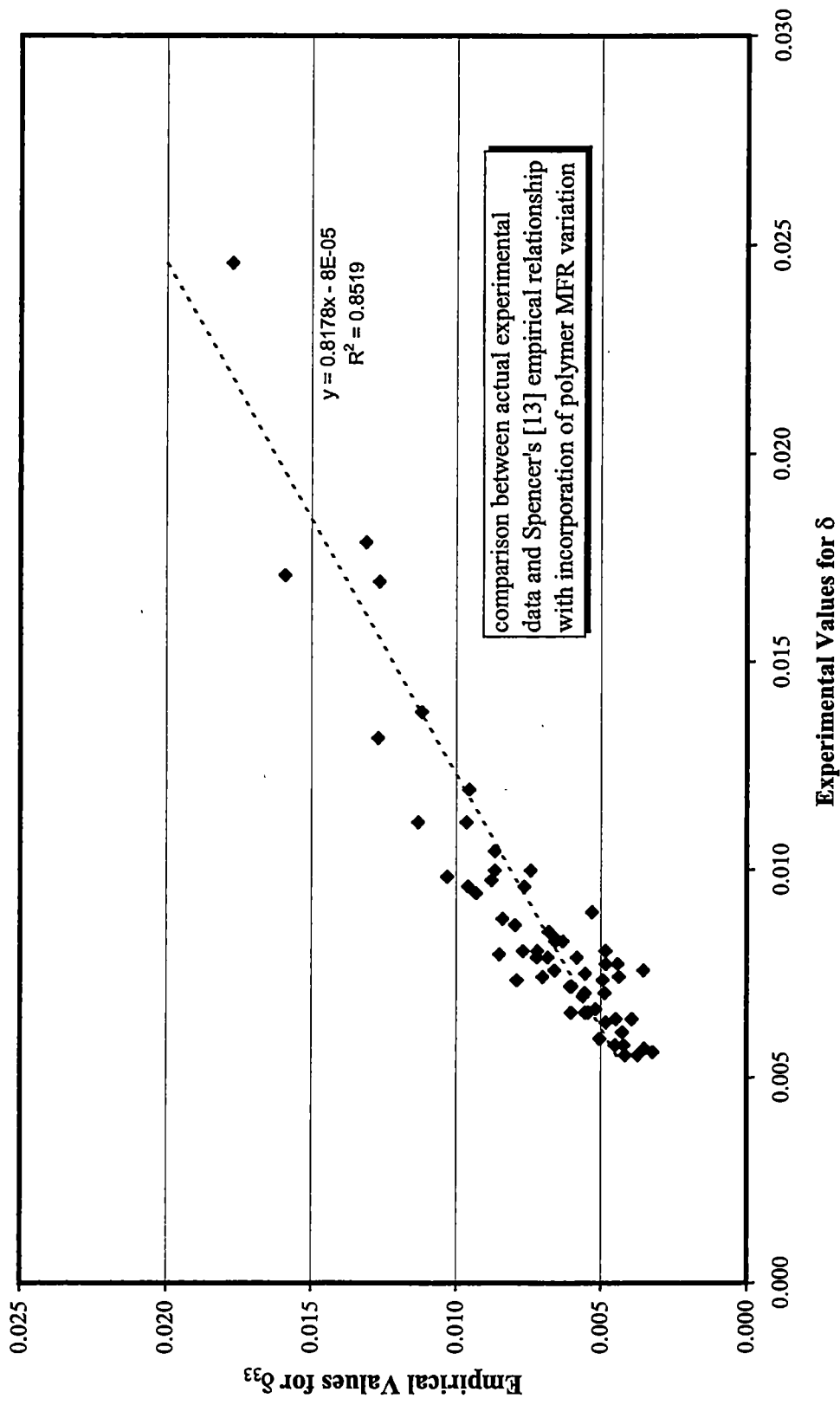


Figure 5.25: Experimental average fiber diameter ratio vs. empirical fiber diameter ratio

attenuation process before impacting the collector. The filament collision theory of shot production is most often applied to multi-hole dies. However, since other investigators have shown that the broken filament theory of shot production is invalid, the filament collision theory is applicable to the single hole die configuration used in this investigation. A single hole die melt blowing line could only have filament fusion if the single filament looped back on itself and fused in a manner shown Figure 5.26. Any fiber that has enough flapping motion to loop back on itself would have a variable aerodynamic form drag applied to the filament. This variable form drag would cause the melt blown web to have variable fiber diameters.

It has been proposed that the source of the single hole shot production is possibly due to the variable aerodynamic form drag of a flapping fiber. It has also been proposed that variable aerodynamic forces are the source of variable fiber diameters in the final web sample. If both these proposals are valid then there could be a relationship between shot production and a parameter that relates to fiber diameter uniformity. The fiber diameter uniformity is represented by the coefficient of variation of the measured fibers. The coefficient of variation is the ratio of the standard deviation to the average fiber diameter [19]. This coefficient was used in order to express the uniformity results on a percentage basis [19]. Figure 5.27 is a plot of number of shot per in² versus average fiber diameter. This figure indicates that, as expected, the same processing parameter values that allow the production of fine fibers also produce shot. Figure 5.28 is a plot of number of shot per in² versus the fiber diameter coefficient of variation. This figure indicates no relationship

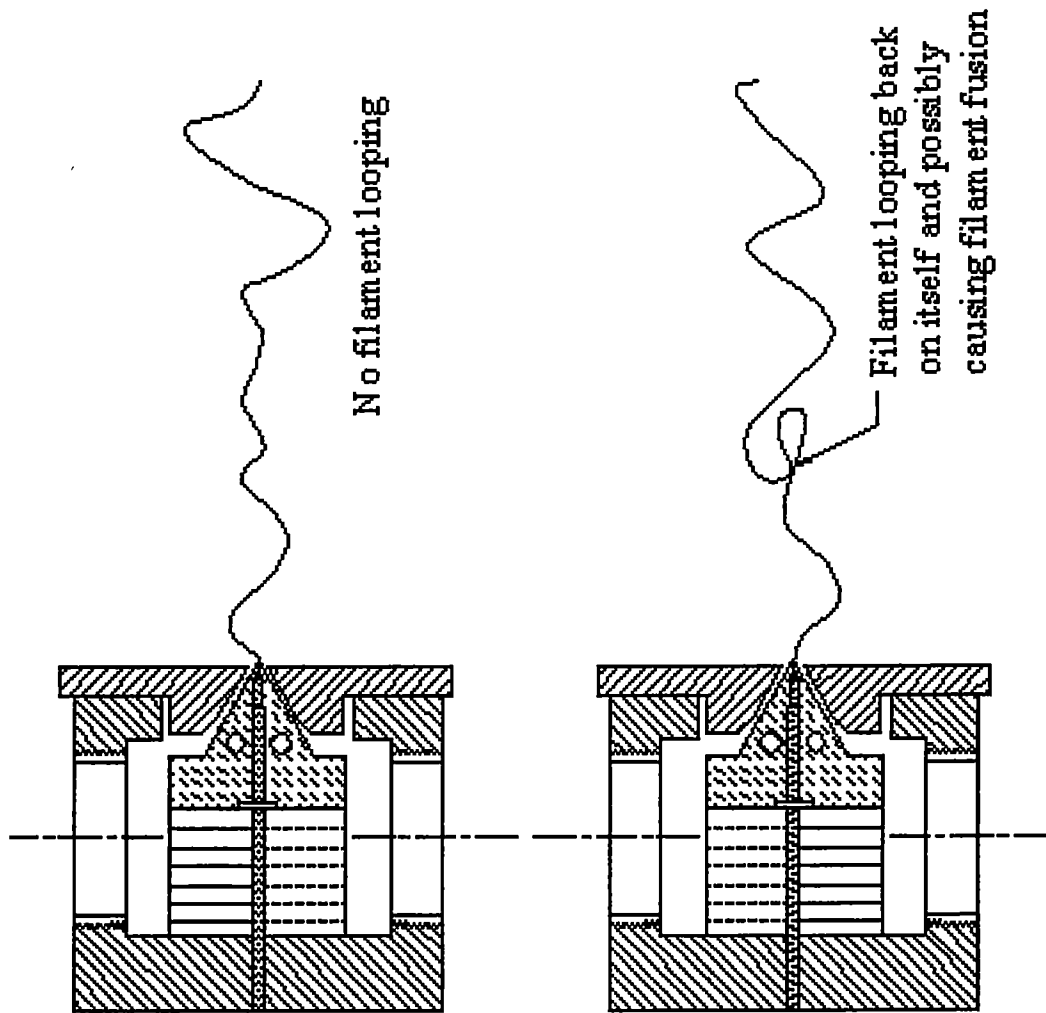


Figure 5.26: Single hole melt blowing line filament flight dynamics

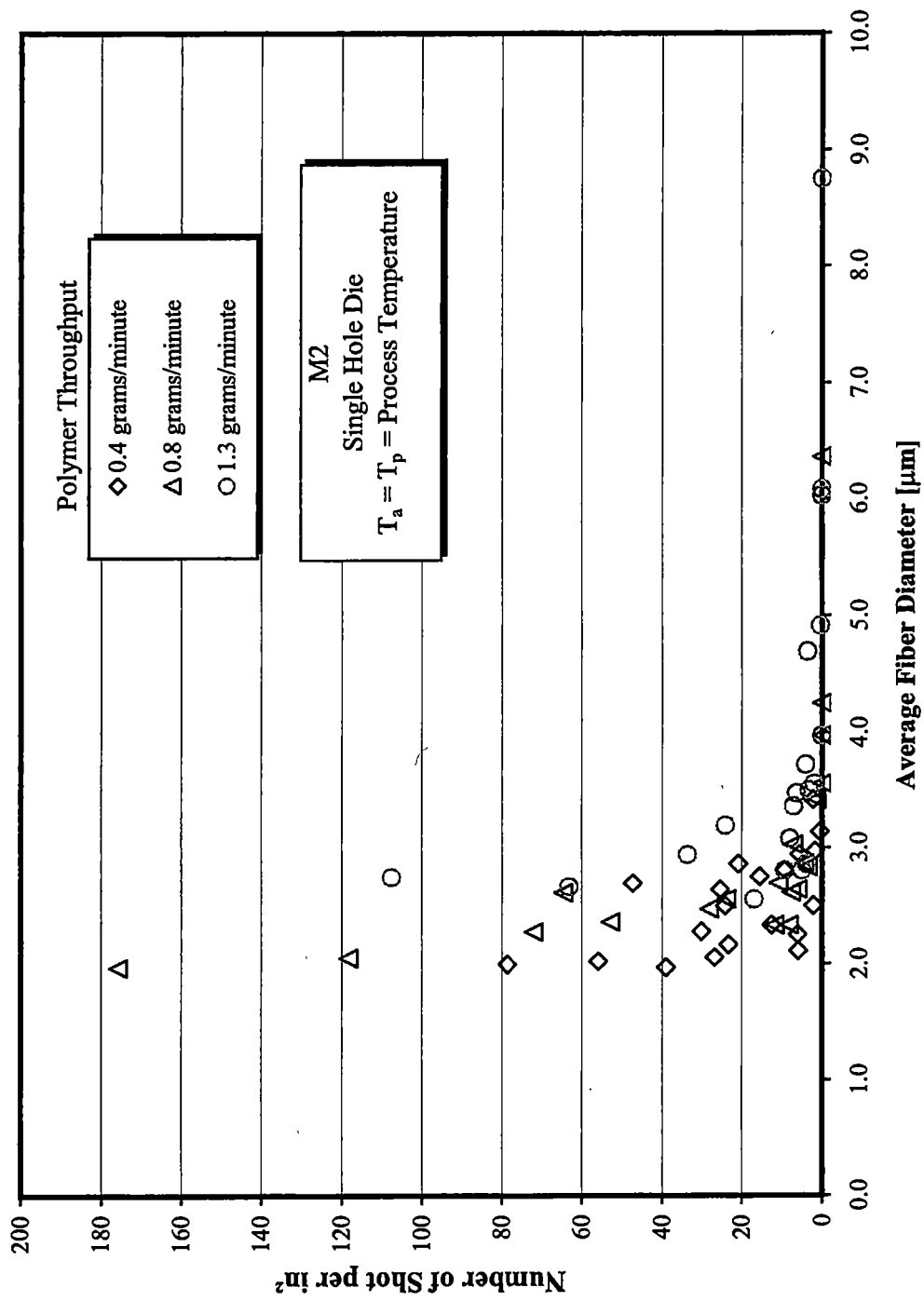


Figure 5.27: Number of shot per in² vs. average fiber diameter

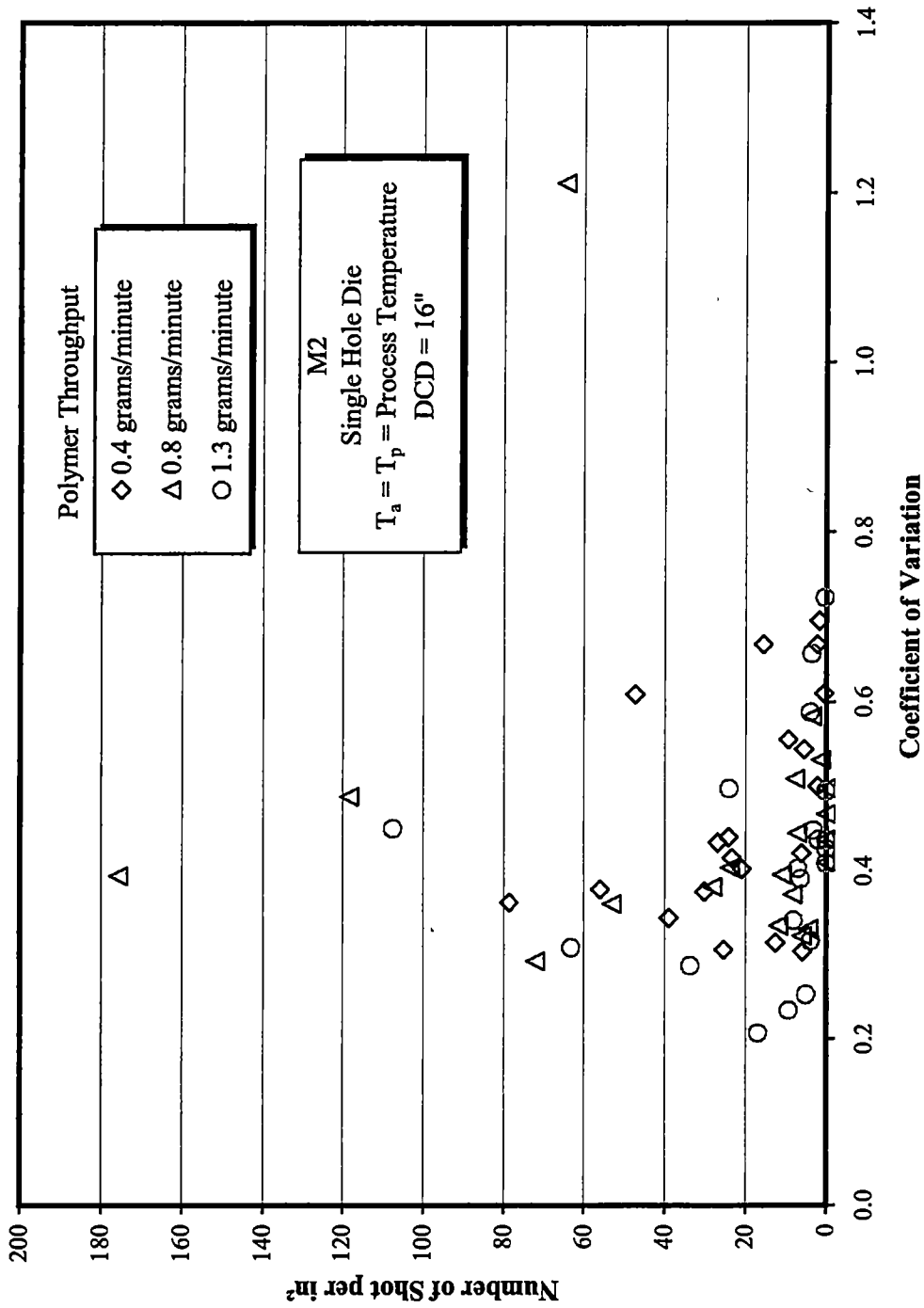


Figure 5.28: Number of shot per in² vs. web fiber diameter coefficient of variation

between shot production and fiber variation. Figure 5.28 is very cluttered since it includes all the M2 resin single hole data. For this reason, Figure 5.28 is broken up and plotted in a manner which might reveal any trends in the data. Figure 5.29, 5.30 and 5.31 are all plots of number of shot per in² versus the fiber diameter coefficient of variation with different symbols for each process temperature for each polymer throughput. These plots indicate that there is no apparent relationship between web fiber uniformity and web shot content. Again, this is troubling since it is generally accepted that the variable aerodynamic forces that induce fiber diameter attenuation are responsible for shot production in a single hole die case.

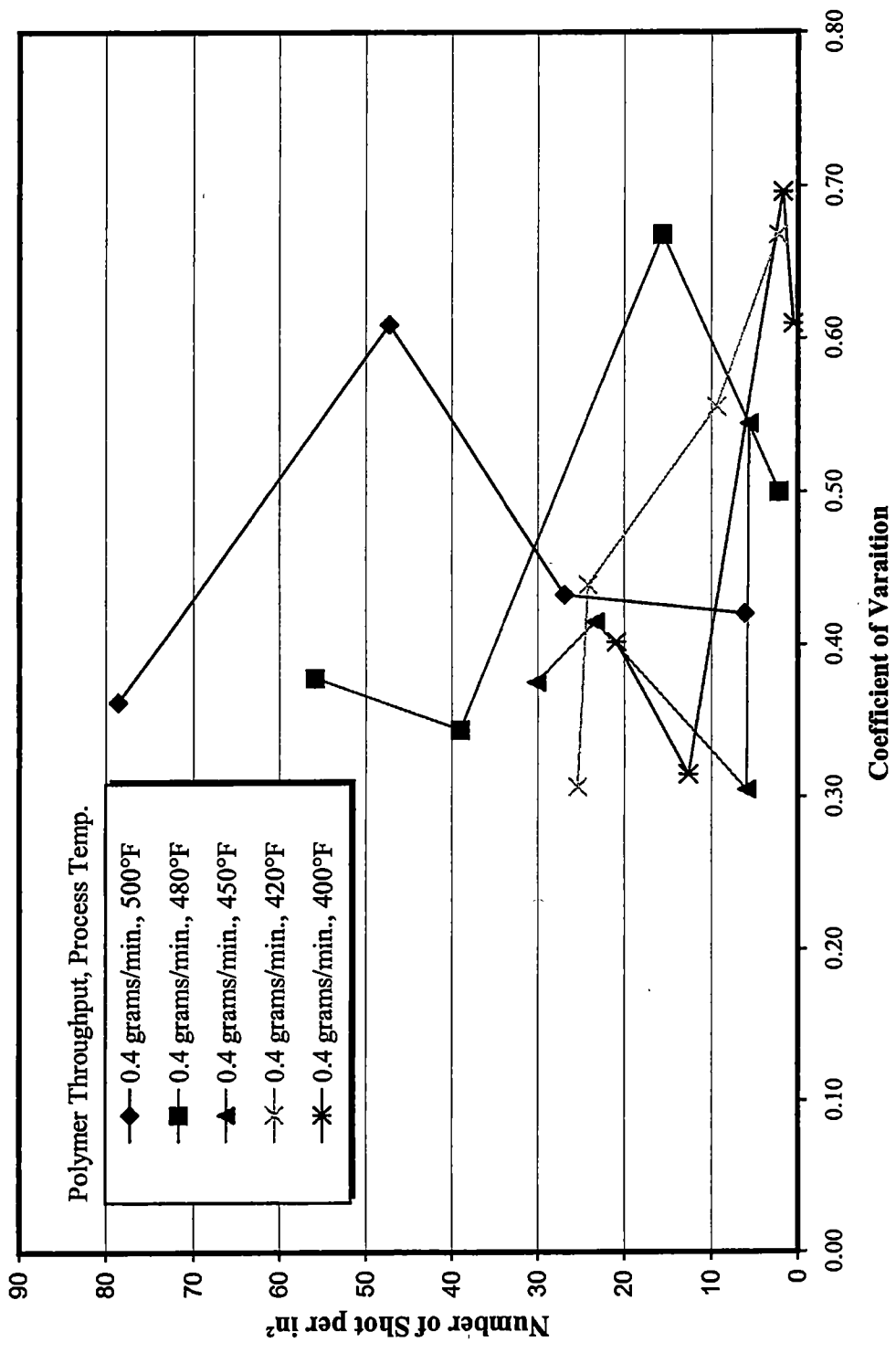


Figure 5.29: Number of shot per in² vs. web fiber diameter coefficient of variation

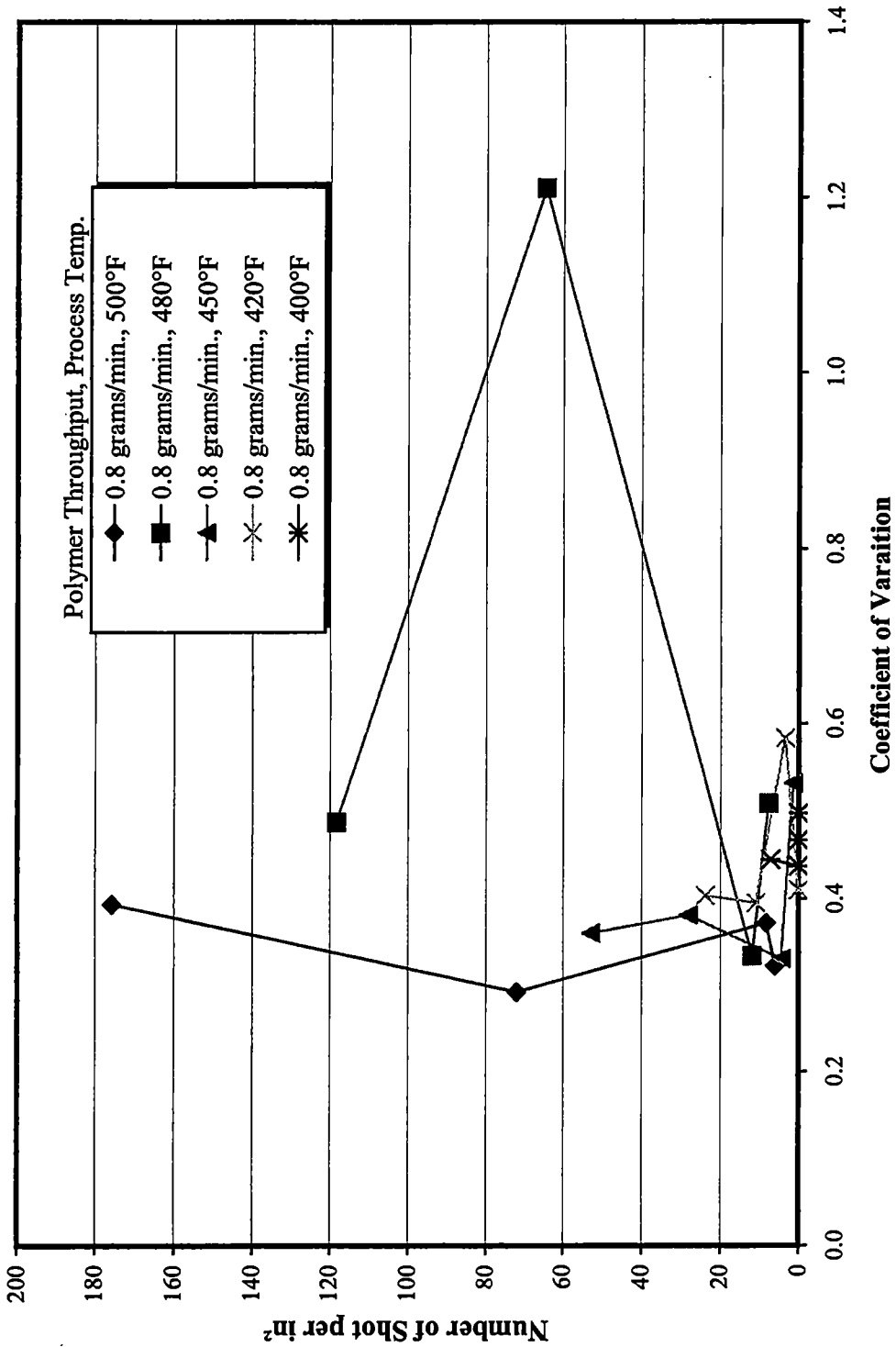


Figure 5.30: Number of shot per in² vs. web fiber diameter coefficient of variation

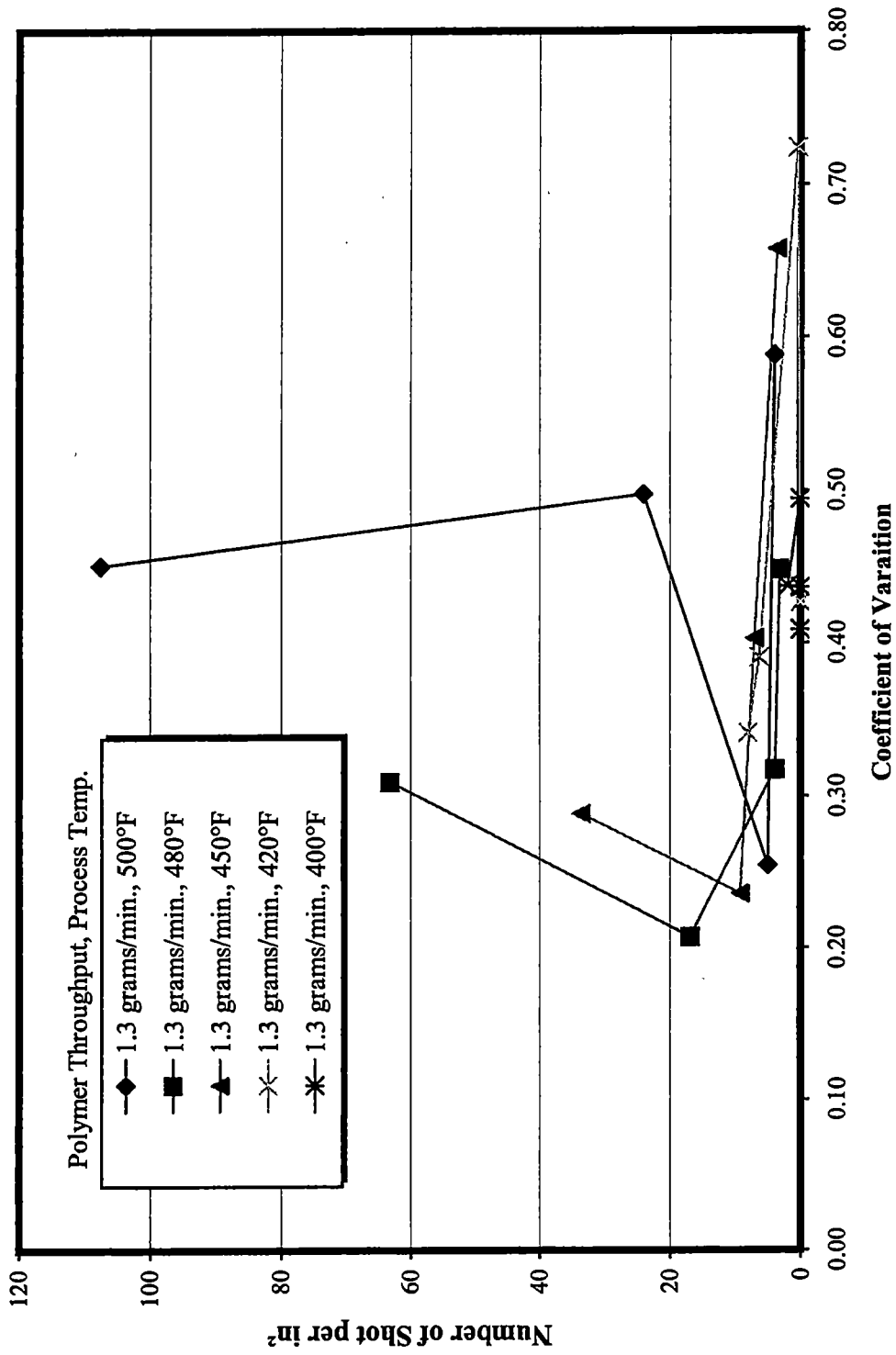


Figure 5.31: Number of shot per in² vs. web fiber diameter coefficient of variation

Chapter VI

Single Hole Shot Production Model

Once the data has been collected and analyzed the next step was to begin the modeling process. This chapter presents the efforts to model the shot production of the single hole die using the data that was presented and discussed in the previous chapter. This is not the first occasion in which researchers have attempted to empirically model a melt blown process. Haynes [16] and Spencer [13] each studied the melt blowing process in order to create an empirical model that could be used to predict the average fiber diameter of a web sample given the processing parameters. Spencer's model was demonstrated in a previous chapter. The shot production model is investigated in the same manner as Haynes and Spencer created their fiber diameter model. It is known from the many figures in Chapter V that a shot model will most likely be nonlinear in nature. The general form of the model is assumed to be of the following nonlinear form:

$$\eta = A + B (C_1)^{e_1} (C_2)^{e_2} (C_3)^{e_3} \dots (C_i)^{e_i} \quad 6.1$$

where:

- η dimensionless number of shot per area ratio
- A constant
- B multiplying constant
- C_i dimensionless variable
- e_i exponent of dimensionless variable

There are numerous dimensionless variables that could be incorporated in the above equation. The use of dimensionless variables was incorporated in order to simplify the constants in Equation 6.1. A list and description of the dimensionless variables that were attempted in this modeling process is provided in Table 6.1. These new variables are simply the experimental shot per in² values and process parameters divided by a corresponding reference value. The number of shot per in² versus processing parameter graphs in Chapter V are then replotted in terms of the new corresponding dimensionless variables. These graphs are represented in Figures 6.1 through 6.10. These dimensionless figures are identical in representing the shot production characteristics of Chapter V's figures regardless of the referenced values used to non dimensionalize the original parameters. A systematic approach to determining the proper model is applied by cycling through the dimensionless variables in Table 6.1 in order to determine if one variable is more dominant than others. This process is trial and error, and many of the variables in Table 6.1 have no influence in the production of shot. However, since this study is the first known attempt at empirically modeling shot production the dimensionless variables that prove to have no influence on shot production may be almost as important as those that do.

Method for Developing the Empirical Model

As previously stated, care was taken to maintain constant processing parameters and limit any human errors in the production and analysis of the melt blown samples. This care was taken in order to optimize the statistical analysis

Table 6.1: List of dimensionless variables

Variable	Expression	Reference Value
β - Polymer Throughput Ratio	$\frac{\dot{m}_p}{(\dot{m}_p)_{ref}}$	0.8 $\left[\frac{\text{grams}}{\text{minute}} \right]$
Γ - Air to Polymer Mass Flux Ratio	$\frac{\dot{m}_a/A_e}{\dot{m}_p/A_{die}}$	Not Applicable
Φ - Die Air Pressure Ratio	$\frac{P_d + P_{atm}}{P_{ref} + P_{atm}}$	5 [psig]
η - Number of Shot per Area Ratio	$\frac{NOS \text{ per Area}}{(NOS \text{ per Area})_{ref}}$	Number of Shot per Area at Reference Conditions
θ - Process Temperature Ratio	$\frac{T_p}{(T_p)_{ref}}$	480°F = 940°R
Ψ - air polymer momentum ratio ratio	$\frac{\dot{m}_a V_{air}/A_e}{\dot{m}_p V_p/A_{die}}$	Not Applicable
Λ - Air Velocity Ratio	$\frac{V_{air}}{V_{ref}}$	Air Velocity at Reference Conditions

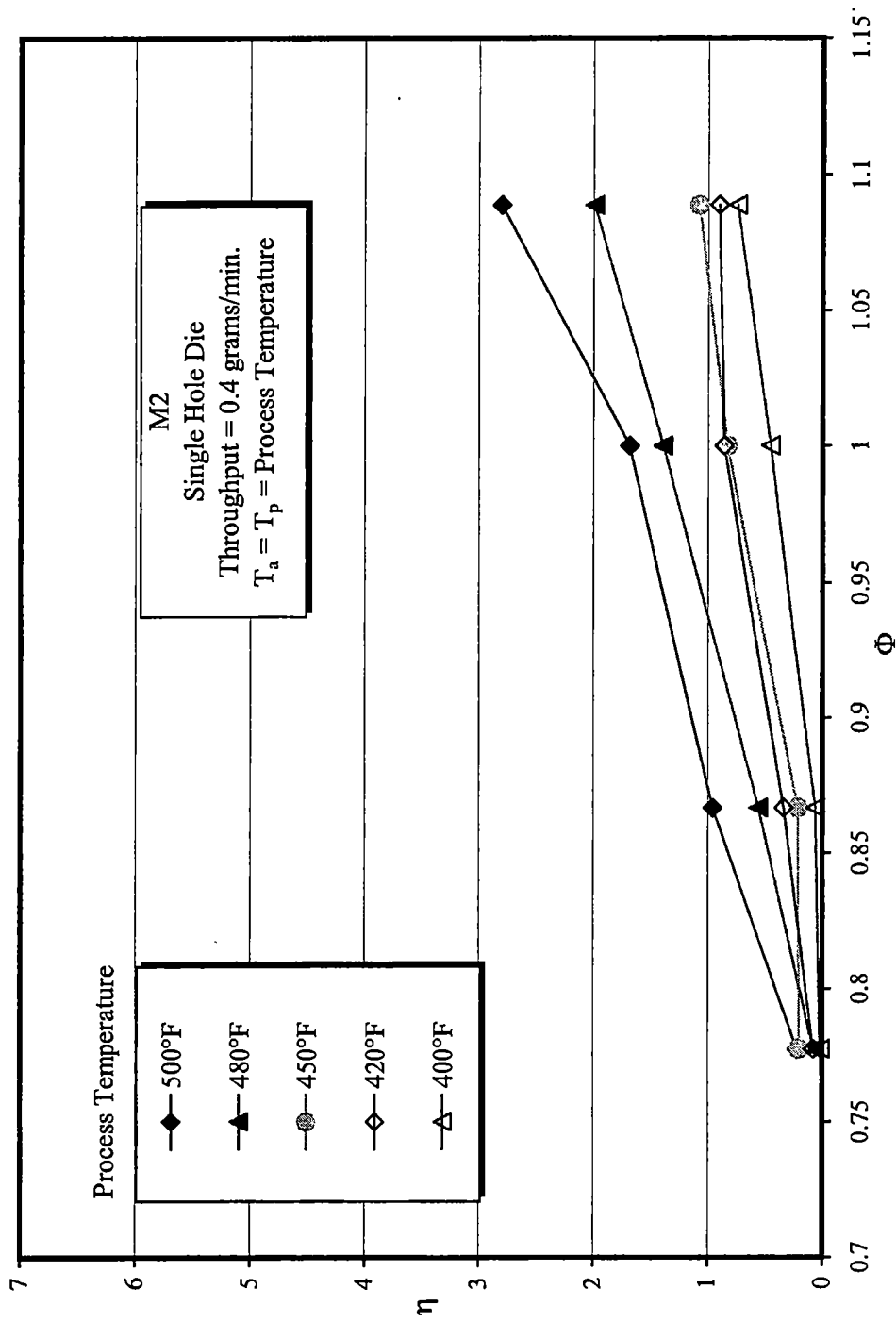


Figure 6.1: Number of shot per area ratio vs. die air pressure ratio

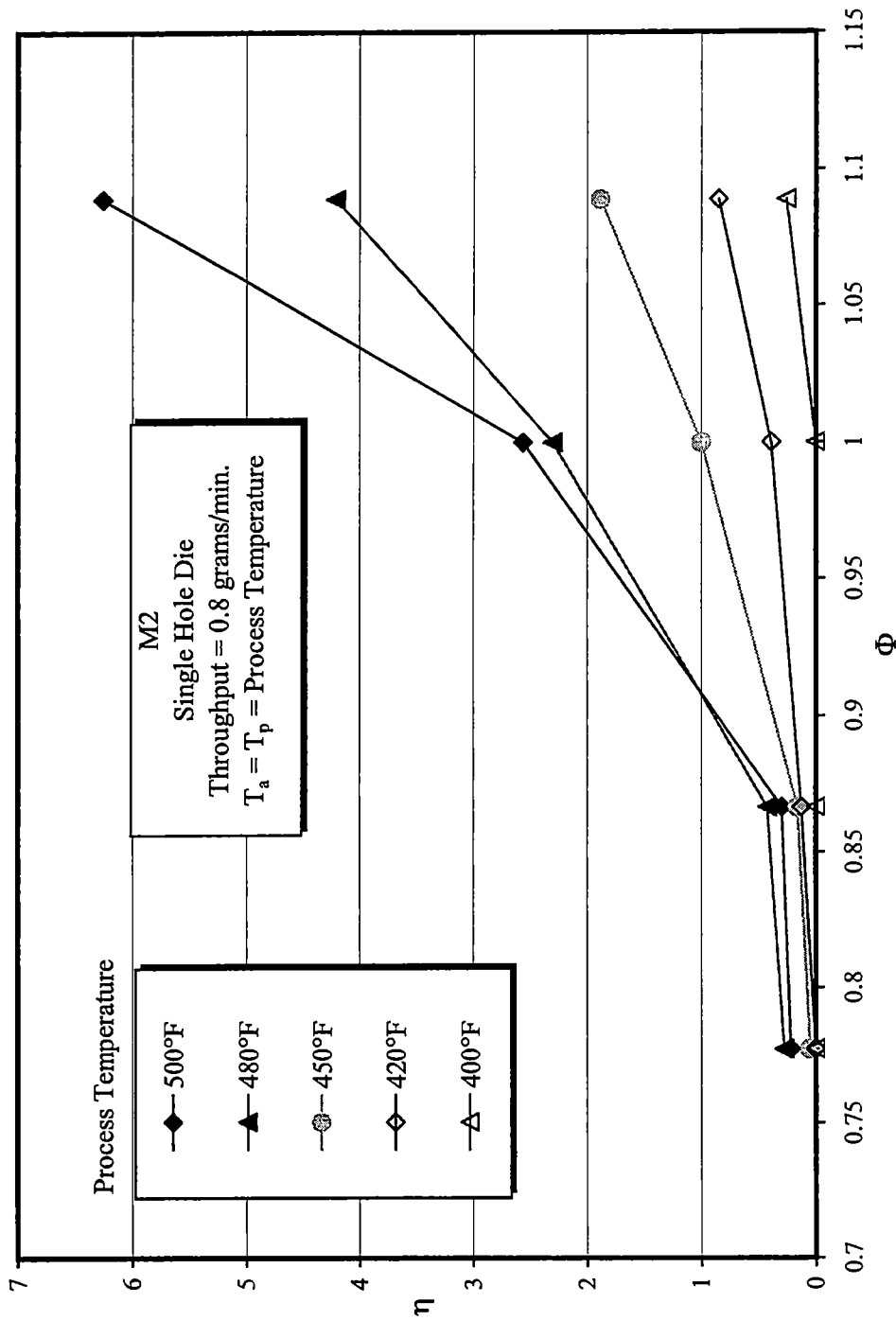


Figure 6.2: Number of shot per area ratio vs. die air pressure ratio

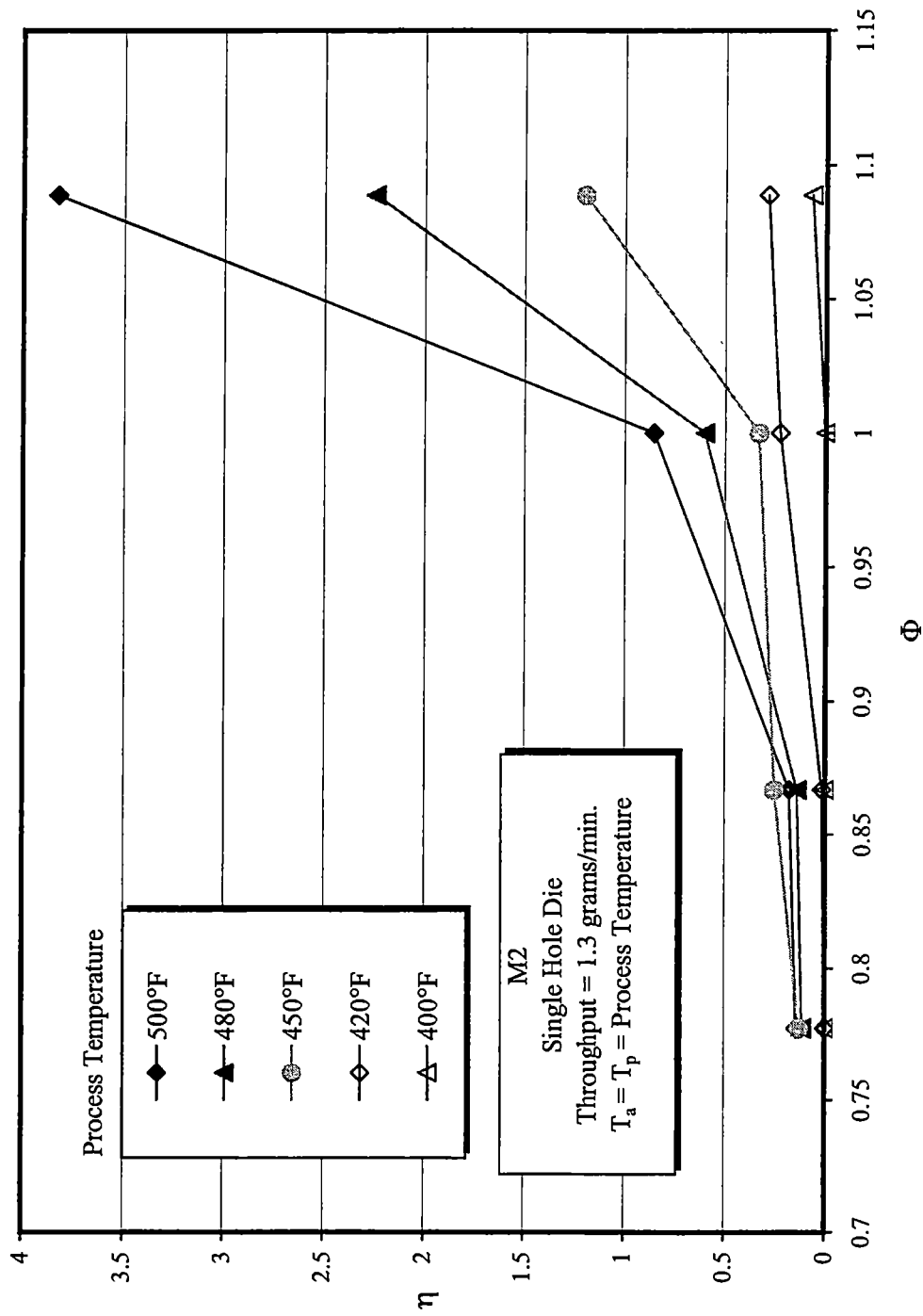


Figure 6.3: Number of shot per area ratio vs. die air pressure ratio

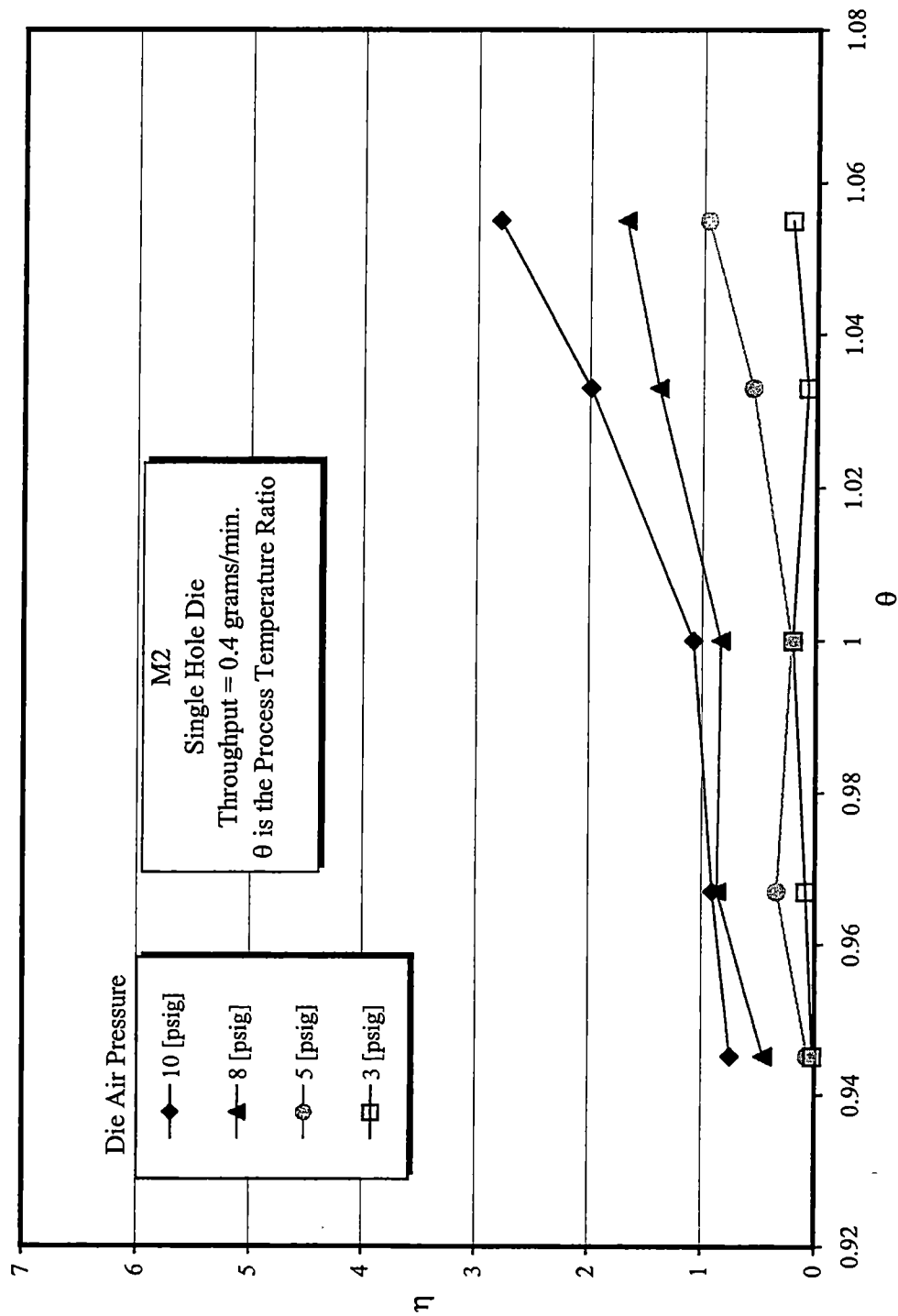


Figure 6.4: Number of shot per area ratio vs. process temperature ratio

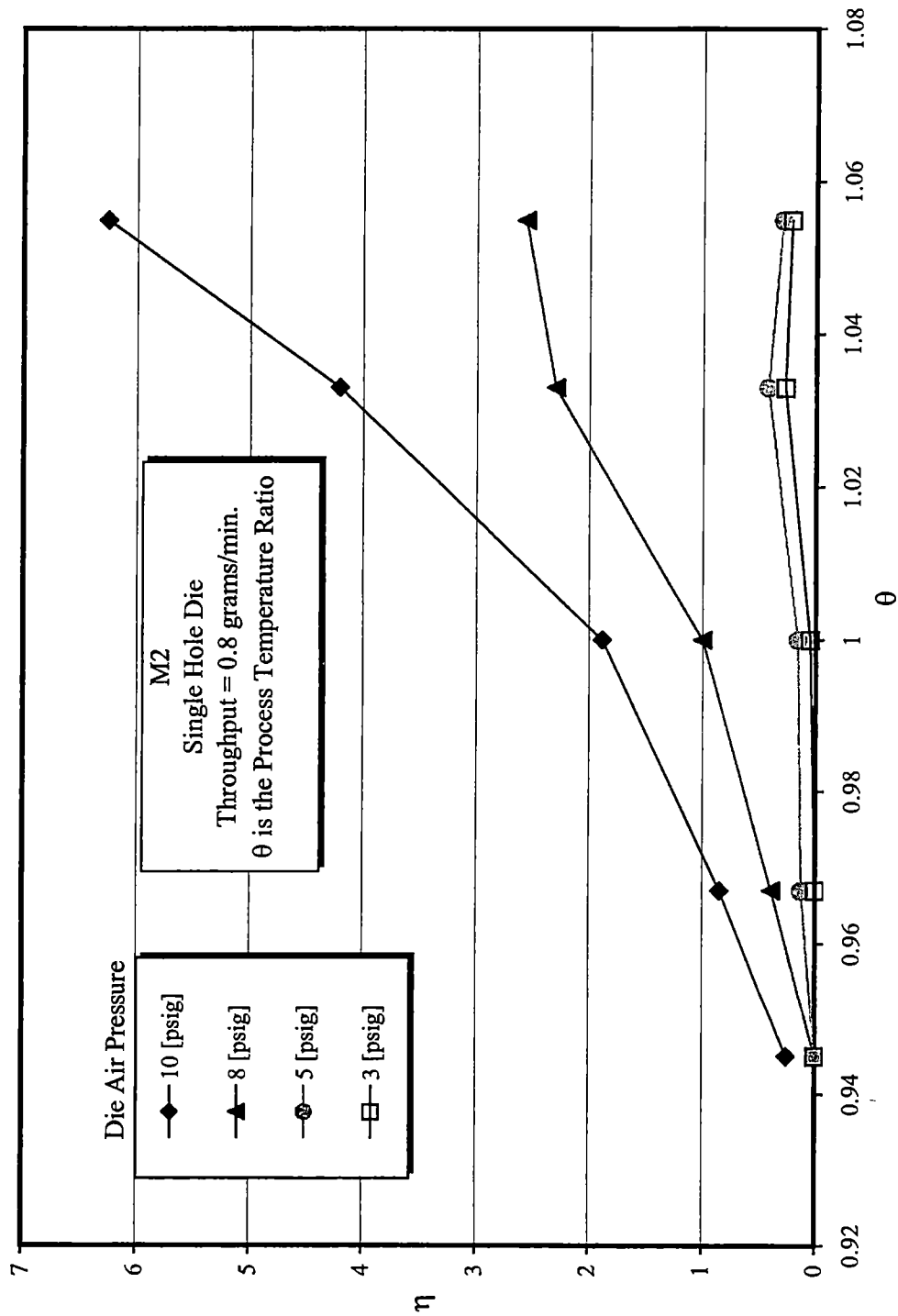


Figure 6.5: Number of shot per area ratio vs. process temperature ratio

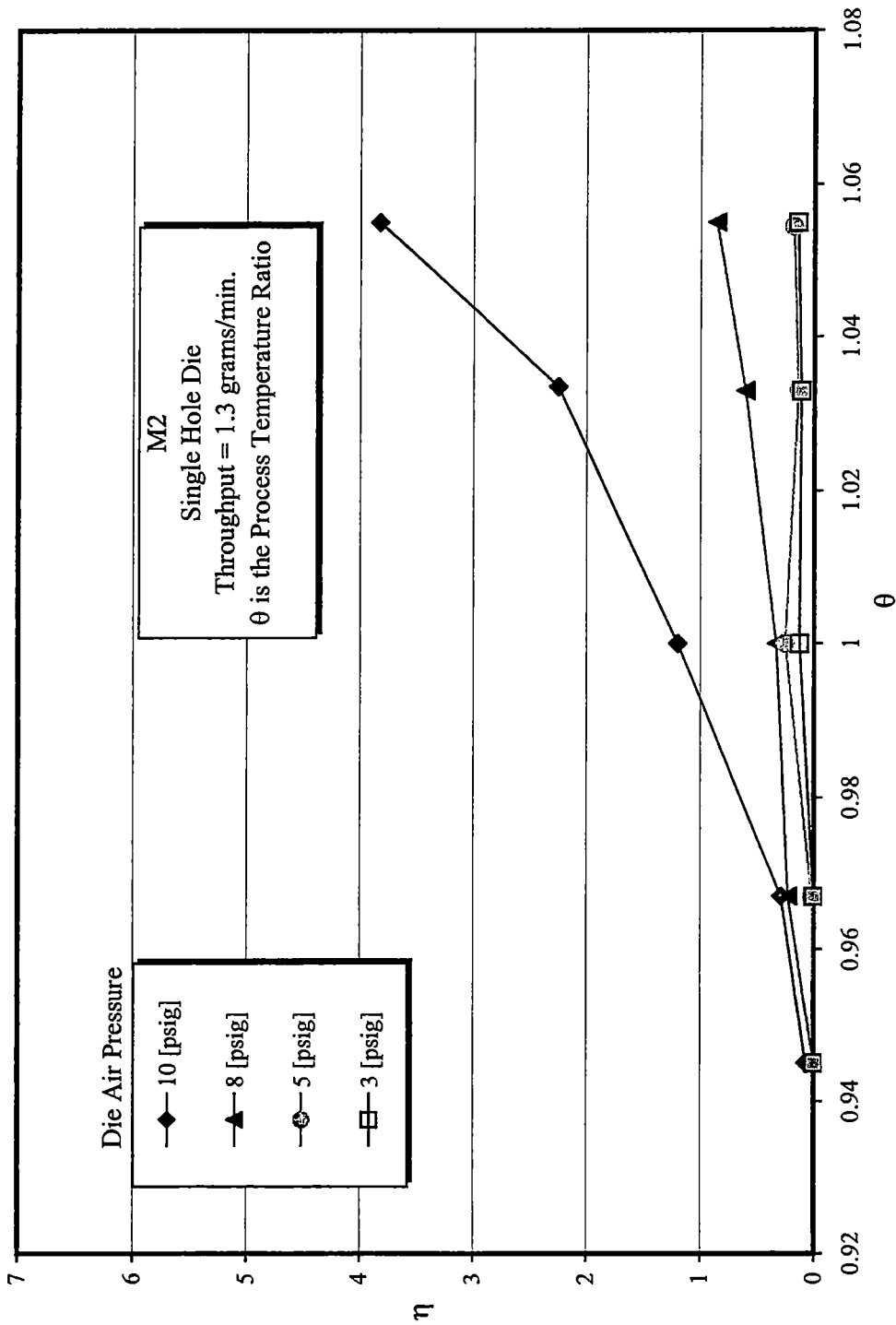


Figure 6.6: Number of shot per area ratio vs. process temperature ratio

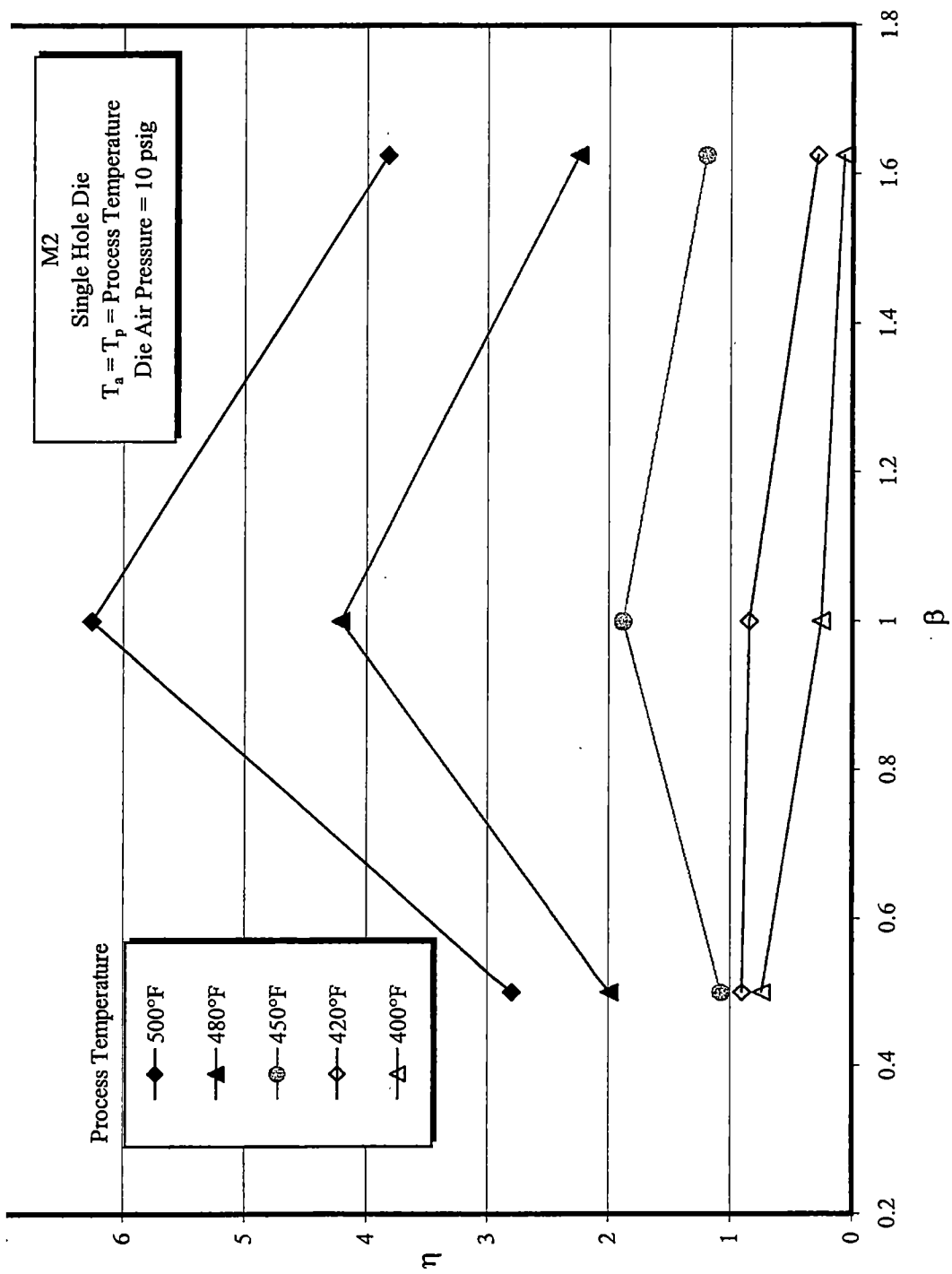


Figure 6.7: Number of shot per area ratio vs. polymer throughput ratio

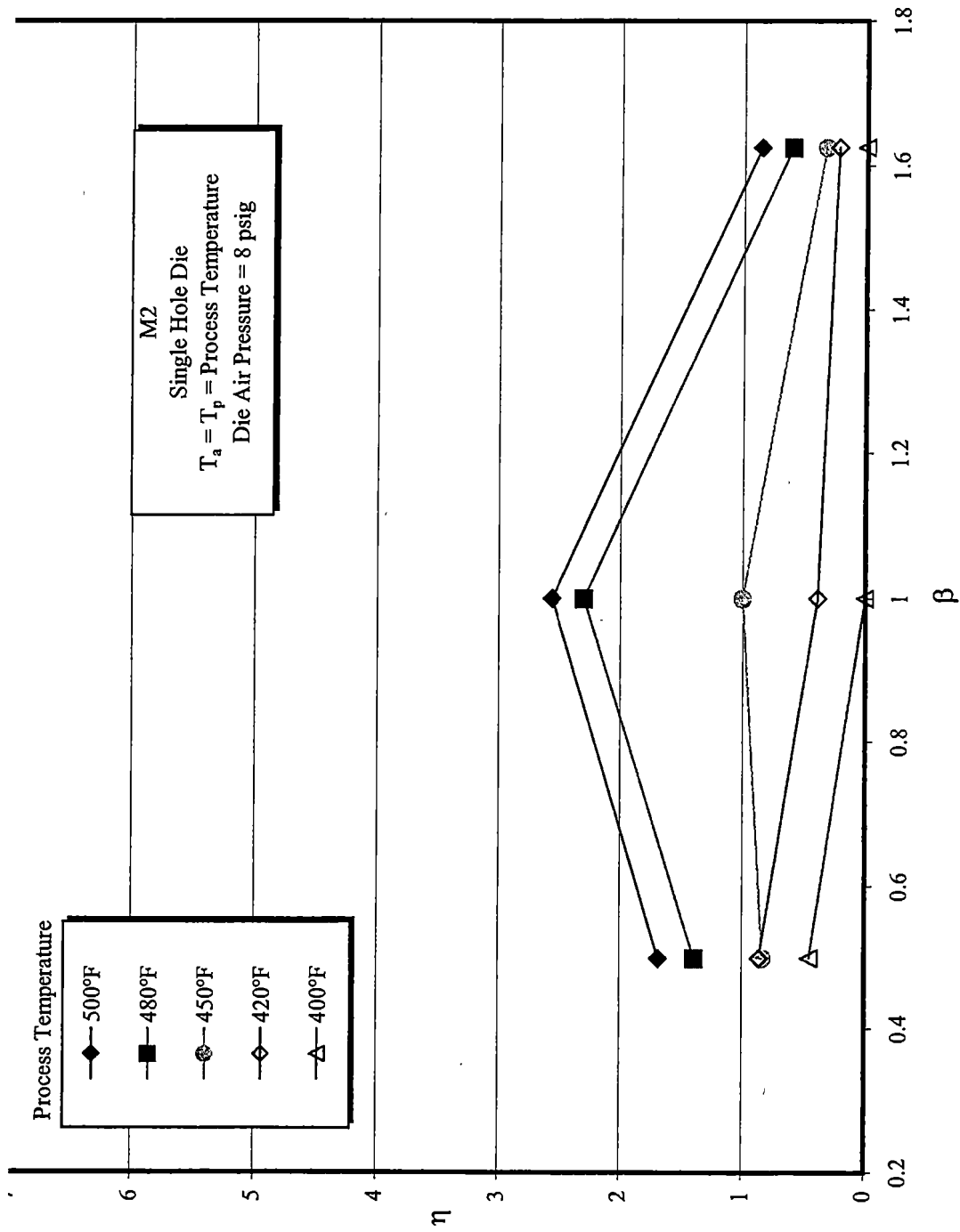


Figure 6.8: Number of shot per area ratio vs. polymer throughput ratio

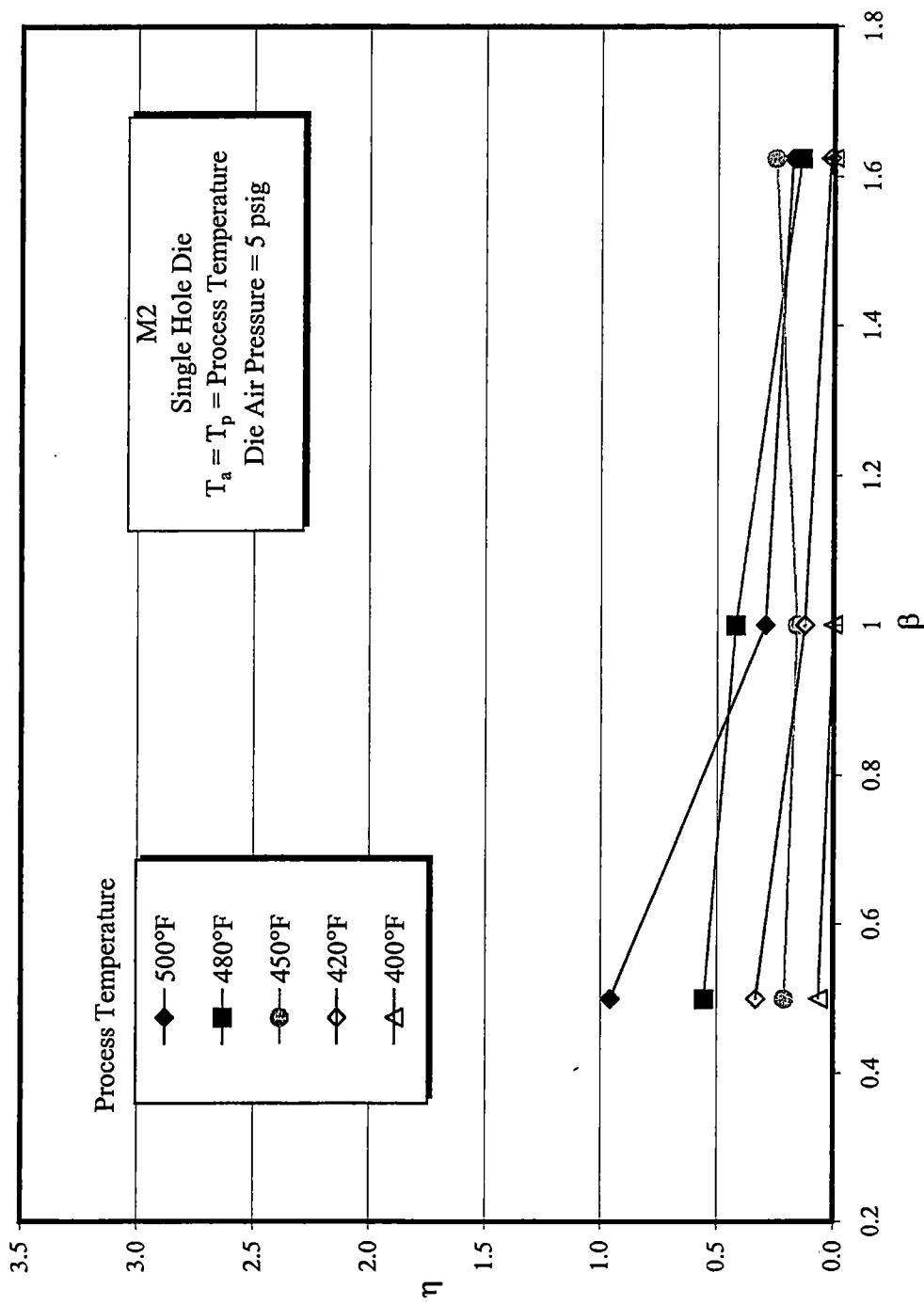


Figure 6.9: Number of shot per area ratio vs. polymer throughput ratio

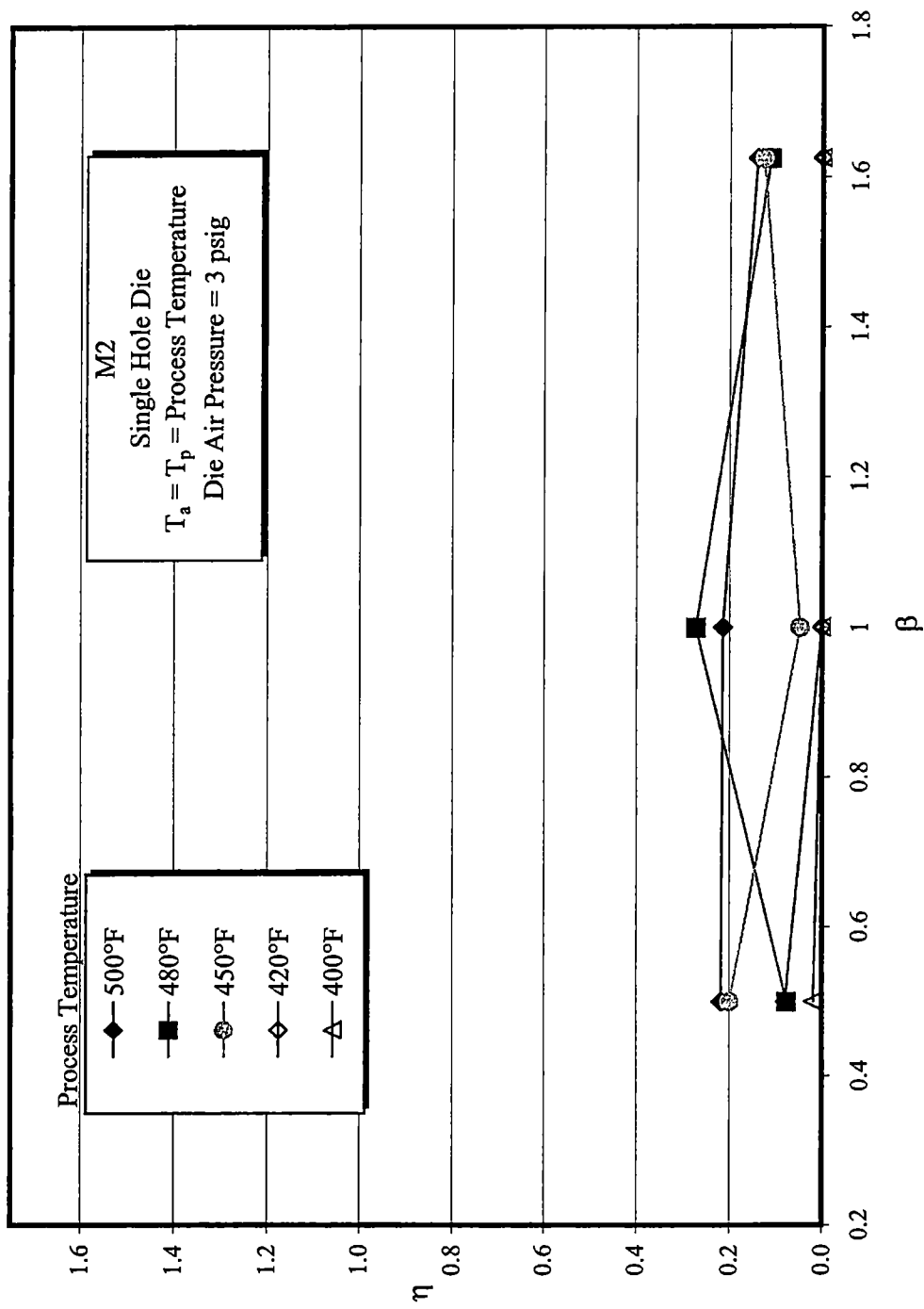


Figure 6.10: Number of shot per area ratio vs. polymer throughput ratio

regression procedure used to create the empirical model. The empirical model is determined by use of a statistical analysis software package. The software used in this effort is SPSS[®] version 8.0. This statistical package predicts the values of the constants and exponents of Equation 6.1 using nonlinear regression techniques. The most difficult part of this procedure is inputting the experimental data into the SPSS program. However, this program is Microsoft Windows[®] based and since proper care was taken in the spreadsheet setup, the data can be directly imported into the SPSS program. With the data in the program, an expression similar to Equation 6.1 is entered. The only other requirement before the analysis can begin is an initial guess for each of the constants and exponents. Figure 6.11 is an example of the SPSS nonlinear model input screen and Figure 6.12 is an example of the SPSS nonlinear model constant initial guess input screen. A sample output from the SPSS non-linear regression is shown in Figure 6.13.

Upon completion of a regression analysis, the program returns the predicted values for the constants and exponents. The program's output also includes the predicted values from the calculated empirical model and the coefficient of regression (R^2). This R^2 term indicates how good of an empirical model the statistical analysis has produced. The R^2 term varies between zero and one, where $R^2 = 1$ is a perfect model. Another piece of information the output provides, is the Asymptotic 95% Confidence Level for the constants. This simply means that the values for A, B, and e_i have a 95% probability of being between the upper and lower levels provided. The magnitude of the difference between the upper and lower level of the Asymptotic

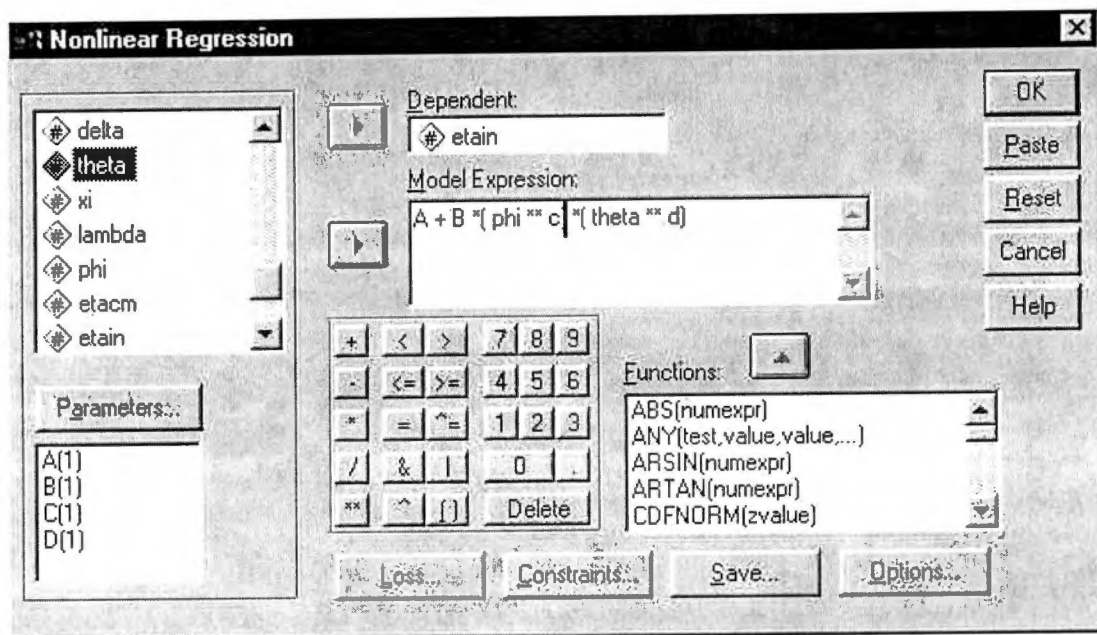


Figure 6.11: Non-linear regression model input window

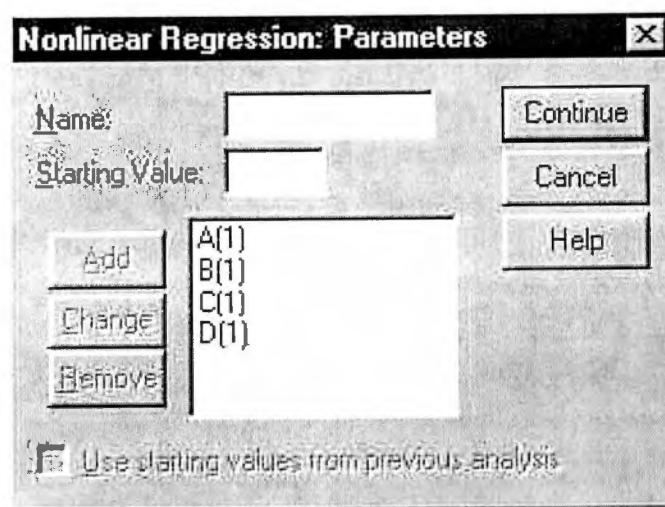


Figure 6.12: Non-linear model constant initial guess window

Non-linear Regression of 3925_spss_1.sav

All the derivatives will be calculated numerically.

The following new variables are being created:

Name	Label
PRED_	Predicted Values

Iteration	Residual SS	A	B	C	D
1	171.7584316	1.00000000	1.00000000	1.00000000	1.00000000
1.1	3186.150923	8.58234842	-8.0222371	12.5891373	14.1951316
1.2	14.55648840	.688724748	-.23821134	2.79459102	4.65319961
~	~	~	~	~	~
12.1	.3731433273	.005547780	.677444248	9.73281919	20.7354464
13	.3731433273	.005547780	.677444248	9.73281919	20.7354464
13.1	.3731433263	.005548968	.677442746	9.73327785	20.7349118

Run stopped after 30 model evaluations and 13 derivative evaluations. Iterations have been stopped because the relative reduction between successive residual sums of squares is at most SSCON = 1.000E-08

Nonlinear Regression Summary Statistics Dependent Variable ETAIN

Source	DF	Sum of Squares	Mean Square
Regression	4	2.67818	.66955
Residual	56	.37314	6.663274E-03
Uncorrected Total	60	3.05133	

(Corrected Total) 59 2.10080

R squared = 1 - Residual SS / Corrected SS = .82238

Parameter	Estimate	Asymptotic Std. Error	Asymptotic 95 % Confidence Interval	
			Lower	Upper
A	.005548968	.019418972	-.033351907	.044449843
B	.677442746	.043294654	.590713133	.764172360
C	9.733277851	1.697269902	6.333237672	13.133318030
D	20.734911844	3.171178686	14.382277574	27.087546114

Asymptotic Correlation Matrix of the Parameter Estimates

	A	B	C	D
A	1.0000	-.2288	.6457	.5933
B	-.2288	1.0000	.1009	.2357
C	.6457	.1009	1.0000	.3825
D	.5933	.2357	.3825	1.0000

Figure 6.13: SPSS non-linear regression output

95% Confidence Level indicates the uncertainty in the regression's coefficient values. If the upper and lower levels of the Asymptotic 95% Confidence Level bound zero then the coefficient might be zero and that term would become insignificant in the empirical model. Therefore, the upper and lower level of the Asymptotic 95% Confidence Level for the constant must not contain zero for the constant to be considered important.

Single Variable Empirical Model

As previously stated a systematic approach to determining the best model was employed by analyzing Equation 6.1 with each dimensionless variable from Table 6.1 in order to determine if one variable is more dominant than the others. The results from this single variable cycle proved to be mixed and are provided in Equations 6.2 through 6.7.

$$\eta_1 = -889.996 + 890.772 \beta^{-0.0001818} \quad 6.2$$

$$(R^2 = 0.00448)$$

$$\eta_2 = -2023.689 + 2024.092 \Gamma^{0.0003061} \quad 6.3$$

$$(R^2 = 0.08366)$$

$$\eta_3 = 0.00056 + 0.894212 \Phi^{8.879518} \quad 6.4$$

$$(R^2 = 0.36991)$$

$$\eta_4 = -0.22806 + 0.867268 \Theta^{14.69899} \quad 6.5$$

$$(R^2 = 0.23337)$$

$$\eta_5 = -77.8894 + 76.1967 \Psi^{0.003945} \quad 6.6$$

$$(R^2 = 0.08170)$$

$$\eta_6 = 0.09501 + 0.74745 \Lambda^{10.30078} \quad 6.7$$

$$(R^2 = 0.57293)$$

Equations 6.2 through 6.6 all have constants (A_i , B_i and e_i) that bound zero in the Asymptotic 95% Confidence Level and therefore these equations are undesirable for model construction regardless of their R^2 value. Equation 6.7 has the highest R^2 value of any of the single variable models and also has B_i and e_i values that do not include zero. Equation 6.7's " A_i " constant is bounded by zero and therefore the non-linear model that best utilizes the single variable Λ is the following:

$$\eta_7 = 0.8453 \Lambda^{9.601} \quad 6.8$$

$$(R^2 = 0.57028)$$

It was shown in Figure 5.2 that die air pressure and air velocity are linearly related and therefore the non similar results of Equations 6.4 and 6.8 is slightly surprising. The most notable difference between the air velocity and the die air pressure variables is that air velocity calculations incorporate the air temperature. Since the air

temperature is the same as the polymer temperature throughout the experimental data, the air velocity variable, Λ , incorporates the polymer temperature effects to a slight degree. The importance of the velocity variable, Λ , above the other single variables hints at the need for a multiple variable empirical model.

Multiple Variable Empirical Model

Even without the single variable lambda data shown in the previous section the logic in using a multiple variable empirical model had been discussed. As previously discussed, the mechanism for shot production has been believed to be the collision of molten fibers in flight and or the breaking of molten fibers in flight. Regardless of which mechanism one prescribes the dominant forces involved in these situations are very similar. The aerodynamic forces acting on the fiber itself are instrumental in either looping the fiber into itself to cause a self-fiber collision or by inducing enough axial force to break the molten fiber. The counterpart to the aerodynamic forces acting in the fiber is the elastic force of the fiber itself. The aerodynamic forces must overwhelm the elastic forces in order to cause self-fiber collisions or axial fiber failure. The dominant parameter in the aerodynamic force is the velocity and the dominant parameter in the elastic force of the fiber is the polymer temperature. With this in mind, one should construct an empirical model that contains the polymer temperature effects and air velocity effects. Since the air and polymer temperature are identical and the air velocity is primarily composed of the die pressure and air temperature with the die exit area being held constant, the following model should incorporate all the necessary variables for now.

$$\eta_8 = A + B (\Phi^c) (\Theta^d) \quad 6.9$$

Once the SPSS regression was completed the constant "A" proved to be unnecessary due to its inclusion of zero in the Asymptotic 95% Confidence Level. The result of the non-linear regression is shown in Equation 6.10.

$$\eta_9 = 0.64745 (\Phi^{9.4116}) (\Theta^{20.20512}) \quad 6.10$$

$$(R^2 = 0.82213)$$

Equation 6.10 represents the best results obtained up to this point. As stated in Chapter III, the shot production results for the lower process temperatures and die air pressures are the judgement of the experimenter since the confidence level of the WebPro results is low. With this in mind, these processing conditions were removed from the sample and another non-linear regression was performed and the results are provided below:

$$\eta_{10} = 0.5438 (\Phi^{9.49745}) (\Theta^{19.64098}) \quad 6.11$$

$$(R^2 = 0.799)$$

Equation 6.11 is essentially the same as Equation 6.10. This means that the exclusion of the lower processing conditions data makes little difference and therefore Equation 6.10 will be used. Figure 6.14 is a plot of η_9 versus $\eta_{\text{experimental}}$ and indicates the variation in the empirical model. The variation in the data and the slope of the data points could be due to the lack of a polymer throughput variable in the empirical relationship. Figures 6.7 through 6.10 indicate that the effect of the polymer throughput is most likely not a power relationship. The majority of the curves in these figures indicate that the polymer throughput variable (β) is a quadratic

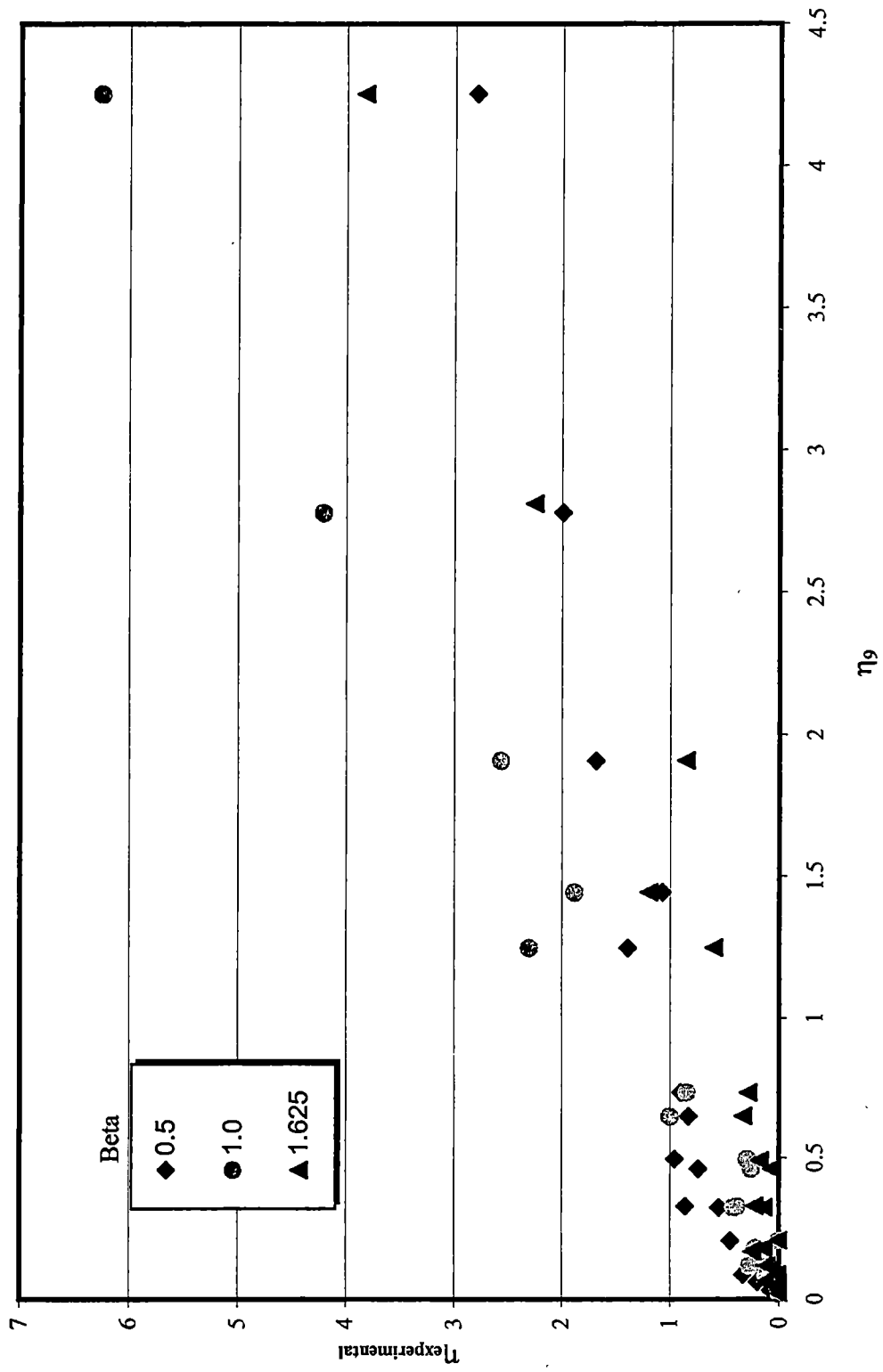


Figure 6.14: Experimental number of shot per area ratio vs. empirical number of shot per area ratio

relationship. In order to determine the effect of the polymer throughput the following modified shot ratio relationship was created. This equation was then analyzed using the same regression techniques as before.

$$H_s = \frac{\eta}{\eta_0} = A\beta^2 + B\beta + C \quad 6.12$$

Once the non-linear regression was performed Equation 6.12 proved not to model the experimental data properly. The value of the modified shot ratio "H" in the above equation has many values where the right side of Equation 6.12 has only three values since the polymer throughput was 0.4, 0.8 or 1.3 grams/minute. With the non-linear regression investigated it was decided to plot the value of "H" versus β in the same manner as Figures 6.7 through 6.10. These figures are shown in Figures 6.15 through 6.18 with trendlines and trendline equations applied to the pertinent curves. For the most part the 500°F, 480°F and 450°F curves are very similar for Figure 6.15, 6.16 and 6.17 which correspond to die pressures of 10 psig, 8 psig, and 5 psig respectively. The entire purpose of these figures is to determine if the shot data would collapse into a single curve and allow for the polymer throughput to be incorporated into the empirical model of Equation 6.10. Since these curves do not collapse into a single curve a trial and error method was employed to determine if one of the similar curves mentioned above would successfully model the polymer throughput variations in the empirical model. The selection of curves to model the polymer throughput was limited to the figures mentioned above as having similar curves. Another factor in the curve selection was the desire not to select a curve from the extreme process parameter conditions. With this in mind the curve that was selected to attempt to

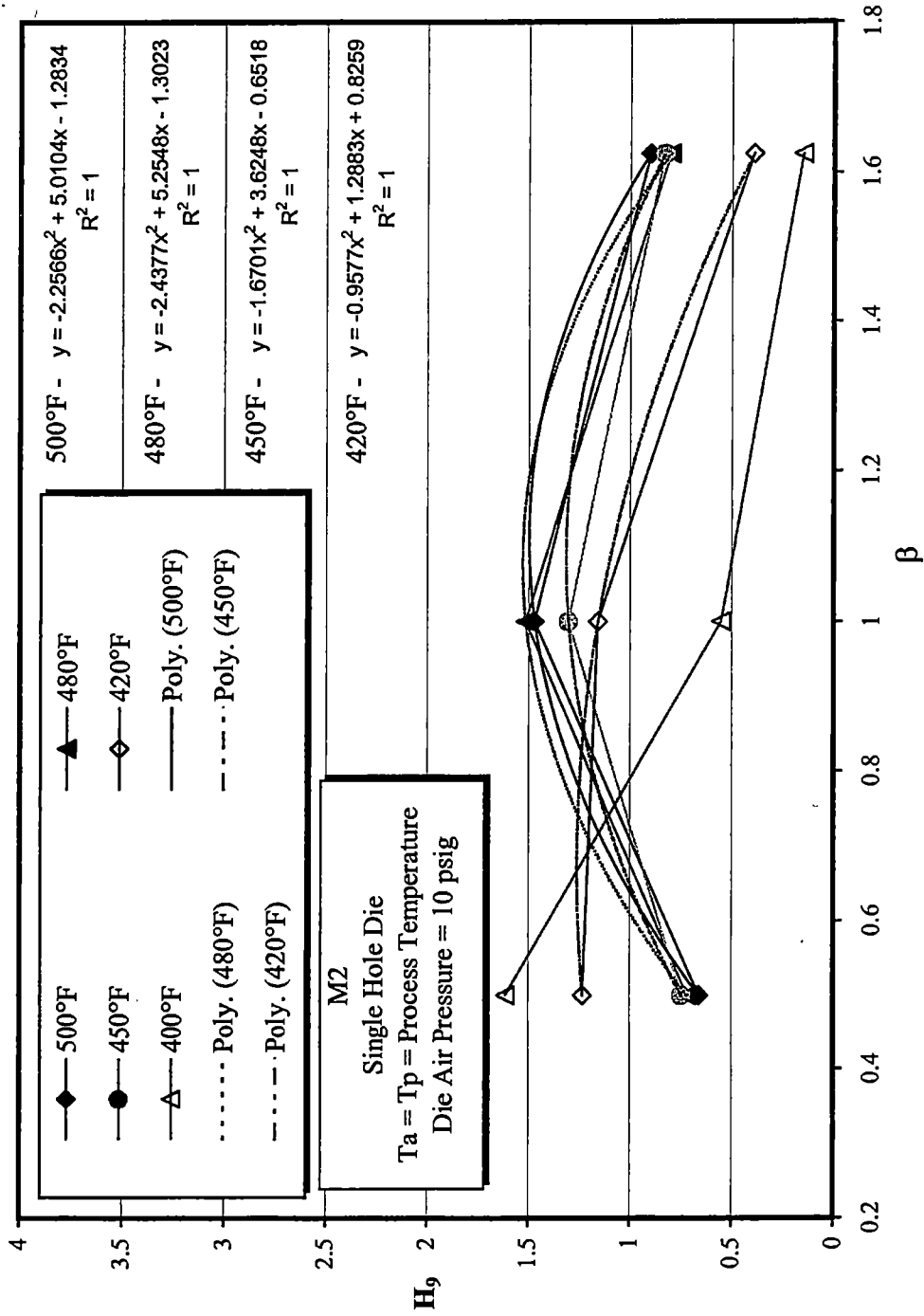


Figure 6.15: Modified number of shot per area ratio vs. polymer throughput ratio for P_d = 10 psig

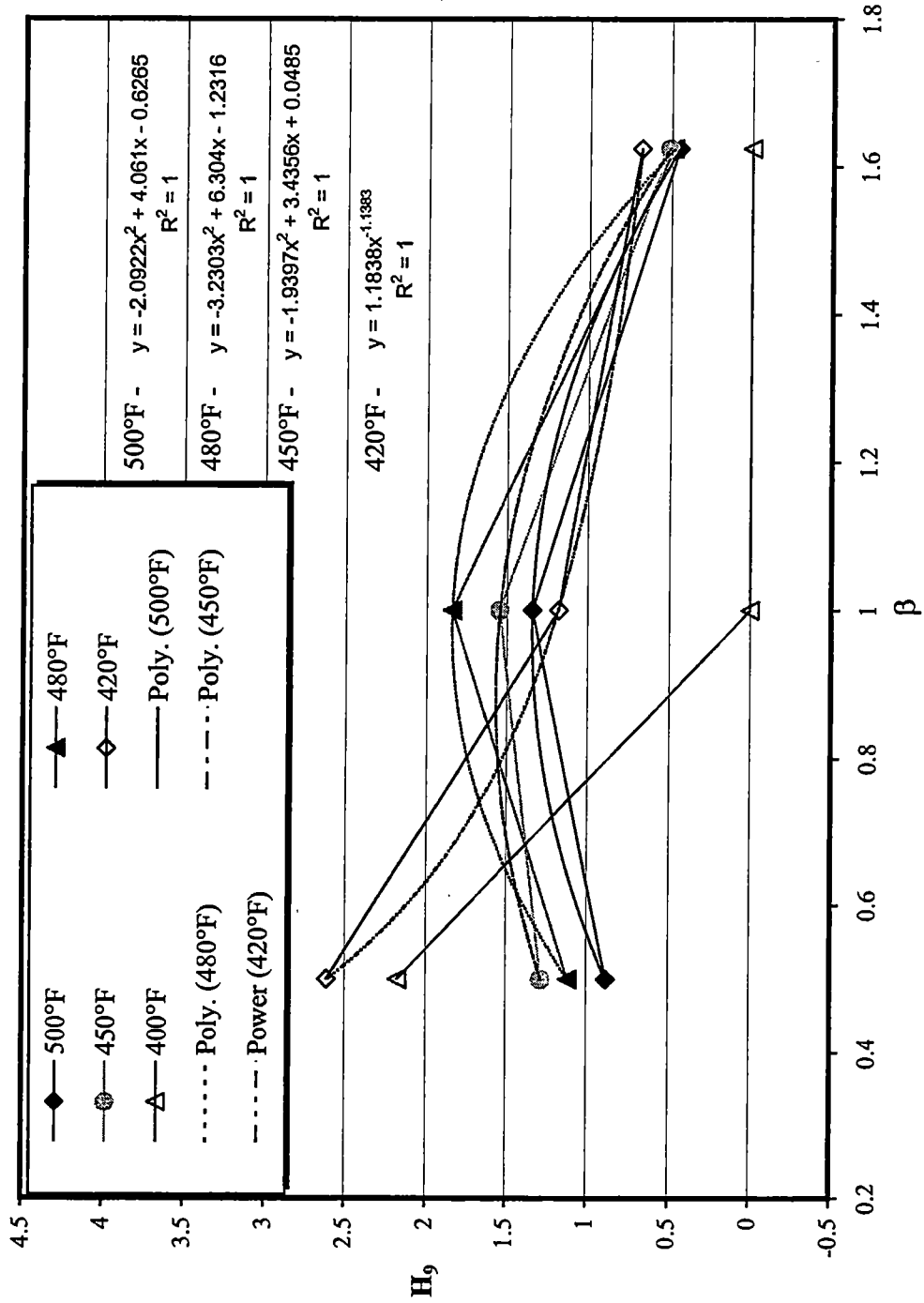


Figure 6.16: Modified number of shot per area ratio vs. polymer throughput ratio for $P_d = 8$ psig

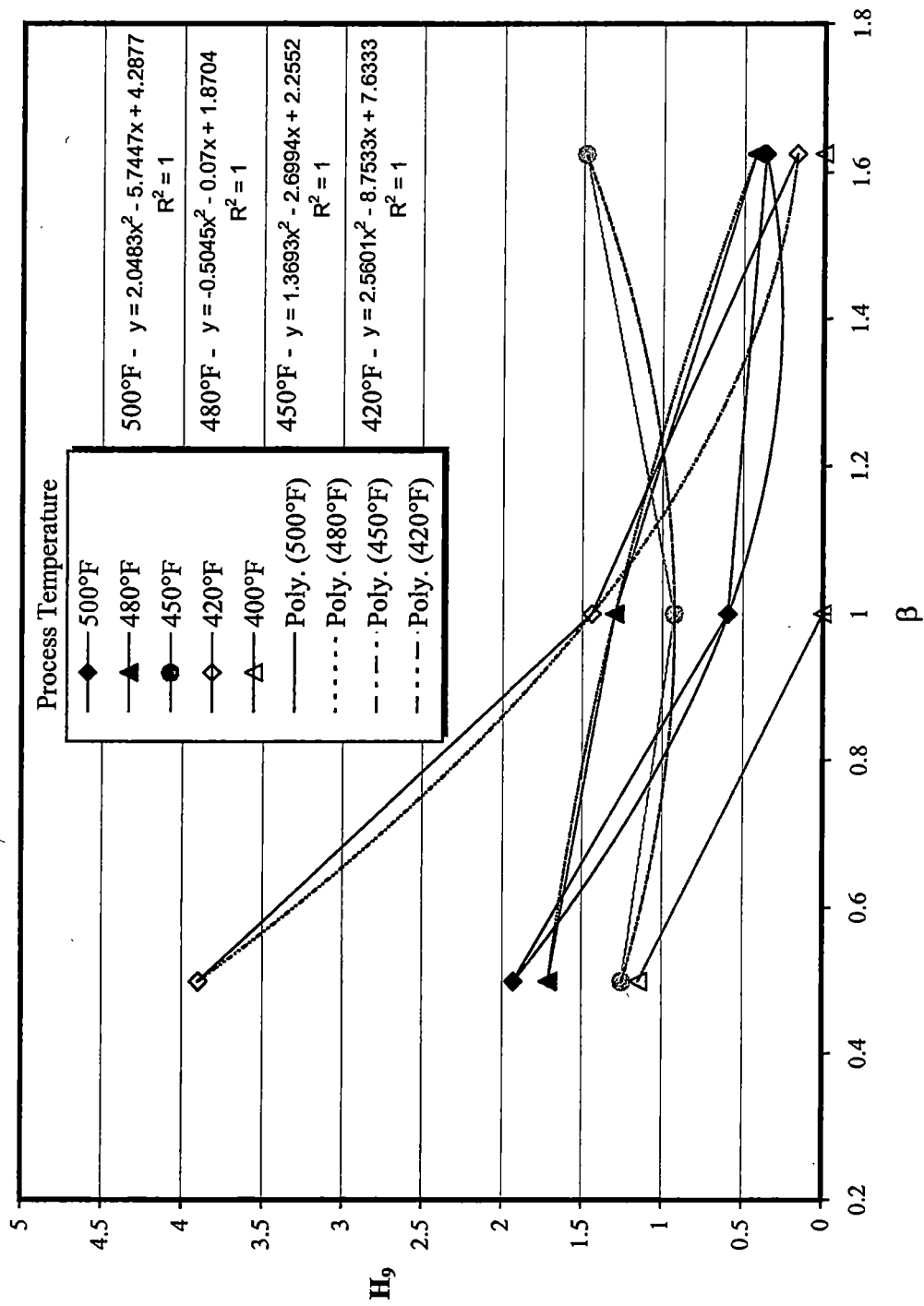


Figure 6.17: Modified number of shot per area ratio vs. polymer throughput ratio for $P_4 = 5$ psig

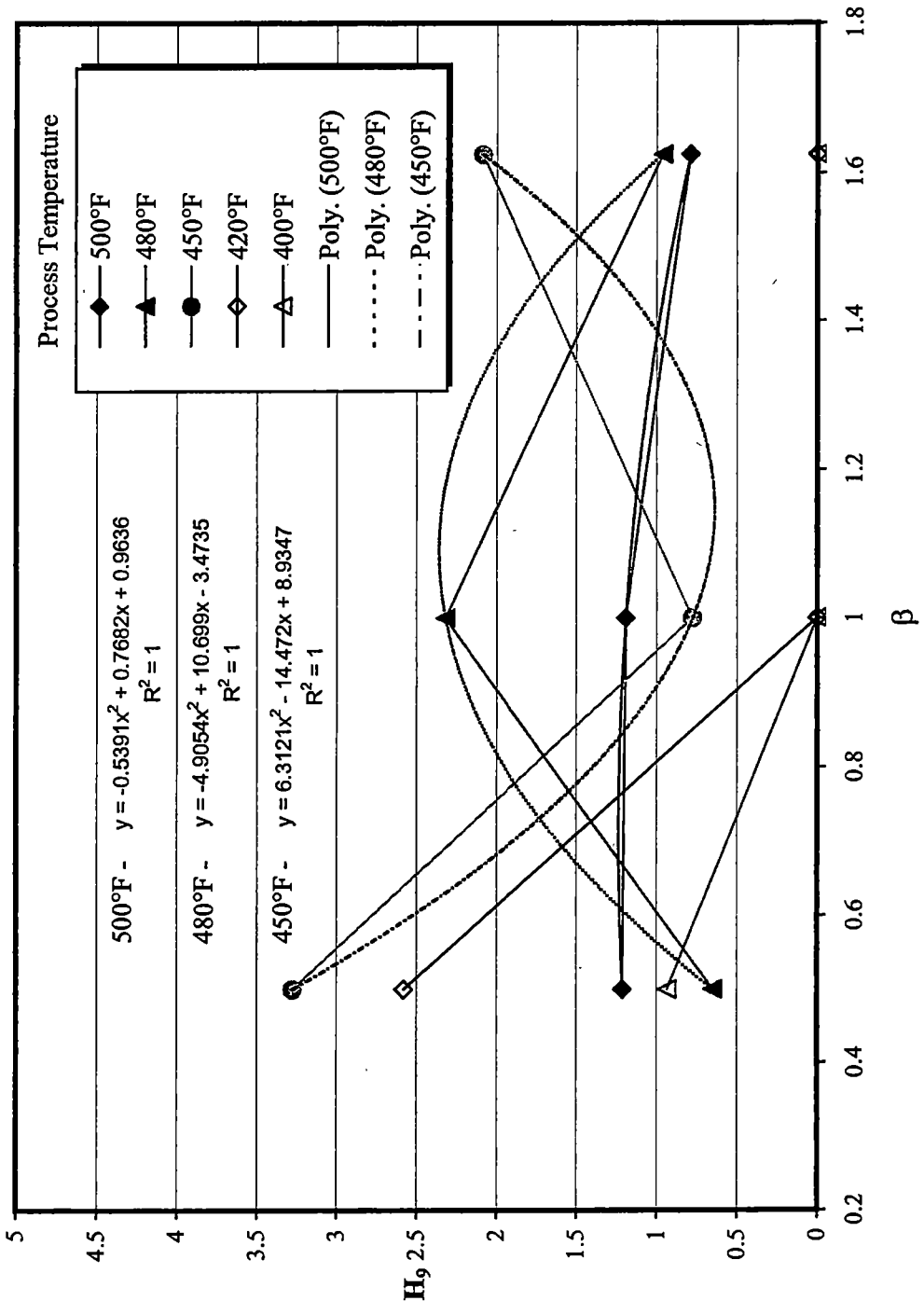


Figure 6.18: Modified number of shot area ratio vs. polymer throughput ratio for $P_d = 3$ psig

model the shot as a function of polymer throughput ratio would be 450°F process temperature and 8 psig die pressure curve. This curve has a trendline and trendline curve equation such that the equation for modified shot ratio becomes:

$$H_9 = \frac{\eta}{\eta_9} = -1.9397 \beta^2 + 3.4356 \beta + 0.0485 \quad 6.13$$

When Equation 6.10 is substituted for η_9 , Equation 6.13 is rearranged to produce the following relationship:

$$\eta_{11} = (-1.9397 \beta^2 + 3.4356 \beta + 0.0485) \left(0.64745 \left(\Phi^{9.4116} \right) \left(\Theta^{20.20512} \right) \right) \quad 6.14$$

Figure 6.19 is a plot of η_{11} versus η and indicates how accurately the experimental data is modeled by Equation 6.14. This figure is plotted with three series since the curves in the H_9 versus β plots did not collapse into a single curve. These three series have been approximated using the trendline curve equations and R^2 values. If Equation 6.14 had been a perfect model the slope of each of these trendlines in Figure 6.19 would have been one with R^2 values equaling one also. The R^2 values for this model are very high for all three series and could not be improved upon without adding more terms to improve the model. The slopes for the three series can be improved by applying slight correction factors for each value of β . If the inverse of the slope was plotted for each curve versus the corresponding β value, the trendline curve equation of such a plot would correct the slopes of Figure 6.19. Figure 6.20 is a plot of Figure 6.19's series slope inverses versus β . This curve is nearly linear and upon adding its linear trendline curve equation to Equation 6.14 the following empirical model is produced.

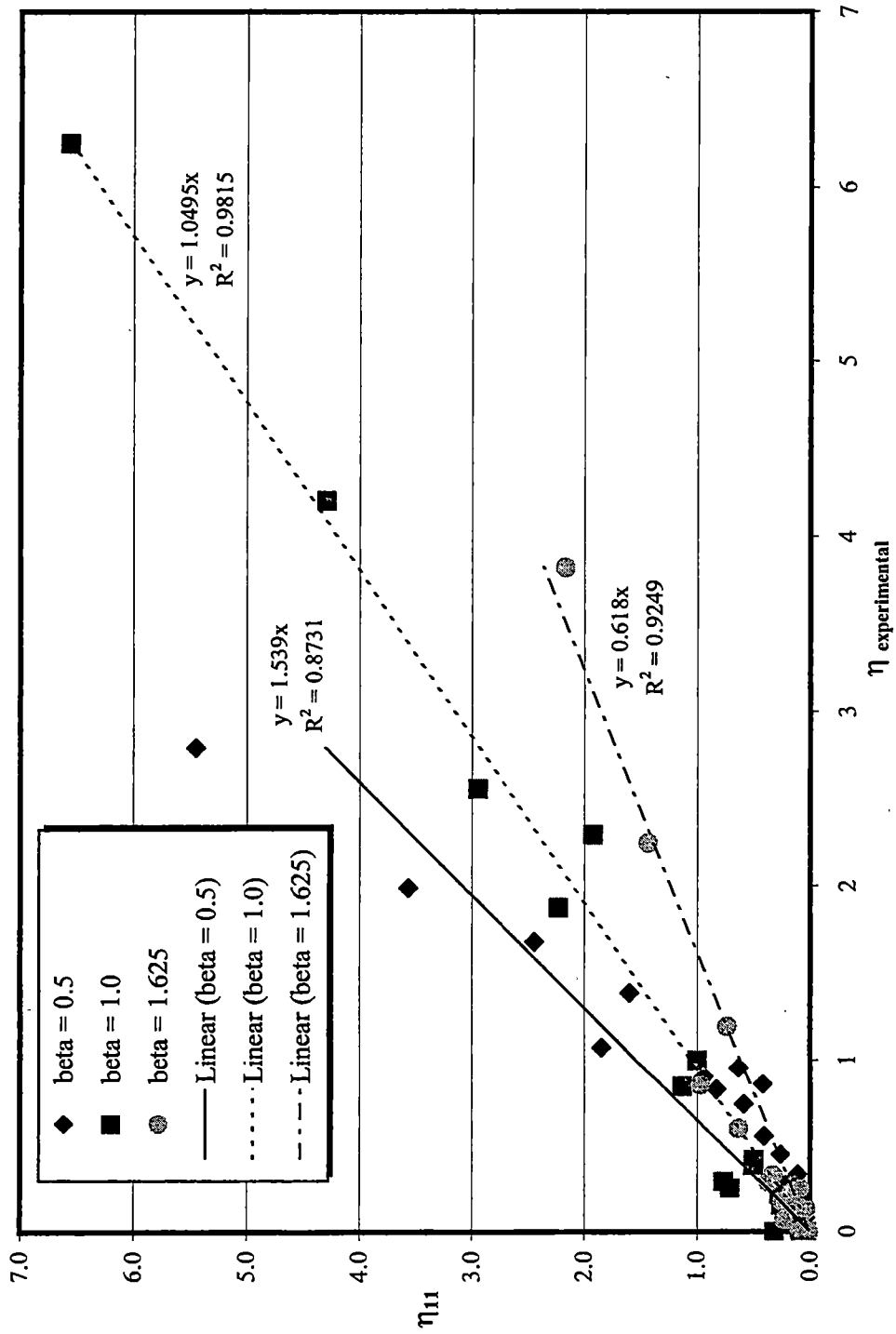


Figure 6.19: Empirical number of shot per area ratio vs. experimental number of shot per area ratio

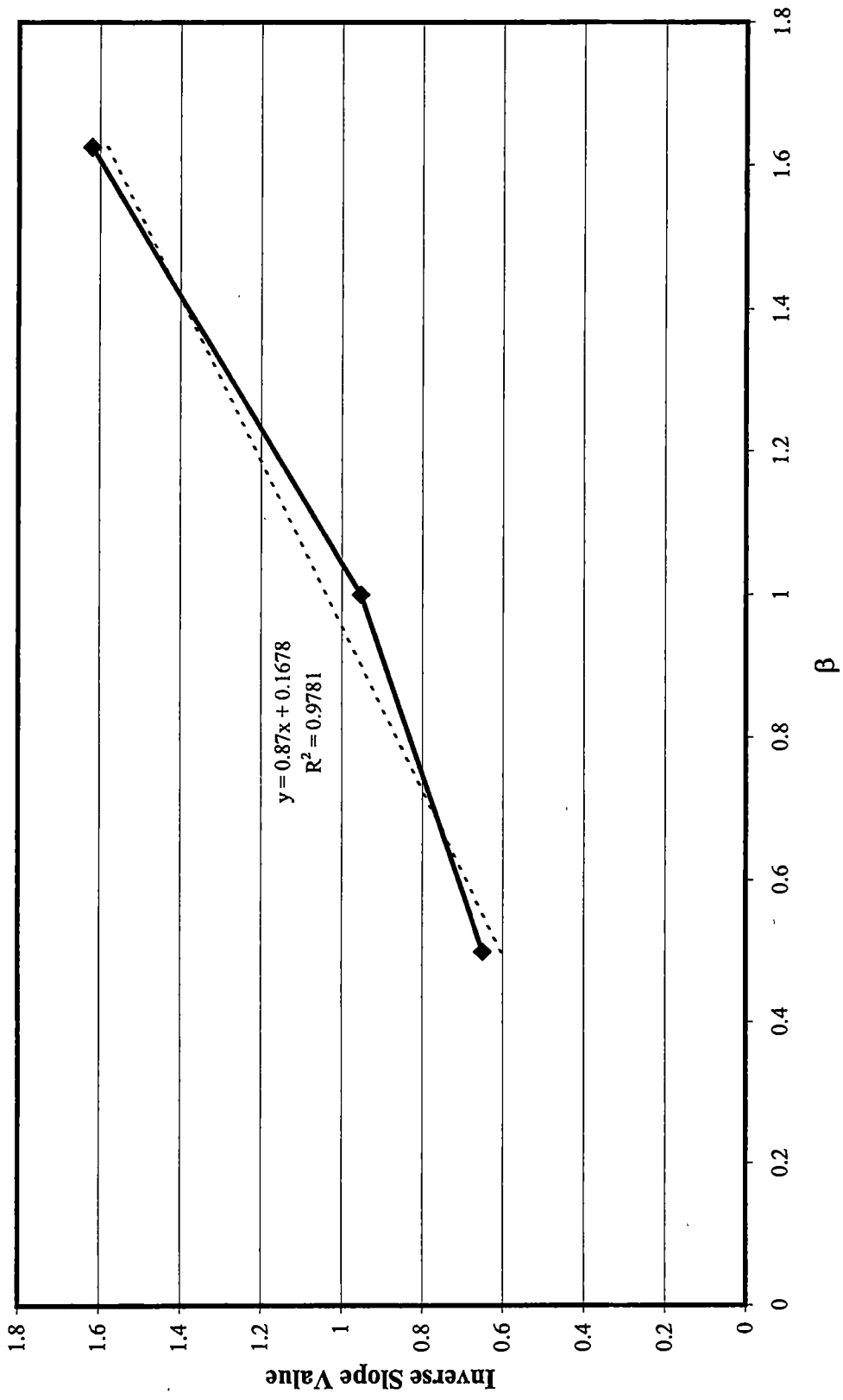


Figure 6.20: Figure 6.19's inverse slope value vs. polymer throughput ratio

$$\eta_{11} = (-1.9397 \beta^2 + 3.4356 \beta + 0.0485)(0.87 \beta + 0.1678)^* \left(0.64745 (\Phi^{9.4116}) (\Theta^{20.20512}) \right) \quad 6.15$$

Upon combining terms the above relationship becomes:

$$\eta_{11} = (-1.0926\beta^3 + 1.7245 \beta^2 + 0.4006 \beta + 0.0053)(\Phi^{9.4116} \Theta^{20.20512}) \quad 6.16$$

This empirical shot ratio relationship is plotted versus the experimental shot ratio and shown in Figure 6.21. This figure demonstrates how well the experimental shot ratio agrees with the empirical model. This figure's trendline curve equations indicate that the R^2 values are no different than that of Figure 6.19. However, the slopes of the trendlines are all nearly one. Therefore, the addition of the slope correction factor equation from Figure 6.20 was successful in transforming Figure 6.19 into the more "one to one" Figure 6.21. Figure 6.21 appears to indicate that Equation 6.16 is a good approximation to the experimental values but a more clear indication of Equation 6.16's accuracy is shown when Figures 6.2 through 6.10 are replotted with Equation 6.16 values incorporated for direct comparison. Figures 6.22 through 6.31 provide this experimental-empirical shot ratio comparison.

Even though Figures 6.22 through 6.31 indicate a comparison between the experimental data and Equation 6.16, it is appropriate to apply Equation 6.16 to other M2 resin, single hole die experimental data. The application of Equation 6.16 to data other than the experimental data used to create the model will test the empirical model. In order to apply this empirical model to other data a modified number of shot per area ratio was created in a manner very similar to that applied to the average

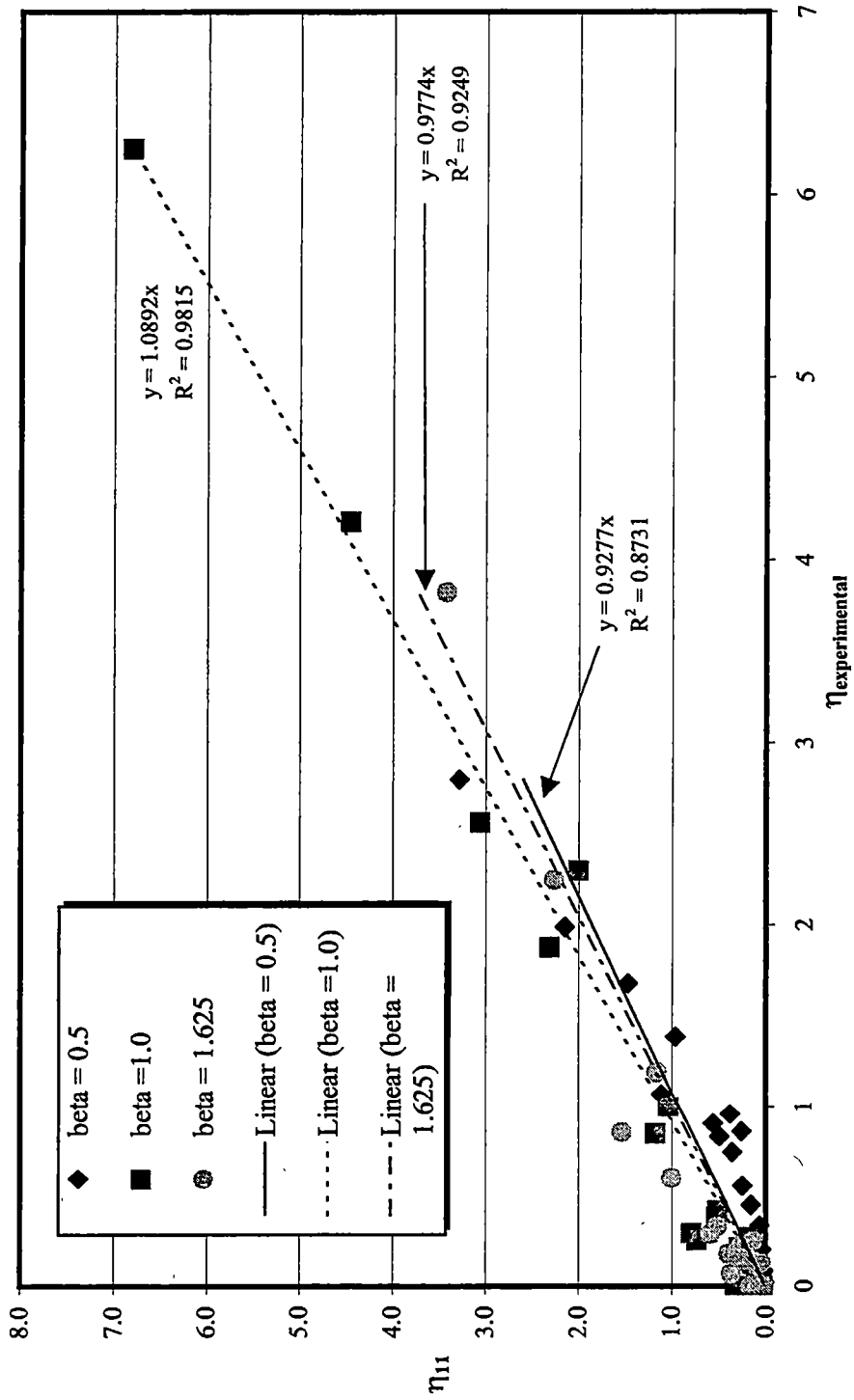


Figure 6.21: Corrected empirical shot per area ratio vs. experimental shot per area ratio

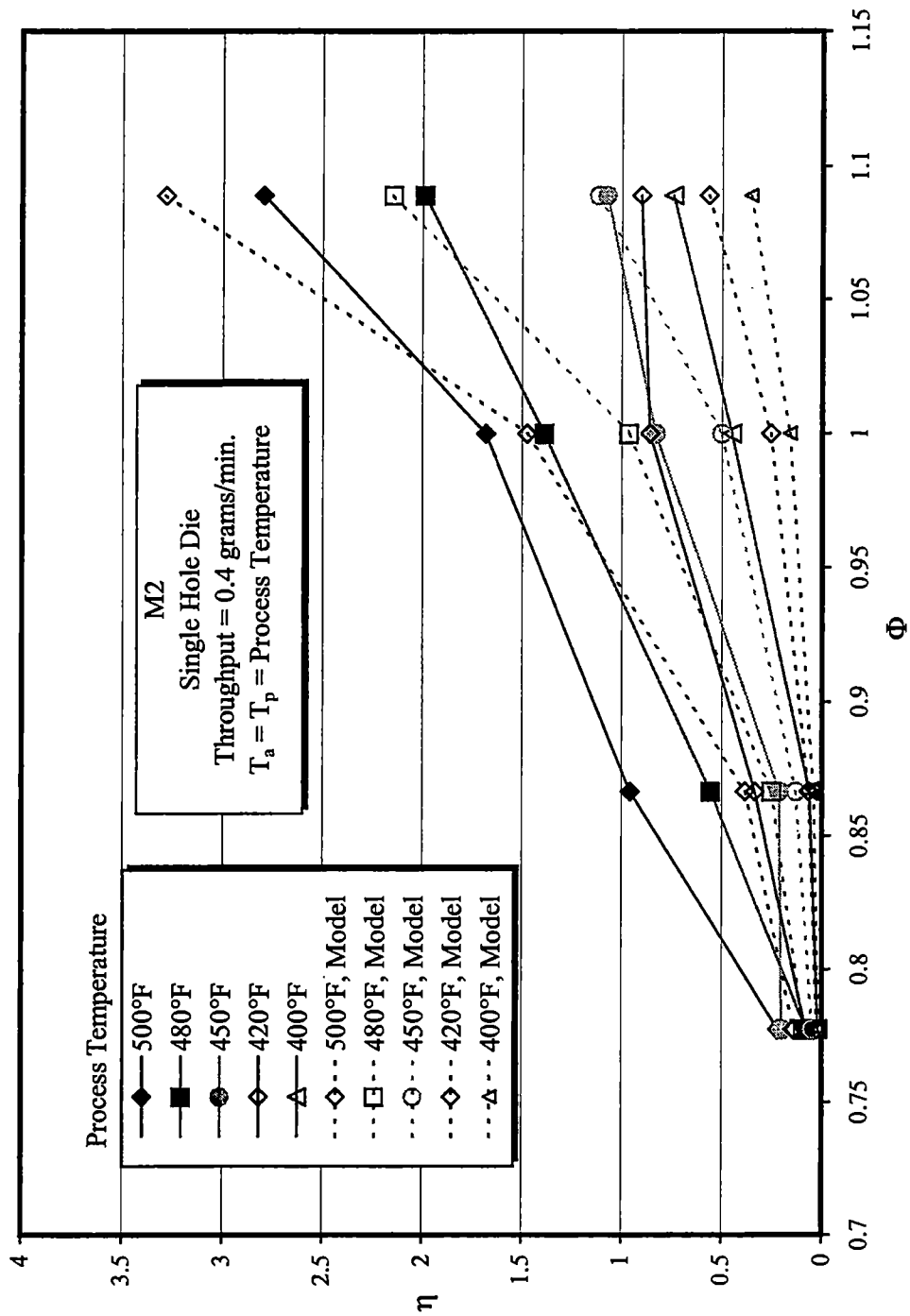


Figure 6.22: Number of shot per area ratio vs. die air pressure ratio

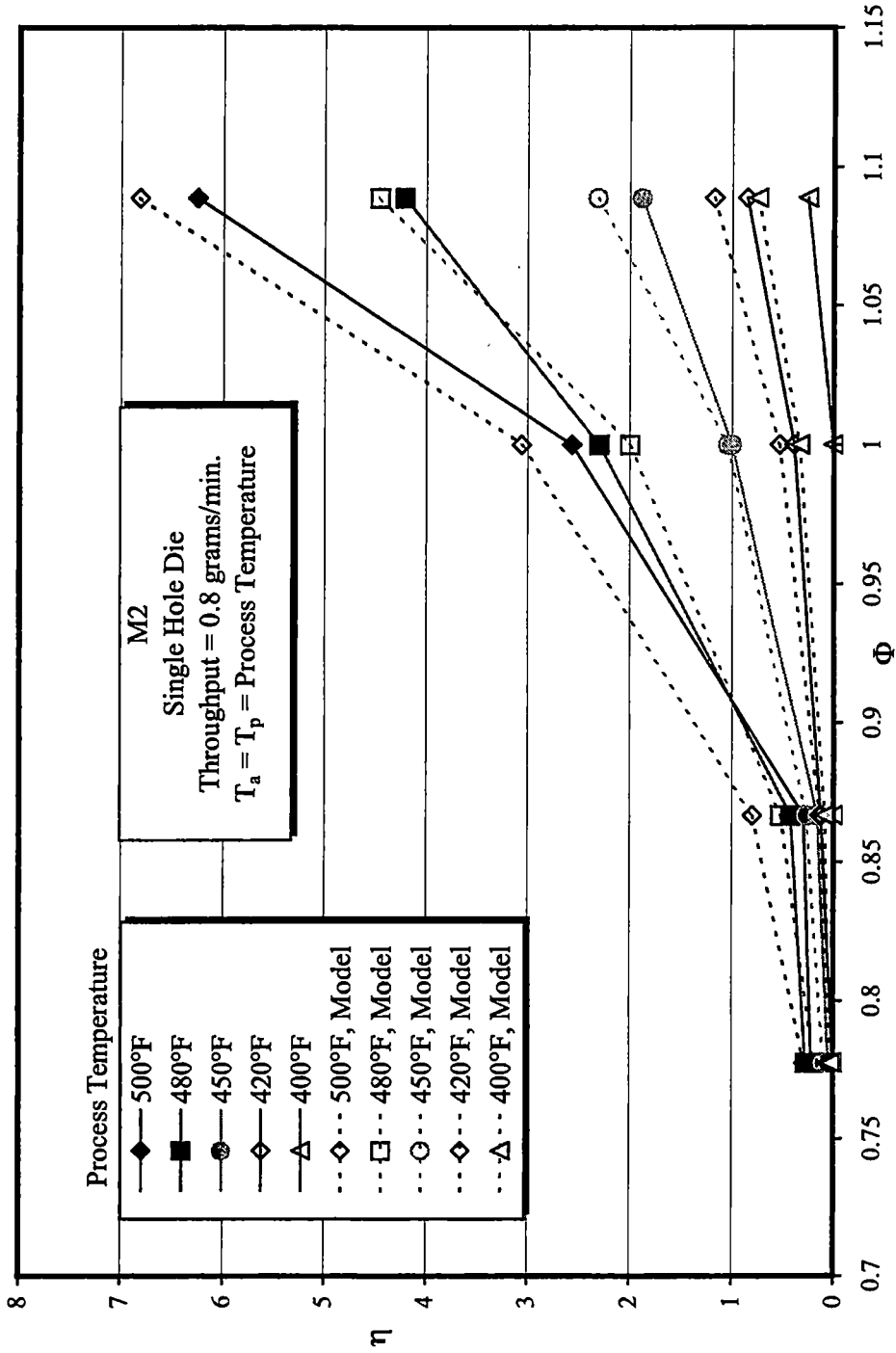


Figure 6.23: Number of shot per area ratio vs. die air pressure ratio

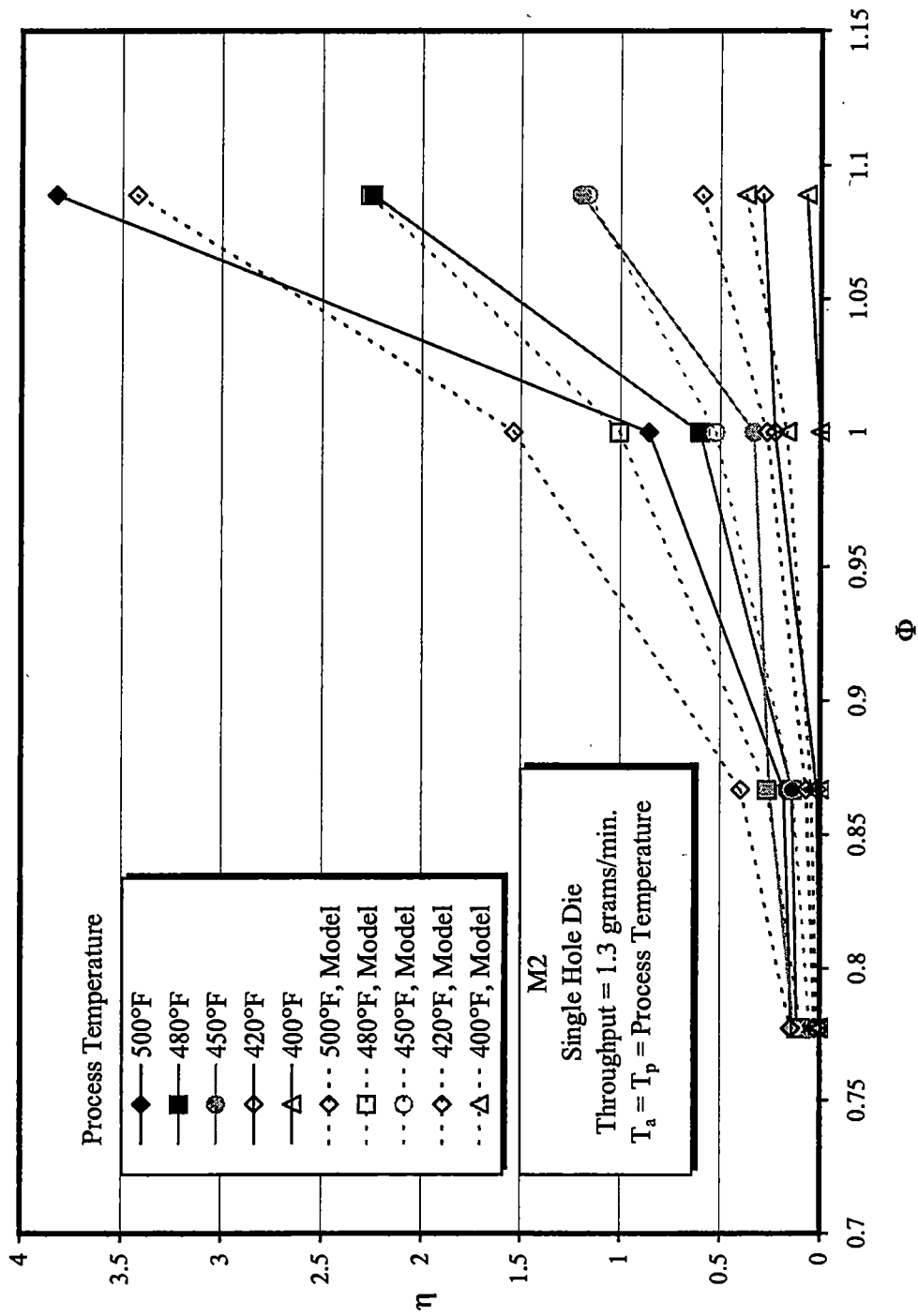


Figure 6.24: Number of shot per area ratio vs. die air pressure ratio

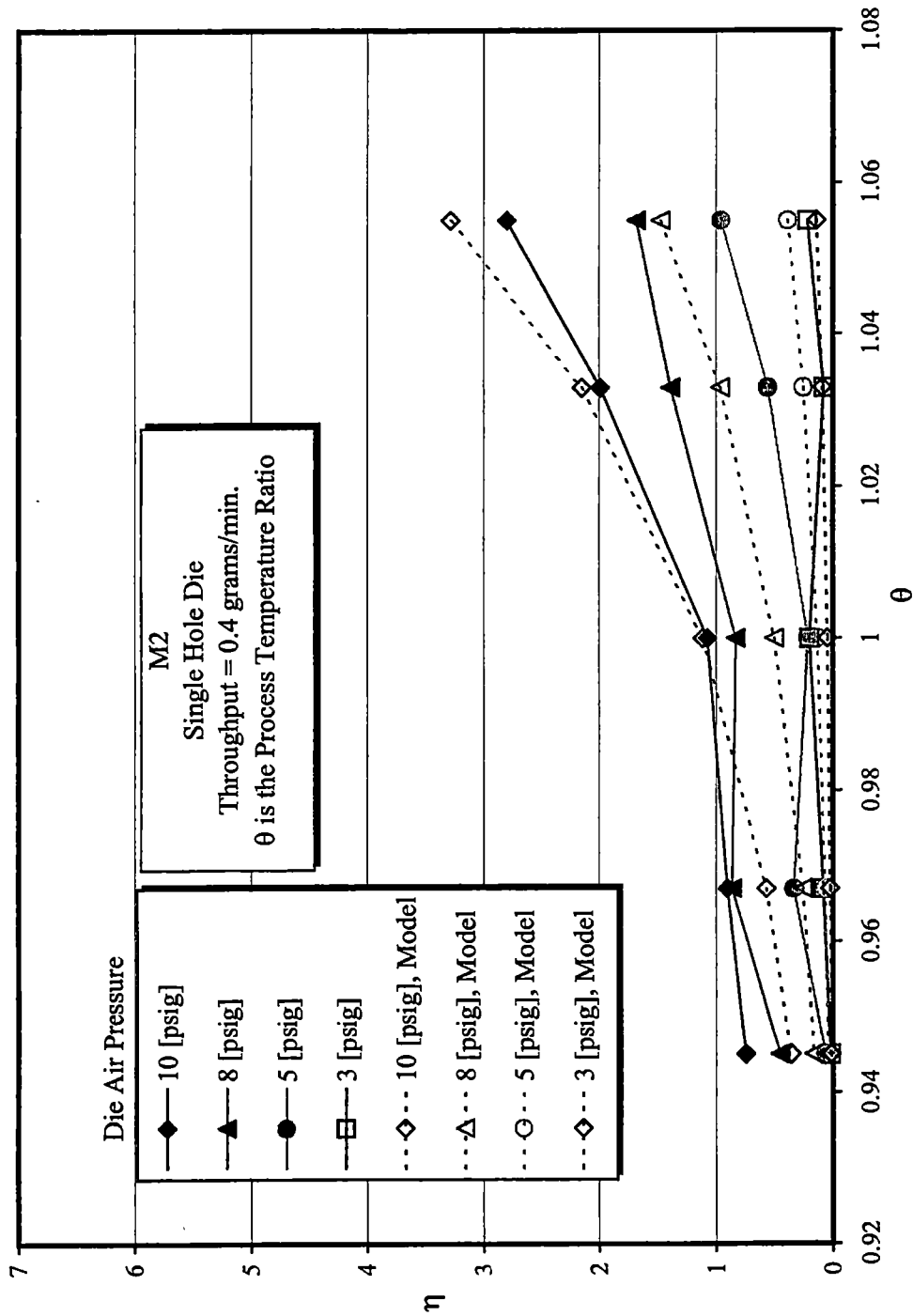


Figure 6.25: Number of shot area ratio vs. process temperature ratio

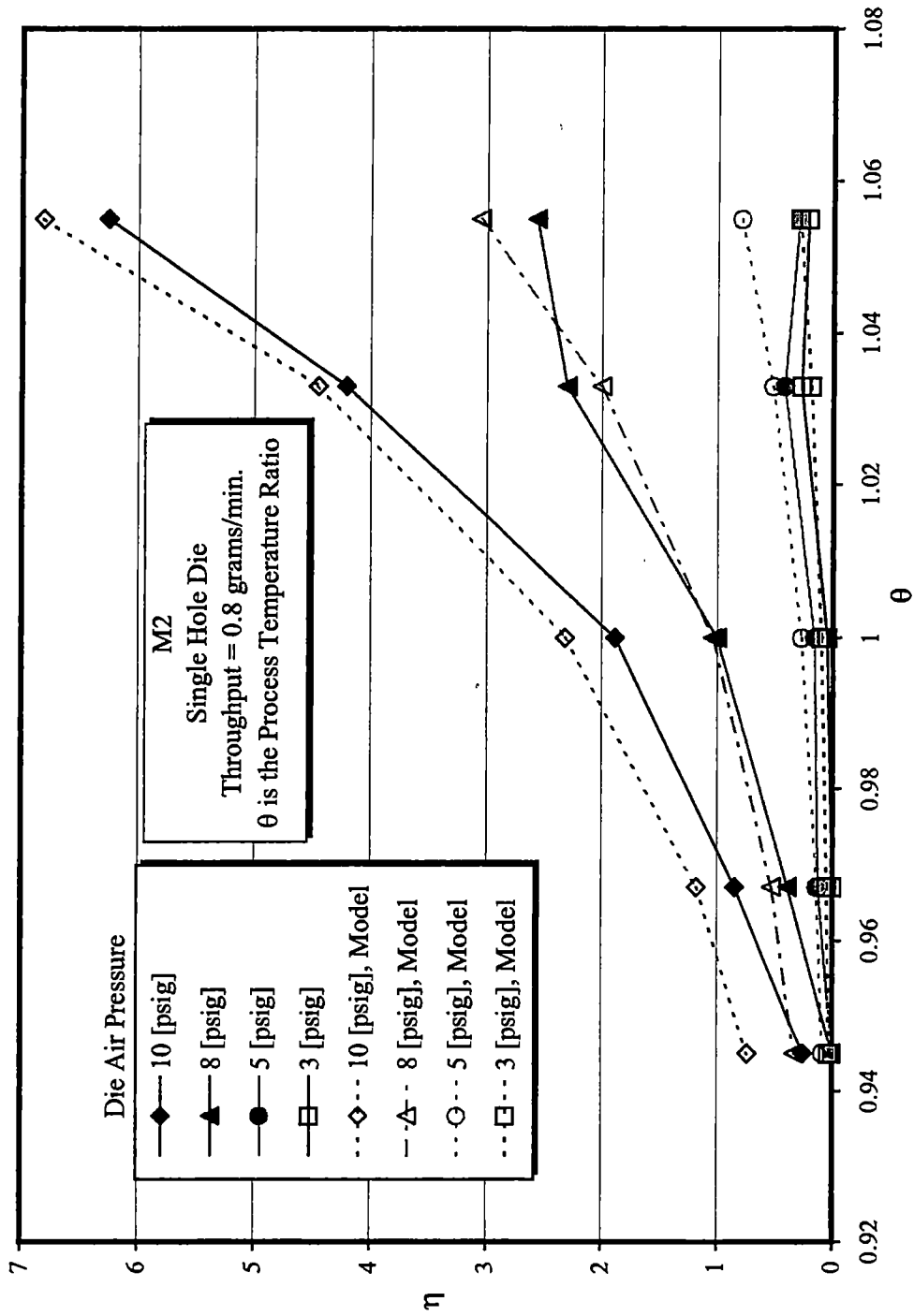


Figure 6.26: Number of shot area ratio vs. process temperature ratio

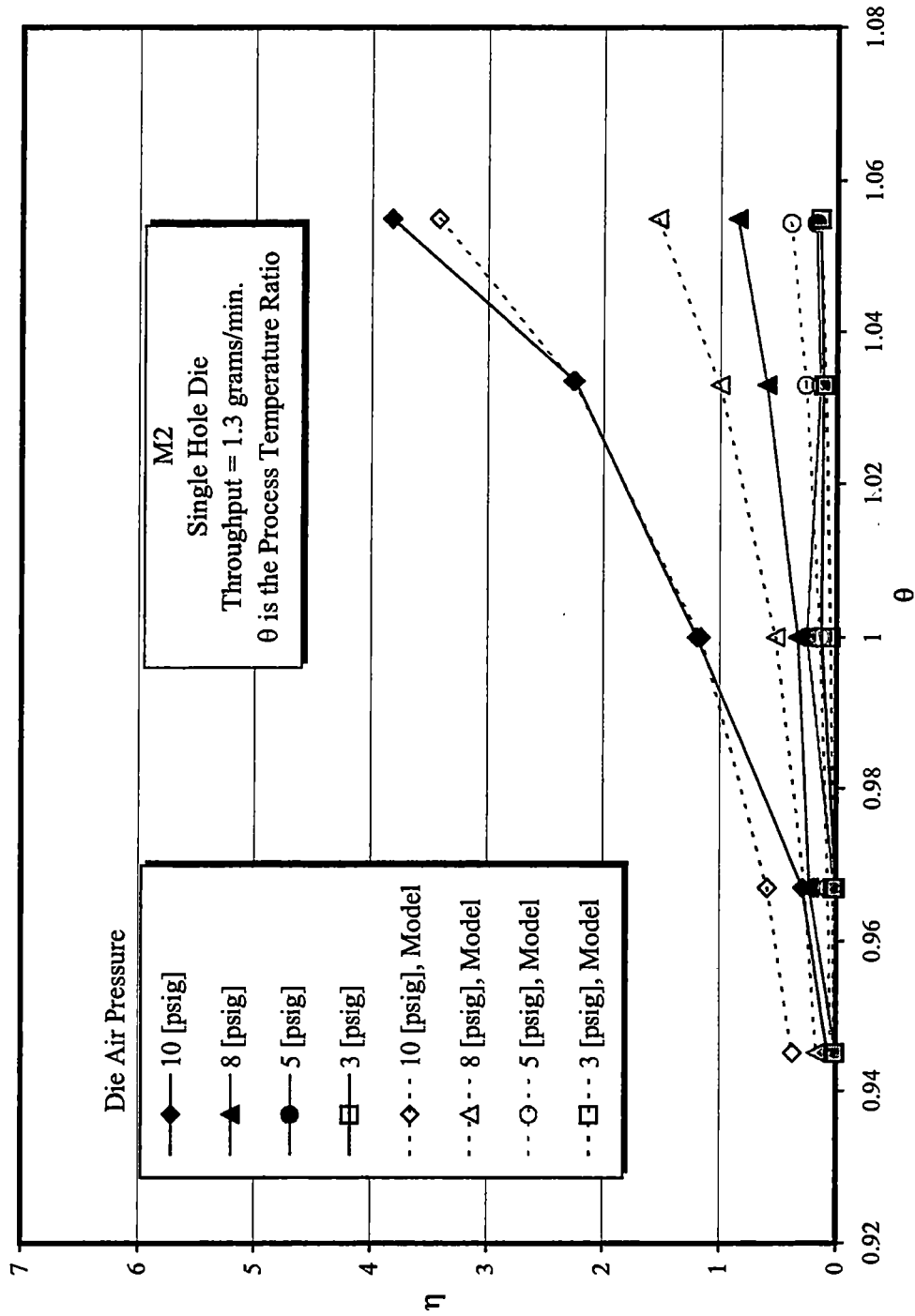


Figure 6.27: Number of shot area ratio vs. process temperature ratio

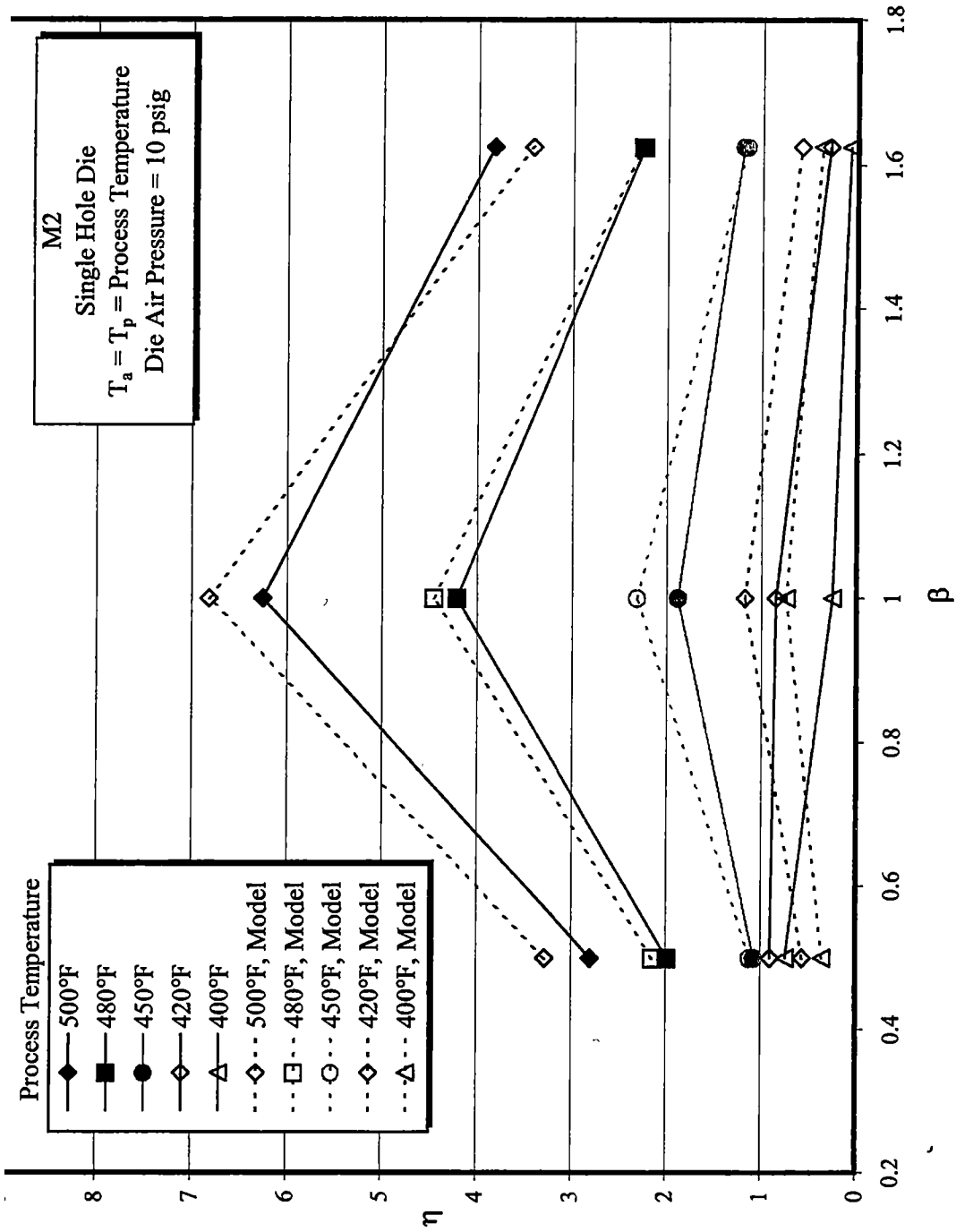


Figure 6.28: Number of shot per area ratio vs. polymer throughput ratio

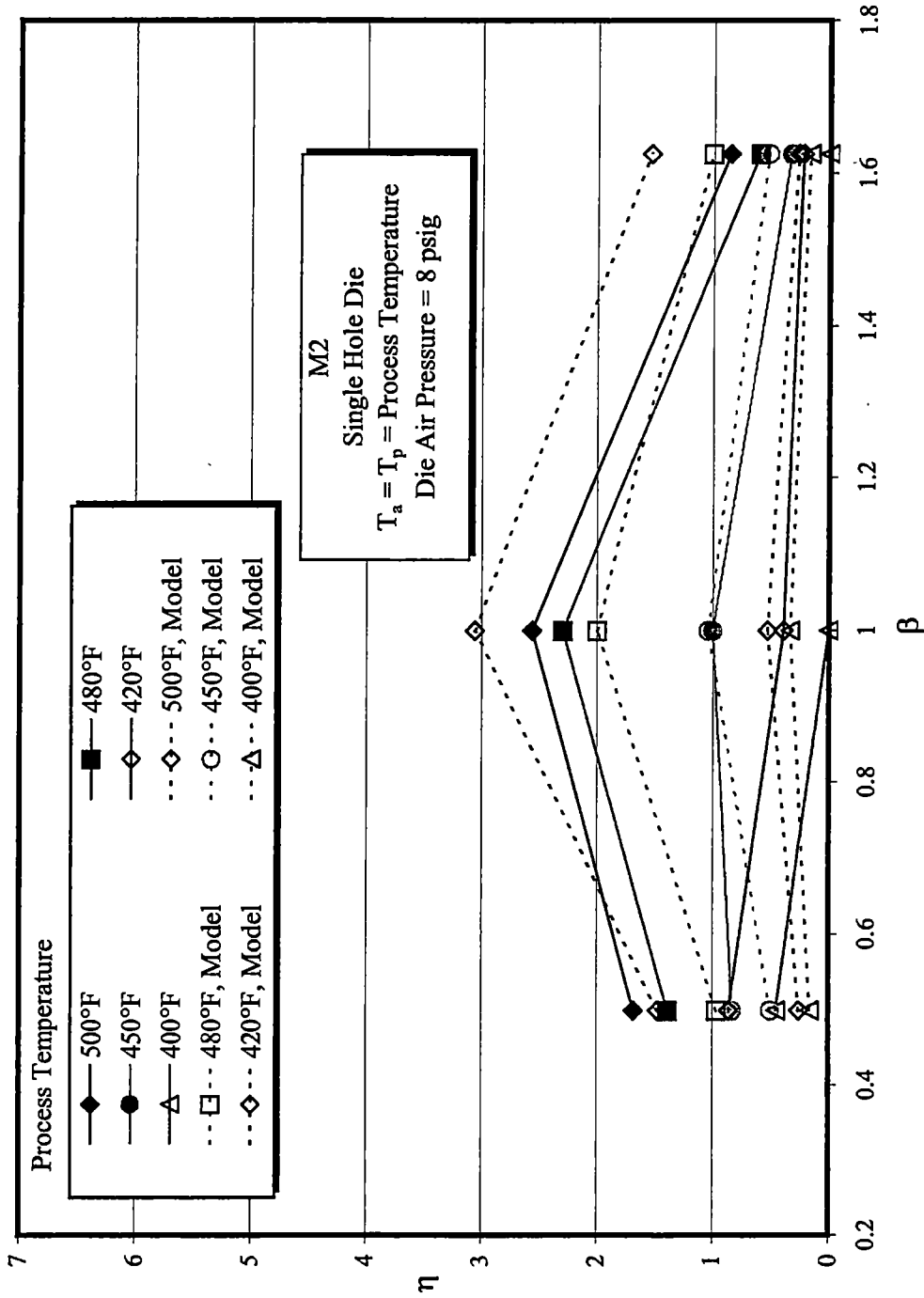


Figure 6.29: Number of shot area ratio vs. polymer throughput ratio

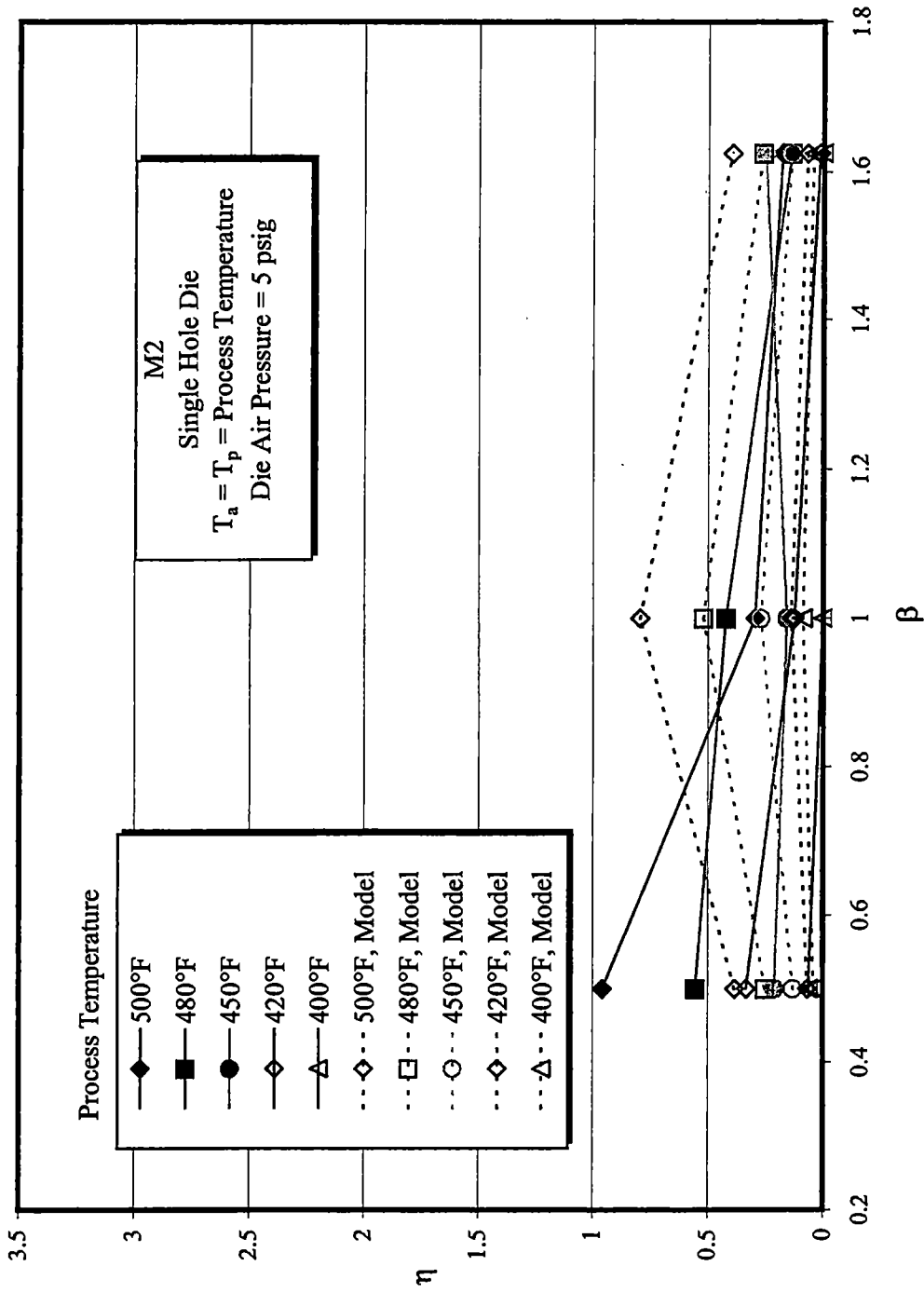


Figure 6.30: Number of shot per area ratio vs. polymer throughput ratio

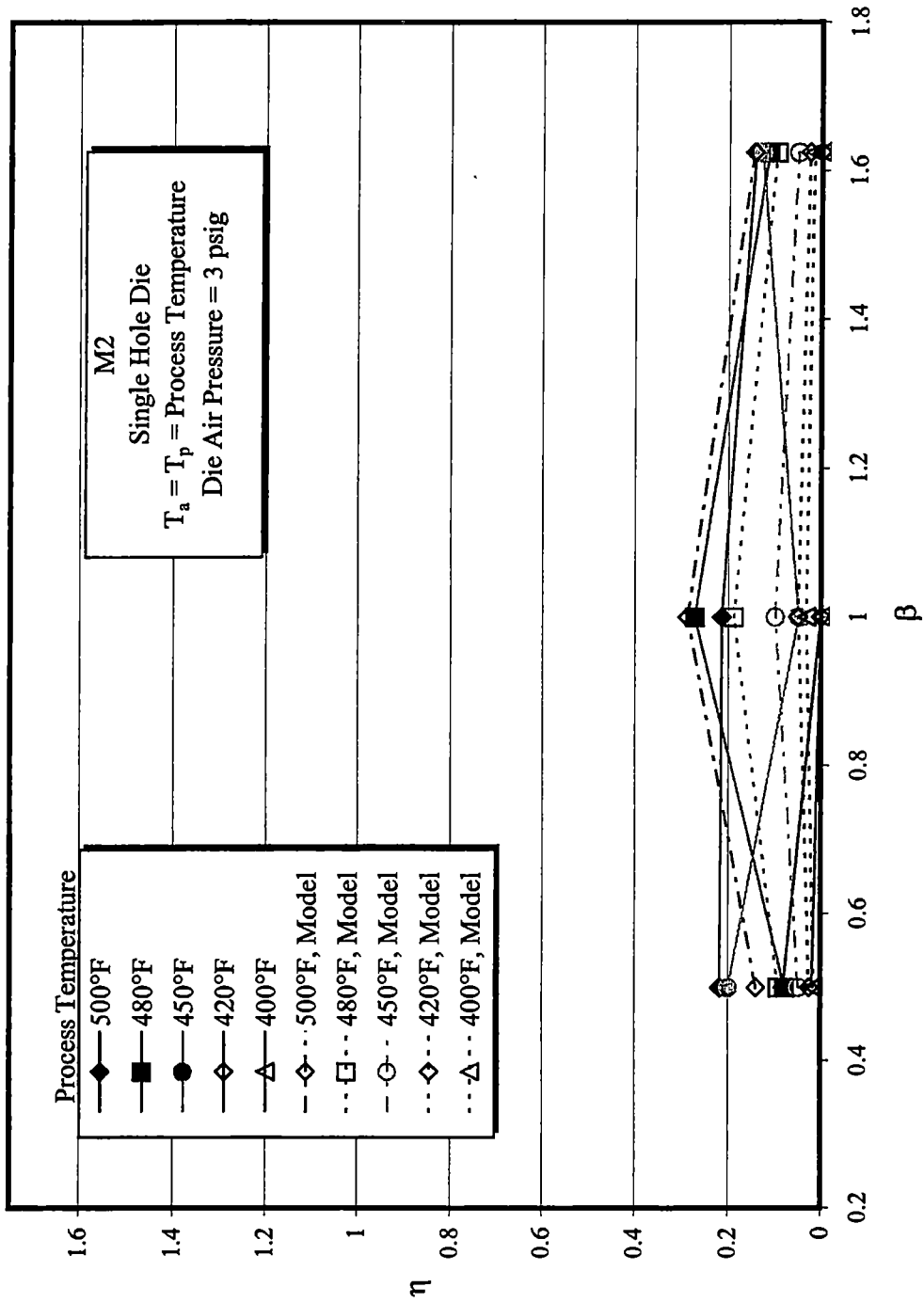


Figure 6.31: Number of shot per area ratio vs. polymer throughput ratio

fiber diameter ratio in the previous chapter. The modified number of shot ratio (H_{11}) is a simple manipulation of Equation 6.16 and is shown in Equation 6.17.

$$H_{11} = \frac{\eta_{11}}{(-1.0926\beta^3 + 1.7245\beta^2 + 0.4006\beta + 0.0053)(\ominus^{20.20512})} \quad 6.17$$

$$H_{11} = f(\Phi) = \Phi^{9.411} \quad 6.18$$

Equation 6.17 is used to plot the experimental data and Equation 6.18 is used to plot the empirical model. Both results are plotted as function of pressure ratio (Φ). Any one of the variables could have been used for the x-axis variable. The other experimental data was obtained in the video taping investigation for a broad range of process temperatures at low pressures, high process temperatures and high die air pressures, and some data at various polymer throughputs. This independent experimental data was plotted with the original set used to create Equation 6.16. Figure 6.32 is a plot of Equation 6.17 versus the pressure ratio for all M2 resin single hole die experimental data. This figure also plots Equation 6.18 as an empirical comparison. This figure indicates more variation in Equation 6.16's results than was previously shown in Figures 6.22 through 6.31. Even with this variation, the newly applied data follows the empirical relationship's curve in the same manner as that of the data used to create the empirical relationship. An attempt was made to understand why the original experimental data did not follow the empirical relationship's curve more closely. The original data points with the maximum variation are low process temperature data points. This was not surprising since these are the data points that had the greatest amount of uncertainty in the WebPro shot measurements. Figure 6.33 is a plot of the original experimental data with the lower process temperature

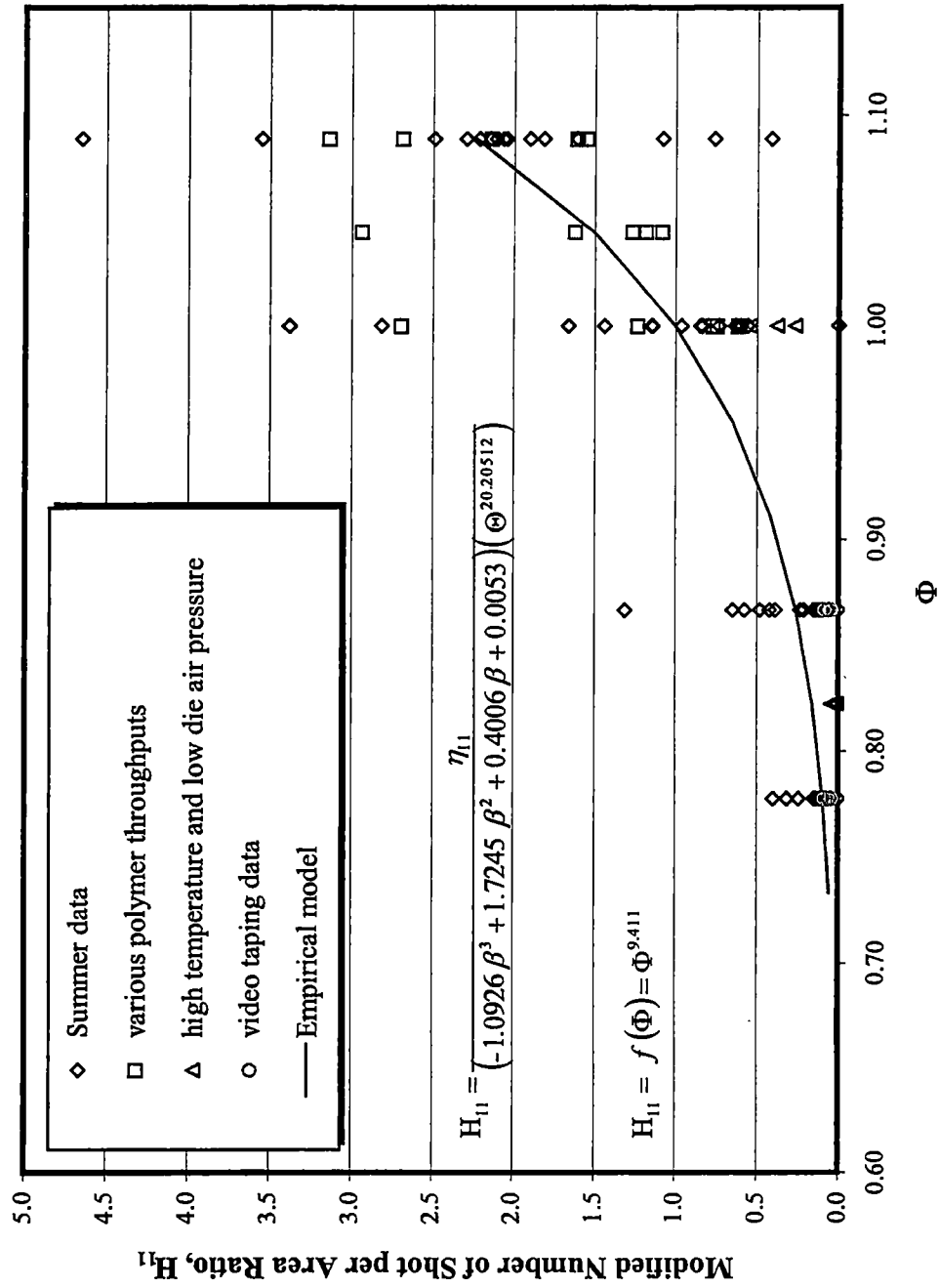


Figure 6.32: Comparison between empirical model and experimental data

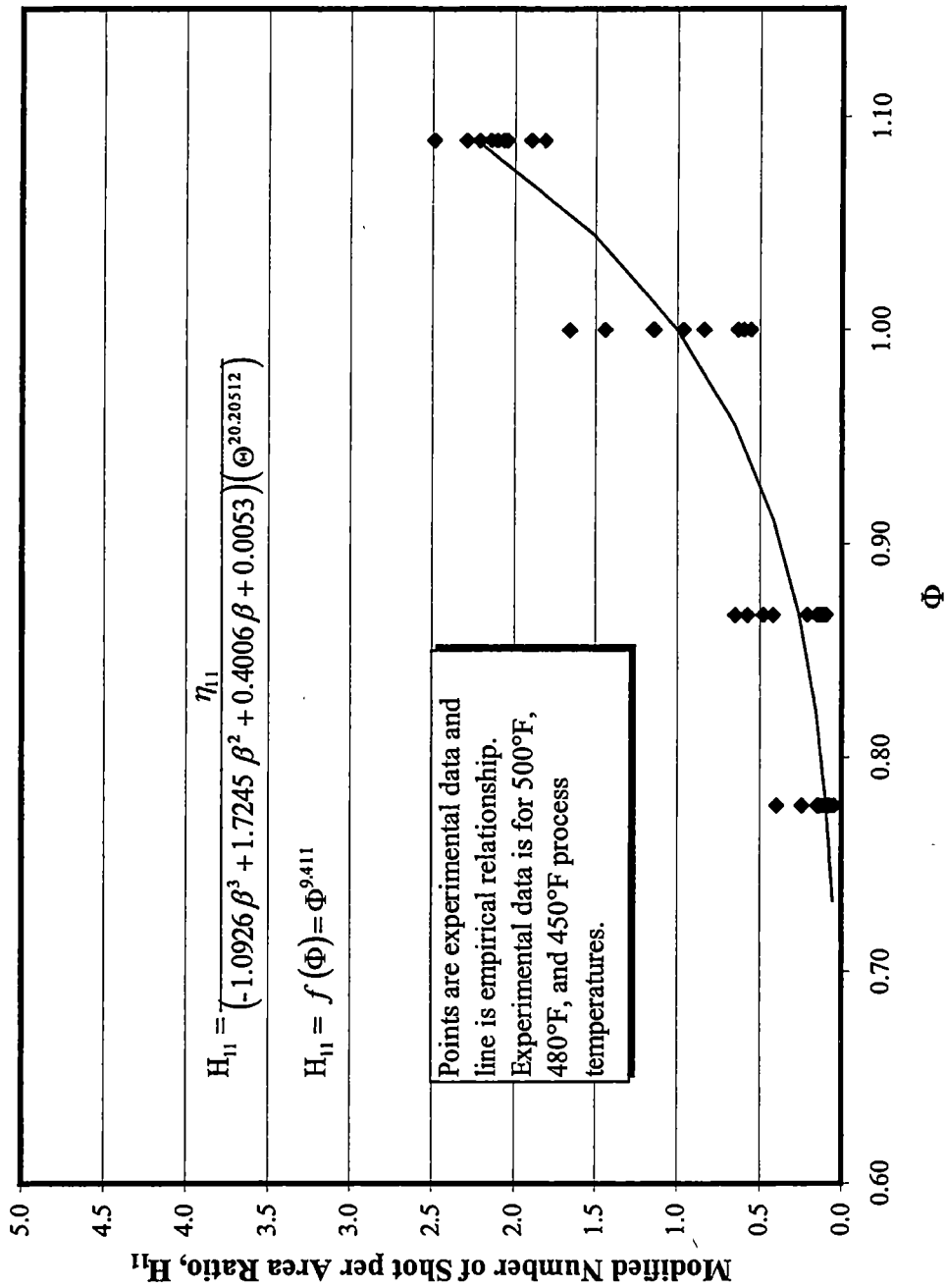


Figure 6.33: Comparison between empirical model and experimental data for modified data set

points (420°F and 400°F) removed. This figure illustrates that the original data points in Figure 6.32 with the maximum variation from the empirical curve were produced at low process temperatures.

Shot Production Model Based on Fundamental Fluid Mechanics Dimensionless Variables

While the processing parameter empirical model of Equation 6.16 is useful in relating the actual process conditions to shot production, it was of interest to determine if traditional fluid flow dimensionless variables could be used to correlate the production of shot. The fluid flow variable most applicable in this investigation would be the air Reynolds number (Re_a). The Reynolds number is a ratio of inertia forces to that of viscous forces. In the melt blowing process the inertia and viscous forces of the air and the polymer are very important and are defined as follows:

$$Re_a = \frac{\rho_a V_a h}{\mu_a} \quad 6.19$$

$$Re_p = \frac{\rho_p V_p d}{\mu_p} \quad 6.20$$

Where the length scale “h” in Equation 6.19 was taken as the air discharge exit height and the length scale “d” in Equation 6.20 to be the die orifice diameter. The calculation of these Reynolds numbers incorporates all the process parameters. The polymer throughput and polymer temperature effects are incorporated into the polymer Reynolds number. The die air pressure and temperature are also incorporated into the air Reynolds number. The determination of the air Reynolds number is calculated using the values of air mass flow rate and air exit height as

determined in Appendix I and II. The air dynamic viscosity (μ_a) was determined from fluid mechanics texts at the process temperature. The polymer Reynolds number was calculated using an elongational viscosity relationship determined by Patel [20].

$$\mu \left[\frac{\text{lbf s}}{\text{ft}^2} \right] = 6.293 \times 10^{-7} e^{\left(\frac{12766.48}{T_p [^\circ\text{F}] + 460} \right)} \quad 6.21$$

Figure 6.34 is a plot of this polymer elongational viscosity versus polymer temperature. Other dimensionless variables to investigate are the momentum flux ratio and the mass flux ratio. These two ratios relate the relative intensities of the air and polymer streams. These dimensionless variables are cycled through Equation 6.22 in the same manner as before.

$$\text{Shot Cover \%} = A + B (C_1)^{e_1} (C_2)^{e_2} (C_3)^{e_3} \dots (C_i)^{e_i} \quad 6.22$$

Using the same experimental data sample as before the SPSS[®] statistical analysis program was again utilized to determine the constants in Equation 6.22. This model uses shot cover percentage as opposed to a number of shot per area ratio. This cover percentage was used because it is already dimensionless and was shown in Figure 5.3 to be related to the number of shot per area. After many trials the best empirical relationship that could be determined is comprised of the polymer and air Reynolds numbers and the air to polymer momentum flux ratio. This empirical relationship is shown in Equation 6.23.

$$\text{Shot Cover \%} = \left(\text{Re}_a^{3.2394} \right) \left(\text{Re}_p^{-1.9563} \right) \left(\Psi^{-3.4106} \right) \left(\Gamma^{8.7937} \right) \quad 6.23$$

$$(R^2 = 0.697)$$

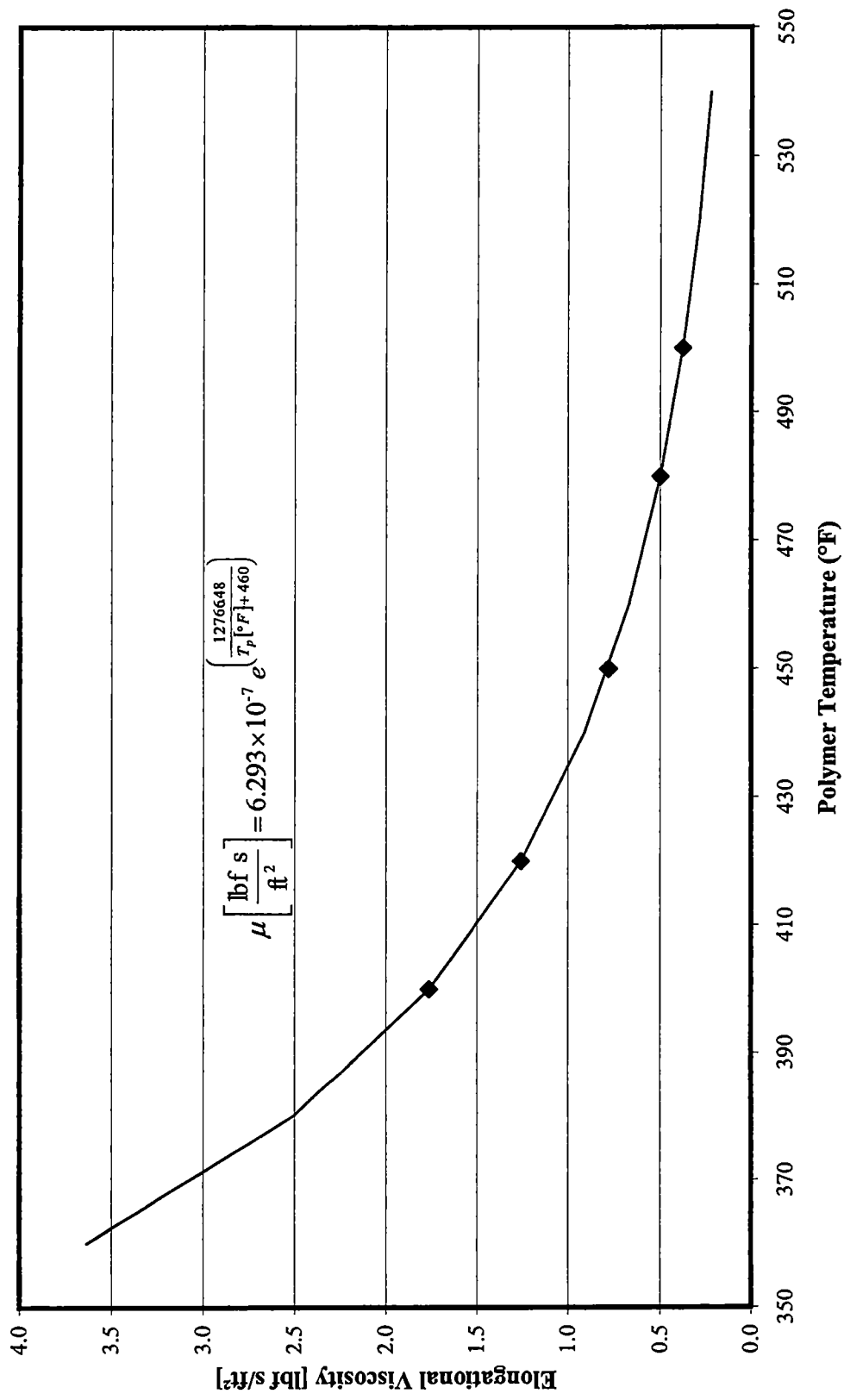


Figure 6.34: Elongational viscosity of 700 MFR polypropylene vs. polymer temperature

This empirical relationship has the highest R^2 term and none of the constants' asymptotic 95% confidence intervals contain zero. Figure 6.35 is a plot of the experimental cover area percentage versus Equation 6.23 results. This figure is very similar to that of Figure 6.14 in that the data points are not along one line and appear to be grouped together with similar polymer throughputs. This seems to indicate that these dimensionless variables do not model the polymer throughput variation effects very well. The process parameter empirical relationship had a similar situation that was corrected by applying a correction factor based on polymer throughput. This was a method that was employed to make the data points in Figure 6.19 coalesce onto a single curve with a slope of one. It was decided not to force or correct the data points in Figure 6.35 in a similar manner. Instead the statistical analysis program would be rerun for individual polymer throughput data. When the statistical analysis was performed for the each polymer throughput the following relationships were created.

$$\text{Shot Cover \%} \left(\dot{m}_p = 0.4 \frac{\text{grams}}{\text{minute}} \right) = \left(\text{Re}_a^{-2.304} \right) \left(\text{Re}_p^{0.7155} \right) \left(\Psi^{2.81} \right) \quad 6.24$$

$$(R^2 = 0.92)$$

$$\text{Shot Cover \%} \left(\dot{m}_p = 0.8 \frac{\text{grams}}{\text{minute}} \right) = \left(\text{Re}_a^{-4.78} \right) \left(\text{Re}_p^{1.5297} \right) \left(\Psi^{6.93} \right) \quad 6.25$$

$$(R^2 = 0.98)$$

$$\text{Shot Cover \%} \left(\dot{m}_p = 1.3 \frac{\text{grams}}{\text{minute}} \right) = \left(\text{Re}_a^{-7.8} \right) \left(\text{Re}_p^{0.461} \right) \left(\Psi^{10.92} \right) \quad 6.26$$

$$(R^2 = 0.93)$$

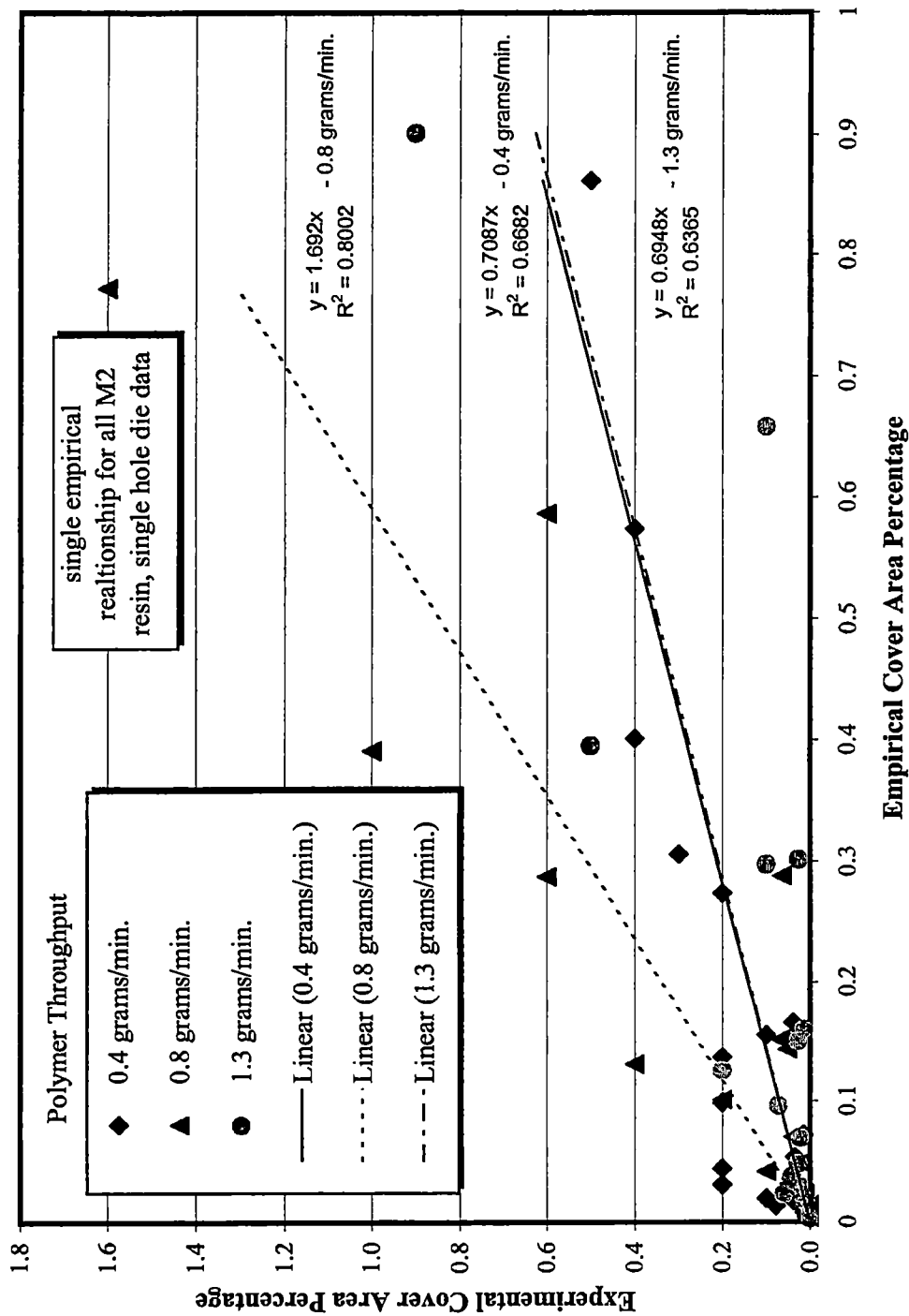


Figure 6.35: Empirical shot cover percentage vs. experimental shot cover percentage

These relationships differ from Equation 6.23 in that Equations 6.24 through 6.26 do not incorporate a polymer mass flux ratio (Γ) term. During the statistical analysis the exponent for the mass flux ratio term always had a asymptotic 95% confidence interval that contained zero as the intervals midpoint and therefore the exponent could be zero and delete the effect of the term altogether. The R^2 terms for each of the three polymer throughput empirical models are very similar. The asymptotic 95% confidence interval for the constants in Equations 6.24, 6.25 and 6.26 do not contain zero for eight out of the nine constants. The polymer Reynolds number's constant in Equation 6.26 had a confidence interval that barely included zero. Since this was the only constant and the zero value was not near the midpoint of the interval it was decided to accept the statistical programs value. Figure 6.36 is a plot of experimental cover area percentage against empirical cover area percentage using the above empirical models. This figure indicates that one empirical model per polymer throughput is much better at predicting the data than that of one empirical model for the dimensionless parameters that are being employed. Future study may create dimensionless variables that aid in capturing the variable polymer throughput effect that eluded this study. Overall, the use of traditional fluid flow dimensionless variables worked reasonably well and could be considered a parallel to the dimensionless parameter empirical model.

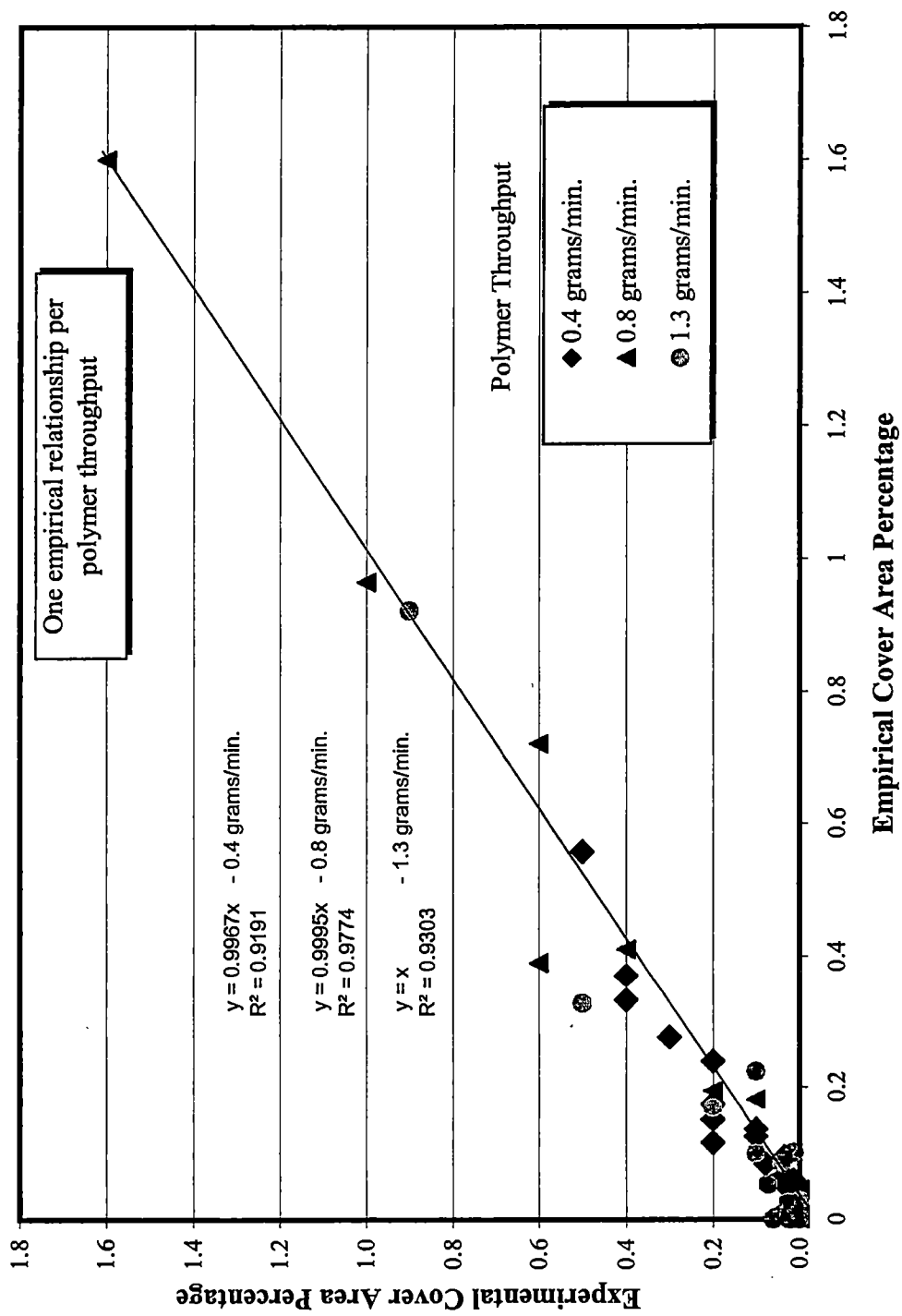


Figure 6.36: Empirical shot cover percentage vs. experimental shot cover percentage

Chapter VII

Investigation into the use of Nucleating Agents to Reduce Shot Production

With the exception of the six resin study in Chapter IV, previous study in this investigation has been concerned with the processing conditions at which the shot was formed. This was primarily done in order to determine the processing conditions at which the shot production is minimized. Little attention has been given to the role the polymer itself might play in reducing the shot production. As previously stated, the theory that shot was caused by melt fracture during attenuation has been mostly discarded since 1991 when Milligan and Haynes used photographic methods to prove that fibers in melt blown webs were actually continuous filaments. This revelation has given rise to the theory that molten filament collisions during attenuation cause more massive filaments, which produce shot upon impact with the collector.

If one subscribes to the filament collision model, shot is caused by molten filaments colliding and fusing in flight. This fused mass then requires more solidification time due to its increased mass to surface area ratio. If more solidification time is not supplied then a semi-molten fused mass will impact the collector surface and create a shot particle in the web sample. Therefore, if molten filament collisions that possibly cause these more massive filaments could be reduced then shot could possibly be reduced. If one wants to reduce the number of molten filament collisions then one must do one of the two following items:

- Create a situation in which fibers do not collide during the attenuation process. This is an aerodynamic problem.
- Create a situation in which fibers are not molten upon collision. This is a material property problem if the rate at which heat is transferred from the filaments remains constant.

Exxon provided this investigator with two sets of resins that each contained a nucleating agent. The purpose of this nucleating agent additive is to accelerate the crystallization process (solidification) during the attenuation process. If the nucleating agent were to successfully accelerate the crystallization process then the probability of filaments fusing would be reduced. The resins differed by the parts per million (ppm) content of nucleating agent and the agent type itself, but the base resin was always the same M2 metallocene resin. These resins were each melt-blown at the following process conditions:

Process Temperatures (Air and Polymer)	-	480°F, 450°F, 420°F
Die Pressure	-	7 [psig], 5 [psig], 3 [psig]
Nosepiece	-	30 hole die
Polymer Throughput	-	0.8 [grams/minute/hole]
Die Setback and Die Gap	-	0.079 [inches]
Die to Collector Distance	-	16 [inches]

The web samples were then analyzed to determine the average fiber diameter and shot production. Since the nucleating agents should reduce the time a filament is molten then the nucleated resins should have a larger average fiber diameter than that of the base resin, M2. The major difference between the samples collected for this analysis and the samples collected in Chapter IV is that these samples were created using a multiple hole die. A multiple hole die is used since this die would have more filament to filament collisions than that of a single hole die.

The first set of resins tested was treated with the nucleating agent NA-1 at two different concentrations. These resins are designated as NR1 and NR2 with NR2 having twice the level of the NA-1 nucleating agent. Again, these nucleated resins are all based on the metallocene resin M2. Figure 7.1 and 7.2 provide the results for the shot production tests and fiber diameter test of these resin's web samples. The base resin's web samples were tested also and the results are included in the figures for comparative purposes. Figure 7.1 indicates that the shot production of the nucleated resins was not reduced below that of the M2 base resin. This figure seems to indicate that the addition of the nucleating agent was not successful in reducing shot production. Figure 7.2 indicates the base resin has the smallest average fiber diameter as expected.

With the previous results in hand, it was decided that maybe the amount of nucleating agent was insufficient to affect the highly dynamic system of the melt blowing air jet. Exxon provided four more nucleated resins with more nucleating agent content or a different nucleating agent altogether. Two of these resins (NR3 and NR4) utilized the same NA-1 nucleating agent as the previous investigation. NR3 has three times the NA-1 nucleating agent of the NR1 resin and NR4 has twenty times the NA-1 nucleating agent of the NR1 resin. The other two provided resins (NR5 and NR6) utilize a different nucleating agent altogether. These resins use a nucleating agent NA-2 at levels equal to that of the level of NA-1 in NR1 and NR2. Figure 7.3 is a plot of shot production versus process temperature for all the NA-1 nucleated resins. Again, this figure indicates the further addition of nucleating agent

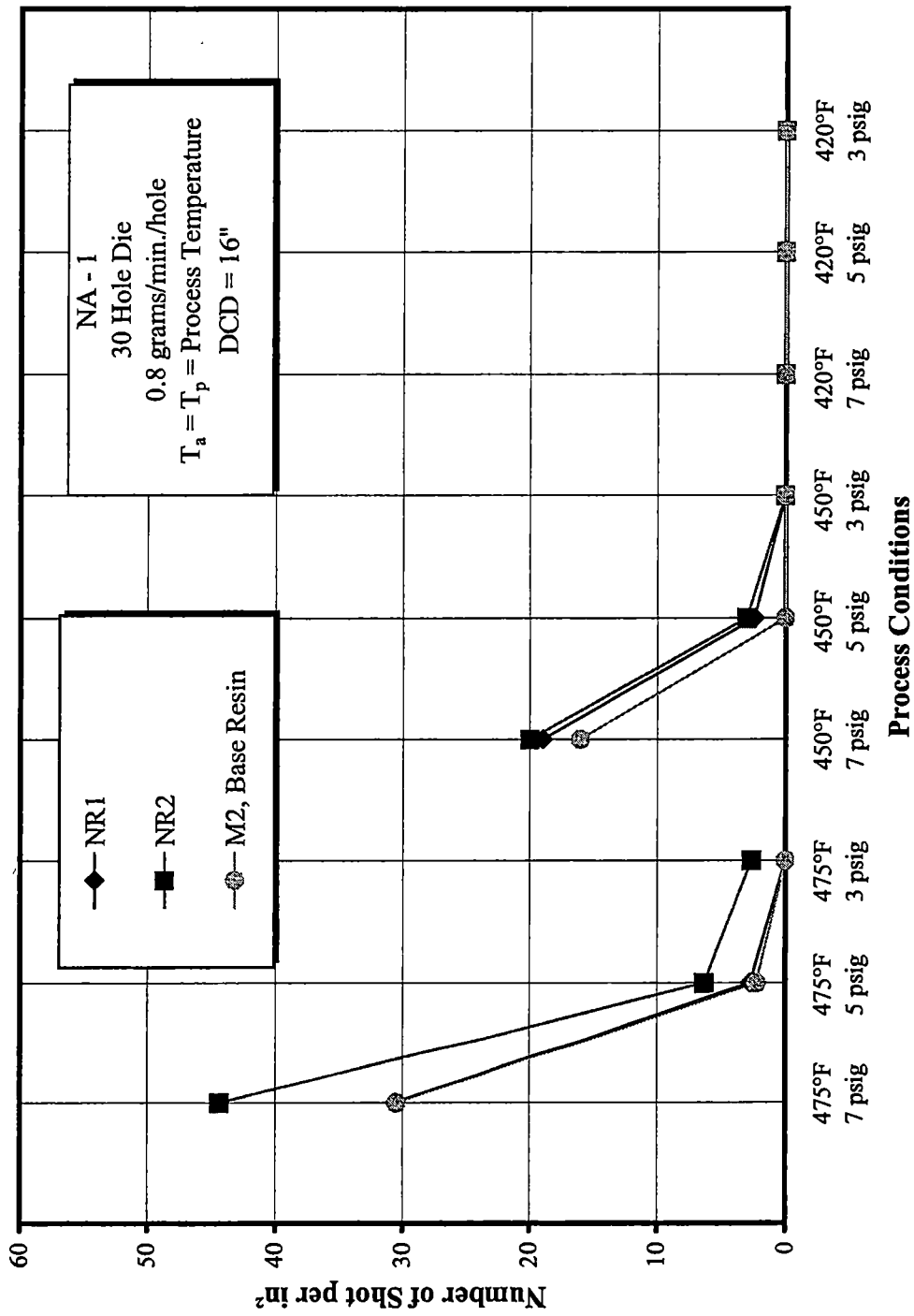


Figure 7.1: Number of shot per in² vs. process conditions

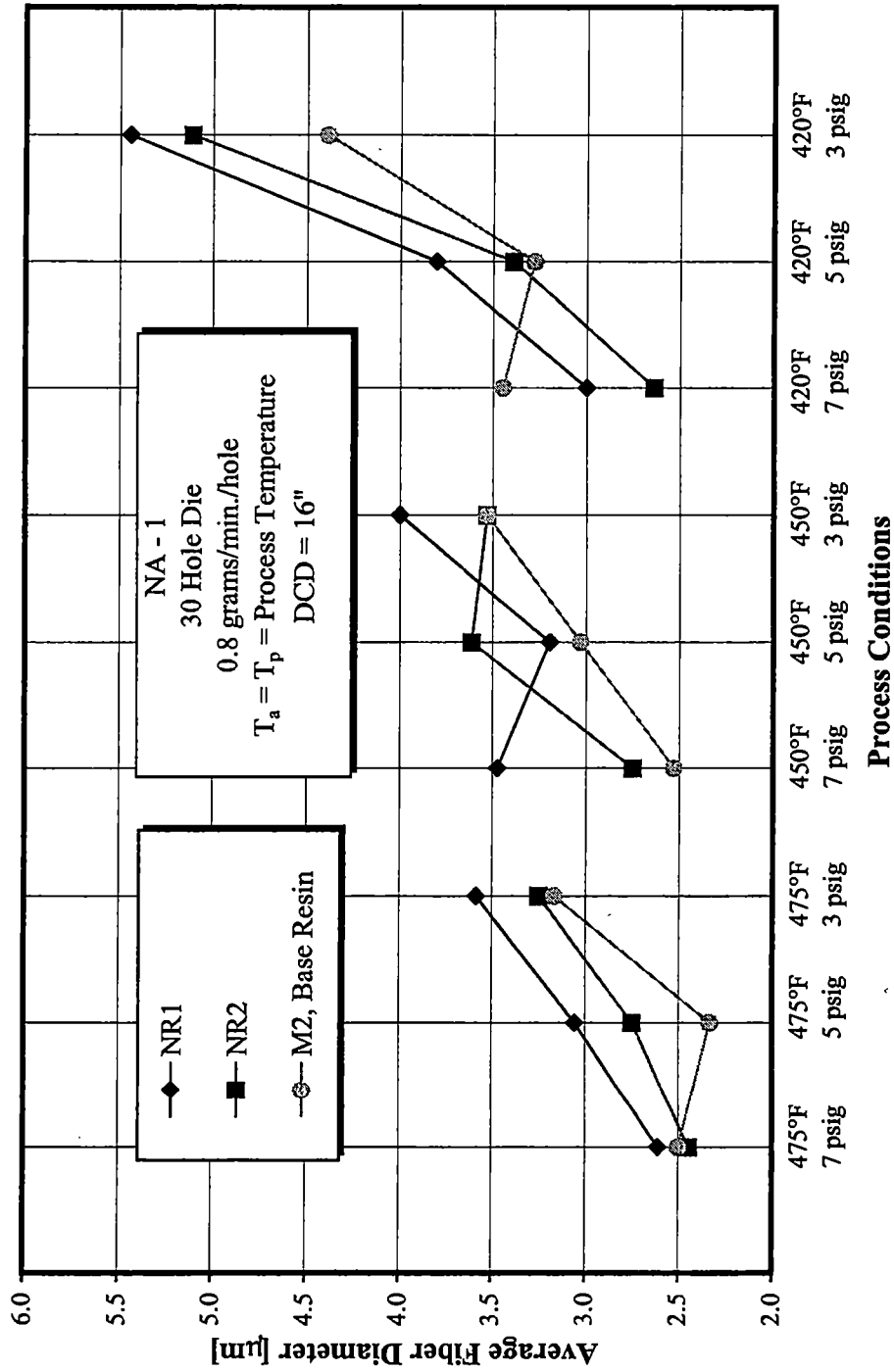


Figure 7.2: Average fiber diameter vs. process conditions

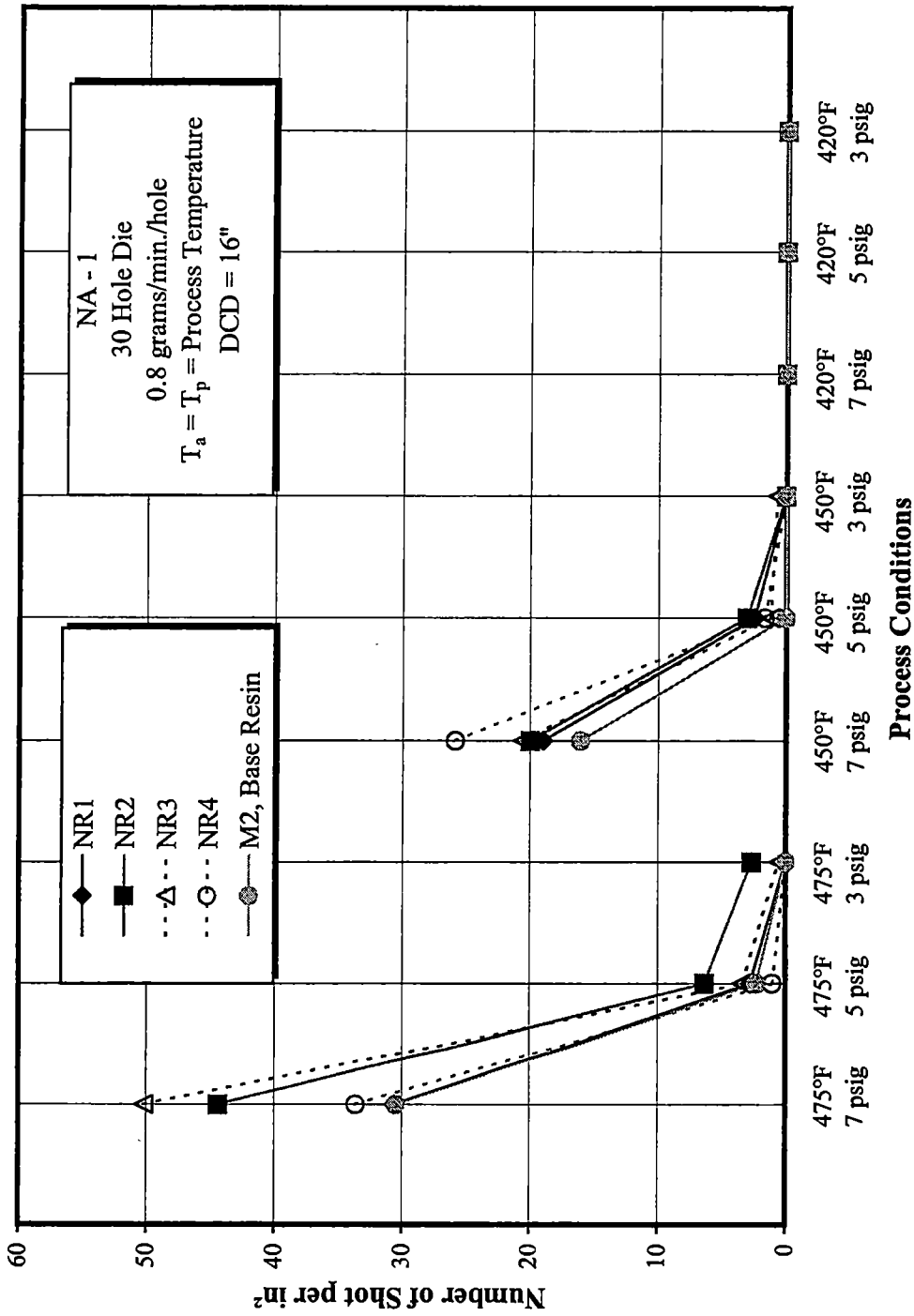


Figure 7.3: Number of shot per in² vs. process conditions

to the base resin made little difference in the shot production. Figure 7.4 is similar to Figure 7.2 in that the smallest fibers are usually created with the base resin but any changes in diameter due to nucleating level are within the diameter measurement's uncertainty. Figure 7.5 indicates that the addition of the nucleating agent NA-2 to the base resin M2 does not reduce the shot production. Figure 7.6 indicates that the smaller fibers are created with the M2 base resin. However, as with the previous resin, any changes in fiber diameter are within the experimental uncertainty of the diameter measurements.

Since Figures 7.3 and 7.5 indicate that the shot production is not reduced by the addition of the nucleating agent one might question whether the nucleating agent had any effect on the resin at all. In order to test this, the produced web samples were subjected to tests that would determine if the crystallization kinetics of the nucleated resins were different than that of the base resin. This was accomplished by performing differential scanning calorimetry (DSC) tests on a portion of a melt blown web sample created with each of the nucleated resins and the base resin. The DSC measures the time required for crystallization in a quiescent cooling environment. Figure 7.7 indicates that the addition of the nucleating agent in various percentages did indeed change the quiescent crystallization kinetics. Figure 7.7 is a plot of crystallization half-time versus environmental temperature which crystallization occurs for an isothermal quiescent process. This figure indicates that the nucleated resins, for the most part, have a shorter crystallization time than that of the base resin. Also, Figure 7.7 indicates that the half-times for a constant environmental

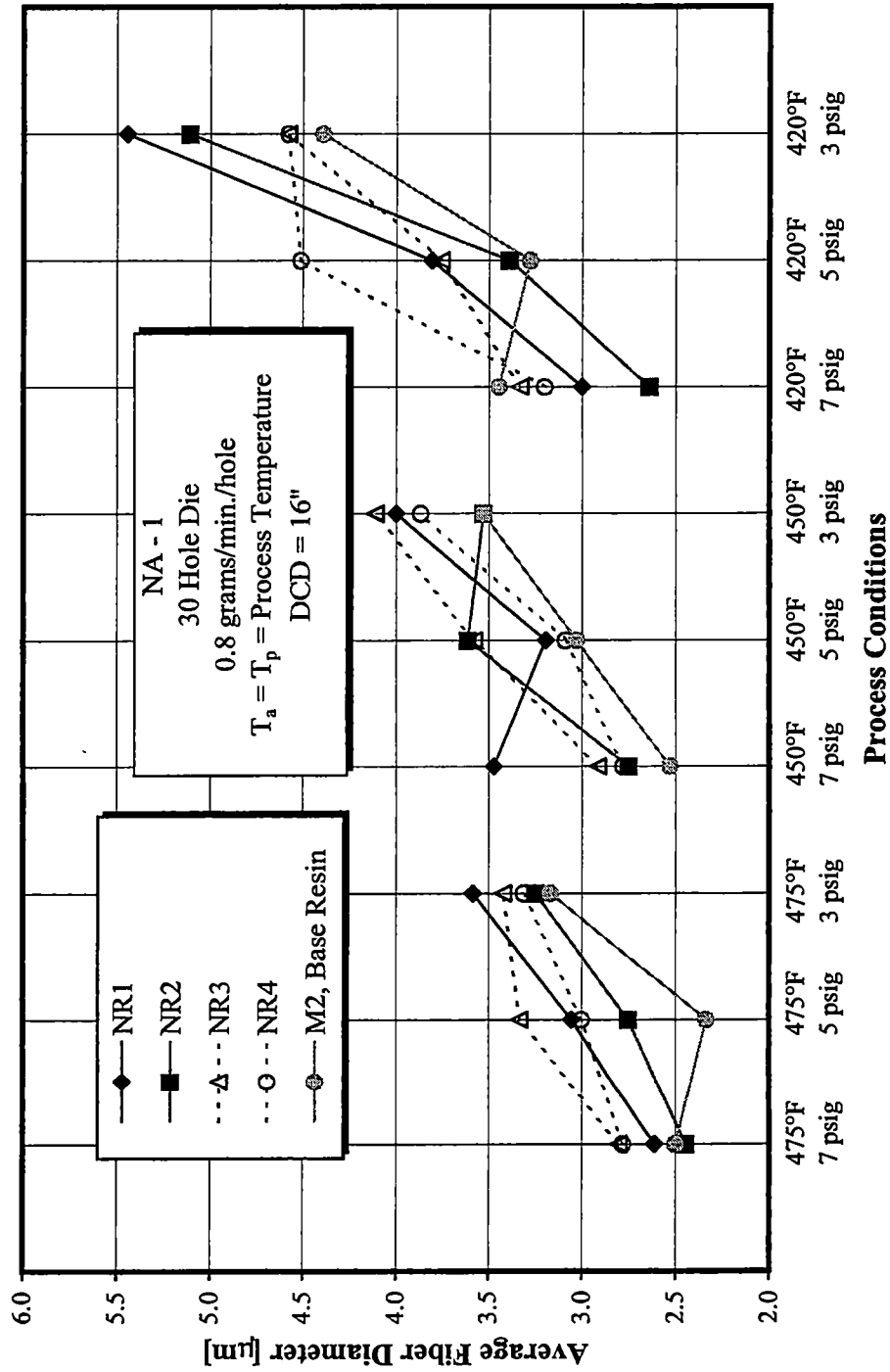


Figure 7.4: Average fiber diameter vs. process conditions

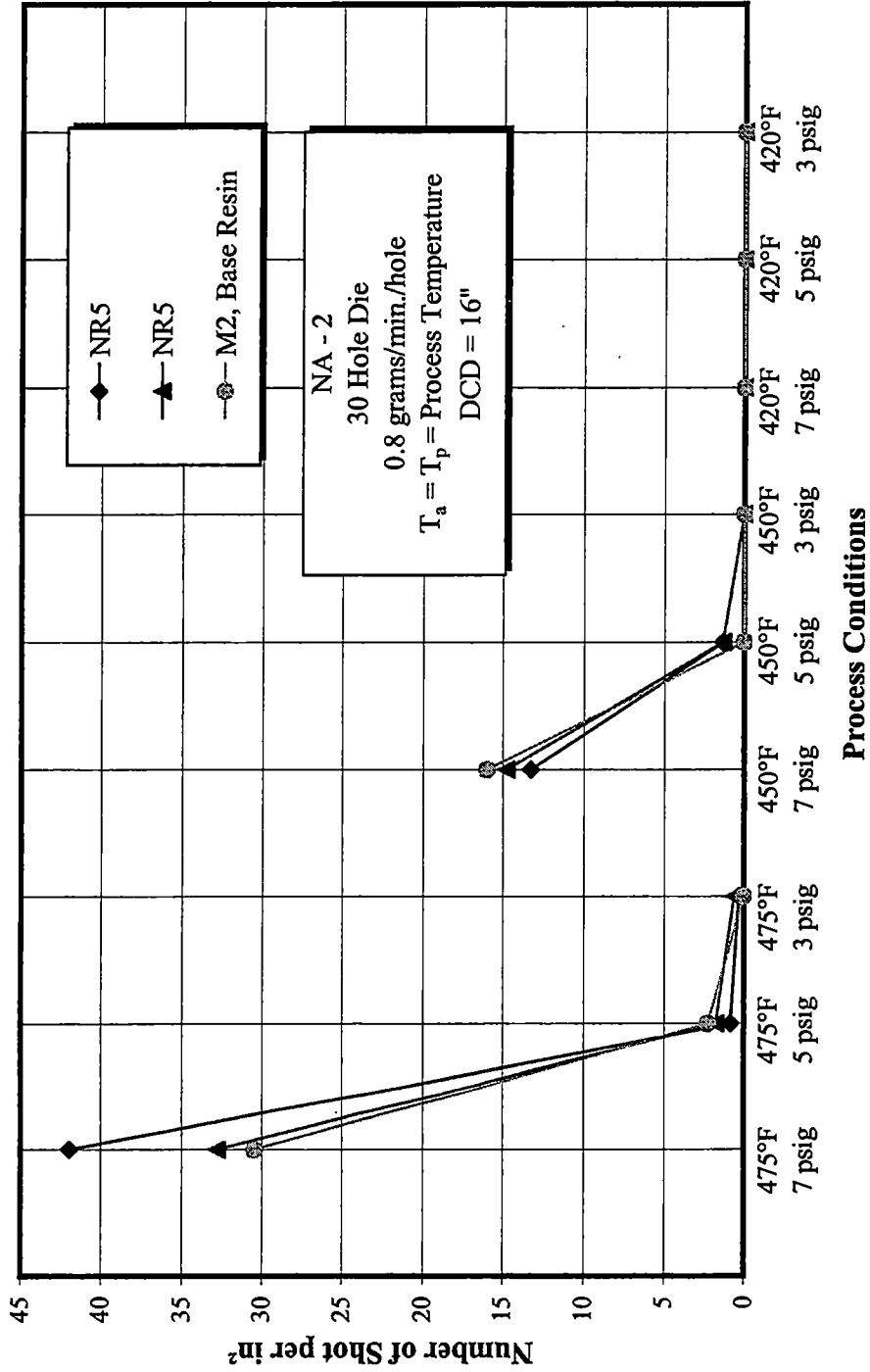


Figure 7.5: Number of shot per in² vs. process conditions

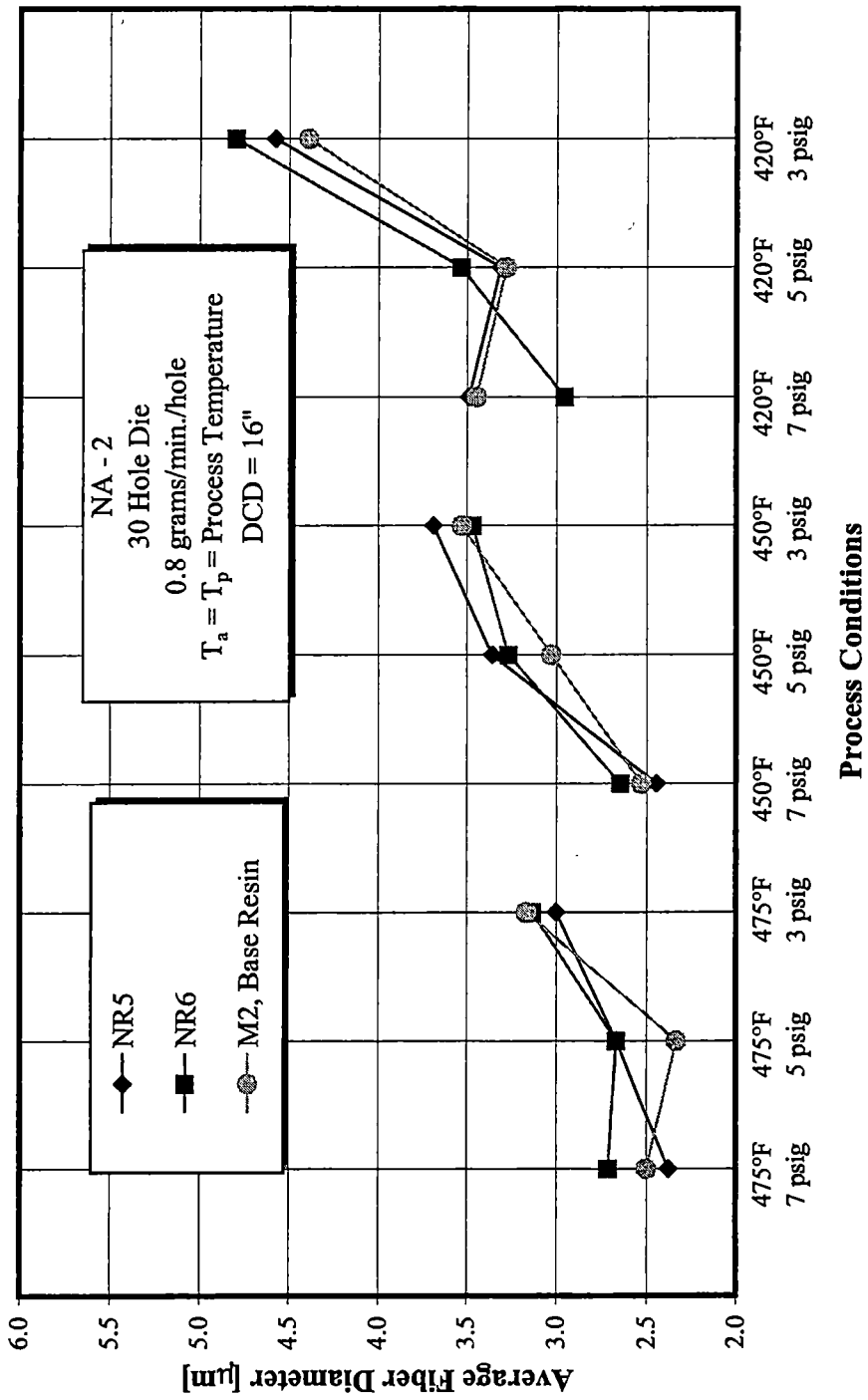


Figure 7.6: Average fiber diameter vs. process conditions

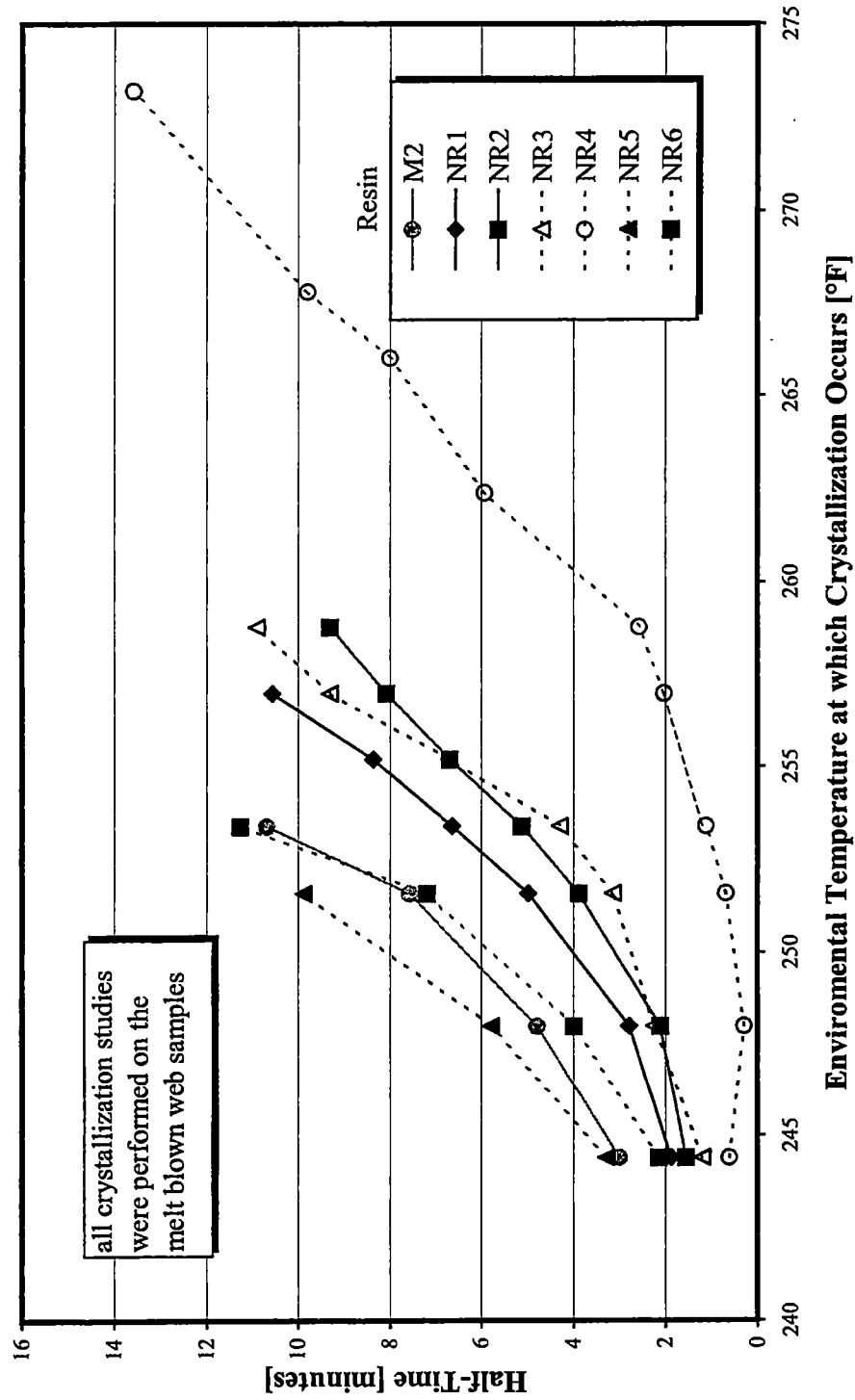


Figure 7.7: Crystallization half-time vs. environmental temperature at which crystallization occurs

temperature decrease as the percentage of nucleating agent is increased. Recall that the resins NR1, NR2, NR3 and NR4 utilize the same NA-1 nucleating agent in increasing percentages. The NR4 resin has the highest percentage of the NA-1 nucleating agent at levels twenty times that of the NR1 resin. Therefore it is understandable why the NR4 half-time curve in Figure 7.7 is so displaced from that of the other resins. This figure also indicates that the NA-2 nucleating agent used in the NR5 and NR6 resins was not nearly as effective as its NA-1 counterpart.

The shot data indicates that the addition of a nucleating agent in the provided concentration does very little to effect the shot production of the M2 metallocene base resin. The conclusions drawn from this nucleating agent investigation are as follows:

- The addition of nucleating agent does effect the crystallization kinetics of the base resin in a quiescent environment in the desired manner for the NA-1 nucleating agent. The NA-2 agent demonstrated no real effect on the base resin crystallization kinetics in the same quiescent environment.
- The nucleating agents do not affect the crystallization kinetics of the filament during the highly dynamic fiber attenuation period or that filament collisions and fusion are not the primary mechanism for shot production.

The previous chapter demonstrated the ability of two different empirical models to estimate the shot production of a melt blowing process using a single hole die. The data collected in this chapter is one of the few instances in which a multiple hole die was used to create web samples. Since these multi hole die web samples had already been analyzed for shot, there was interest to investigate how well the single hole empirical model would estimate the multi-hole shot production. The only

difference between the single hole die and thirty hole die experimental data is the total polymer throughput. The polymer throughput variable used in the process parameter empirical model, Equation 6.15, is based on polymer throughput per hole but since the single hole die has only one hole this parameter could be total polymer throughput also. However, since the single hole die possessed a quadratic polymer throughput relationship the model will not produce realistic results if the total throughput is used for the multi hole die configuration. The total throughput for the multi hole die is approximately 24 grams per minute and the single hole model will return a negative value for the modified number of shot per area ratio (H) if this total polymer throughput is used. Therefore for this comparison, the polymer throughput per hole was used for the multi hole die polymer throughput parameter in the empirical model. The comparison is performed by using the modified number of shot per area ratio in order to compare these data using the single processing variable, Φ . This comparison is shown in Figure 7.8, and demonstrates that the multi hole experimental data follows a similar trend to that of the single hole data and could be used to determine the effect of varying process parameters. The only concern this figure reveals is that the single hole empirical model over estimates the modified number of shot per area ratio for the multi hole situation. Since the model was created using single hole experimental shot data at the same processing conditions one would expect the empirical curve to lie below that of the multi hole experimental shot data. This would be expected since it is known that multi hole dies produce more shot than single hole dies for a constant set of processing conditions. The best explanation for this phenomenon is that the single hole empirical model data has

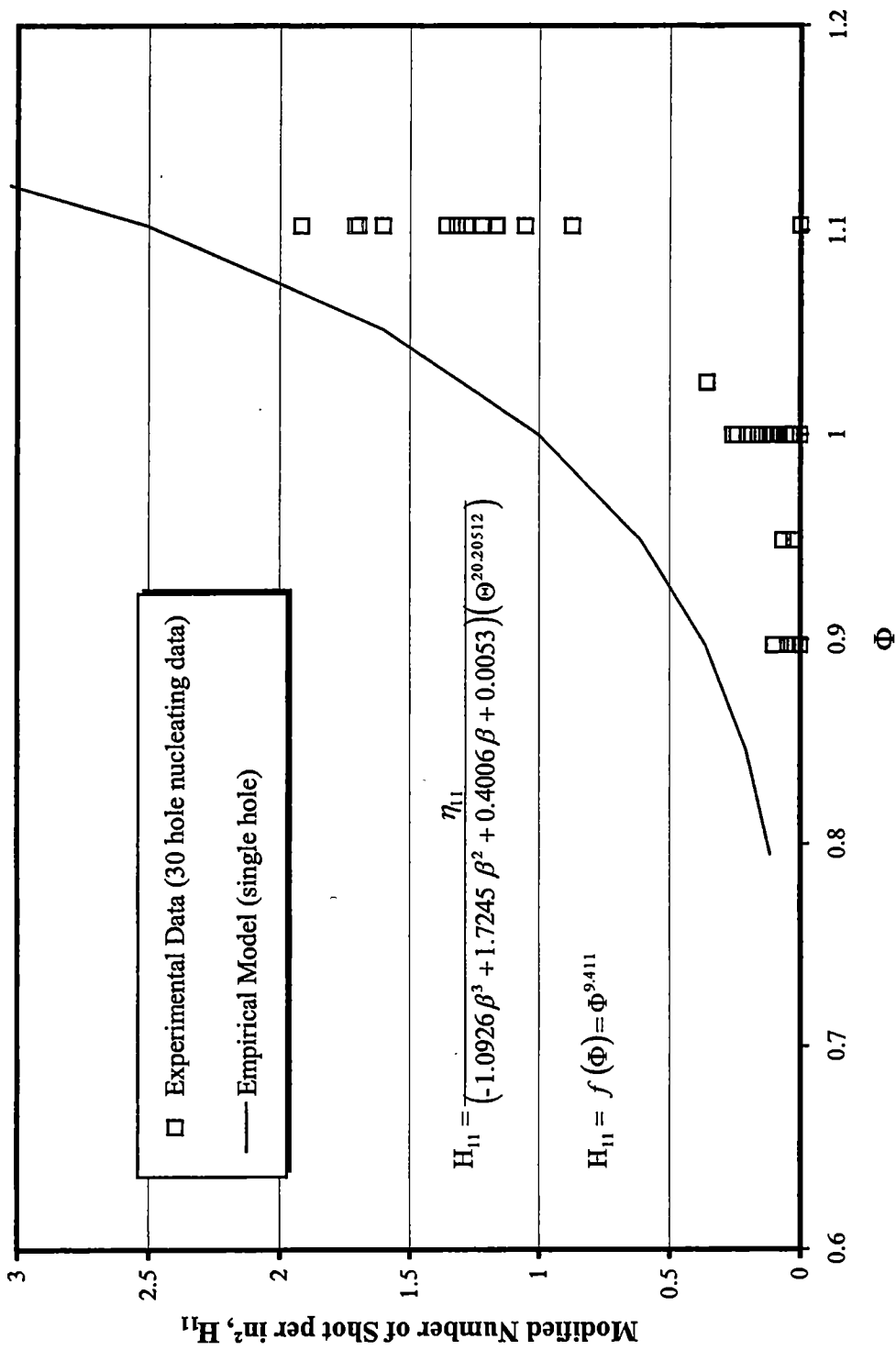


Figure 7.8: Comparison between single hole empirical model and 30 hole nucleating data

higher die air pressure ratios (Φ) than that of the multi hole die experimental data. Since it has been previously shown that the shot production increases with increasing die air pressure ratio (Φ) the model was created to include these higher processing conditions and application of the model to lower values of die air pressure could result in an overestimation. Another area where the two sets of data vary is web sample basis weight. The collector drive ratio limitations would not allow the collector to operate at a RPM level that would enable the single hole experimental data and the thirty hole experimental data to be collected at the same basis weight. Therefore the thirty hole web samples have a higher basis weight and hence are thicker. This thickness could have allowed some of the shot to be missed during the WebPro analysis. This is only a possible explanation for the difference and this difference should not overshadow the observation that the single hole model does a respectable job in modeling the shot production trend of the multi hole die experimental.

Chapter VIII

Conclusions and Recommendations

The following conclusions have been stated in the previous chapters and are presented here for clarity and conciseness. These conclusions have been developed based on the experimental data collected in this investigation.

Experimental Investigation Processes Summary

1. Average fiber diameter measurements performed with the optical microscope, scanning electron microscope and the WebPro diameter analysis were agreeable in that the fiber diameter trends were the same for each procedure. With this in mind the optical method was preferred since this investigation possessed the optical microscope and would need to enlist outside help for the other two methods.
2. The WebPro shot analysis method worked very well for web samples that possessed fine fibers and were produced at an optically opaque basis weight. For a given basis weight the web samples with fine fibers were very dense optically and light would pass through any shot particle much easier than through the surrounding fine fibered web. This type of web would tend to produce very reliable and repeatable shot analysis results. However, webs with larger fibers would not be as optically dense and allow much more light transmittance than that of the fine fibered webs. This light transmittance could be (and quite often is) interpreted by the WebPro as a shot particle.

Experimental Investigation Summary

Six resin study

1. Metallocene resins produce more shot than the conventional Zigler-Natta resins with all other parameters being constant. Therefore it might be implied that the narrower molecular weight distribution resins do not produce less shot than that of the standard molecular weight distribution.

2. Melt blown web samples created using the thirty hole die contain more shot than web samples created using a single hole die with all other parameters being constant.

Experimental investigation into process parameters

1. Average fiber diameter decreases with increasing die air pressure (air velocity) for a constant process temperature and polymer throughput.
2. Average fiber diameter decreases with increasing process temperature for a constant die air pressure and polymer throughput.
3. Average fiber diameter increases with increasing polymer throughput for a constant process temperature and die air pressure.
4. Shot production increases with increasing die air pressure (air velocity) for a constant process temperature and polymer throughput.
5. Shot production increases with increasing process temperature for a constant die air pressure and polymer throughput.
6. Shot production depends on polymer throughput and may increase or decrease with increasing polymer throughput for a constant process temperature and die air pressure.
7. There is an inverse relationship between shot production and average fiber diameter processing trends. The same process parameters that produce small fiber diameters aid in the production of shot for constant polymer throughput.
8. There is no apparent correlation between shot production and average fiber diameter uniformity (coefficient of variation or standard deviation). Variable aerodynamic forces generate non uniform fiber diameters and logically increase filament collisions. If this was the case then there should have been a relationship between shot production and web sample fiber diameter non uniformity.

Comparison between experimental average fiber diameter ratio and Spencer's [13] empirical average fiber diameter ratio

1. Empirical average fiber diameter ratio relationship created by Spencer [13] compares very well with the experimental average fiber diameter ratio of this investigation.
2. Addition of polymer MFR term to empirical average fiber diameter ratio relationship does not increase the accuracy of the relationship very much if at all.

Single hole shot production model

1. Single variable models did not model the shot production well. The best single variable was the air velocity ratio and this indicated that a multi variable model might apply since air velocity is comprised of air temperature and air pressure.
2. Incorporation of polymer throughput term was most difficult due to its quadratic nature. This parameter was incorporated by trial and error and using a modified number of shot per area ratio. The trial and error results were then incorporated into the temperature and pressure statistical relationship. This relationship modeled the experimental data very well. The model does not necessarily agree with the experimental data at every point but the model does indicate the proper trends of the experimental output for a given process parameter variation.
3. Application of independent experimental data demonstrated that the model does capture the trends of these data as well.
4. The largest variation of experimental data from that of the empirical model occurs at the lower process conditions (both temperature and pressure).

5. Modeling the shot production using classical dimensionless parameters (air and polymer Reynolds Numbers and air momentum flux ratio) worked quite well when the models were derived for individual polymer throughputs. A previous attempt to model all the experimental data using a single model was unsuccessful in that one model could not capture the affect of polymer throughput.

Investigation into the use of Nucleating Agents to Reduce Shot Production

1. The addition of nucleating agents to the M2 metallocene resin in various percentages had little effect on the shot production.
2. The use of the nucleating agents in resins does reduce the crystallization time of the resins in a quiescent isothermal environment. Therefore the nucleating agents do effect the resin's solidification time in a quiescent isothermal environment but evidently these agents do not effect the solidification time in the highly dynamic environment of the attenuation air jet or else the solidification time is not important in shot production.

Recommendations

1. Investigate the effect of polymer throughput on the shot production further. The quadratic form of the polymer throughput variable became a dominant parameter in the empirical relationship determination. The effect of the polymer throughput variation on shot production is very puzzling even though the results were confirmed with more investigation. Further study might alleviate the inherent skepticism in the inverse relationship between polymer throughput and shot production for polymer throughputs greater than 0.8 grams/minute.
2. Reinvestigate the melt blowing process through the use of high speed video. The previous tests did not capture enough time to confirm that a shot causing situation had been captured on tape and therefore little was learned in the previous high speed video taping experiments.

List of References

List of References

- [1] American Society for Testing and Materials: Annual Book of Standard, Philadelphia, Pennsylvania, 1989.
- [2] www.nonwovens.com, Miller Freeman Paper Newsgroup, San Francisco, CA, July 1998.
- [3] Nutter, W.: Textile Month, No. 5, 1970, pp.94-100.
- [4] Malkin, S.R. et. al. :Nonwovens: An Advanced Tutorial, Turbak, A.F. and Vigo, T.L., Editors, TAPPI Press, Atlanta, USA, 1989, p.101-129.
- [5] Wadsworth, L.C. and McCulloch, W.J.G. :Meltblown Technology Today, Miller Freeman Publications, San Francisco, 1989, pp. 28-40.
- [6] Wente, V.A., "Superfine Thermoplastic Fibers," Industrial and Engineering Chemistry, Vol. 48, No. 8, 1956, pp. 1342-1346.
- [7] Buntin, R.R. and Lohkamp, D.T., "Melt Blowing – A One-Step Web Process for New Nonwoven Products", TAPPI, Vol. 56, No. 4, April 1973, pp. 74-77.
- [8] Shambaugh, R.L., "A Macroscopic View of the Melt-Blowing Process for Producing Microfibers", Ind. Eng. Chem. Res., 1988, Vol. 27, No. 12, pp. 2363-2372.
- [9] Malkin, S.R., Process-Structure-Property Relationship in Different Molecular Weight Polypropylene Melt Blown Webs, Ph.d. Dissertation, University of Tennessee, Knoxville, May 1990.
- [10] Milligan, M.W. and Haynes, B.D., "Experimental Investigation of Melt Blowing", INDA Journal, Vol. 3, No. 4, Fall 1991, pp. 20-25.
- [11] Utsman, F.M., An Experimental Investigation on the Production of Microfibers and the Web Defect Known as Shot for the Melt Blowing Process, Thesis, University of Tennessee, Knoxville, 1995.
- [12] Milligan, M.W. and Bogard, J., "Model for Shot Formation in Melt Blowing", 7th Textile and Nonwoven Development Center Meeting, Knoxville, TN, Nov. 1997.
- [13] Spencer, E.G., An Experimental Investigation of Processing Parameters for the Production of Micro Fibers Using the Melt Blowing Process, Thesis, University of Tennessee, Knoxville, 1994.

- [14] Rodriguez, Ferdinand, Principles of Polymer Systems, fourth edition, Taylor and Francis, New York, 1996.
- [15] Flow Measurement, "ASME, Power Test Code," PTC 19.5:4, 1959.
- [16] Haynes, B.D., An Experimental and Analytical Investigation of the Production of Microfibers Using a Single Hole Melt Blowing Process, Ph.D. Dissertation, University of Tennessee, Knoxville, 1991.
- [17] Bogard, John, Master's Thesis yet to be completed, University of Tennessee, 1999.
- [18] Yan, Z. and Bresse, R.R., "Characterizing Nonwoven-web Structure by Using Image-analysis Techniques Part V: Analysis of Shot in Meltblown Webs", The Journal of Textile Institute, Volume 89, 1998, p. 328.
- [19] Neville, A.M. and Kennedy, J.B., Basic Statistical Methods for Engineers and Scientist, International Textbook Company, Scranton, PA, 1964.
- [20] Patel, R., Rheological Properties of Low Molecular Weight Polypropylenes, Thesis, University of Tennessee, Knoxville, 1988.

Appendices

Appendix I

Derivation of Air Jet Exit Area Expression

This section is taken in its entirety from Spencer [13] and presented here for completeness. There have been a few slight modifications to Spencer's original section for conformity sake.

Figure AI.1 shows an exploded view of the die tip and face plates. The distance between the inclined surface of the die and inner inclined surface of the face plates is called the air gap (d_g). The air gap reduces/increases the flow area available for the air to flow through the test section. Setback (d_s) is the distance between the tip of the nose piece and the exit plane of the test section. The included angle (α) of the die is also shown in Figure AI.1. The angle θ represents the angle at which the top and bottom air jet streams converge at the tip of the die. This angle is one half of the die included angle ($\theta = \alpha/2$).

From the geometry of the die and the face plates shown in Figure AI.1, the following relationships can be written from fundamental geometry principles:

$$d_s = x_3 + x_1 \quad \text{AI.1}$$

$$h = 2 x_4 + d_{\text{die}} \quad \text{AI.2}$$

$$x_3 = d_g \sin \theta \quad \text{AI.3}$$

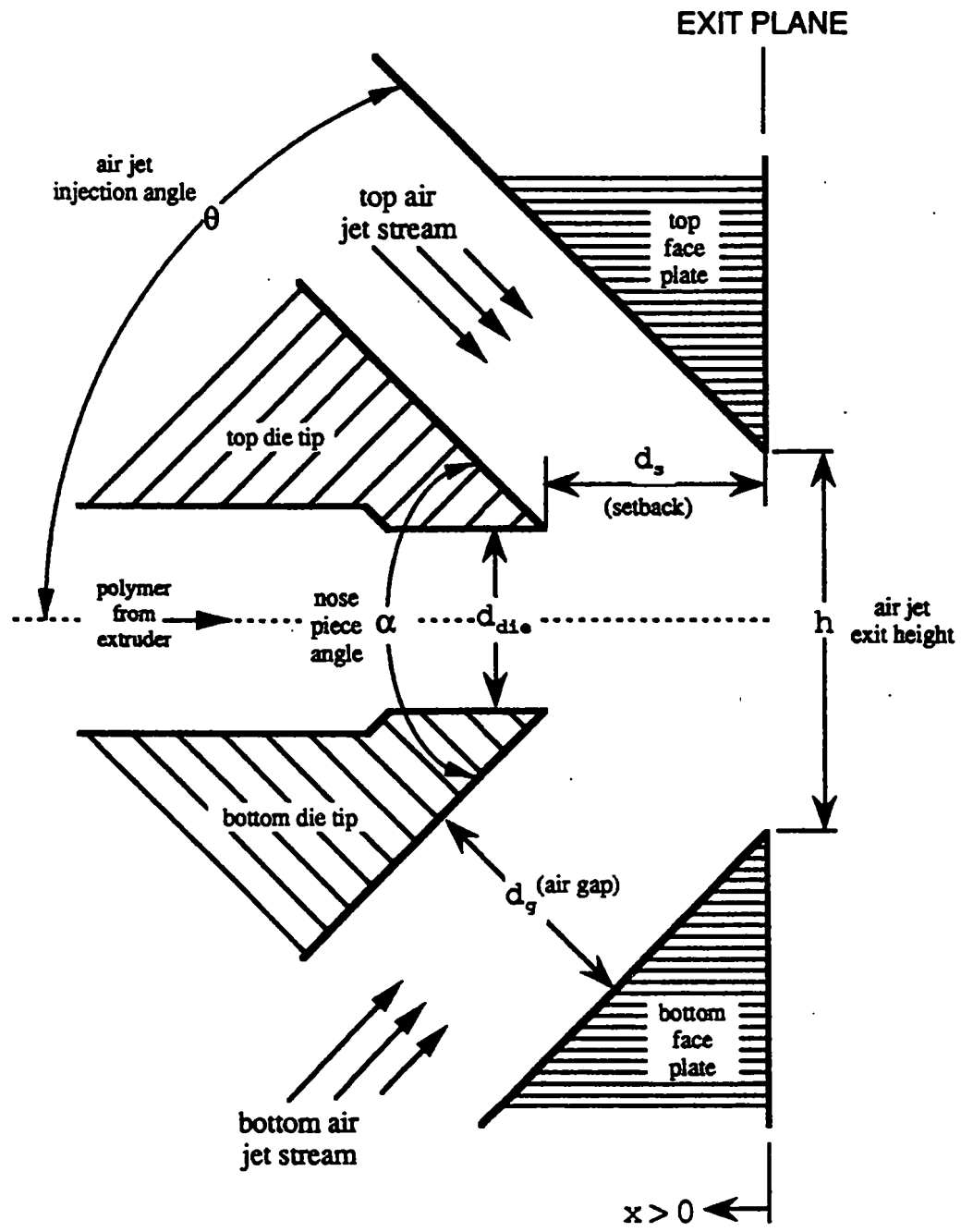


Figure AI.1: Exploded view of the die tip and face plates

Source: Spencer, E.G., An Experimental Investigation of Processing Parameters for the Production of Micro Fibers Using the Melt Blowing Process, Thesis, University of Tennessee, Knoxville, 1994.

$$x_2 = x_1 \tan \theta \quad \text{AI.4}$$

$$(d_g)^2 = (x_3)^2 + (x_4 + x_2)^2 \quad \text{AI.5}$$

where

$$\theta = \alpha/2$$

$$d_{die} = 356 \mu\text{m}$$

Solving equation AI.5 for x_4 and substituting into equation AI.2:

$$h = 2 \left[\sqrt{(d_g)^2 - (x_3)^2} - x_2 \right] + d_{die} \quad \text{AI.6}$$

Substituting x_3 from equation AI.3 into equation AI.6:

$$h = 2 \left[\sqrt{(d_g)^2 - (d_g \sin \theta)^2} - x_2 \right] + d_{die}$$

$$h = 2 [d_g \cos \theta - x_2] + d_{die} \quad \text{AI.7}$$

Substituting x_2 from Equation AI.4 into Equation AI.7:

$$h = 2 [d_g \cos \theta - x_2 \tan \theta] + d_{die} \quad \text{AI.8}$$

Substituting x_1 from Equation AI.1 into Equation AI.8:

$$h = 2 [d_g \cos \theta - (d_s - x_3) \tan \theta] + d_{die} \quad \text{AI.9}$$

Substituting x_3 from Equation AI.3 into Equation AI.9:

$$h = 2 [d_g \cos \theta - d_s \tan \theta + d_g \sin \theta \tan \theta] + d_{die} \quad \text{AI.10}$$

Rearranging Equation AI.10, the expression for the air jet exit height at the test section exit plane becomes:

$$h = 2 \left[d_g (\cos \theta + \sin \theta \tan \theta) - d_s \tan \theta \right] + d_{die} \quad \text{AI.11}$$

Equation AI.11 expresses the air jet exit height in terms of variables that are easily measured; air gap, setback, and air jet injection angle. Both the 60° and 90° included angle dies are four inches wide. Therefore, the air jet exit area is given by multiplying the air jet exit height by the width of the die:

$$A_e = w [\text{in}] \left(2 \left[d_g (\cos \theta + \sin \theta \tan \theta) - d_s \tan \theta \right] + d_{die} \right) \quad \text{AI.12}$$

where:

A_e	air jet exit in in^2
w	air jet exit width
d_s	setback in inches
d_g	air gap in inches
θ	air jet injection angle in degrees
d_{die}	air orifice diameter in inches

Appendix II

Derivation of Air Flow Rate Expression

The following derivation is based in the ASME Flow Measurement Standard Code [15] and is presented by Haynes [16] and Spencer [13]. The purpose of this rederivation is to completely show the manner in which the mass flow rate is determined from measured data. The mass flow rate of air through the system is constant and therefore we will determine the mass flow rate at the orifice. The air flow through an orifice is given by Equation AII.1 [15]:

$$\dot{m}_o = [359(C)(F)(d_{\text{orifice}})^2(F_e)\sqrt{h_m\rho_a}] \left[\frac{\text{lbm}}{\text{hr}} \right] \quad \text{AII.1}$$

- Where:
- C coefficient of discharge, from ASME Flow Measurement Code, (dimensionless)
 - F Velocity approach factor, from ASME Flow Measurement Code, (dimensionless)
 - d_{orifice} measuring orifice diameter in inches.
 - F_e Thermal Expansion Factor, from ASME Flow Measurement Code, (dimensionless)
 - h_m pressure drop across orifice in inches of water.
 - ρ_a density of air in lbm/ft^3 .

The coefficient of discharge, C, is considered to be constant at 0.61625 for the range of Reynolds numbers at which the air experiences at the orifice. This constant coefficient of discharge value was also used in work by Haynes [16] and Spencer

[13]. The Velocity approach factor, F, is determined from a relationship which utilizes the ratio of the orifice diameter to that of the internal pipe diameter. This relationship for F is given by:

$$F = \frac{1}{\sqrt{1 - \left(\frac{d_{\text{orifice}}}{d_{\text{pipe}}}\right)^4}} \quad \text{AII.2}$$

With d_{orifice} equal to 1.0346 [in.] and d_{pipe} equal to 2.0 [in.], the value for the velocity approach factor is equal to 1.0328. From the ASME Flow Measurement Standard Code [15] and information presented by Haynes [16] and Spencer [13], the value used for the thermal expansion factor, F_e , is considered to be unity for the temperature range experienced at the orifice location. For these known values of C, F, d_{orifice} and F_e , equation AII.1 becomes:

$$\dot{m}_o = \left[244.6 \sqrt{h_m \rho_a} \right] \left[\frac{\text{lbm}}{\text{hr}} \right] \quad \text{AII.3}$$

Thermodynamic texts allow for the density of air to be modeled with the following ideal gas relationship:

$$\rho_a = \frac{p}{T_{\text{pipe}} R} \left[\frac{\text{lbm}}{\text{ft}^3} \right] \quad \text{AII.4}$$

The pressure (p) in the ideal gas relationship is the absolute pressure directly upstream of the measuring orifice. The pressure regulator upstream of the orifice was set at 50 [psig] and the atmospheric pressure is noted to be p_∞ [psia]. Therefore the pressure (p) in the ideal gas relationship is $(50 + p_\infty)$ [psia].

$$p = (50 + p_{\infty}) \left[\frac{\text{lbf}}{\text{in}^2} \right] = \left[(50 + p_{\infty}) \left[\frac{\text{lbf}}{\text{in}^2} \right] \left(\frac{144 \left[\text{in}^2 \right]}{\left[\text{ft}^2 \right]} \right) \right] \left[\frac{\text{lbf}}{\text{ft}^2} \right]$$

Where R is the ideal gas constant for air:

$$R = 53.3 \left[\frac{\text{ft lbf}}{\text{lbm R}} \right]$$

The Temperature of the air at the orifice (T_{pipe}) is read in degrees Fahrenheit [$^{\circ}\text{F}$] from the thermometer. Upon substitution the relationship for air density becomes:

$$\rho_a = \frac{\left[(50 + p_{\infty}) \left[\frac{\text{lbf}}{\text{in}^2} \right] \left(\frac{144 \left[\text{in}^2 \right]}{\left[\text{ft}^2 \right]} \right) \right] \left[\frac{\text{lbf}}{\text{ft}^2} \right]}{T_{\text{pipe}} [^{\circ}\text{R}] * 53.3 \left[\frac{\text{ft lbf}}{\text{lbm R}} \right]} \quad \text{AII.5}$$

Upon substituting the air density relationship into equation AII.3 we get:

$$\dot{m}_o \left[\frac{\text{lbm}}{\text{hr}} \right] = 244.6 \sqrt{h_m [\text{in. of H}_2\text{O}] \left[\left[2.702 \left[\frac{\text{lbm } ^{\circ}\text{R in}^2}{\text{ft}^3 \text{ lbf}} \right] \left(\frac{(50 + p_{\infty}) \left[\frac{\text{lbf}}{\text{in}^2} \right]}{(T_{\text{pipe}} [^{\circ}\text{F}] + 460) [^{\circ}\text{R}]} \right) \right] \right] \left[\frac{\text{lbm}}{\text{ft}^3} \right]}$$

or

$$\dot{m}_o \left[\frac{\text{lbm}}{\text{s}} \right] = 0.1122 \sqrt{h_m [\text{in. of H}_2\text{O}] \left(\frac{(50 + p_{\infty}) \left[\frac{\text{lbf}}{\text{in}^2} \right]}{(T_{\text{pipe}} [^{\circ}\text{F}] + 460) [^{\circ}\text{R}]} \right)} \quad \text{AII.6}$$

The units for the constant 0.1122 are such that the entire right side of the above equation renders units of [lbm/s] when evaluated.

Appendix III

Derivation of Air Jet Exit Velocity Expression

The following is a derivation of the air test section exit velocity (V_e). The air mass flow rate is derived in Appendix II and we know that for our test apparatus the mass flow rate of air at the test section (\dot{m}_{ts}) is equal to that of the mass flow rate of air at the measuring orifice (\dot{m}_o). Therefore, from the conservation of mass relationship:

$$\dot{m}_o = \dot{m}_{ts}$$

Since the test section has a single inlet and a single outlet the continuity equation for this configuration can be written as:

$$\dot{m}_o = \dot{m}_{ts} = \rho_{ts} A_e V_e \quad \text{AIII.1}$$

Appendix II demonstrated that the mass flow rate at the measuring orifice is calculated to be:

$$\dot{m}_o \left[\frac{\text{lbm}}{\text{s}} \right] = 0.1122 \sqrt{h_m [\text{in. of H}_2\text{O}] \left(\frac{(50 + p_\infty) \left[\frac{\text{lbf}}{\text{in}^2} \right]}{(T_{\text{pipe}} [\text{°F}] + 460) [\text{°R}]} \right)} \quad \text{AII.6}$$

Therefore the velocity at the test section exit plane can be expressed as:

$$V_e \left[\frac{\text{ft}}{\text{s}} \right] = \frac{\left(0.1122 \sqrt{h_m [\text{in. of H}_2\text{O}] \left(\frac{(50 + p_\infty) \left[\frac{\text{lbf}}{\text{in}^2} \right]}{(T_{\text{pipe}} [^\circ\text{F}] + 460) [^\circ\text{R}]} \right)} \right) \left[\frac{\text{lbf}}{\text{s}} \right]}{\rho_{ts} \left[\frac{\text{lbf}}{\text{ft}^3} \right] A_e [\text{ft}^2]} \quad \text{AIII.2}$$

Now the density of air at the test section is needed. As in Appendix II the density of air at the test section exit can be modeled with the ideal gas relationship:

$$\rho_{ts} = \frac{p_{ts}}{T_{ts} R} \left[\frac{\text{lbf}}{\text{ft}^3} \right] \quad \text{AIII.3}$$

Where:

p_{ts}	-	static pressure of air at test section exit [lbf/ft ²]
T_{ts}	-	static temperature of air at the test section exit [°R]
R	-	ideal gas constant for air (53.3 [(ft lbf)/(lbfm °R)])

Since the static pressure at the test section's exit is not a experimentally measured quantity, this pressure must be found by other means. Haynes [16] and Spencer [13] both modeled the air moving through the test section as an isentropic process. This modeling process is valid since the irreversibilities of friction and heat transfer are considered insignificant. For an isentropic process the following relationship between temperature and pressure can be written:

$$\frac{T_1}{T_2} = \left[\frac{P_1}{P_2} \right]^{\left(\frac{\gamma-1}{\gamma} \right)} \quad \text{AIII.4}$$

Where: γ is the specific heat ratio of the gas being modeled.

In our situation, state 1 is considered to be static condition of the air jet at the test section exit and state 2 is the stagnation condition of the air jet at the test section exit.

Therefore, the above relationship can be written as:

$$T_{ts} = T_{ts_0} \left[\frac{P_{ts}}{P_{ts_0}} \right]^{\left(\frac{\gamma-1}{\gamma} \right)} \quad \text{AIII.5}$$

Where:

T_{ts}	static temperature of air at the exit of test section [°R]
T_{ts_0}	stagnation temperature of air at the exit of the test section [°R]
P_{ts}	static pressure of air at the exit of the test section [lbf/in ²]
P_{ts_0}	stagnation pressure of air at the exit of the test section [lbf/in ²]

Upon substituting the above equation for T_{ts} into the equation for density the density equation becomes:

$$\rho_{ts} = \left(\frac{P_{ts}}{R T_{ts_0} \left[\frac{P_{ts}}{P_{ts_0}} \right]^{\left(\frac{\gamma-1}{\gamma} \right)}} \right) \left[\frac{\text{lbm}}{\text{ft}^3} \right] \quad \text{AIII.6}$$

Now substitute the above density relationship into the air jet velocity exit at the exit plane relationship:

$$V_e \left[\frac{\text{ft}}{\text{s}} \right] = \frac{\left(0.1122 \sqrt{h_m [\text{in. of H}_2\text{O}] \left(\frac{(50 + p_\infty) \left[\frac{\text{lb}_f}{\text{in}^2} \right]}{(T_{\text{pipe}} [^\circ\text{F}] + 460) [^\circ\text{R}]} \right)} \right) \left[\frac{\text{lbm}}{\text{s}} \right]}{\left(\frac{p_{ts}}{R T_{ts0} \left[\frac{p_{ts}}{p_{ts0}} \right]^{\frac{\gamma-1}{\gamma}}} \right) \left[\frac{\text{lbm}}{\text{ft}^3} \right] A_e [\text{ft}^2]} \quad \text{AIII.7}$$

The p_{ts} term is still unknown and is not easily measured therefore this pressure must be evaluated in another manner. This pressure is determined by applying the properties of a converging nozzle during an isentropic process. A converging nozzle has a maximum Mach number of one that can be obtained at the exit of the test section. When the Mach number at the exit of the test section is one then the flow is said to be "choked". Gas dynamics texts state that for choked flow, Mach number equal one, the isentropic pressure ratio is given to be:

$$\frac{p_{ts}}{p_{ts0}} = 0.52828 \Rightarrow p_{ts0} = \frac{p_{ts}}{0.52828} \quad \text{AIII.8}$$

Another property of converging nozzles in isentropic flow is that if the flow is not choked then the discharge pressure of the nozzle is equal to that of the surroundings (p_∞). However, if the flow is choked then the discharge pressure is equal to 0.52828 times the upstream stagnation pressure. In this investigation the stagnation pressure (p_{ts0}) is considered to be the die air pressure due to the fact that the air velocity in the

test section is so much lower than that of the air exit velocity. Therefore, one would like to know what test section pressure (p_{ts0}) will cause the discharge air at the test section exit to be choked. Using the algebraically manipulated version of the isentropic pressure ratio, we can calculate the test section pressure that will cause choked flow at the test section exit for a known surrounding or atmospheric pressure (p_{∞}). For example, if the atmospheric pressure is known to be 14.5 [psia] then the corresponding test section pressure for choked flow to occur at the test section exit would be:

$$\frac{14.5 \text{ [psia]}}{0.52828} = 27.45 \text{ [psia]} \therefore p_{ts0} \text{ (psig)} = (27.45 - 14.5) = 12.95 \text{ [psig]}$$

With this known, it can be seen that if the test section pressure at or above 12.95 [psig] then the flow is choked and air pressure ratio at the test section exit is equal to:

$$\frac{p_{ts}}{p_{ts0}} = 0.52828 \text{ and } p_{ts} = (0.52828) p_{ts0}$$

If the test section pressure is below 12.95 [psig] then p_{ts} is equal to 14.5 [psia] and the pressure ratio at the exit is equal to:

$$\frac{p_{ts}}{p_{ts0}} = \frac{14.5 \text{ [psia]}}{p_{ts0} \text{ [psig]} + 14.5 \text{ [psia]}}$$

These example calculations are based on (p_{∞}) being 14.5 [psia] and should be corrected if this value of (p_{∞}) is not representative of the atmospheric pressure in the testing area. This same process for determining p_{ts} [psig] was used by Haynes [16] and Spencer [13].

VITA

William Todd Taylor was born in Memphis, Tennessee on March 17, 1971. He attended high school at Memphis Preparatory School and graduated in 1989. He attended Christian Brothers University in Memphis, Tennessee where he obtained a Bachelors of Science in Mechanical Engineering in 1993.

In January of 1994, he began work at Office of Griffith C. Burr, Inc. in Memphis, Tennessee where he worked as a consulting engineer. He married the former Miss Rachele Therese Pascual in July of 1997 in Memphis, Tennessee. He then left his employment as a consulting engineer in August of 1997 in order to attend school at the University of Tennessee in Knoxville and obtain a Master of Science degree in Mechanical Engineering. The focus of his graduate study has been in the thermal and fluid science area.